DECOMPOSITION OF HYDROGEN PEROXIDE AND ORGANIC COMPOUNDS IN THE PRESENCE OF IRON AND IRON OXIDES

by

Wai P. Kwan

B. S., California Institute of Technology (1997)
S. M., Massachusetts Institute of Technology (1999)

Submitted to the Department of Civil and Environmental Engineering
In Partial Fulfillment of the Requirements for the Degree of

Doctor of Philosophy in Environmental Engineering

at the

Massachusetts Institute of Technology
May 2003
[June 2003]

© 2003 Massachusetts Institute of Technology
All rights reserved

MASSACHUSETTS INSTITUTE OF TECHNOLOGY
JUN 0 2 2003
LIBRARIES

Signature of the Author_____
Department of Civil and Environmental Engineering
May 9, 2003

Certified by_____
Bettina M. Voelker
Associate Professor of Civil and Environmental Engineering
Thesis Supervisor

Accepted by_____
Oral Buyukozturk, Chairman
Departmental Committee on Graduate Students

Decomposition of Hydrogen Peroxide and Organic Compounds in the Presence of Iron and Iron Oxides

by

Wai P. Kwan

Submitted to the Department of Civil and Environmental Engineering on May 9, 2003
in Partial Fulfillment of the Requirements for the Degree of Doctor of Philosophy in
Environmental Engineering

Abstract

Most advanced oxidation processes use the hydroxyl radical (•OH) to treat pollutants found in wastewater and contaminated aquifers because •OH reacts with numerous compounds at near diffusion-limited rates. •OH can be made by reacting hydrogen peroxide (H_2O_2) with either Fe(II) (the Fenton reaction), Fe(III), or iron oxide. This dissertation investigated the factors that influence the decomposition rates of H_2O_2 and organic compounds, as well as the generation rate of •OH (V_{OH}), in the presence of dissolved Fe(III) and iron oxide.

The Fe(III)-initiated chain reaction could be the dominant mechanism for the decomposition of H_2O_2 and organic compounds. The degradation rates of $H^{14}COOH$, an •OH probe, and H_2O_2 were measured in experiments at pH 4 containing either dissolved Fe(III) or ferrihydrite. Combined with the results from experiments using a radical chain terminator, we concluded that a solution chain reaction was important only in the Fe(III) system. In the ferrihydrite system the amount of dissolved Fe was insufficient to effectively propagate the chain reaction. In addition, a nonradical producing H_2O_2 loss pathway exists at the oxide surface.

The oxidation rate of any dissolved organic compound can be predicted from V_{OH} if the main sinks of •OH in the solution are known. Experiments using $H^{14}COOH$ and ferrihydrite, goethite, or hematite showed that V_{OH} was proportional to the product of the concentrations of surface area and H_2O_2. Based on these results, a model was created for predicting the pseudo-first-order oxidation rate coefficients of dissolved organic compounds (k_{org}) in systems containing iron oxide and H_2O_2. While our model successfully predicted k_{org} in aquifer sand experiments, it yielded mixed results when compared to measurements from previously published studies.

Some factors that could have caused the disagreements between model predictions and measurements were examined to refine our model. Results from experiments containing goethite, $H^{14}COOH$, and 2-Chlorophenol showed that $H^{14}COOH$ detected more •OH, which is produced at the oxide surface, than did 2-Chlorophenol. This was attributed to electrostatic attraction between the formate anions and the positively charged oxide surface, and could explain why our model, based on $H^{14}COOH$, overpredicted the k_{org} values of many neutral compounds.

Thesis Supervisor: Bettina M. Voelker
Title: Associate Professor of Civil and Environmental Engineering

Acknowledgments

First and foremost, I gratefully thank my advisor Tina Voelker, who has provided me with enormous amounts of guidance and freedom for the past six years. She taught me to write well, and more importantly, to think deeply about science, and to analyze the details carefully. Her door was always open for the numerous questions that I have had. She is also a very generous and caring person, inviting people to her home every year to celebrate Thanksgiving.

The input from my committee members, Scot Martin and Phil Gschwend, were invaluable. Their expertise and advice are sprinkled throughout this dissertation.

I have enjoyed many stimulating interactions with the past and present members of the Voelker research group. They are all brilliant individuals who have sat through many of my group meetings and gave me useful feedback. Jed Goldstone, Megan Kogut, and Barbara Southworth, in particular, toiled with me for most of these past six years as we progressed toward our Ph.D. Now that I am done, all of Tina's first generation of students has graduated.

The rest of Parsons Lab, including John MacFarlane, Sheila Frankel, Sheila Anderson, and the many post-docs and graduate students, are all wonderful people who are eager to help each other in any endeavor.

Lastly, I thank my parents and my sister for their support.

Table of Contents

ABSTRACT 3
ACKNOWLEDGMENTS 4

CHAPTER 1: INTRODUCTION 16

LITERATURE CITED 19

CHAPTER 2: DECOMPOSITION OF HYDROGEN PEROXIDE AND ORGANIC COMPOUNDS IN THE PRESENCE OF DISSOLVED IRON AND FERRIHYDRITE 21

ABSTRACT 22
INTRODUCTION 22
MATERIALS AND METHODS 25
Materials 25
Analytical Techniques 25
Kinetic Experiments 27
Dissolved Iron 28
Ferrihydrite 28
Kinetic Modeling 28
RESULTS 30
Reactions of Dissolved Fe at pH 4 30
Reactions in the Presence of Ferrihydrite at pH 4 34
DISCUSSION 38
Importance of the Chain Reaction at pH > 3 38
Mechanisms of Decomposition of Hydrogen Peroxide and Organic Compounds in Iron Oxide/H_2O_2 Systems 38
ACKNOWLEDGMENTS 42
LITERATURE CITED 42

CHAPTER 3: RATES OF HYDROXYL RADICAL GENERATION AND ORGANIC COMPOUND OXIDATION IN MINERAL-CATALYZED FENTON-LIKE SYSTEMS 59

ABSTRACT 60
INTRODUCTION 60
MATERIALS AND METHODS 62
Materials 62
Analytical Techniques 63
Kinetic Experiments 64
Calculating V_{OH} 64
RESULTS 65
DISCUSSION 68
Relationship between [H_2O_2], Iron Oxide, and V_{OH} 68
Predicting V_{OH} and Organic Compound Degradation Rate 70
ACKNOWLEDGMENTS 76
LITERATURE CITED 76

CHAPTER 4: INFLUENCE OF ELECTROSTATICS ON THE OXIDATION RATES OF ORGANIC COMPOUNDS IN HETEROGENEOUS FENTON SYSTEMS 89

ABSTRACT 90
INTRODUCTION 90
MATERIALS AND METHODS 93
Materials 93
Analytical Techniques 93
Experimental Setup 93
RESULTS 94
DISCUSSION 98
Lifetime of •OH 98
Quantifying Electrostatic Effects 98
Implications For Our Model 100
ACKNOWLEDGMENTS 103
LITERATURE CITED 103
CHAPTER 5: CONCLUSIONS AND FUTURE RESEARCH TOPICS 119
CONTRIBUTIONS OF THIS THESIS 120
FUTURE WORK 122
LITERATURE CITED 123
APPENDIX A 125
KELVIN EFFECT 128
LITERATURE CITED 128
APPENDIX B 129
pH INCREASE DUE TO OXIDATION OF FORMIC ACID 130
EXPERIMENTS WITH H_2O_2 AS THE DOMINANT •OH SINK 130
EXPERIMENTS WITH FORMIC ACID AS THE DOMINANT •OH SINK 130
LITERATURE CITED 130
APPENDIX C 143
APPENDIX D 146

List of Tables

Table 2-1. Mechanism of the Fe(III)-initiated chain reaction. The rate constants are listed in M^{-1} s^{-1}. 45

Table 2-2. Some published rate constants for the reactions of •OH with formic acid, formate, and hydrogen peroxide, in M^{-1} s^{-1}. We included all rate constants except those where the reaction pH was outside of 2-5. 46

Table 2-3. Experimental pseudo first-order decomposition rates of $H^{14}COOH/H^{14}COO^-$ and H_2O_2, and the corresponding γ in pH 4 solutions with dissolved iron, in day^{-1}. The uncertainty in the rate coefficients represents one standard deviation calculated from non-linear regressions of the raw data (concentration of $H^{14}COOH/H^{14}COO^-$ and H_2O_2 versus time). The uncertainty in γ represents one standard deviation calculated by propagating the errors from the rate coefficients. Measured dissolved Fe (0.02-μm filtered) was 0.41-2.55 μM, but no relationship between reaction rates and dissolved Fe was observed. 47

Table 2-4. Experimental pseudo first-order decomposition rates of benzoic acid and formic acid in pH 4 solutions containing ferrihydrite. The uncertainty in the observed rate coefficients represents one standard deviation calculated from nonlinear regressions of the raw data. The uncertainty in the ratio represents one standard deviation calculated by propagating the errors from the rate coefficients. Also listed are the averages of the literature values of the second-order rate constants with •OH that meet the criterion stated in Table 2-2, with an uncertainty of one standard deviation. 48

Table 2-5. Estimated solution chain lengths vs. pH, assuming [Fe(III)] is at equilibrium with amorphous ferric hydroxide ($K_{sp} = 10^{-38.8}$). 49

Table 3-1. Relevant information from the publications used in Figure 3-4. 78

Table 3-2. Relevant information from the publications used in Figure 3-5.* 79

Table 4-1. Effect of ionic strength and pH on Ψ_0. 105

Table A-1. Concentration of dissolved iron (defined as iron that passed through a 0.02-μm filter) in the ferrihydrite experiments. Ferrihydrite was diluted from a freshly prepared 4 x 10^{-4} M stock solution, except where noted, into 200 mL. The detection limit for Fe is 0.03 μM. 126

Table C-1. Final pH of experiments using goethite and H_2O_2 to oxidize 2-CP. The initial pH was 4.0. 144

Table C-2. $\int_0^\infty k_{OH,HCOO^-}[\bullet OH]_{ss}(x)[HCOO^-]_{bulk}\, e^{-\Delta Z F \Psi(x)/RT} dx$ (ζ) as a function of pH. Ψ_0 was calculated in the same manner as described in chapter 4, and ζ was evaluated at I = 10 mM and $[H_2O_2]_0$ = 160 mM. 145

List of Figures

Figure 2-1. Schematic diagram of the Fe(III)-initiated Fenton-like chain reaction. 50

Figure 2-2. A typical data set of the concentration of hydrogen peroxide (●) and ^{14}C-labeled formic acid (▽) over time in an experiment with only dissolved Fe at pH 4. Error bars represent one standard deviation. The lines are non-linear regression fits of the data to the function $[C] = [C]_0 \exp(-kt)$, with $[C]_0$ values of 819 μM and 110 nM and k values of 0.046 day^{-1} and 0.89 day^{-1}, for H_2O_2 and HCOOH, respectively. 51

Figure 2-3a. Experimental (○) pseudo-first-order decomposition rates of H_2O_2 in the ferrihydrite/H_2O_2 system. Also included are data from experiments where 10 μM *tert*-butyl alcohol (■) or 100 μM *tert*-butyl alcohol (▲) were added. Error bars represent one standard deviation of rate coefficients calculated from non-linear regressions of the raw data. 52

Figure 2-3b. Experimental (○) pseudo-first-order decomposition rates of $H^{14}COOH/H^{14}COO^-$ in the ferrihydrite/H_2O_2 system. Also included are data from experiments where 10 μM *tert*-butyl alcohol (■) or 100 μM *tert*-butyl alcohol (▲) were added. Error bars represent one standard deviation of rate coefficients calculated from non-linear regressions of the raw data. 53

Figure 2-4. Comparison of predictions from Models A-D to the experimental γ values (●) of the ferrihydrite/H_2O_2 system. Error bars represent one standard deviation, calculated by propagating the errors shown in Figures 2-3a,b or from iron measurements. Note that lines for Models A and D are nearly identical. 54

Figure 2-5a. Pseudo-first-order decomposition rates of H_2O_2 in an iron oxide/H_2O_2 system from Models A and B, with and without 100 μM *tert*-butyl alcohol. 55

Figure 2-5b. Pseudo-first-order decomposition rates of $H^{14}COOH/H^{14}COO^-$ in an iron oxide/H_2O_2 system from Models A and B, with and without 100 μM *tert*-butyl alcohol. 56

Figure 2-5c. Pseudo-first-order decomposition rates of H_2O_2 in an iron oxide/H_2O_2 system from Models C and D, with and without 100 μM *tert*-butyl alcohol. 57

Figure 2-5d. Pseudo-first-order decomposition rates of $H^{14}COOH/H^{14}COO^-$ in an iron oxide/H_2O_2 system from Models C and D, with and without 100 μM *tert*-butyl alcohol. 58

Figure 3-1a. V_{OH} of three different iron oxides plotted as a function of the amount of surface area and hydrogen peroxide at pH 4. Ferrihydrite concentrations varied from 6-400 μM, with $[H_2O_2]_0 \leq 1$ mM (●) and ≥ 5 mM (○); goethite concentrations of 0.02 (◈), 0.2 (◆), and 0.6 g/L (◇), and hematite concentrations of 0.2 (▲) and 1 g/L (△) are also shown. The initial concentration of formic acid for all experiments was 74-244 nM. The lines are regression fits of the data to eq 10-12. 81

Figure 3-1b. Decomposition rate of formic acid in the experiments described in Figure 3-1a (same symbols), normalized to the concentration of total Fe and plotted as a function of the initial amount of hydrogen peroxide. The lines are the expected values based on the regressions. 82

Figure 3-2a. V_{OH} from experiments containing 0.6 g/L of goethite with either H_2O_2 ($[HCOOH]_{T,0}$ = 100 nM (◇) or 50 μM (◆)) or formic acid ($[HCOOH]_{T,0}$ = 50 μM (□), 0.3 mM (■) or 10 mM (▼)) as the dominant •OH sink at pH 4. The line is the predicted V_{OH} calculated from eq 10. 83

Figure 3-2b. Decomposition rate of formic acid in the experiments described in Figure 3-2a (same symbols), normalized to the concentration of total Fe and plotted as a function of the

initial amount of hydrogen peroxide. The data for $[HCOOH]_{T,0}$ = 100 nM is the same as Figure 3-1b. The lines are the expected $(d[HCOOH]_T/dt)/[Fe]_T$ for each starting amount of formic acid, given the calculated V_{OH} shown in Figure 3-2a. ____ 84
Figure 3-3a. V_{OH} from experiments at pH 4 with H_2O_2 as the dominant •OH sink and either 25 (●) or 60 g/L (▽) of sand and with formic acid as the dominant •OH sink and 60 g/L of sand (■). We assumed that all of the crystalline surface iron in the sand was goethite, and plotted all of the data points using a surface area of 40 m^2/g, with a range of 8-200 m^2/g depicted by the error bars. The line is the predicted V_{OH} calculated from eq 10. ____ 85
Figure 3-3b. Decomposition rate of formic acid in the experiments described in Figure 3-3a (same symbols), normalized to the concentration of total Fe and plotted as a function of the initial amount of hydrogen peroxide. The two sets of dashed lines represent the possible range of predicted values for the two systems, assuming that all of the crystalline iron in the sand was goethite, with a surface area ranging from 8 to 200 m^2/g. ____ 86
Figure 3-4. Comparison of measured V_{OH} from refs *9* (●), *16* (▽), *17* (■), and *18* (◇), versus our predictions. The line represents perfect agreement between predicted and measured V_{OH} values. Petigara et al. (*18*) did not have measurements of the surface area of their iron oxide because they used natural soils. Thus, we estimated the V_{OH} values using typical ranges of surface areas for goethite and hematite and presented the results with error bars. ____ 87
Figure 3-5. Comparison of the measured pseudo-first-order loss rate of various organic compounds, obtained from refs *36* (▼), *8* (○), *11* (▽), *12* (●), *37* (□), and *19* (■), versus our predictions. The line represents perfect agreement between predicted and measured k_{org} values. The error bars show the range of estimated k_{org} values using typical ranges of surface areas for goethite in studies where the surface area was not measured. ____ 88
Figure 4-1. Typical data set of the concentration of ^{14}C-labeled formic acid (●) and 2-CP (▽) in an experiment containing 0.6 g/L goethite, $[H_2O_2]_0$ = 2 M, $[2\text{-CP}]_0$ = 300 μM, and initial ^{14}C of 10000 DPM at pH 4. The lines are linear regression fits to log transformed data._ 106
Figure 4-2a. $[•OH]_{ss,\ interval}$ for ^{14}C-labeled formic acid (●, ○) and 2-CP (▼, ▽) in experiments containing 0.6 g/L goethite, $[H_2O_2]_0$ = 2 M, initial ^{14}C of 20000 (●) or 10000 (○)DPM, and $[2\text{-CP}]_0$ = 130 (▼) or 300 (▽) μM at pH 4. The horizontal bars denote the time interval between the two consecutive data points that were used to calculate $[•OH]_{ss,\ interval}$. ____ 107
Figure 4-2b. $[•OH]_{ss,\ interval}$ for ^{14}C-labeled formic acid (●, ○) and NB(■, □) in experiments containing 0.6 g/L goethite, $[H_2O_2]_0$ = 2 M, $[NB]_0$ = 100 μM, and initial ^{14}C of 40000 (●) or 10000 (○) DPM at pH 4. The horizontal bars denote the time interval between the two consecutive data points that were used to calculate $[•OH]_{ss,\ interval}$. ____ 108
Figure 4-2c. $[•OH]_{ss,\ interval}$ for ^{14}C-labeled formic acid (●, ○), 2-CP (▼, ▽), and NB (■, □) in experiments containing 0.6 g/L goethite, $[H_2O_2]_0$ = 2 M, $[2\text{-CP}]_0 = [NB]_0$ = 100 μM, and initial ^{14}C of 40000 (●) or 20000 (○) DPM at pH 4. The horizontal bars denote the time interval between the two consecutive data points that were used to calculate $[•OH]_{ss,\ interval}$. ____ 109
Figure 4-3a. ^{14}C activity of $H^{14}COOH$ in four experiments containing 0.6 g/L goethite, $[H_2O_2]_0$ = 2 M, and $[2\text{-CP}]_0$ = 0.3 (●), 3 (○), 30 (◆), or 300 (◇) μM at pH 4. The experiments with $[2\text{-CP}]_0$ = 0.3 and 3 μM were re-spiked with $H^{14}COOH$ after ~20 hours. ____ 110
Figure 4-3b. $[•OH]_{ss,\ interval}$ for the data shown in Figure 4-3a. The horizontal bars denote the time interval between the two consecutive data points that were used to calculate $[•OH]_{ss,\ interval}$. ____ 111

Figure 4-4a. Photos of two test tubes containing 0.6 g/L of goethite, $[H_2O_2]_0$ = 2 M and $[2\text{-CP}]_0$ = 3 (left) or 300 (right) μM at pH 4. (A) was taken immediately after the test tubes had been shaking for 1.5 hours. They were then left undisturbed for 15 minutes before (B) was taken. 112

Figure 4-4b. Continuation of the experiment described in Figure 4-4a. (A) was taken immediately after the test tubes had been shaking for 10 hours. They were then left undisturbed for 15 minutes before (B) was taken. 113

Figure 4-5a. ^{14}C activity of $H^{14}COOH$ (●) and [2-CP] (▽) in an experiment with [Fe(III)] = 25 μM, $[H_2O_2]_0$ = 2 M, and $[2\text{-CP}]_0$ = 170 μM at pH 3. 114

Figure 4-5b. ^{14}C activity of $H^{14}COOH$ (●) and [2-CP] (▽) in an experiment with [Fe(III)] = 75 μM, $[H_2O_2]_0$ = 2 M, and $[2\text{-CP}]_0$ = 200 μM at pH 3. 115

Figure 4-6a. $[\bullet OH]_{ss,\ interval}$ for the data shown in Figure 4-5a. The horizontal bars denote the time interval between the two consecutive data points that were used to calculate $[\bullet OH]_{ss,\ interval}$. 116

Figure 4-6b. $[\bullet OH]_{ss,\ interval}$ for the data shown in Figure 4-5b. The horizontal bars denote the time interval between the two consecutive data points that were used to calculate $[\bullet OH]_{ss,\ interval}$. 117

Figure 4-7. Comparison of the measured pseudo-first-order loss rate of various organic compounds, obtained from refs *36* (▼), *16* (○), *10* (▽), *17* (●), *11* (□), and *21* (■), versus our model predictions that account for electrostatic effects. The line represents perfect agreement between predicted and measured k_{org} values. The horizontal bars show the range of estimated k_{org} values using typical ranges of surface areas for goethite in studies where the surface area was not measured. 118

Figure B1a. Representative data set of the concentration of ^{14}C-labeled formic acid (given as disintegrations per minute) and hydrogen peroxide over time in experiments at pH 4, containing 20 μM (●), 200 μM (▽), or 280 μM (■) ferrihydrite. $[HCOOH]_{T,\ 0}$ was 110 nM. 131

Figure B1b. Representative data set of the concentration of ^{14}C-labeled formic acid (given as disintegrations per minute) over time in experiments at pH 4, 190 μM ferrihydrite, $[HCOOH]_{T,\ 0}$ = 212-219 nM, and $[H_2O_2]_0$ = 50 mM(●), 100 mM (□), 200 mM (▲), or 400 mM(▽). 132

Figure B1c. Representative data set of the concentration of ^{14}C-labeled formic acid (given as disintegrations per minute) and hydrogen peroxide over time in experiments at pH 4, containing 0.6 g/L of goethite, $[HCOOH]_{T,\ 0}$ = 92-112 nM, and $[H_2O_2]_0$ = 2 mM (●), 40 mM (□), 0.4 M (▲), or 1 M (▽). 133

Figure B1d. Representative data set of the concentration of ^{14}C-labeled formic acid (given as disintegrations per minute) and hydrogen peroxide over time in experiments at pH 4, containing 1 g/L of hematite, $[HCOOH]_{T,\ 0}$ = 201-210 nM, and $[H_2O_2]_0$ = 10 mM (●), 100 mM (□), 1 M (▲), or 2 M (▽). 134

Figure B1e. Representative data set of the concentration of ^{14}C-labeled formic acid (given as disintegrations per minute) and hydrogen peroxide over time in experiments at pH 4, containing 60 g/L of Georgetown sand, $[HCOOH]_{T,\ 0}$ = 162-166 nM, and $[H_2O_2]_0$ = 5 mM (●), 110 mM (▽), 675 mM (■), or 2.7 M (◇). 135

Figure B2a. Concentration of HCOOH versus time from experiments containing 0.6 g/L of goethite, $[HCOOH]_{T,\ 0}$ = 10 mM, and $[H_2O_2]_0$ = 2 mM (●) or 10 mM (○). (A) shows the nonlinear regression fits to the data, while (B) shows the linear regression fits. 136

Figure B2b. Concentration of HCOOH versus time from experiments containing 0.6 g/L of goethite, $[HCOOH]_{T,0}$ = 10 mM, and $[H_2O_2]_0$ = 10 mM (●), 50 mM (▽), or 100 mM (■). (A) shows the nonlinear regression fits to the data, while (B) shows the linear regression fits. 137
Figure B2c. Concentration of HCOOH versus time from experiments containing 0.6 g/L of goethite, $[HCOOH]_{T,0}$ = 10 mM, and $[H_2O_2]_0$ = 50 mM (●) or 100 mM (▼). (A) shows the nonlinear regression fits to the data, while (B) shows the linear regression fits. 138
Figure B2d. Concentration of HCOOH versus time from experiments containing 0.6 g/L of goethite, $[HCOOH]_{T,0}$ = 0.3 mM, and $[H_2O_2]_0$ = 700 μM (●), 500 μM (▽), 250 μM (■), or 100 μM (◇). (A) shows the nonlinear regression fits to the data, while (B) shows the linear regression fits. 139
Figure B2e. Concentration of HCOOH versus time from experiments containing 0.6 g/L of goethite, $[HCOOH]_{T,0}$ = 50 μM, and $[H_2O_2]_0$ = 600 μM. (A) shows the nonlinear regression fit to the data, while (B) shows the linear regression fit. 140
Figure B2f. Concentration of HCOOH versus time from experiments containing 0.6 g/L of goethite, $[HCOOH]_{T,0}$ = 50 μM, and $[H_2O_2]_0$ = 500 μM (●), 250 μM (▽), or 100 μM (■). (A) shows the nonlinear regression fits to the data, while (B) shows the linear regression fits. 141
Figure B3. Concentration of H_2O_2 versus time for the experiments shown in Figures B2a-f. 142
Figure D1. (A) ^{14}C activity in experiments with [Fe(III)] = 0.79 (●) or 2.11 (▼) μM, and k = 0.53 and 1.45 d^{-1}, respectively. (B) $[H_2O_2]$ in experiments described in (A), with k = 0.033 (○) and 0.066 (▽) d^{-1}. (C) ^{14}C activity in experiments with [Fe(III)] = 1.30 (●), 0.58 (▼), or 0.73 (■) μM, and k = 0.76, 0.21, and 0.32 d^{-1}, respectively. (D) $[H_2O_2]$ in experiments described in (C), with k = 0.072 (○), 0.0082 (▽), and 0.017 (□) d^{-1}. 148
Figure D2. (A) ^{14}C activity in experiments with [ferrihydrite] = 5.59 (●), 37.66 (▼) or 85.69 (■) μM, and k = 0.36, 0.49, and 0.41 d^{-1}, respectively. (B) $[H_2O_2]$ in experiments described in (A), with k = 0.016 (○), 0.035 (▽), and 0.040 (□) d^{-1}. (C) ^{14}C activity in experiments with [ferrihydrite] = 16.85 (●), 178.56 (▼) or 276.19 (■) μM, and k = 0.63, 2.30, and 3.89 d^{-1}, respectively. (D) $[H_2O_2]$ in experiments described in (C), with k = 0.039 (○), 0.18 (▽), and 0.35 (□) d^{-1}. 149
Figure D3. (A) ^{14}C activity in experiments with [ferrihydrite] = 20.31 (●), 192.93 (▼), or 276.76 (■) μM, and k = 0.36, 0.49, and 0.41 d^{-1}, respectively. (B) $[H_2O_2]$ in experiments described in (A), with k = 0.11 (○), 0.035 (▽), and 0.040 (□) d^{-1}. (C) ^{14}C activity in experiments with [ferrihydrite] = 6.35 (●), 23.74 (▼), 85.34 (■), or 133.91 (◆) μM, and k = 0.11, 0.31, 0.31, and 1.84 d^{-1}, respectively. (D) $[H_2O_2]$ in experiments described in (C), with k = 0.0067 (○), 0.013 (▽), 0.024 d^{-1} (□), and 0.12 (◇) d^{-1}. 150
Figure D4. (A) ^{14}C activity in experiments with [ferrihydrite] = 44.86 (●), 84.41 (▼), or 378.99 (■) μM, and k = 0.53, 0.56, and 4.00 d^{-1}, respectively. (B) $[H_2O_2]$ in experiments described in (A), with k = 0.040 (○), 0.038 (▽), and 0.54 (□) d^{-1}. (C) ^{14}C activity in experiments with [ferrihydrite] = 323.31 (●) or 411.83 (▼) μM, and k = 1.91 and 4.97 d^{-1}, respectively. (D) $[H_2O_2]$ in experiments described in (C), with k = 0.26 (○) and 0.61 (▽) d^{-1}. 151
Figure D5. (A) ^{14}C activity in experiments with [ferrihydrite] = 178.22 μM and k = 1.77 d^{-1}. (B) $[H_2O_2]$ in experiments described in (A), with k = 0.13 d^{-1}. (C) ^{14}C activity in experiments with [ferrihydrite] = 306.45 μM and k = 2.20 d^{-1}. (D) $[H_2O_2]$ in experiments described in (C), with k = 0.43 d^{-1}. 152

Figure D6. (A) ^{14}C activity in experiments with [ferrihydrite] = 166.77 (●) or 183.94 (▼) μM, and k = 2.63 and 2.13 d^{-1}, respectively. (B) $[H_2O_2]$ in experiments described in (A), with k = 0.14 (○) and 0.18 (▽) d^{-1}. (C) ^{14}C activity in experiments with [ferrihydrite] = 212.85 (●) or 61.80 (▼) μM, and k = 2.22 and 0.83 d^{-1}, respectively. (D) $[H_2O_2]$ in experiments described in (C), with k = 0.21 (○) and 0.036 (▽) d^{-1}. 153

Figure D7. (A) ^{14}C activity in experiments with [Fe(III)] = 1.30 μM and k = 0.89 d^{-1}. (B) $[H_2O_2]$ in experiments described in (A), with k = 0.046 d^{-1}. (C) ^{14}C activity in experiments with [ferrihydrite] = 83.68 μM and k = 1.15 d^{-1}. (D) $[H_2O_2]$ in experiments described in (C), with k = 0.071 d^{-1}. 154

Figure D8. (A) ^{14}C activity in experiments with 0.1 mM *tert*-butyl alcohol and [ferrihydrite] = 192.63 (●) or 196.87 (▼) μM, and k = 0.62 and 1.16 d^{-1}, respectively. (B) $[H_2O_2]$ in experiments described in (A), with k = 0.27 (○) and 0.34 (▽) d^{-1}. (C) ^{14}C activity in experiments with [Fe(III)] = 2.70 (●) or 2.73 and 0.1 mM *tert*-butyl alcohol (▼) μM, and k = 0.23 and 0.0095 d^{-1}, respectively. (D) $[H_2O_2]$ in experiments described in (C), with k = 0.0090 (○) and 0.0031 (▽) d^{-1}. 155

Figure D9. (A) ^{14}C activity in experiments with 10 μM *tert*-butyl alcohol (except ●) and [ferrihydrite] = 85.70 (●), 78.34 (▼), 85.08 (■), or 84.93 and 1 μM Fe(III) (◆) μM, and k = 0.75, 0.20, 0.22, and 0.23 d^{-1}, respectively. (B) $[H_2O_2]$ in experiments described in (A), with k = 0.039 (○), 0.020 (▽), 0.018 (□), and 0.015 (◇) d^{-1}. (C) ^{14}C activity in experiments with [ferrihydrite] = 185.46 (●), 192.95 and 10 μM *tert*-butyl alcohol (▼), or 181.93 and 1.5 μM Fe(III) (■) μM, and k = 1.86, 1.43, and 2.74 d^{-1}, respectively. (D) $[H_2O_2]$ in experiments described in (C), with k = 0.088 (○), 0.11 (▽), and 0.15 (□) d^{-1}. 156

Figure D10. (A) ^{14}C activity in experiments with [ferrihydrite] = 42.68 (●), 48.93 and 10 μM *tert*-butyl alcohol (▼), or 42.15 and 1.5 μM Fe(III) (■) μM, and k = 0.77, 0.27, and 0.76 d^{-1}, respectively. (B) $[H_2O_2]$ in experiments described in (A), with k = 0.031 (○), 0.0037 (▽), and 0.028 (□) d^{-1}. (C) ^{14}C activity in experiments with [ferrihydrite] = 190.11 (●), 187.86 and 10 μM *tert*-butyl alcohol (▼), or 187.77 and 10 μM *tert*-butyl alcohol (■) μM, and k = 1.73, 0.12, and 0.13 d^{-1}, respectively. (D) $[H_2O_2]$ in experiments described in (C), with k = 0.44 (○), 0.036 (▽), and 0.057 (□) d^{-1}. 157

Figure D11. (A) ^{14}C activity in experiments with [Fe(III)] = 0.90 (●) or 1.18 and 1 mM NaCl (▼) μM, [ferrihydrite] = 197.95 (■) or 197.35 and 1 mM NaCl (◆) μM, and k = 0.14, 0.14, 2.85, and 2.63 d^{-1}, respectively. (B) $[H_2O_2]$ in experiments described in (A), with k = 0.011 (○), 0.0087 (▽), 0.25 (□), and 0.19 (◇) d^{-1}. (C) ^{14}C activity in experiments with [ferrihydrite] ~200 μM and k = 2.93 d^{-1}. (D) $[H_2O_2]$ in experiments described in (C), with k = 0.28 d^{-1}. 158

Figure D12. (A) ^{14}C activity in experiments with [ferrihydrite] = 198.75 μM and k = 2.40 d^{-1}. (B) $[H_2O_2]$ in experiments described in (A), with k = 0.17 d^{-1}. (C) ^{14}C activity in experiments with [ferrihydrite] ~200 μM and k = 1.71 d^{-1}. (D) $[H_2O_2]$ in experiments described in (C), with k = 0.19 d^{-1}. 159

Figure D13. (A) Concentration of benzoic acid (●) and formic acid (▼) in a control experiment containing H_2O_2 and no iron. (B) $[H_2O_2]$ in the experiment described in (A). (C) Concentration of benzoic acid (●) and formic acid (▼) in a control experiment with [ferrihydrite] = 300 μM and no H_2O_2. 160

Figure D14. (A) Concentration of benzoic acid in duplicate experiments with [ferrihydrite] = 190 μM, and k = 1.26 (●) and 0.66 (▽) d^{-1}. (B) Concentration of benzoic acid in duplicate

experiments with [ferrihydrite] = 190 μM, and k = 0.59 (●) and 0.23 (▽) d^{-1}. (C) $[H_2O_2]$ in experiments described in (A) and (B), with k = 0.078 (●) and 0.090 (▽) d^{-1}. 161
Figure D15. (A) ^{14}C activity in experiments with [ferrihydrite] = 190 μM and $[H_2O_2]_0$ = 5 (●), 10 (▼) or 30 (■) mM, and k = 0.13, 0.12, and 0.17 h^{-1}, respectively. (B) ^{14}C activity in experiments with [ferrihydrite] = 190 μM and $[H_2O_2]_0$ = 50 (●), 100 (▼), 200 (■) or 400 (◆) mM, and k = 0.22, 0.26, 0.23, and 0.20 h^{-1}, respectively. (C) ^{14}C activity in experiments with [ferrihydrite] = 90 μM and $[H_2O_2]_0$ = 5 (●), 10 (▼) or 30 (■) mM, and k = 0.11, 0.098, and 0.084 h^{-1}, respectively. (D) ^{14}C activity in experiments with [ferrihydrite] = 90 μM and $[H_2O_2]_0$ = 50 (●), 100 (▼), 200 (■) or 400 (◆) mM, and k = 0.093, 0.080, 0.068, and 0.072 h^{-1}, respectively. 162
Figure D16. (A) ^{14}C activity in experiments with [ferrihydrite] = 100 μM and $[H_2O_2]_0$ = 75 (●) or 300 (▼) mM, or [ferrihydrite] = 200 μM and $[H_2O_2]_0$ = 75 (■) or 300 (◆) mM, and k = 0.061, 0.099, 0.16 and 0.19 h^{-1}, respectively. (B) ^{14}C activity in experiments with [ferrihydrite] = 160 μM and $[H_2O_2]_0$ = 0.3 (●) or 0.4 (▼) M, or [ferrihydrite] = 230 μM and $[H_2O_2]_0$ = 0.2 (■) or 0.3 (◆) M, and k = 0.16, 0.14, 0.18 and 0.20 h^{-1}, respectively. (C) ^{14}C activity in experiments with 0.2 g/L goethite and $[H_2O_2]_0$ = 10 (●) or 100 (▼) mM, or [hematite] = 0.2 g/L and $[H_2O_2]_0$ = 10 (■) or 100 (◆) mM, and k = 0.26, 0.40, 0.024 and 0.031 h^{-1}, respectively. 163
Figure D17. (A) ^{14}C activity in experiments with 0.2 g/L goethite and $[H_2O_2]_0$ = 50 (●) or 300 (▼) mM, or 0.2 g/L hematite and $[H_2O_2]_0$ = 50 (■) or 300 (◆) mM, and k = 0.53, 0.47, 0.040 and 0.014 h^{-1}, respectively. (B) ^{14}C activity in experiments with 0.2 g/L hematite with k = 0.0089 (●) and 0.013 (▼) h^{-1}. (C) $[H_2O_2]$ in experiments described in (B), with $[H_2O_2]_0$ = 0.7 (○) or 0.9 (▽) M. 164
Figure D18. (A) ^{14}C activity in experiments with 0.2 g/L goethite and k = 0.53 (●) and 0.27 (▼) h^{-1}, or 0.2 g/L hematite and k = 0.027 (■) and 0.015 (◆) h^{-1}. (B) $[H_2O_2]$ in experiments described in (A), with $[H_2O_2]_0$ = 0.2 (○), 0.6 (▽), 0.8 (□), or 0.9 (◇) M. (C) ^{14}C activity in experiments with 0.2 g/L goethite and k = 0.12 (●) and 0.14 (▼) h^{-1}, or 0.6 g/L goethite and k = 0.76 (■) and 1.21 (◆) h^{-1}. (D) $[H_2O_2]$ in experiments described in (C), with $[H_2O_2]_0$ = 0.002 (○), 2 (▽), 0.010 (□), or 0.1 (◇) M. 165
Figure D19. (A) ^{14}C activity in experiments with 0.6 g/L goethite and k = 0.32 (●), 1.20 (▼), 1.26 (■) and 1.03 (◆) h^{-1}. (B) $[H_2O_2]$ in experiments described in (A), with $[H_2O_2]_0$ = 2 (○) or 40 (▽) mM, or 0.4 (□) or 1.0 (◇) M. (C) ^{14}C activity in experiments with 0.02 g/L goethite and $[H_2O_2]_0$ = 2 (●), 50 (▼), 140 (■) or 440 (◆) mM, with k = 0.062, 0.027, 0.076, and 0.11 h^{-1}, respectively. (D) ^{14}C activity in experiments with 0.2 g/L goethite and $[H_2O_2]_0$ = 0.9 (●) or 3.7 (▼) M, or 1.0 g/L hematite and $[H_2O_2]_0$ = 50 (●) or 540 (▼) mM, with k = 0.12, 0.062, 0.096, and 0.041 h^{-1}, respectively. 166
Figure D20. (A) ^{14}C activity in experiments with 1.0 g/L hematite and k = 0.081 (●), 0.11 (▼), 0.039 (■) and 0.050 (◆) h^{-1}. (B) $[H_2O_2]$ in experiments described in (A), with $[H_2O_2]_0$ = 10 (○) or 110 (▽) mM, or 1.0 (□) or 2.0 (◇) M. (C) ^{14}C activity in control experiments with 0.02 g/L goethite (●) or hematite (▼) and no H_2O_2. 167
Figure D21. (A) ^{14}C activity in experiments with 0.6 g/L goethite, I = [NaHCOO] = 10 mM, and k = 0.0020 (●) and 0.010 (▼) h^{-1}. (B) $[H_2O_2]$ in experiments described in (A), with $[H_2O_2]_0$ = 2 (○) or 10 (▽) mM. (C) ^{14}C activity in experiments with 0.6 g/L goethite, I = [NaHCOO] = 10 mM, and k = 0.010 (●), 0.051 (▼) and 0.079 (■) h^{-1}. The second and third k values were obtained using the data points from the first four hours as the pH of the

solutions rose above 5 afterwards. (D) $[H_2O_2]$ in experiments described in (C), with $[H_2O_2]_0$ = 10 (○), 50 (▽), or 100 (□) mM. 168
Figure D22. (A) ^{14}C activity in experiments with 0.6 g/L goethite, I = [NaHCOO] = 10 mM, and k = 0.054 (●) and 0.099 (▼) h^{-1}. The k values were obtained using the data points from the first four hours as the pH of the solutions rose above 5 afterwards. (B) $[H_2O_2]$ in experiments described in (A), with $[H_2O_2]_0$ = 50 (○) or 110 (▽) mM. (C) ^{14}C activity in experiments with 0.6 g/L goethite, [NaHCOO] = 50 μM (I = 10 mM), and k = 0.088 h^{-1}. (D) $[H_2O_2]$ in experiments described in (C), with $[H_2O_2]_0$ = 610 μM and k = 0.032 h^{-1}. 169
Figure D23. (A) ^{14}C activity in experiments with 0.6 g/L goethite, [NaHCOO] = 50 μM (I = 10 mM), and k = 0.15 (●), 0.078 (▼), and 0.021 (■) h^{-1}. (B) $[H_2O_2]$ in experiments described in (A), with $[H_2O_2]_0$ = 530 (○), 260 (▽), or 110 (□) μM, and k = 0.055, 0.050, and 0.043 h^{-1}, respectively. (C) ^{14}C activity in experiments with 0.6 g/L goethite, [NaHCOO] = 300 μM (I = 10 mM), and k = 0.028 (●), 0.019 (▼), 0.010 (■), and 0.0018 (◆) h^{-1}. (D) $[H_2O_2]$ in experiments described in (C), with $[H_2O_2]_0$ = 700 (○), 500 (▽), 250 (□), or 100 (◇) μM and k = 0.037, 0.037, 0.030, and 0.023 h^{-1}, respectively. 170
Figure D24. (A) ^{14}C activity in experiments with 0.6 g/L goethite, [NaHCOO] = 50 μM (I = 10 mM), and k = 1.10 (●) and 0.74 (▼) h^{-1}. (B) $[H_2O_2]$ in experiments described in (A), with $[H_2O_2]_0$ = 0.5 (○) or 1.9 (▽) M. (C) ^{14}C activity in experiments with 25 g/L Georgetown sand, and k = 0.042 (●), 0.035 (▼), and 0.052 (■) h^{-1}. (◆) is the control experiment with k = 0.0044 h^{-1}. (D) $[H_2O_2]$ in experiments described in (C), with $[H_2O_2]_0$ = 4.8 (○) or 100 (▽) mM, or 1.1 (□) M. 171
Figure D25. (A) ^{14}C activity in experiments with 60 g/L Georgetown sand and k = 0.043 (●), 0.095 (▼), 0.052 (■), and 0.073 (◆) h^{-1}. (B) $[H_2O_2]$ in experiments described in (A), with $[H_2O_2]_0$ = 5.0 (○), 110 (▽), 675 (□), or 2700 (◇) mM. (C) ^{14}C activity in experiments with 60 g/L Georgetown sand, and k = 0.0091 (●), 0.012 (▼), 0.00034 (■), and 0.0024 (◆) h^{-1}. (■) and (◆) contained 10 mM NaHCOO instead of $NaClO_4$. (D) $[H_2O_2]$ in experiments described in (C), with $[H_2O_2]_0$ = 85 (○) or 630 (▽) μM, or 1.0 (□) or 10 (◇) mM. 172
Figure D26. (A) ^{14}C activity in experiments with 25 g/L Georgetown sand (●), or 60 g/L Georgetown sand and [NaHCOO] = 10 mM (▼) or [NaHCOO] = 300 μM (I = 10 mM) (■), (◆). k = 0.057, 0.0058, 0.0083, and 0.0083 h^{-1}, respectively. (B) $[H_2O_2]$ in experiments described in (A), with $[H_2O_2]_0$ = 30 (○), 60 (▽), 0.086 (□), or 0.6 (◇) mM. 173
Figure D27. (A) [2-CP] in an experiment with 2.5 g/L goethite and k = 0.17 h^{-1}. (B) $[H_2O_2]$ in the experiment described in (A), with k = 0.030 h^{-1}. (C) [2-CP] in an experiment with 2.5 g/L goethite and k = 0.14 h^{-1}. (D) $[H_2O_2]$ in the experiment described in (C), with k = 0.050 h^{-1}. 174
Figure D28. (A) ^{14}C activity in an experiment with [Fe(III)] = 25 μM, $[H_2O_2]_0$ = 1.9 M, and $[2\text{-CP}]_0$ = 200 μM, with k = 0.0038 h^{-1}. (B) [2-CP] in an experiment with [Fe(III)] = 25 μM and $[H_2O_2]_0$ = 2.0 M, with k = 0.039 h^{-1}. (C) ^{14}C activity in an experiment with [Fe(III)] = 75 μM, $[H_2O_2]_0$ = 1.7 M, and $[2\text{-CP}]_0$ = 200 μM, with k = 0.032 h^{-1}. (D) [2-CP] in an experiment with [Fe(III)] = 75 μM and $[H_2O_2]_0$ = 1.8 M, with k = 0.97 h^{-1}. 175
Figure D29. (A) ^{14}C activity in an experiment with 0.6 g/L goethite, $[H_2O_2]_0$ = 2 M, and $[2\text{-CP}]_0$ = 130 μM, with k = 0.28 h^{-1}. (B) [2-CP] in an experiment with 0.6 g/L goethite, $[H_2O_2]_0$ = 2 M, and k = 0.049 h^{-1}. (C) $[H_2O_2]$ in the experiments described in (A, ○) and (B, △), with k = 0.0016 (△) h^{-1}. 176

Figure D30. (A) ^{14}C activity in an experiment with 0.6 g/L goethite, $[H_2O_2]_0$ = 2 M, and $[2\text{-CP}]_0$ = 300 μM, with k = 0.075 h^{-1}. (B) [2-CP] in an experiment with 0.6 g/L goethite, $[H_2O_2]_0$ = 2 M, and k = 0.052 h^{-1}. (C) $[H_2O_2]$ in the experiments described in (A, ○) and (B, △), with k = 0.0026 (△) h^{-1}. 177
Figure D31. (A) ^{14}C activity in an experiment with 0.6 g/L goethite, $[H_2O_2]_0$ = 2 M, and $[NB]_0$ = 100 μM, with k = 0.55 h^{-1}. (B) [NB] in an experiment with 0.6 g/L goethite, $[H_2O_2]_0$ = 2 M, and k = 0.058 h^{-1}. (C) $[H_2O_2]$ in the experiments described in (A, ○) and (B, ◇), with k = 0.0042 (◇) h^{-1}. 178
Figure D32. (A) ^{14}C activity in an experiment with 0.6 g/L goethite, $[H_2O_2]_0$ = 2 M, and $[NB]_0$ = 100 μM, with k = 0.73 h^{-1}. (B) [NB] in an experiment with 0.6 g/L goethite, $[H_2O_2]_0$ = 2 M, and k = 0.072 h^{-1}. (C) $[H_2O_2]$ in the experiments described in (A, ○) and (B, ◇), with k = 0.0064 (◇) h^{-1}. 179
Figure D33. (A) ^{14}C activity in an experiment with 0.6 g/L goethite, $[H_2O_2]_0$ = 2 M, and $[2\text{-CP}]_0$ = $[NB]_0$ = 90 μM, with k = 0.20 h^{-1}. (B) [2-CP] (▲) and [NB] (◆) in an experiment with 0.6 g/L goethite, $[H_2O_2]_0$ = 2 M, with k = 0.028 (▲) and 0.012 (◆) h^{-1}. (C) $[H_2O_2]$ in the experiments described in (A, ○) and (B, △), with k = 0.0016 (△) h^{-1}. 180
Figure D34. (A) ^{14}C activity in an experiment with 0.6 g/L goethite, $[H_2O_2]_0$ = 2 M, and $[2\text{-CP}]_0$ = $[NB]_0$ = 100 μM, with k = 0.25 h^{-1}. (B) [2-CP] (▲) and [NB] (◆) in an experiment with 0.6 g/L goethite, $[H_2O_2]_0$ = 2 M, with k = 0.046 (▲) and 0.019 (◆) h^{-1}. (C) $[H_2O_2]$ in the experiments described in (A, ○) and (B, △), with k = 0.0014 (△) h^{-1}. 181
Figure D35. (A) ^{14}C activity in an experiment where the iron was from the supernatant of a 0.6 g/L goethite suspension (see chapter 4 for details) and $[H_2O_2]_0$ = 1 M at pH 4 (●) or 5 (○), with k = 0.081 and 0.032 h^{-1}, respectively. (B) ^{14}C activity in an experiment with 0.6 g/L goethite, $[H_2O_2]_0$ = 1 M, and I = 0.9 M $NaClO_4$, with k = 0.016 h^{-1}. (C) ^{14}C activity in four experiment with 0.6 g/L goethite, $[H_2O_2]_0$ = 2 M, and $[2\text{-CP}]_0$ = 0.3 (●), 3 (▽), 30 (■), or 300 (◇) μM, with k = 0.55, 0.52, 0.42 and 0.043 h^{-1}, respectively. The experiments with $[2\text{-CP}]_0$ = 0.3 and 3 μM were re-spiked with $H^{14}COOH$ after ~20 hours. (D) [2-CP] in the experiment described in (C) with $[2\text{-CP}]_0$ = 300 μM, with k = 0.052 h^{-1}. 182

Chapter 1: Introduction

or

-OH, you're one radical dude!-

The hydroxyl radical (•OH) is a powerful inorganic oxidant that reacts with numerous compounds at or near diffusion-limited rates (10^{10} M^{-1} s^{-1}; *1-3*). It is of great research interest because it is used in the remediation of wastewater and polluted groundwater (*4-9*), and is found naturally in surface waters (*10-14*), clouds (*15, 16*), and living cells (*17-19*).

A source of •OH common to all of the systems listed above is the oxidation of Fe(II) by hydrogen peroxide (H_2O_2), also known as the Fenton reaction (*20*). A wealth of information exists regarding the mechanism and kinetics of •OH production during the decomposition of H_2O_2 by Fe(II) and Fe(III) (*21-30*). For example, the generally accepted mechanism of the decomposition of H_2O_2 by Fe(III) consists of a chain reaction where the iron cycles between Fe(III) and Fe(II) as H_2O_2 is consumed (*21, 24, 30*).

While the pure solution phase Fenton system has been researched extensively, work on elucidating the mechanism of H_2O_2 decomposition and •OH generation in the presence of iron oxide has only just begun (*31-36*). The goal of this dissertation work was to further the understanding of the heterogeneous Fenton-like system and to determine the factors that control the decomposition rates of H_2O_2 and organic compounds, as well as the generation rate of •OH (V_{OH}), in the presence of iron and iron oxide. This knowledge can help to increase the efficacy of hydrogen peroxide-based treatment processes of contaminated aquifers.

The contribution of solution phase reactions to the decomposition of H_2O_2 and organic compounds in the presence of dissolved iron and ferrihydrite at pH 4 was examined in chapter 2. One aspect that was explored in detail was the importance of the chain reaction mechanism in this system because it could determine the lifetimes of H_2O_2 and organic compounds. ^{14}C-labeled formic acid was the main •OH probe since its reactions with •OH and subsequent reactants are well-characterized. It also has a detection limit on the order of nanomolar, meaning that it can be used at concentrations so low that its presence will not drastically alter the kinetics of the system. The experimental results agreed reasonably well with those predicted by a kinetic model of the chain reaction mechanism that is based on published rate constants extrapolated to pH 4. The results from experiments where *tert*-butyl alcohol was added supported the conclusion that the solution chain reaction mechanism controlled the decomposition kinetics of H_2O_2 and formic acid when Fe was introduced as dissolved Fe(III). In contrast, the solution chain reaction was not the dominant decomposition pathway of H_2O_2 and formic acid when ferrihydrite was the iron source. The heterogeneous system was modeled using four different hypothetical mechanisms,

and the one that produced the best fits to the data had a nonradical producing H_2O_2 loss pathway at the iron oxide surface, as well as insufficient amounts of dissolved Fe to effectively propagate the solution phase chain reaction.

In chapter 3, a model was created for predicting the pseudo-first-order oxidation rate coefficient of a dissolved organic compound (k_{org}) in mineral-catalyzed Fenton-like systems based on the factors that control V_{OH}. This was the first time anyone has attempted to formulate a generally applicable approach for predicting k_{org} in mineral-catalyzed Fenton-like systems. ^{14}C-labeled formic acid was used to measure V_{OH} in pH 4 slurries of H_2O_2 and either synthesized ferrihydrite, goethite, or hematite or a natural iron oxide-coated quartzitic aquifer sand. V_{OH} was proportional to the product of the concentrations of surface area of the iron oxide and H_2O_2, although different solids produced •OH at different rates. Using these results, a model was developed that predicts the degradation rate of an organic compound based on its initial concentration, its second order rate constant with •OH, the initial concentration of H_2O_2, the concentration and reaction rates of any other important •OH sinks in the system, and the surface area, type and quantity of iron oxide. The model successfully predicted V_{OH} and k_{org} in the aquifer sand experiments and in a number of previously published works, but overpredicted V_{OH} and k_{org} from other studies.

The work to refine the model discussed in chapter 3 is presented in chapter 4. Three hypotheses that could explain why the model overpredicted V_{OH} and k_{org} in some instances were tested: (1) laboratory synthesized iron oxide was significantly different from those used in other studies, (2) electrostatic attraction between formate anions and the iron oxide surface must be accounted for, and (3) the compound being degraded or its oxidation products interfered with the generation of •OH. Experimental results indicated that the discrepancies between model and measured values for V_{OH} and k_{org} were mainly due to electrostatics. The concentration of formate anions in the double layer was greater than its bulk concentration because it was attracted to the positively charged iron oxide surface. Consequently, the bulk ^{14}C-labeled formic acid loss rate was faster than that for neutral compounds because more of the probe reacted with •OH, which is generated at the oxide surface, than it would have in the absence of electrostatic attraction. As time progressed, the decomposition rate of ^{14}C-labeled formic acid decreased, but the oxidation rates of the neutral compounds remained relatively constant. This was a result of the reduction of the positive charge on the iron oxide surface due to sorption of the oxidation products of the

organic compound that was being degraded. This conclusion was supported by the observation that the goethite particles coagulated during the experiment, which had never occurred in all of our previous experiments where the organic compound was not present.

Literature Cited

(1) Ross, F.; Ross, A. B. *Selected Specific Rates of Reactions of Transients from Water in Aqueous Solution*; U. S. National Bureau of Standards (NSRDS-NBS59): Gaithersburg, MD, 1977.

(2) Buxton, G. V.; Greenstock, C. L.; Helman, W. P.; Ross, A. B. *J. Phys. Chem. Ref. Data* **1988**, *17*, 513-886.

(3) Haag, W. R.; Yao, C. C. D. *Environ. Sci. Technol.* **1992**, *26*, 1005-1013.

(4) Ravikumar, J. X.; Gurol, M. D. *Environ. Sci. Technol.* **1994**, *28*, 394-400.

(5) Bigda, R. J. *Chem. Eng. Prog.* **1995**, *91*, 62-65.

(6) Kakarla, P. K. C.; Watts, R. J. *J. Environ. Eng.* **1997**, *123*, 11-17.

(7) Kong, S. H.; Watts, R. J.; Choi, J. H. *Chemosphere* **1998**, *37*, 1473-1482.

(8) De Laat, J.; Gallard, H.; Ancelin, S.; Legube, B. *Chemosphere* **1999**, *39*, 2693-2706.

(9) Chen, G.; Hoag, G. E.; Chedda, P.; Nadim, F.; Woody, B. A.; Dobbs, G. M. *J. Hazard. Mater.* **2001**, *87*, 171-186.

(10) Haag, W. R.; Hoigné, J. *Chemosphere* **1985**, *14*, 1659-1671.

(11) Zhou, X.; Mopper, K. *Mar. Chem.* **1990**, *30*, 71-88.

(12) Vaughan, P. P.; Blough, N. V. *Environ. Sci. Technol.* **1998**, *32*, 2947-2953.

(13) Goldstone, J. V.; Pullin, M. J.; Bertilsson, S.; Voelker, B. M. *Environ. Sci. Technol.* **2002**, *36*, 364-372.

(14) Southworth, B. A.; Voelker, B. M. *Environ. Sci. Technol.* **2003**, *37*, 1130-1136.

(15) Graedel, T. E.; Mandich, M. L.; Weschler, C. J. *J. Geophys. Res.* **1986**, *91*, 5205-5221.

(16) Sedlak, D. L.; Hoigné, J. *Atmos. Environ.* **1993**, *27A*, 2173-2185.

(17) Li, B.; Gutierrez, P. L.; Blough, N. V. *Anal. Chem.* **1997**, *69*, 4295-4302.

(18) Madigan, M. T.; Martinko, J. M.; Parker, J. *Biology of Microorganisms*; Prentice Hall: Upper Saddle River, New Jersey, 1997.

(19) Blokhina, O.; Virolainen, E.; Fagerstedt, K. V. *Ann. Bot.* **2003**, *91*, 179-194.

(20) Fenton, H. J. H. *J. Chem. Soc.* **1894**, *65*, 899-910.

(21) Haber, F.; Weiss, J. *P. Roy. Soc. Lond.* **1934**, *147*, 332-351.

(22) Barb, W. G.; Baxendale, J. H.; George, P.; Hargrave, K. R. *Trans. Faraday Soc.* **1951**, *97*, 462-500.

(23) Barb, W. G.; Baxendale, J. H.; George, P.; Hargrave, K. R. *Trans. Faraday Soc.* **1951**, *97*, 591-616.

(24) Walling, C.; Goosen, A. *J. Am. Chem. Soc.* **1973**, *95*, 2987-2991.

(25) Abbot, J.; Brown, D. G. *Int. J. Chem. Kinet.* **1990**, *22*, 963-974.

(26) Millero, F. J.; Sotolongo, S.; Stade, D. J.; Vega, C. A. *J. Solution Chem.* **1991**, *20*, 1079-1092.

(27) Lipczynska-Kochany, E.; Sprah, G.; Harms, S. *Chemosphere* **1995**, *30*, 9-20.

(28) Voelker, B. M.; Sulzberger, B. *Environ. Sci. Technol.* **1996**, *30*, 1106-1114.

(29) Kozlov, Y. N.; Dribinskii, V. L. *Russ. J. Phys. Chem. USSR* **1997**, *71*, 1612-1614.

(30) De Laat, J.; Gallard, H. *Environ. Sci. Technol.* **1999**, *33*, 2726-2732.

(31) Lin, S.-S.; Gurol, M. D. *Environ. Sci. Technol.* **1998**, *32*, 1417-1423.

(32) Valentine, R. L.; Wang, H. C. A. *J. Environ. Eng.* **1998**, *124*, 31-38.

(33) Miller, C. M.; Valentine, R. L. *Water Res.* **1999**, *33*, 2805-2816.

(34) Kwan, W. P.; Voelker, B. M. *Environ. Sci. Technol.* **2002**, *36*, 1467-1476.

(35) Lu, M.-C.; Chen, J.-N.; Huang, H.-H. *Chemosphere* **2002**, *46*, 131-136.

(36) Kwan, W. P.; Voelker, B. M. *Environ. Sci. Technol.* **2003**, *37*, 1150-1158.

Chapter 2: Decomposition of Hydrogen Peroxide and Organic Compounds in the Presence of Dissolved Iron and Ferrihydrite

or

-Welcome to the Kwan and Voelker modeling agency-

Reproduced with permission from Kwan, Wai P. and Voelker, Bettina M. "Decomposition of hydrogen peroxide and organic compounds in the presence of dissolved iron and ferrihydrite." *Environmental Science and Technology*, **2002**, 36(7), 1467-1476.

© 2002 American Chemical Society

Abstract

This work examines the contribution of solution phase reactions, especially those involving a chain reaction mechanism, to the decomposition of hydrogen peroxide (H_2O_2) and organic compounds in the presence of dissolved iron and ferrihydrite. In solutions at pH 4, where Fe was introduced as dissolved Fe(III), both H_2O_2 and ^{14}C-labeled formic acid decomposed at measurable rates that agreed reasonably well with those predicted by a kinetic model of the chain reaction mechanism, using published rate constants extrapolated to pH 4. The ratio of the formic acid and H_2O_2 decomposition rates, as well as the dramatic effect of *tert*-butyl alcohol on these rates, confirmed that a solution chain reaction mechanism involving •OH controlled the decomposition kinetics of both compounds. In the presence of ferrihydrite as the iron source, the ratio of the rate of formic acid decomposition to that of H_2O_2 decomposition was significantly lower than that observed in the presence of only dissolved Fe. Moreover, neither rate diminished drastically upon addition of *tert*-butyl alcohol, indicating that the solution phase chain reaction is not a dominant decomposition pathway of H_2O_2 and formic acid. Relative decomposition rates of formic acid and a second •OH probe, benzoic acid, were consistent with oxidation of these compounds by •OH. These observations can be reproduced by a kinetic model including (a) decomposition of H_2O_2 at the iron oxide surface, producing •OH with lower yield than the reaction sequence with dissolved Fe, and (b) low concentrations of dissolved Fe in the presence of ferrihydrite, preventing propagation of the solution phase chain reaction.

Introduction

Fenton's reagent [Fe(II) + hydrogen peroxide] has been used to oxidize organic pollutants in many applications, from treatment of wastewaters to remediation of contaminated aquifers (*1-4*). These applications exploit the high reactivity of the hydroxyl radical (•OH) that is generated when hydrogen peroxide (H_2O_2) oxidizes Fe(II) to Fe(III) (the Fenton reaction). A disadvantage of using Fenton's reagent as a treatment method is that the Fe(III) produced is only sparingly soluble, especially at circumneutral pH, so that high concentrations of ferric oxyhydroxide precipitates are generated when stoichiometric quantities of Fe(II) are used. An alternative is to use catalytic quantities of Fe and regenerate the Fe(II) needed for the Fenton reaction by continuously reducing Fe(III). In batch reactor treatment schemes, UV irradiation can be used to reduce Fe(III) (*5-7*). For treatment of soils, the slow reduction of dissolved Fe(III) by hydrogen peroxide itself has been found to be sufficient (*8*, *9*).

In hydrogen peroxide solutions in which Fe(II) constitutes a minor fraction of the total dissolved Fe, the overall kinetics of hydrogen peroxide and contaminant decomposition may be controlled by a chain reaction (*5*, *10-12*). In the absence of light, the chain initiation reaction is the reduction of Fe(III) by hydrogen peroxide (Table 2-1, reaction T1.1), producing two chain-propagating species Fe(II) and HO_2/O_2^- (superoxide radical and its conjugate acid) (*10*, *11*). Fe(II) is quickly oxidized by another molecule of H_2O_2, and the chain is then propagated by reactions T1.3 and T1.4. Thus, reactions T1.2, T1.3, and T1.4 form a cycle that sustains itself by regenerating Fe(II) (Figure 2-1). Reactions that will terminate the chain include reactions T1.5 and T1.6. Reactions of •OH with organic solutes or other solution constituents may propagate the chain if they produce HO_2/O_2^- or another species capable of reducing Fe(III) (e.g., CO_2^- and some organic radical products); otherwise, they act as termination steps (*13*). For the chain reaction to be significant (with chain lengths much greater than 1), either the concentration of H_2O_2 must be high enough so that it outcompetes other solution constituents for •OH or the reactions of •OH with the other solutes must be able to propagate the chain. In addition, there must be enough dissolved Fe(III) in solution to ensure that most of the HO_2/O_2^- reacts with it to form Fe(II) [either directly or via an intermediate, e.g., Cu(I) (*14*)].

Investigators have expanded the range of treatment applications of Fenton chemistry by demonstrating that an iron oxide/H_2O_2 system can effectively oxidize pollutants at pH values ranging from 3 to circumneutral (*15-17*). However, a consensus on the mechanism of this process does not exist. Proposed mechanisms for the decomposition of hydrogen peroxide generally include reactions analogous to reactions T1.1 and T1.2 taking place on the iron oxide surface (*17-20*). Many studies suggest that the oxidation of organic compounds takes place via dissolved •OH released into solution when the surface analogue of reaction T1.2 occurs. Lin and Gurol (*19*) postulate that •OH formed by a surface reaction would be too reactive to diffuse into the bulk solution. Therefore, they propose that their organic compound may be oxidized either in the sorbed state by near-surface •OH or in solution by dissolved •OH generated when Fe(II), formed by the surface versions of reactions T1.1 and T1.4, is first released into solution and then oxidized by H_2O_2 (*21*). Miller and Valentine (*22*) propose that HO_2/O_2^- diffuses into the bulk solution to generate •OH by reacting with H_2O_2. Watts and co-workers invoke an additional surface species capable of oxidizing sorbed compounds at very high (>2%) concentrations of H_2O_2 (*18*). In summary, the relative contributions of surface and solution reactions to the

decomposition of H_2O_2 and organic compounds in iron oxide/H_2O_2 systems remain unclear.

Furthermore, the postulated release of •OH, HO_2/O_2^- or Fe(II) from surface reactions into the dissolved phase implies that a chain reaction can take place in solution if enough dissolved Fe is present for the chain propagation steps, as is likely in acidic suspensions of iron oxide-containing particles. The chain reaction could even be the dominant mechanism for the decomposition of both hydrogen peroxide and organic compounds. The role of the iron oxide surface would then be restricted to just initiating the solution phase chain reaction. The ability of different solutes present in the solution to participate in chain propagation and termination reactions would become a crucial factor in predicting the overall rates of decomposition of H_2O_2 and organic compounds. This possibility has not been considered by previous studies.

An important question is whether the chain reaction mechanism is possible at pH values greater than 3. A number of studies have examined the kinetics of H_2O_2 decomposition in the Fe(III)/H_2O_2 system in acidic solutions (*10*, *11*, *23-25*). More recently, De Laat and Gallard (*12*, *26*) presented a detailed kinetic model of the chain reaction that successfully described the kinetics of both H_2O_2 and atrazine decomposition under a wide range of conditions at pH values of 3 or less. While H_2O_2 decomposition rates in the Fe(III)/H_2O_2 system were observed to decrease dramatically at pH values greater than 3 (*5*, *12*), these studies do not rule out the possibility of a solution phase chain reaction, especially if another initiation reaction besides T1.1 (for example, a surface reaction) can occur.

The objective of this work was to examine the importance of solution phase reactions, especially the Fe(III)-initiated chain reaction, in the decomposition of organic compounds and H_2O_2. Experiments at pH 4 with only dissolved Fe(III) added to H_2O_2 solutions in the presence and absence of the chain terminator *tert*-butyl alcohol demonstrate that the chain reaction mechanism can still control the kinetics of H_2O_2 and organic compound decomposition at this pH. Experiments in the presence of ferrihydrite reveal that a surface-initiated chain reaction was not significant in our experimental system. The decomposition kinetics of two organic compounds used as •OH probes (formic and benzoic acids) indicate that release of dissolved •OH is likely to be the main mechanism of oxidation of these compounds, but the yield of •OH was lower than expected.

Materials and Methods

Materials

All reagents were reagent grade and were used without further purification except for 2-nitrophenyl hydrazine (NPH), which was recrystallized once from hot water. H_2O_2 (30%, unstabilized) was from Fluka. All solutions were prepared using 18 MΩ Milli-Q water from a Millipore system unless otherwise noted. NPH and 1-ethyl-3-(3-dimethylaminopropyl) carbodiimide hydrochloride (EDC, protein sequencing grade) were stored frozen until use. Peroxidase (type II from horseradish) and *N*,*N*-diethyl-*p*-phenylenediamine (DPD) solutions were kept in the dark at 4 °C for no more than 2 weeks. Stock solutions of Fe(III) were made fresh daily by dissolving $Fe(ClO_4)_3 \bullet 9H_2O$ in Milli-Q water that was first acidified to pH < 1 with concentrated $HClO_4$.

All glassware and other containers used in this work were soaked in 1N HCl for more than 10 h and rinsed with Milli-Q water. The Teflon bottles in which the kinetic experiments were performed were soaked in concentrated nitric acid for more than 10 h and washed with Milli-Q water. Glassware used in the HPLC procedures were soaked in 10% HNO_3, rinsed with Milli-Q water, and then combusted in an oven at 450 °C for a minimum of 8 h. Samples for HPLC analysis were derivatized and stored in borosilicate glass vials with Teflon-lined caps. The pH measurements were made using an Orion model 420A benchtop pH meter calibrated against standard buffers. All spectrophotometric measurements were done on an HP 8453 diode array spectrophotometer. ^{14}C activity was measured in a Beckman LS 6500 multipurpose scintillation counter. HPLC data were obtained from an HP 1050 series HPLC coupled to a diode array detector. A Spherisorb ODS-2 column (5 μm particle size, 25 cm length x 4.6 mm i.d.) was used for the HPLC separation.

Ferrihydrite was prepared from $FeCl_3 \bullet 6H_2O$ according to the method described by Wells et al. (*27*). $FeCl_3 \bullet 6H_2O$ was dissolved to make a 4×10^{-4} M solution (5×10^{-4} M for experiments with high ferrihydrite concentrations). Within 1 h, the solution was heated in a 90 °C water bath for 5 min and then quickly cooled back to room temperature. It was used within 2 days without further purification.

Analytical Techniques

Hydrogen peroxide was measured spectrophotometrically using the DPD method (*28*) as modified by Voelker and Sulzberger (*29*) to minimize interference by Fe(II) and Fe(III). Samples

were diluted so that the H_2O_2 concentration never exceeded 25 μM in the 1-cm path length cuvette.

The ferrozine method (*30*), as modified by Voelker and Sulzberger (*29*), was used to measure the concentration of dissolved and total (dissolved plus solid) iron. Dissolved iron was defined as iron that passed through a 0.02-μm filter (Anotop, aluminum oxide membrane, Whatman).

We used ^{14}C-labeled formic acid as our main •OH probe for various reasons. The reactions of formate and formic acid with •OH are fast (Table 2-2) and are well-characterized (*31*):

$$\bullet OH + HCOO^- \xrightarrow{-H_2O} CO_2^{\bullet -} \xrightarrow{+O_2} CO_2 + O_2^- \quad (1)$$

$$\bullet OH + HCOOH \xrightarrow{-H_2O} HCOO\bullet \xrightarrow{+O_2, -H^+} CO_2 + O_2^- \quad (2)$$

In an oxygenated environment, the carbon radicals create almost no side products besides CO_2 and O_2^- because they react with oxygen at nearly diffusion-limited rates (*13*). This means that any reactions between the iron and the carbon radicals are insignificant. The superoxide produced in reaction 1 propagates the chain reaction (see Figure 2-1). Also, low concentrations (~100 nM) of $H^{14}COOH$ can be used since our detection limit (three times the standard deviation of the typical background radiation level) is on the order of 1 nM. These probe properties allow us to investigate •OH formation without any danger of significantly perturbing the system, for example, by adding a chain termination reaction.

To measure the amount of ^{14}C-labeled $HCOOH/HCOO^-$ in the reactor, a 4-mL aliquot was transferred into a 15-mL polystyrene conical tube. It was subsequently air sparged vigorously with house air using a gas dispersion tube with a fritted cylinder for 30 s or more to drive out the ^{14}C-labeled carbon dioxide. A total of 1 mL of the aliquot was then mixed with 6 mL of scintillation fluid (ScintiSafe Econo 1, Fisher) in a 7-mL glass scintillation vial. The frit was washed with Milli-Q water and wiped dry with Kimwipes after each sparge. At the end of the day, it was soaked in 1 N HCl overnight to remove any traces of iron. The vials were kept at room temperature, and their ^{14}C content was measured en masse within 1 day. The ^{14}C content of an aliquot measured immediately after extraction did not differ from that measured 1 day later. Vigorous air sparging of aliquots for 5 min did not remove ^{14}C-labeled $HCOOH/HCOO^-$ from an iron-free solution containing 1 mM H_2O_2 and 50 nM $H^{14}COOH/H^{14}COO^-$ at pH 3. We also

performed a control experiment to demonstrate that all of the $^{14}CO_2$ is removed by sparging: 5 mM each of $Fe(NH_4)_2(SO_4)_2 \cdot 6H_2O$ (99+%, Sigma-Aldrich) and H_2O_2 were added to a pH 3 solution containing 50 nM $H^{14}COOH/H^{14}COO^-$. Under these conditions, all of the $H^{14}COOH/H^{14}COO^-$ should be rapidly oxidized to $^{14}CO_2$ via the Fenton reaction. The ^{14}C activity of this solution after sparging was indistinguishable from background radiation. To show that sorption of $H^{14}COOH/H^{14}COO^-$ to ferrihydrite was insignificant, a pH 4 solution containing no H_2O_2, 300 μM ferrihydrite, and 70 nM $H^{14}COOH/H^{14}COO^-$ was stirred for 3 days. There was no statistical difference in ^{14}C content between samples that were filtered through a 0.02-μm filter and ones that were not. These controls are described in more detail elsewhere (*32*).

We also performed experiments in which benzoic acid and (nonlabeled) formic acid were used simultaneously as •OH probes. Benzoic acid is a well-characterized •OH-specific probe (*33*). The two probes were detected using HPLC (*34*). A total of 0.2 mL of a pyridine (HPLC grade)/HCl (99.999%) buffer (1.25:1.00, v/v), 0.2 mL of 0.3 M EDC, and 0.4 mL of 0.1 M NPH were added to 2 mL of reaction solution. After waiting 90 min or longer, 0.2 mL of 40% (w/v) KOH was added to neutralize the acid. Finally, the vials were put in a 70 °C water bath for 10 min to complete the derivatization. The products were kept frozen until analysis. A total of 0.5 mL of the derivatized sample was injected into a guard cartridge (Dionex IonPac NG1, 4 x 35 mm), which acted as a concentrator, followed by 1 mL of Milli-Q water to flush out the strong KOH. The elution gradient was as follows: water at pH 2.5 (A) and acetonitrile (UV spectrophotometric grade) (B); 0-2 min 10% B, 2-11 min 30% B, and 11-20 min 50% B, at a flow rate of 1.0 mL/min. The column was kept in a 35 °C water bath. The analytes were detected by absorbance at 400 nm. Control experiments showed benzoic acid sorption to ferrihydrite was insignificant.

Kinetic Experiments

All experiments were performed in 250-mL Teflon bottles covered completely with black electrical tape to exclude light. Milli-Q water was treated for approximately 45 min with ozone bubbled through a gas dispersion tube with a fritted cylinder. This was done to oxidize any trace impurities that could interfere with the chain reaction and cause, for example, lag periods before the decomposition of H_2O_2 accelerates (see Results) (*32*). The water was stirred for a couple of hours prior to adding NaOH to raise the pH above 9, which facilitates the decomposition of dissolved ozone (*35*). It was left stirring overnight to ensure that all of the ozone was removed

and acidified to pH ~5 before use. Unless noted otherwise, 200 mL of solution contained 10 mM $NaClO_4$ (for ionic strength control) and 100 nM $H^{14}COOH/H^{14}COO^-$. During the course of an experiment, the bottles were loosely capped, and the solutions were kept in a recirculating water bath set at 25 ± 0.5 °C while being stirred by a magnetic stirrer. Experiments lasted from 1 to 4 days. Pseudo-first-order decomposition rate coefficients for $H^{14}COOH/H^{14}COO^-$ and H_2O_2, i.e., k_{HCOOH} and $k_{H_2O_2}$, were obtained by performing nonlinear least squares regression fits to the concentration versus time data from each experiment using the built-in nonlinear curve-fitting routine in SigmaPlot (graphing software from SPSS Inc.).

Dissolved Iron

The experimental solutions contained ~1 mM H_2O_2 and were adjusted to pH 4 with $HClO_4$ and/or NaOH. A small volume of an acidified Fe(III) stock solution (typically 20-200 μL to avoid changing the solution pH dramatically) was added to start the experiment. The pH of the solutions remained within ±0.2 unit of their initial pH for the entire experiment without further adjustments.

Ferrihydrite

The setup is similar to above except that the experimental solutions were adjusted to pH 4 with $HClO_4$ and/or NaOH after the ferrihydrite was added. Care was taken to avoid making the solution too basic (pH > 6) during the adjustment. H_2O_2 was added at time zero. The solution pH remained steady (±0.2 unit of initial pH) throughout the experiment.

In two of the ferrihydrite experiments, $H^{14}COOH/H^{14}COO$ was replaced with 50 μM nonlabeled formic acid; 15 μM benzoic acid was also added. Before collecting the aliquots that would be used for derivatization, the 3-mL syringe and 0.02-μm filter were prerinsed five times with 3 mL of Milli-Q water and once with 3 mL of the experimental solution to remove any residual organic acids. The samples were collected and frozen immediately until they could be derivatized in one batch.

Kinetic Modeling

All of the modeling results were calculated with the computer program Acuchem (*36*). At first glance, the kinetic model that we used to investigate the Fenton system (Table 2-1) appears to differ significantly from the recent work of De Laat and Gallard (*12*), which describes a mechanism for the homogeneous decomposition of hydrogen peroxide by Fe(III) in aqueous solutions at pH < 3. In fact, they are the same with only cosmetic changes. Our model has fewer

reactions than the DeLaat and Gallard model because we have incorporated both equilibrium and rate expressions into composite rate constants instead of using individual rate constants for each species. We chose to use composite rate constants because they are the easiest way to include equilibrium in the Acuchem format and because they make it more apparent which reactions are important to the system at the pH of interest.

The concept of the composite rate constant is illustrated in the following example. HO_2 and O_2^- ($pK_a = 4.8$; *37*) react with Fe^{2+} at different rates to form $Fe^{III}(HO_2)^{2+}$ and are considered as two separate reactions in the De Laat and Gallard model:

$$Fe^{2+} + HO_2 \rightarrow Fe^{III}(HO_2)^{2+} \quad (3)$$

$$Fe^{2+} + O_2^- + H^+ \rightarrow Fe^{III}(HO_2)^{2+} \quad (4)$$

In our model (reaction T1.6), they are considered as a single reaction between Fe(II) and HO_2/O_2^-, whose rate constant (i.e., the composite rate constant) is a weighted sum of the two individual rate constants:

$$k_{T1.6} = \frac{[HO_2]}{[HO_2]_T} k_3 + \frac{[O_2^-]}{[HO_2]_T} k_4 \quad (5)$$

The weights are determined by the percentage of HO_2 and O_2^- in solution, which is a function of pH. Other reactions including HO_2 and O_2^- were treated in the same manner. Since $Fe^{III}(HO_2)^{2+}$ is not a significant species in our system (see below), reaction T1.6 in our model only shows Fe(III) and H_2O_2 as the products.

Reactions II.1-II.6b in De Laat and Gallard (*12*) can be expressed as our composite reaction T1.1 if the two Fe(III)-hydroperoxy complexes are not major H_2O_2 or Fe(III) species. Using the stability constants of the hydrolysis products of Fe^{3+} from Morel and Hering (*38*) along with eq 15 and the equilibrium constants in Table 2-2 of De Laat and Gallard (*12*), we calculated that at pH 3 the Fe(III)-hydroperoxy complexes make up less than 5% of the total dissolved Fe(III) if $[H_2O_2]$ is less than 0.11 M. [The stability constants in the De Laat and Gallard model were calculated for an ionic strength I of 0.1 M. Instead of using those, we referred to literature values and corrected them for $I = 0.01$ M.] If additional hydroperoxy species do not become important at higher pH values (for which the De Laat and Gallard model was not calibrated), Fe(III)-hydroperoxy complexes are insignificant (<5%) to Fe speciation at $[H_2O_2] <$ 0.088 M at pH 4. The complexes will make up even smaller fractions of the total H_2O_2 if $[H_2O_2]_T$ is greater than $[Fe(III)]_T$. Therefore, the assumption that Fe(III)-hydroperoxy complexes are not

significant is always valid under our experimental conditions.

Table 2-1 shows the rate constants, in composite form where appropriate, that were used in our model. All of these were derived from the values used in the De Laat and Gallard model except for the rate constants for two reactions. We used equations from Millero et al. (*39*) to calculate the rate constants for reaction T1.2 at pH values higher than 3. As for the composite rate constants for reaction T1.1, we computed them based on the literature values of the hydrolysis equilibrium constants of Fe(III) (*38*), corrected for $I = 0.01$ M, along with the other rate constants in the De Laat and Gallard model. We did not include ionic strength corrections for rate constants because, at our low ionic strength, these should be negligible for reactions of monovalent species with each other or of divalent species with neutral species. These two categories include all of the reactions in Table 2-1, since in reaction T1.4, the main species reacting are $Fe(OH)_2^+$ with O_2^-, while in reaction T1.6, the main species are Fe^{2+} and HO_2. As we used formic acid as a hydroxyl radical probe, its oxidation reaction (reaction T1.10) was also included in the model calculations. This rate constant was calculated by averaging the literature values of rate constants obtained at pH 2-5, shown in Table 2-2. Using the recommended values from Buxton of 1.3×10^8 and 3.2×10^9 M^{-1} s^{-1} for HCOOH and $HCOO^-$ gives a nearly identical rate constant of 2.1×10^9 M^{-1} s^{-1} at pH 4. The reaction between *tert*-butyl alcohol and •OH was added when we explored its effects on the Fenton system. We used 6.0×10^8 M^{-1} s^{-1}, the recommended value from Buxton et al. (*40*), instead of averaging because there were not many independent measurements of this rate constant.

The direct reaction of HO_2/O_2^- with H_2O_2, suggested by Miller and Valentine (*22*) to play a role at circumneutral pH, was not included in our models because, at all of the Fe(III) and H_2O_2 concentrations considered here, the rate of the direct reaction is negligible as compared to the Fe-catalyzed rate (reaction T.1.4 followed by T.1.2). Furthermore, it remains unclear whether this reaction can proceed at all in the absence of metal catalysis (*41*).

Results

Reactions of Dissolved Fe at pH 4

The purpose of our first set of experiments was to show that chain reaction kinetics can control the rate of hydrogen peroxide and formic acid decomposition and •OH formation at pH 4 with only dissolved Fe(III) present. The pseudo-first-order decomposition rate coefficients for $H^{14}COOH/H^{14}COO^-$ and H_2O_2 (k_{HCOOH} and $k_{H_2O_2}$) were measurable but low (Figure 2-2 and

Table 2-3). The total iron concentrations in all of our experiments were slightly above the theoretical saturation limit of amorphous $Fe(OH)_3(s)$, which we calculated to be 0.42 μM at pH 4 (*38*). In theory, then, solubility should have controlled the amount of dissolved Fe, and it should have been equal to 0.42 μM in all of the experiments. We extrapolated the De Laat and Gallard model to pH 4 as explained in the Methods section (Table 2-1), then ran it in Acuchem with dissolved Fe equal to 0.42 μM and particulate Fe assumed to be unreactive. The resulting model calculations were well-described by pseudo-first-order kinetics with k_{HCOOH} equal to 1.41 day^{-1} and $k_{H_2O_2}$ equal to 0.043 day^{-1}. Our measured values of k_{HCOOH} and $k_{H_2O_2}$, 0.68 ± 0.13 and 0.030 ± 0.015 day^{-1}, respectively (Table 2-3), agree reasonably well with those of the model.

The scatter among the data points in these experiments may be due to two factors. First, if small amounts of chain terminating •OH scavengers were present in the Milli-Q water, they could decrease $k_{H_2O_2}$ and k_{HCOOH} by prematurely terminating the chain reaction. The effect of such scavengers was clearly visible in early phases of this work, where we often observed long lag periods before H_2O_2 decomposition ensued (*32*). Pretreating the Milli-Q water with ozone decreased the occurrence of these dramatic lag periods, but residual concentrations of •OH scavenging contaminants from, for example, the reagent solutions could still be present. Short lag periods (0.5-1 day) remained in three of the seven experiments shown in Table 2-3. In these cases, initial time points were excluded from the data used to obtain the experimental k_{HCOOH} and $k_{H_2O_2}$.

A second possible reason for the scatter in the data is iron speciation. Since we worked at Fe concentrations slightly above saturation, colloids and microscopic-sized solids could have formed throughout each experiment. On the basis of our work with ferrihydrite, colloidal and precipitated iron should not have a large effect on $k_{H_2O_2}$ and k_{HCOOH} at total Fe concentrations of a few micromolar (see Figure 2-3a,b). However, since the dynamics of colloid formation and precipitation could have changed from experiment to experiment, the concentration of dissolved Fe may also have varied, resulting in scatter in the data. (The model calculations predict a strong dependence of $k_{H_2O_2}$ and k_{HCOOH} on the concentration of dissolved Fe.) We did not observe a relationship between observed values of $k_{H_2O_2}$ and k_{HCOOH} and measured concentrations of dissolved Fe (Table 2-3), but this might merely mean that the concentration of Fe that passed

through a 0.02-μm filter did not correspond to the concentration of reactive dissolved Fe.

If most of the $H^{14}COOH/H^{14}COO^-$ and H_2O_2 were consumed by the chain reaction, then we would expect their decomposition rates to drop drastically when a chain terminator is introduced into the system. In one experiment, we added 100 μM *tert*-butyl alcohol, which reacts with •OH to form an organic radical that does not participate in the chain reaction (*13*). The pseudo-first-order decomposition rate coefficients for $H^{14}COOH/H^{14}COO^-$ and H_2O_2 that we measured in the presence of 100 μM *tert*-butyl alcohol were 0.0095 ± 0.0070 and 0.0031 ± 0.0065 day^{-1}, respectively, a factor of 102 and 14 less than the rate coefficients measured in the absence of *tert*-butyl alcohol. In contrast, this amount of *tert*-butyl alcohol decreases the fraction of •OH radical reacting with H_2O_2 and $H^{14}COOH/H^{14}COO^-$ from 0.99 and 0.0066 to 0.35 and 0.0024, respectively (see eq 7 below). Clearly, the competition for •OH radical by *tert*-butyl alcohol is not sufficient to explain the observed decrease in H_2O_2 and $H^{14}COOH/H^{14}COO^-$ decomposition rates, so the main effect of *tert*-butyl alcohol must be to decrease the rate of •OH production by acting as an efficient chain terminator. This effect is reproduced by a kinetic model calculation including 100 μM *tert*-butyl alcohol and, as before, 0.42 μM dissolved Fe, which yields 0.0034 day^{-1} for k_{HCOOH} and 0.00048 day^{-1} for $k_{H_2O_2}$, a decrease by a factor of 415 and 90 as compared to the model's prediction in the absence of *tert*-butyl alcohol. This calculation neglects the possibility of reactions of Fe with organic radical products of •OH oxidation of *tert*-butyl alcohol, which could both propagate the chain by reducing Fe(III) or terminate it by oxidizing Fe(II). However, since our experimental result shows that *tert*-butyl alcohol acts as an efficient chain terminator, we can assume that chain propagation by organic radicals is insignificant.

While the effect of *tert*-butyl alcohol is a good indicator of a chain reaction mechanism involving •OH, we used another tool to provide evidence that the decomposition of formic acid is caused by reaction with •OH. This tool is based on work describing the oxidation of organic contaminants by hydroxyl radicals produced during ozone decomposition (*35*). In a well-mixed aqueous solution, the ratio of the decomposition rate of a chemical species (M) versus that of hydrogen peroxide can be defined as the product of the yield of hydroxyl radicals from hydrogen peroxide (Y) and the fraction of hydroxyl radicals that react with the various contaminants (F):

$$\frac{d[M]}{d[H_2O_2]} = \left(\frac{\text{moles of } \bullet OH \text{ produced}}{\text{moles of } H_2O_2 \text{ consumed}}\right) \times \left(\frac{\text{moles of M consumed}}{\text{moles of } \bullet OH \text{ produced}}\right) = YF \qquad (6)$$

where eq 6 is true if •OH is the only sink of M. The yield is dependent on the reaction conditions and is equal to 0.5 for the chain reaction described by reactions T1.2-T1.4. If the chain length is sufficiently long, then the initiation and termination steps will not significantly affect this number because they occur once, whereas the propagation steps happen many times. F can be computed from the concentrations of the chemical species in solution and their second order reaction rate constants of reaction with •OH ($k_{OH,M}$):

$$F = \frac{k_{OH,M}[M]}{k_{OH,M}[M] + k_{OH,H_2O_2}[H_2O_2] + \sum k_{OH,i}[S_i]} \qquad (7)$$

where S is all other •OH sinks besides hydrogen peroxide and M, e.g., *tert*-butyl alcohol.

In our experiments, $H^{14}COOH/H^{14}COO^-$ is the chemical species of interest (M), and the largest term in the denominator of eq 7 is $k_{OH,H_2O_2}[H_2O_2]$ because $k_{OH,[HCOOH]_T}[HCOOH]_T$ (where $[HCOOH]_T = [HCOOH] + [HCOO^-]$, so the rate constant is the composite rate constant) is very small and we have removed all other •OH sinks. (This was not true for the experiments that included *tert*-butyl alcohol, but those were a small subset of this work.) Thus, we can rewrite eq 6 as

$$\frac{d[HCOOH]_T}{d[H_2O_2]} = Y\frac{k_{OH,[HCOOH]_T}[HCOOH]_T}{k_{OH,H_2O_2}[H_2O_2]}, \qquad (8)$$

which, when integrated, gives

$$\frac{[HCOOH]_T}{[HCOOH]_0} = \left(\frac{[H_2O_2]}{[H_2O_2]_0}\right)^{\gamma} \qquad (9)$$

where

$$\gamma = Y\frac{k_{OH,[HCOOH]_T}}{k_{OH,H_2O_2}} \qquad (10)$$

If the decomposition of $HCOOH/HCOO^-$ and H_2O_2 follow pseudo-first-order kinetics, γ is also equivalent to the ratio of the observed pseudo-first-order decomposition rates of $HCOOH/HCOO^-$ over that of H_2O_2.

The γ values from our experiments average to a value of 22.3 ± 9.9 (Table 2-3) as compared to a value of 33 obtained from the De Laat and Gallard model. Both fall within the

uncertainty of the expected value of γ of 43 ± 27, which was computed using eq 10, the average rate constants from Table 2-2, and a value of 0.5 for Y. The discrepancy between the model value and the expected value arises from the fact that our model used DeLaat and Gallard's value for k_{OH,H_2O_2} instead of the average value in Table 2-2. The large uncertainty in the expected γ is mainly attributable to the uncertainty of k_{OH,H_2O_2}. The scatter in the measured values of γ is much less than the scatter in the measured values of $k_{H_2O_2}$ and k_{HCOOH}; this is consistent with the proposed causes of scatter in the rate coefficients because they would affect both decomposition rates equally.

In summary, our experimental results in solutions containing mostly dissolved Fe show that the •OH chain reaction can proceed at pH 4 and dictate the rates at which H_2O_2 and $H^{14}COOH/H^{14}COO^-$ decompose in Fe(III)/H_2O_2 systems. Furthermore, the model of the chain reaction proposed by De Laat and Gallard, extrapolated to pH 4 with no additional adjustable parameters, produces reasonable approximations of the behavior of this system in the presence and absence of *tert*-butyl alcohol.

Reactions in the Presence of Ferrihydrite at pH 4

After having established that the solution phase chain reaction occurs at pH 4, we conducted experiments to determine whether the prime effect of iron oxides could be to initiate the solution chain reaction. The difference in this set of experiments from the previous one was that the source of iron was laboratory-synthesized ferrihydrite instead of dissolved Fe(III).

Some initial experiments were performed with 200 μM ferrihydrite at pH 3. At this pH, some of the ferrihydrite (~6 μM) dissolved rapidly and the observed pseudo-first-order decomposition rate coefficients of both H_2O_2 and formic acid were comparable to those expected from the measured levels of dissolved Fe(III), indicating that the effect of ferrihydrite was negligible (except as the source of the dissolved Fe). We therefore worked at pH 4.

The decomposition rates of both H_2O_2 and $H^{14}COOH/H^{14}COO^-$ rose as we increased the ferrihydrite concentration (Figure 2-3a,b), with $k_{H_2O_2}$ increasing more steeply than k_{HCOOH} and resulting in a decrease in γ with increasing ferrihydrite concentrations (Figure 2-4). Addition of 10 or 100 μM *tert*-butyl alcohol did not significantly affect $k_{H_2O_2}$ and only slightly decreased k_{HCOOH}. Scatter in the data is most likely due to variations in the reactivity of different batches of ferrihydrite. The amount of dissolved iron released from the ferrihydrite may also have varied.

Our attempts to measure dissolved Fe in these experiments were inconclusive. We observed a lot of variation in measured values of Fe passing through a 0.02-μm filter, but as before, no clear relationship between measured filterable Fe and reaction rate coefficients was observed. About a third of the measurements were less than the detection limit of 0.03 μM; another third were between 0.03 and 1 μM; and the rest were more than 1 μM, often dramatically greater (Appendix A). The abnormally high filterable Fe measurements are likely due to partial breakage of the filter material from high pressures during the filtering process, and it is not clear to what extent the same artifact affected the rest of the measurements. Blank values were consistently low, indicating that contamination was not an issue in these measurements.

To determine the extent to which different simplified mechanisms for the decomposition of H_2O_2 and HCOOH can explain these experimental results and especially to examine the importance of the solution phase chain reaction in this system, we used a qualitative kinetic model combining both solution phase and surface reactions. Our model of solution phase reactions is identical to the DeLaat and Gallard model discussed in the previous section. The only addition is two or three reactions describing the interactions of H_2O_2 with the surface of the ferrihydrite. It is important to note that modeling of this kind cannot validate a certain mechanism; our intention is merely to be able to rule out mechanisms inconsistent with the data.

To model the possibility of a surface initiation of the solution chain reaction, we added only two heterogeneous reactions, analogous to reactions T1.1and T1.2, to the solution phase reactions used for the model of the homogeneous system:

$$\equiv Fe^{III} + H_2O_2 \rightarrow \equiv Fe^{II} + HO_2 + H^+ \quad (11)$$

$$\equiv Fe^{II} + H_2O_2 \rightarrow \equiv Fe^{III} + {}^{\bullet}OH + OH^- \quad (12)$$

We did not include surface •OH and HO_2 species in this model and instead assumed that the radicals would diffuse rapidly into the bulk solution where they would react primarily with H_2O_2 and Fe(III), respectively, to initiate the chain reaction (reactions T1.3 and T1.4). Unknown parameters in this model are the rate constants of reactions 11 and 12 and the concentration of total dissolved Fe(III). Reaction 12 was assumed to be fast and an arbitrarily large rate constant; $1 \times 10^5\ M^{-1}\ s^{-1}$ was chosen. The total dissolved Fe(III) concentration (assumed to be invariant with ferrihydrite concentration) [65 nM Fe(III)] and the rate constant of reaction 11 ($1 \times 10^{-4}\ M^{-1}\ s^{-1}$) were chosen to produce k_{HCOOH} values that lie within the uncertainty of the data at ferrihydrite concentrations of less than 50 μM and at 190 μM.

The model calculations show that if the decomposition rates of H_2O_2 and $H^{14}COOH/H^{14}COO^-$ were both controlled by a surface-initiated solution chain reaction, we would expect to observe three effects (model A in Figures 2-4 and 2-5a,b). First, increasing the amount of ferrihydrite would increase the decomposition rates of both compounds by increasing the rate of the initiation reaction. Second, γ would be equal to the value observed in the presence of only dissolved Fe, independent of the ferrihydrite concentration. Third, addition of *tert*-butyl alcohol as a chain terminator would drastically decrease both decomposition rates. On the basis of the observed decrease in γ with increasing ferrihydrite along with the lack of effect of *tert*-butyl alcohol, we conclude that the chain reaction is not the major mechanism controlling the decomposition of H_2O_2 and $H^{14}COOH/H^{14}COO^-$ in this system.

The decrease in γ with increasing ferrihydrite concentration probably indicates that some of the H_2O_2 disproportionates to O_2 and H_2O at the iron oxide surface without producing dissolved radicals that can initiate a solution chain reaction. This scenario is depicted as "model B" in Figures 2-4 and 2-5a,b, which extends model A by adding a reaction through which the iron oxide surface acts as a catalyst:

$$\equiv Fe^{III} + H_2O_2 \rightarrow \equiv Fe^{III} + \text{non-reactive products} \qquad (13)$$

Model B uses the same parameters as model A, and a rate constant of 7×10^{-3} M^{-1} s^{-1} for reaction 13 was chosen to produce good agreement of modeled and measured $k_{H_2O_2}$ values at 190 μM ferrihydrite. Model B generated results that behaved qualitatively similar to our observations in the absence of *tert*-butyl alcohol. However, it was unable to adequately reproduce $H^{14}COOH/H^{14}COO^-$ decomposition rates when *tert*-butyl alcohol was included, because in the model, the rate of decomposition of $H^{14}COOH/H^{14}COO^-$ was still controlled by the chain reaction.

One possible explanation for the lack of effect of *tert*-butyl alcohol is that there was not enough dissolved Fe(III) present to sustain a chain reaction. This scenario is illustrated by "model C" in Figures 2-4 and 2-5c,d, which is identical to model B except that we chose a lower concentration of total dissolved Fe(III), 15 nM, and adjusted the rate constants of reactions 11 and 13 to values of 7×10^{-4} and 8×10^{-3} M^{-1} s^{-1}, respectively, to produce values of both $k_{H_2O_2}$ and k_{HCOOH} falling within the range of uncertainty of the observed values at ferrihydrite concentrations of less than 50 and at 190 μM. A fourth model (model D in Figures 2-4 and 2-

5c,d) shows that having a low amount of dissolved Fe(III) but no H_2O_2 sink at the iron oxide surface cannot reproduce the decrease in γ with increasing ferrihydrite concentration. Model D is a duplicate of model A except that the amount of total dissolved Fe(III) is 15 nM and the rate constant of reaction 11 is 8×10^{-4} M^{-1} s^{-1}.

An alternative explanation for the low γ values and the small effect of *tert*-butyl alcohol we observed is that another oxidant besides •OH is responsible for the oxidation of formic acid. We examined this idea by adding 50 μM formic acid and 15 μM benzoic acid simultaneously as probe compounds to solutions containing 190 μM ferrihydrite and 1 mM H_2O_2. The ratio of pseudo-first-order decomposition rate coefficients of benzoic acid and formic acid that we measured were in good agreement with the ratio calculated from the literature rate constants for •OH with formic and benzoic acids (Table 2-4). This suggests that •OH was the main oxidant in our system.

If the concentration of Fe(III) in the ferrihydrite/H_2O_2 system is too low to sustain a chain reaction despite release of chain-propagating radicals by surface reactions, then one reason for this may be slow dissolution of ferrihydrite at pH 4. To test whether adding some dissolved Fe(III) to this system would increase the importance of the chain reaction, we compared $k_{H_2O_2}$ and k_{HCOOH} in solutions with 1 mM H_2O_2 and 40 or 180 μM ferrihydrite with and without an addition of 1.5 μM dissolved Fe(III) at time zero. The additional dissolved Fe(III) either had no effect on the pseudo-first-order rate constants (40 μM ferrihydrite) or increased them by less than a factor of 2 (180 μM ferrihydrite) (data not shown).

In summary, comparing our qualitative model calculations to experimental results shows that the decomposition rates of neither H_2O_2 nor HCOOH are controlled by a surface initiated chain reaction and that the yield of •OH from H_2O_2 was much lower than in the presence of dissolved Fe. It should be emphasized that the intention of our model was only to illustrate key characteristics of different proposed mechanisms that could describe the heterogeneous system. While the patterns we discussed did not depend on the values of the rate constants chosen, different sets of fitting parameters (rate constants of reactions 11-13 and total dissolved Fe concentrations) may produce similar or better fits to the data. We did not explore this issue further since our intent was only to constrain the mechanistic possibilities using reasonable values for these parameters.

Discussion

Importance of the Chain Reaction at pH > 3

Our work shows that the chain reaction controls the decomposition rates of both H_2O_2 and formic acid in an aqueous solution containing only ~0.4 μM dissolved Fe at pH 4. The behavior of this system is described reasonably well by De Laat and Gallard's kinetic model of the chain reaction mechanism, which is based on experiments conducted at pH 3 or less. The only reaction in Table 2-1 for which the pH dependence of the effective rate constant is not well understood is the initiation reaction, T1.1. At higher pH, other Fe(III)-hydroperoxy complexes [for example, $Fe(OH)_2(HO_2)$] could become important contributors to this effective rate constant. Our results show that such additional complexes do not need to be invoked in a kinetic model for pH 4. Extrapolations of the model to higher pH values, still assuming that no new Fe(III)-hydroperoxy complexes become important, predict that if the concentration of dissolved Fe(III) is limited by the solubility of ferrihydrite ($K_{sp} = 10^{-38.8}$; *38*), the decomposition of H_2O_2 and organic compounds will be very slow at pH values higher than 4 (Table 2-5). However, even at pH 5, chain lengths in the hundreds are predicted by the model, where the chain length is equal to the propagation rate, 0.5 x $k_{H_2O_2}$ $[H_2O_2]$, divided by the initiation rate, $k_{T1.1}[Fe(III)][H_2O_2]$ (the factor of 0.5 in the propagation rate accounts for the 2 mol of H_2O_2 consumed per cycle, see Figure 2-1) (*42*). The model calculations therefore show that sufficient dissolved Fe can be present at pH 3-5 to effectively propagate the chain reaction, making the chain reaction a potentially important pathway for the decomposition of hydrogen peroxide and organic compounds in an Fe(III)/H_2O_2 system, especially if it is initiated by a different reaction than T1.1 (for example, a photochemical reaction). However, the modeling result above pH 4 must be treated with caution since the kinetic model does not account for the greater potential of trace species to interfere with the chain reaction as the concentrations of dissolved Fe decrease. The model also does not account for the large variability in the solubility product of ferrihydrite (-log K_{sp} = 37.0-39.4; *43*), or other potential influences on solubility such as the Kelvin effect (*44*) (Appendix A).

Mechanisms of Decomposition of Hydrogen Peroxide and Organic Compounds in Iron Oxide/H_2O_2 Systems

While most previous works assumed that •OH is the intermediate primarily responsible for the decomposition of organic compounds in iron oxide/H_2O_2 systems, few have performed

experiments that could invalidate this hypothesis. Miller and Valentine (*22*) showed that the addition of 100 mM butanol dramatically decreased the total decomposition of 0.08 mM quinoline (or 0.11 mM phenol) in a solution containing 58 mM H_2O_2 and 0.2 g/mL of sterilized sand. They attributed this to the competition between butanol and quinoline or phenol for dissolved •OH, but they did not attempt a quantitative comparison of the competition kinetics. A recent study (*20*) used a highly selective spin-trap technique in conjunction with competition kinetics to show that •OH is produced upon the decomposition of H_2O_2 in the presence of Fe-containing soil samples but did not relate the •OH production rate to the rate of decomposition of organic compounds. Our results show that the decomposition kinetics of two nonsorbing probes having very different chemical structures are consistent with •OH being the only important oxidant.

If dissolved •OH is released from the surface reaction, it is somewhat surprising that no chain reaction occurs in our ferrihydrite/H_2O_2 systems since some Fe must have dissolved from the ferrihydrite. The most plausible explanation for this observation is that dissolved Fe is too low for the chain reaction to take place. We intended to constrain the dissolved Fe value by measuring 0.02-μm filterable Fe in our experiments, but our measurements did not yield reliable results. One-third of our samples were lower than the detection limit of 0.03 μM, suggesting that dissolved Fe was lower during the experiments with ferrihydrite than during those without. This is reasonable since aging the ferrihydrite could have decreased its solubility. The lack of effect of adding dissolved Fe to the ferrihydrite systems could be due to rapid removal of the dissolved Fe by precipitation of additional ferrihydrite.

Despite the lack of dependable dissolved Fe data, we were able to use our modeling results to examine at what range of dissolved Fe concentrations the chain reaction would not be important in the heterogeneous system. This is illustrated by Models C and D; they both have a dissolved Fe(III) concentration of 15 nM, and their predicted k_{HCOOH} was barely affected by the presence of *tert*-butyl alcohol. In contrast, Models A and B showed that a dissolved Fe(III) concentration of 65 nM could sustain a chain reaction because their predicted k_{HCOOH} was greatly decreased by *tert*-butyl alcohol. As our model has other fitting parameters, it is possible that a different set of values would show the chain reaction to be unimportant at even higher dissolved Fe concentrations.

The decrease in γ values observed with increasing ferrihydrite indicates a sink of H_2O_2 at

the iron oxide surface other than the radical-producing reactions 11 and 12. In other words, assuming that •OH is the oxidizing species, the yield of •OH per H_2O_2 consumed, as defined by eq 6, is lower than the value of 0.5 that is expected if either the solution chain reaction occurs or, in the absence of a chain reaction, if the main reaction sequence is 11 (or T1.1), 12 (or T1.2), T1.3, and T.1.7. In the latter case, the yield of •OH is 0.5 because 3 mol of H_2O_2 are consumed and 1 mol each of H_2O_2 and •OH are produced by this reaction sequence; hence, the predicted γ is the same as when the chain reaction occurs (this is illustrated by the overlap between the lines for models A and D in Figure 2-4). Previous studies [except the direct measurements in Petigara and Blough (*20*)] have not attempted to calculate a yield of •OH per H_2O_2 consumed, as defined here. Furthermore, most studies have been performed either using natural soil or aquifer solid samples instead of pure mineral phases (e.g., refs *15* and *22*) where H_2O_2 may be consumed by reactions with solids other than iron oxide, e.g., manganese oxide (*22*). Other studies used pure mineral phases but examined systems where not all of the organic compound was dissolved and only the decrease of total concentration over time was measured (e.g., ref *18*), making calculation of the observed γ impossible.

Thus, we were able to calculate values of the observed γ from data presented in only two other studies. The experiments of Valentine and Wang (*17*) examined quinoline loss at pH 7.0 in the presence of three different iron oxide phases. We estimated quinoline and H_2O_2 decomposition rates from Figure 2-4 of their work, using only the data before H_2O_2 was replenished. Since they observed no detectable loss of quinoline in the ferrihydrite solution, its γ was approximately zero. γ for semicrystalline iron oxide was ~0.1, and for goethite it was ~0.3. Using Miller and Valentine's (*22*) estimate of the second-order rate constant of •OH with quinoline, 9.28×10^9 M^{-1} s^{-1} (no direct measurements of this rate constant have been published), we calculate an expected γ of 140. In the other study, Gurol et al. (*45*) used goethite to catalyze the decomposition of hydrogen peroxide and *n*-chlorobutane (BuCl) at pH 7.5. Calculation of γ from their data is complicated by the fact that they observed significant sorptive loss of BuCl (~35%) from their solutions. We attempted to account for this by neglecting the first hour of the data in their Figure 2-3, when sorptive losses were fast, and using the remainder to estimate the rate of loss of BuCl due to oxidation. The decomposition rate of H_2O_2 was computed from their eq 2. The values of γ calculated from their experiments with 44, 75, and 170 mg/L H_2O_2 are ~0.1, ~0.2, and ~2, in contrast to the expected γ of 45, using 3×10^9 M^{-1} s^{-1} as the second-order

rate constant of •OH with BuCl (*46*). In both of these studies, the differences between the expected and the observed γ values were much greater than in ours. H_2O_2 concentration and the type of iron oxide seem to influence the yield of •OH in these systems, but clearly more studies need to be done to better understand the large variability in this parameter.

While kinetic arguments illustrated by the model calculations show that a sink of H_2O_2 other than reactions 11 and 12 is needed to explain the observed decrease in γ with increasing ferrihydrite concentration, we cannot distinguish among different mechanisms whose overall effect could be represented by reaction 13. The possibility of a two-electron transfer process has been suggested both for iron oxides and manganese oxides (*20*). Loss of •OH by reaction with reduced iron sites at the iron oxide surface has also been suggested (*22*). However, for the latter mechanism to affect γ, this reaction would have to become the major sink reaction of •OH. Since we expect surface Fe(II) to be a short-lived intermediate, and hence present in low concentrations, this appears implausible.

Most of our conclusions still hold if nearly all of the •OH formed at the surface of the iron oxide reacts away in the stagnant surface film before diffusing into the bulk solution, as suggested by Lin and Gurol (*19*). Since our probe compounds and hydrogen peroxide decompose on time scales that are much too long to be controlled by their diffusion to the surface, their concentration in the surface film must be approximately equal to their concentration in the bulk solution. Therefore, the fraction of •OH that reacts with H_2O_2 and the probe compounds should still be the same as that of the bulk solution, so the conclusions we drew from the observed values of γ and the ratio of decomposition rates of the two probes remain unchanged. Furthermore, a chain reaction in the bulk solution should still be initiated by the surface processes, since the rate constants in Table 2-1 imply that HO_2/O_2^- and Fe(II) are sufficiently long-lived to diffuse out of the stagnant surface film. However, while reactions of bulk solution radicals with iron oxide surfaces cannot be important due to collision frequency limitations, such reactions are plausible for radicals formed in the surface film. Rapid loss of HO_2/O_2^- to a surface reaction is therefore a possible alternative explanation for the lack of a surface initiated solution chain reaction. Loss of •OH at the surface could explain the low apparent yield of •OH from H_2O_2 (low γ values), although the reaction would have to be with a more abundant surface species than surface Fe(II), such as sorbed hydrogen peroxide.

Distinguishing among these different possible mechanisms for organic matter and

hydrogen peroxide decomposition is important for optimizing water and soil treatment processes based on these reactions. We show that chain reaction mechanisms can play a role in these processes even at pH values above 3, implying that small concentrations of chain-terminating species could have dramatic effects on the overall decomposition kinetics. The yield of •OH from H_2O_2 appears to vary over several orders of magnitude; to achieve proper dosing of the hydrogen peroxide, we need to understand what controls these variations. Further work is also needed to determine whether organic compounds are oxidized by •OH or other oxidants in the bulk solution or near iron oxide surfaces, all of which are critical for optimizing the effectiveness of hydrogen peroxide-based treatment processes in more complicated systems, such as soils in which contaminants are mostly present as sorbed species.

Acknowledgments

We thank Michael Pullin for his help with the HPLC measurements and Phil Gschwend and Scot Martin for helpful discussions. This work was funded by a Parsons fellowship awarded to W.P.K. and by a grant from the American Chemical Society's Petroleum Research Fund.

Literature Cited

(1) Aronstein, B. N.; Lawal, R. A.; Maka, A. *Environ. Toxicol. Chem.* **1994**, *13*, 1719-1726.

(2) Ravikumar, J. X.; Gurol, M. D. *Environ. Sci. Technol.* **1994**, *28*, 394-400.

(3) Bigda, R. J. *Chem. Eng. Prog.* **1995**, *91*, 62-65.

(4) Ho, C. L.; Shebl, M. A.-A.; Watts, R. J. *Hazard. Waste Hazard. Mater.* **1997**, *12*, 15-25.

(5) Pignatello, J. J. *Environ. Sci. Technol.* **1992**, *26*, 944-951.

(6) Li, Z. M.; Comfort, S. D.; Shea, P. J. *J. Environ. Qual.* **1997**, *26*, 480-487.

(7) Pignatello, J. J.; Liu, D.; Huston, P. *Environ. Sci. Technol.* **1999**, *33*, 1832-1839.

(8) Watts, R. J.; Stanton, P. C. *Water Res.* **1999**, *33*, 1405-1414.

(9) Lu, M.-C. *Chemosphere* **2000**, *40*, 125-130.

(10) Barb, W. G.; Baxendale, J. H.; George, P.; Hargrave, K. R. *Trans. Faraday Soc.* **1951**, *97*, 591-616.

(11) Walling, C.; Goosen, A. *J. Am. Chem. Soc.* **1973**, *95*, 2987-2991.

(12) De Laat, J.; Gallard, H. *Environ. Sci. Technol.* **1999**, *33*, 2726-2732.

(13) Staehelin, J.; Hoigné, J. *Environ. Sci. Technol.* **1985**, *19*, 1206-1213.

(14) Kozlov, Y. N.; Dribinskii, V. L. *Russ. J. Phys. Chem. USSR* **1997**, *71*, 1612-1614.

(15) Watts, R. J.; Udell, M. D.; Rauch, P. A.; Leung, S. W. *Hazard. Waste Hazard. Mater.* **1990**,

7, 335-345.

(16) Khan, A. J.; Watts, R. J. *Water Air Soil Pollut.* **1996**, *88*, 247-260.

(17) Valentine, R. L.; Wang, H. C. A. *J. Environ. Eng.* **1998**, *124*, 31-38.

(18) Watts, R. J.; Jones, A. P.; Chen, P.-H.; Kenny, A. *Water Environ. Res.* **1997**, *69*, 269-275.

(19) Lin, S.-S.; Gurol, M. D. *Environ. Sci. Technol.* **1998**, *32*, 1417-1423.

(20) Petigara, B. R.; Blough, N. V.; Mignerey, A. C. *Environ. Sci. Technol.* **2002**, *36*, 639-645.

(21) Lin, S.-S. Ph.D. Thesis, Drexel University, Philadelphia, PA, 1997.

(22) Miller, C. M.; Valentine, R. L. *Water Res.* **1999**, *33*, 2805-2816.

(23) Jones, P.; Tobe, M. L.; Wynne-Jones, W. F. K. *Trans. Faraday Soc.* **1959**, *55*, 91-97.

(24) Kremer, M. L.; Stein, G. *Trans. Faraday Soc.* **1959**, *55*, 959-973.

(25) Walling, C.; Weil, T. *Int. J. Chem. Kinet.* **1974**, *6*, 507-516.

(26) Gallard, H.; De Laat, J. *Water Res.* **2000**, *34*, 3107-3116.

(27) Wells, M. L.; Mayer, L. M.; Guillard, R. R. L. *Mar. Chem.* **1991**, *33*, 23-40.

(28) Bader, H.; Sturzenegger, V.; Hoigne´, J. *Water Res.* **1988**, *22*, 1109-1115.

(29) Voelker, B. M.; Sulzberger, B. *Environ. Sci. Technol.* **1996**, *30*, 1106-1114.

(30) Stookey, L. L. *Anal. Chem.* **1970**, *42*, 779-781.

(31) Ross, F.; Ross, A. B. *Selected Specific Rates of Reactions of Transients from Water in Aqueous Solution*; (NSRDS-NBS59); U.S. National Bureau of Standards: Gaithersburg, MD, 1977.

(32) Kwan,W.P. M.Sc. Thesis, Massachusetts Institute of Technology, Cambridge, MA, 1999.

(33) Zhou, X.; Mopper, K. *Mar. Chem.* **1990**, *30*, 71-88.

(34) Albert, D. B.; Martens, C. S. *Mar. Chem.* **1997**, *56*, 27-37.

(35) Hoigné, J. In *Process Technologies for Water Treatment*; Stucki, S., Ed.; Plenum: New York, 1988; pp. 121-143.

(36) Braun, W.; Herron, J. T. *Acuchem/Acuplot*; National Bureau of Standards: Gaithersburg, MD, 1986.

(37) Bielski, B. H. J.; Cabelli, D. E.; Arudi, R. L.; Ross, A. B. *J. Phys. Chem. Ref. Data* **1985**, *14*, 1041-1100.

(38) Morel, F. M. M.; Hering, J. G. *Principles and Applications of Aquatic Chemistry*; John Wiley & Sons: New York, 1993.

(39) Millero, F. J.; Sotolongo, S.; Stade, D. J.; Vega, C. A. *J. Solution Chem.* **1991**, *20*, 1079-

1092.

(40) Buxton, G. V.; Greenstock, C. L.; Helman, W. P.; Ross, A. B. *J. Phys. Chem. Ref. Data* **1988**, *17*, 513-886.

(41) Weinstein, J.; Bielski, B. H. J. *J. Am. Chem. Soc.* **1979**, *101*, 58-62.

(42) Atkins, P. W. *Physical Chemistry*;W.H. Freeman and Company: New York, 1986.

(43) Schwertmann, U.; Cornell, R. M. *Iron Oxides in the Laboratory*; VCH Publishers: New York, 1991.

(44) Stumm, W.; Morgan, J. J. *Aquatic Chemistry*; John Wiley & Sons, Inc.: New York, 1996.

(45) Gurol, M. D.; Lin, S.-S.; Bhat, N. In *Emerging Technologies in Hazardous Waste Management*; Tedder, D. W., Pohland, F. G., Eds.; Plenum Press: New York, 1997; pp. 9-21.

(46) Haag, W. R.; Hoigné, J. *Chemosphere* **1985**, *14*, 1659-1671.

(47) Elliot, A. J.; McCracken, D. R.; Buxton, G. V.; Wood, N. D. *J. Chem. Soc. Faraday Trans.* **1990**, *86*, 1539-1547.

Table 2-1. Mechanism of the Fe(III)-initiated chain reaction. The rate constants are listed in M^{-1} s^{-1}.

	pH 3	pH 4	pH 5	Reaction
$Fe(III) + H_2O_2 \rightarrow Fe(II) + HO_2/O_2^- + H^+$	2.0×10^{-3}	2.5×10^{-3}	2.6×10^{-3}	(T1.1)
$Fe(II) + H_2O_2 \rightarrow Fe(III) + \bullet OH + OH^-$	63	1.2×10^{2}	5.7×10^{2}	(T1.2)
$H_2O_2 + \bullet OH \rightarrow HO_2/O_2^- + H_2O$	3.3×10^{7}	3.3×10^{7}	3.3×10^{7}	(T1.3)
$Fe(III) + HO_2/O_2^- \rightarrow Fe(II) + O_2 + H^+$	7.8×10^{5}	6.8×10^{6}	3.1×10^{7}	(T1.4)
$Fe(II) + \bullet OH \rightarrow Fe(III) + OH^-$	3.2×10^{8}	3.2×10^{8}	3.2×10^{8}	(T1.5)
$Fe(II) + HO_2/O_2^- \rightarrow Fe(III) + HO_2$	1.3×10^{6}	2.4×10^{6}	6.6×10^{6}	(T1.6)
$HO_2/O_2^- + HO_2/O_2^- \rightarrow H_2O_2$	2.3×10^{6}	1.2×10^{7}	2.3×10^{7}	(T1.7)
$\bullet OH + HO_2/O_2^- \rightarrow H_2O + O_2$	7.1×10^{9}	7.5×10^{9}	8.9×10^{9}	(T1.8)
$\bullet OH + \bullet OH \rightarrow H_2O_2$	5.2×10^{9}	5.2×10^{9}	5.2×10^{9}	(T1.9)
$\bullet OH + HCOOH/HCOO^- \rightarrow CO_2 + O_2^-$	6.5×10^{8}	2.2×10^{9}	3.2×10^{9}	(T1.10)

Table 2-2. Some published rate constants for the reactions of •OH with formic acid, formate, and hydrogen peroxide, in M^{-1} s^{-1}. We included all rate constants except those where the reaction pH was outside of 2-5.

	$k_{OH, HCOOH}$	$k_{OH, HCOO^-}$	k_{OH, H_2O_2}
	1.3×10^{8} [a]	4.3×10^{9} [c]	2.7×10^{7} [a]
	6.5×10^{8} [b]	3.2×10^{9} [a]	4.5×10^{7} [b]
	1.6×10^{8} [b]	3.8×10^{9} [a]	1.2×10^{7} [b]
		2.2×10^{9} [b]	1.7×10^{7} [b]
		3.4×10^{9} [b]	
Average:	$3.1 (\pm 2.9) \times 10^{8}$	$3.4 (\pm 0.8) \times 10^{9}$	$2.5 (\pm 1.5) \times 10^{7}$

[a] Buxton et al. (*40*)

[b] Ross and Ross (*31*)

[c] Elliot et al. (*47*)

Table 2-3. Experimental pseudo first-order decomposition rates of $H^{14}COOH/H^{14}COO^-$ and H_2O_2, and the corresponding γ in pH 4 solutions with dissolved iron, in day^{-1}. The uncertainty in the rate coefficients represents one standard deviation calculated from non-linear regressions of the raw data (concentration of $H^{14}COOH/H^{14}COO^-$ and H_2O_2 versus time). The uncertainty in γ represents one standard deviation calculated by propagating the errors from the rate coefficients. Measured dissolved Fe (0.02-μm filtered) was 0.41-2.55 μM, but no relationship between reaction rates and dissolved Fe was observed.

Experiment #	k_{HCOOH}	$k_{H_2O_2}$	γ
1	1.21 ± 0.14	0.066 ± 0.0019	18.3 ± 2.2
2	2.23 ± 0.17	0.084 ± 0.012	26.5 ± 4.3
3	1.73 ± 0.034	0.075 ± 0.0086	23.1 ± 1.8
4	0.21 ± 0.0094	0.0082 ± 0.0016	25.6 ± 5.1
5	0.32 ± 0.033	0.017 ± 0.002	18.8 ± 2.9
6	0.89 ± 0.060	0.046 ± 0.0049	19.3 ± 2.4
7	0.23 ± 0.0090	0.0090 ± 0.0035	25.6 ± 10.0
Average[†]:	0.68 ± 0.13	0.030 ± 0.015	22.2 ± 11.7

[†]Each value is the geometric average of the data set because the data is log-normally distributed.

Table 2-4. Experimental pseudo first-order decomposition rates of benzoic acid and formic acid in pH 4 solutions containing ferrihydrite. The uncertainty in the observed rate coefficients represents one standard deviation calculated from nonlinear regressions of the raw data. The uncertainty in the ratio represents one standard deviation calculated by propagating the errors from the rate coefficients. Also listed are the averages of the literature values of the second-order rate constants with •OH that meet the criterion stated in Table 2-2, with an uncertainty of one standard deviation.

	$k_{C_6H_5COOH}$ (day^{-1})	k_{HCOOH} (day^{-1})	$\frac{k_{C_6H_5COOH}}{k_{HCOOH}}$
Experiment 1	1.26 ± 0.22	0.59 ± 0.13	2.1 ± 0.6
Experiment 2	0.66 ± 0.042	0.23 ± 0.034	2.9 ± 0.5

	k_{OH, C_6H_5COOH} (M^{-1} s^{-1})	$k_{OH, [HCOOH]_T}$ (M^{-1} s^{-1})	Expected $\frac{k_{OH, C_6H_5COOH}}{k_{OH, [HCOOH]_T}}$
Literature values	4.0 (±1.3) x 10^9	2.2 (±0.5) x 10^9	1.7 ± 0.7

Table 2-5. Estimated solution chain lengths vs. pH, assuming [Fe(III)] is at equilibrium with amorphous ferric hydroxide ($K_{sp} = 10^{-38.8}$).

pH	$[Fe(III)]_{sat}$	$k_{H_2O_2}$ (day^{-1})	k_{HCOOH} (day^{-1})	Chain length
3	15 μM	~0.47	~4.6	~90
4	0.42 μM	~0.043	~1.4	~230
5	33 nM	~0.0063	~0.3	~430

Figure 2-1. Schematic diagram of the Fe(III)-initiated Fenton-like chain reaction.

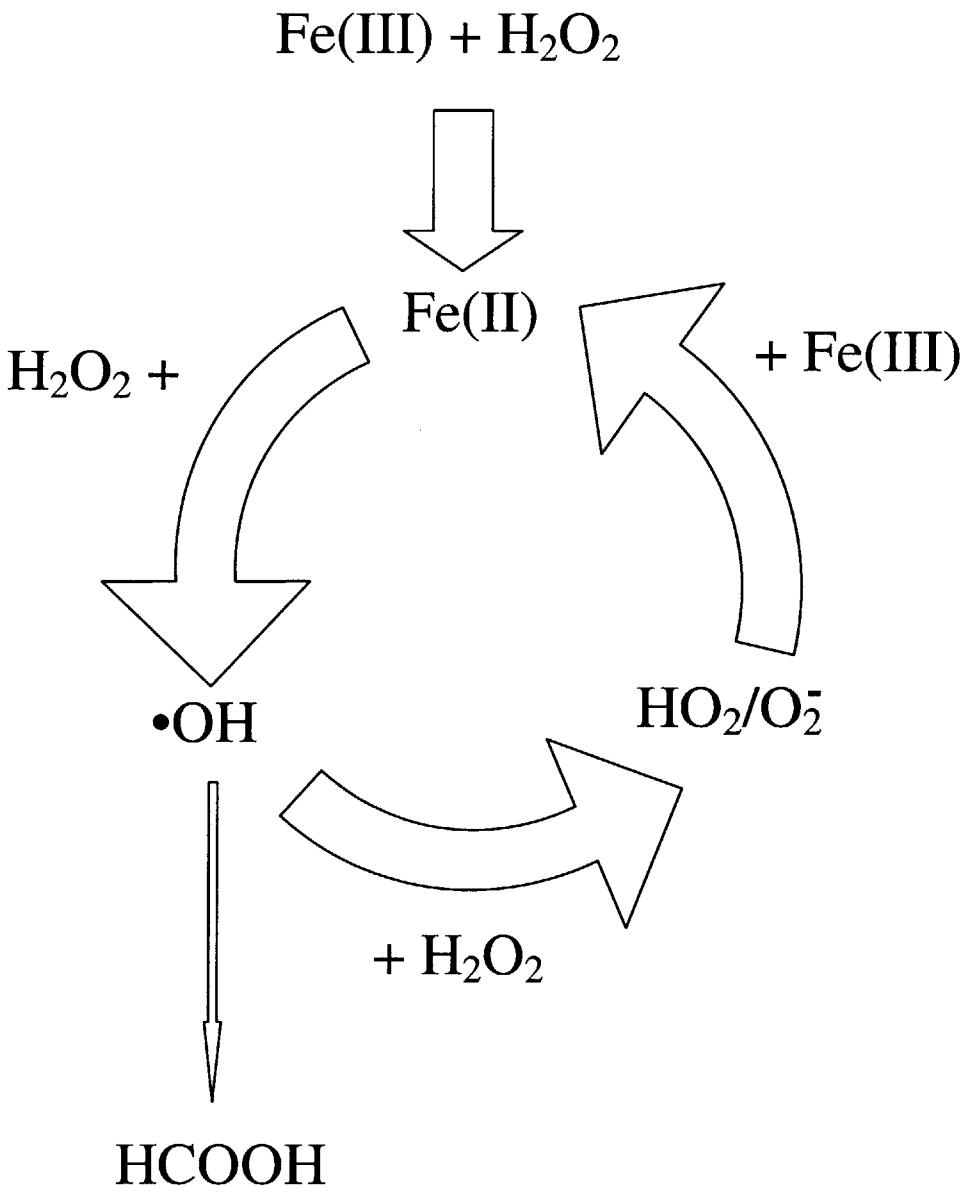

Figure 2-2. A typical data set of the concentration of hydrogen peroxide (•) and ^{14}C-labeled formic acid (∇) over time in an experiment with only dissolved Fe at pH 4. Error bars represent one standard deviation. The lines are non-linear regression fits of the data to the function $[C] = [C]_0 \exp(-kt)$, with $[C]_0$ values of 819 μM and 110 nM and k values of 0.046 day^{-1} and 0.89 day^{-1}, for H_2O_2 and HCOOH, respectively.

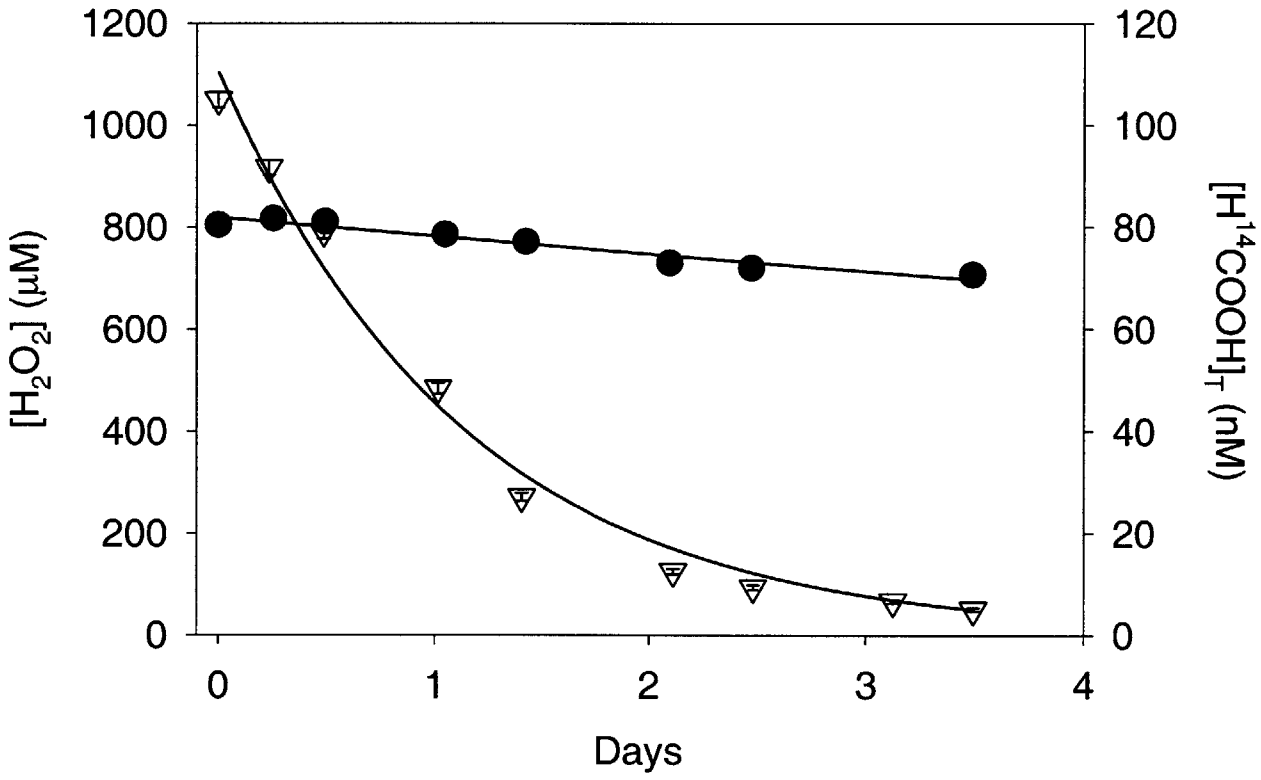

Figure 2-3a. Experimental (○) pseudo-first-order decomposition rates of H_2O_2 in the ferrihydrite/H_2O_2 system. Also included are data from experiments where 10 μM *tert*-butyl alcohol (■) or 100 μM *tert*-butyl alcohol (▲) were added. Error bars represent one standard deviation of rate coefficients calculated from non-linear regressions of the raw data.

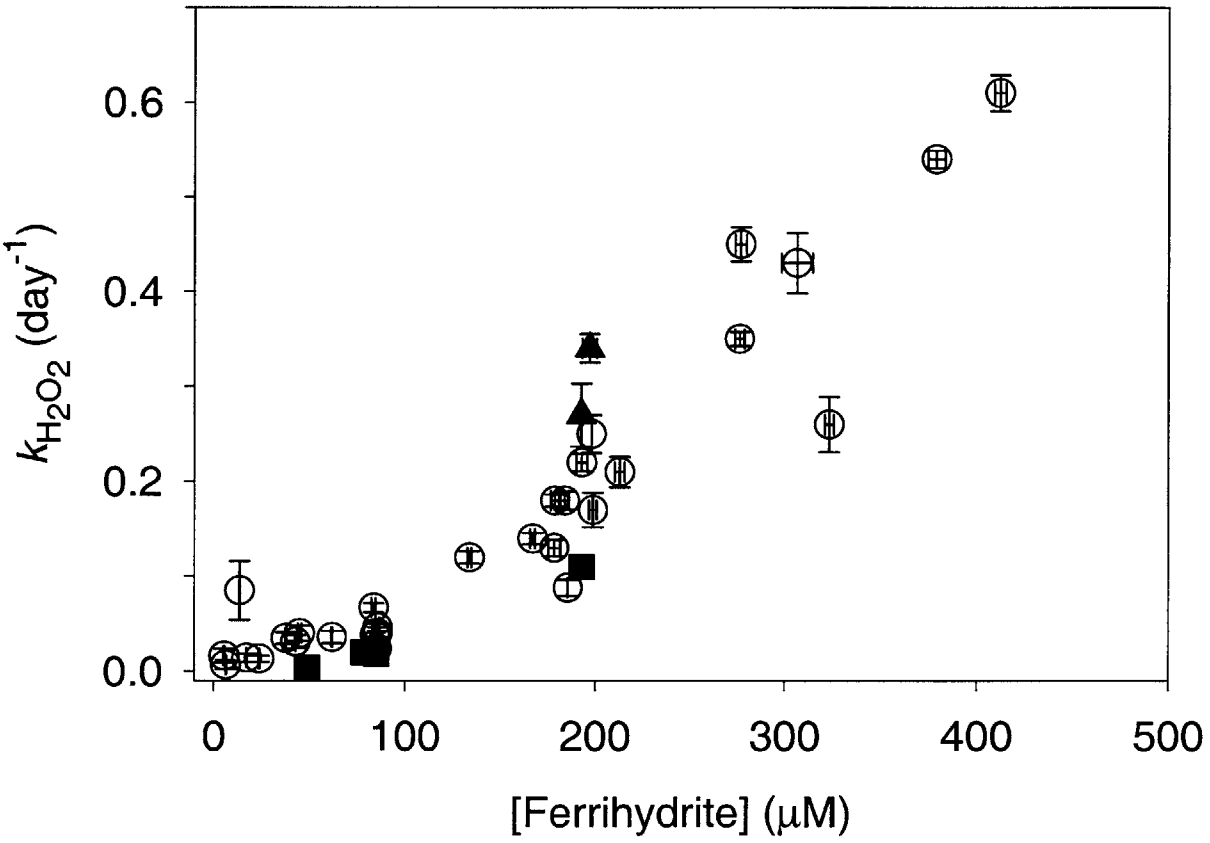

Figure 2-3b. Experimental (○) pseudo-first-order decomposition rates of $H^{14}COOH/H^{14}COO^-$ in the ferrihydrite/H_2O_2 system. Also included are data from experiments where 10 μM *tert*-butyl alcohol (■) or 100 μM *tert*-butyl alcohol (▲) were added. Error bars represent one standard deviation of rate coefficients calculated from non-linear regressions of the raw data.

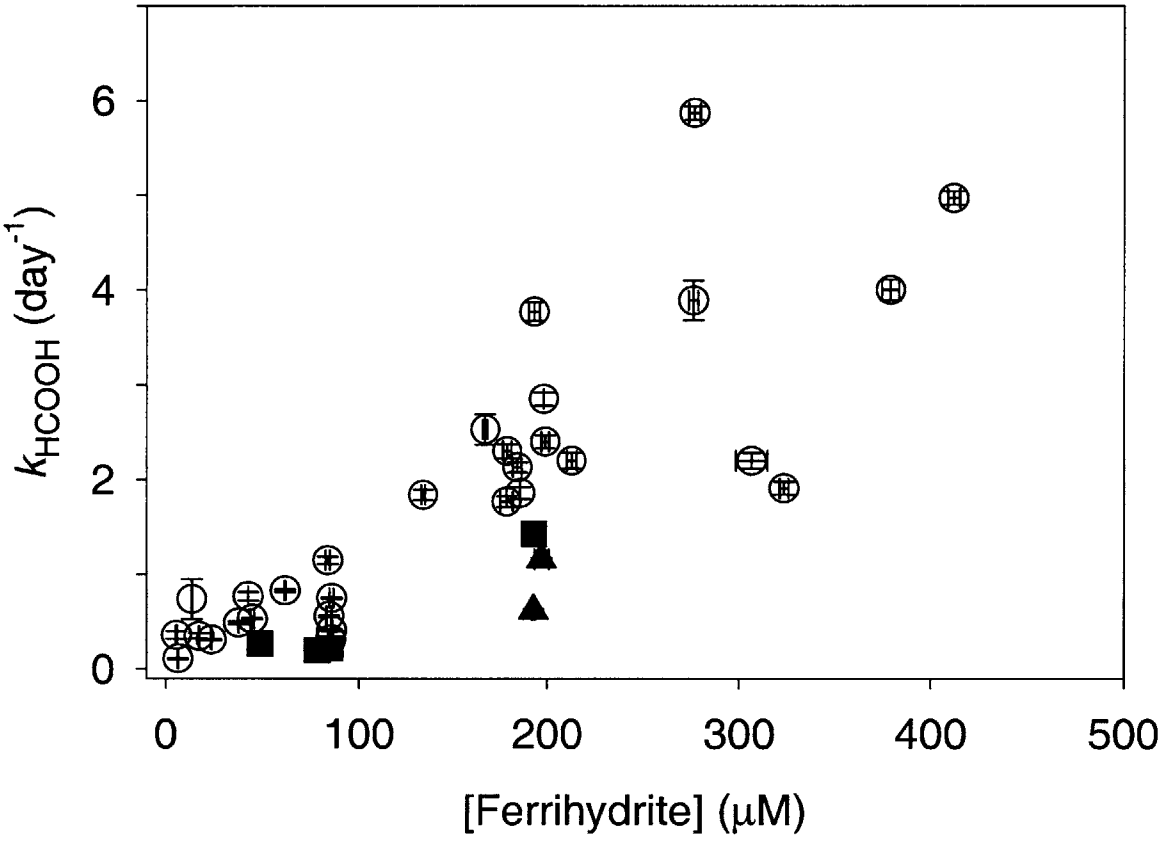

Figure 2-4. Comparison of predictions from Models A-D to the experimental γ values (●) of the ferrihydrite/H_2O_2 system. Error bars represent one standard deviation, calculated by propagating the errors shown in Figures 2-3a,b or from iron measurements. Note that lines for Models A and D are nearly identical.

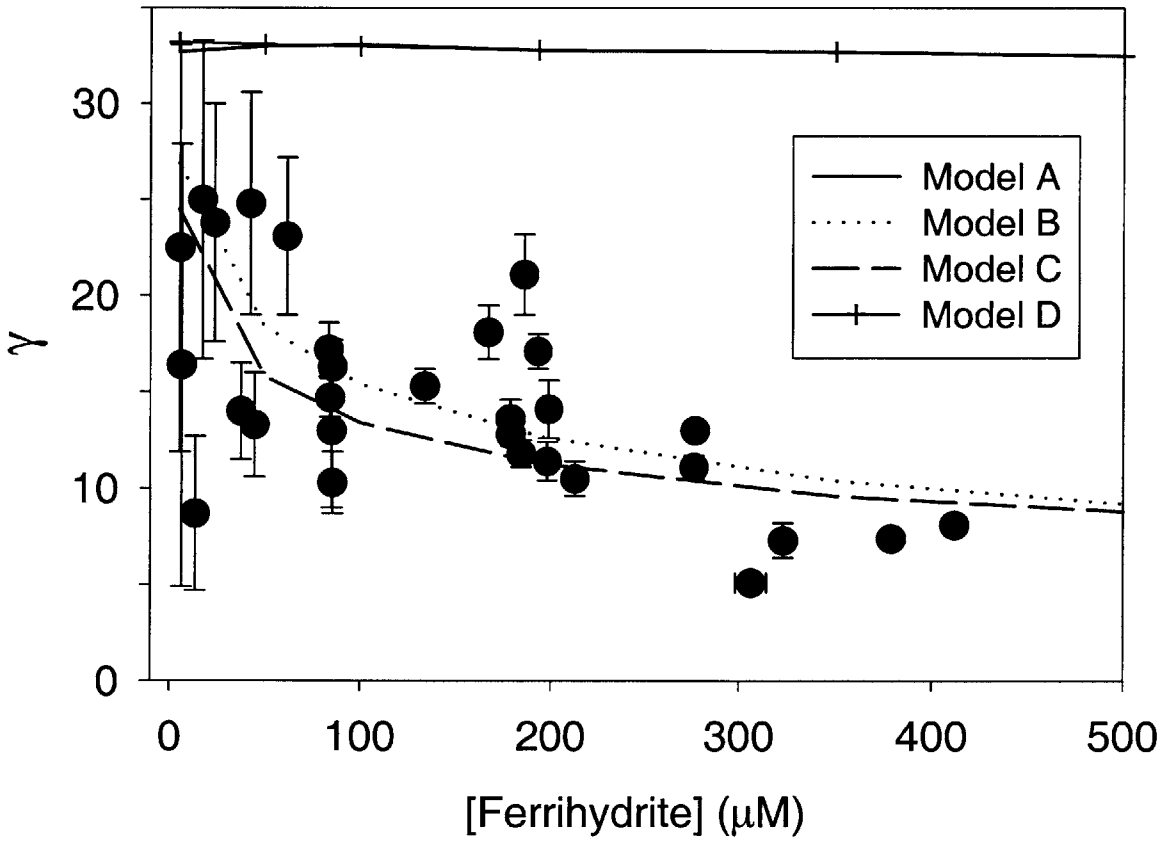

Figure 2-5a. Pseudo-first-order decomposition rates of H_2O_2 in an iron oxide/H_2O_2 system from Models A and B, with and without 100 μM *tert*-butyl alcohol.

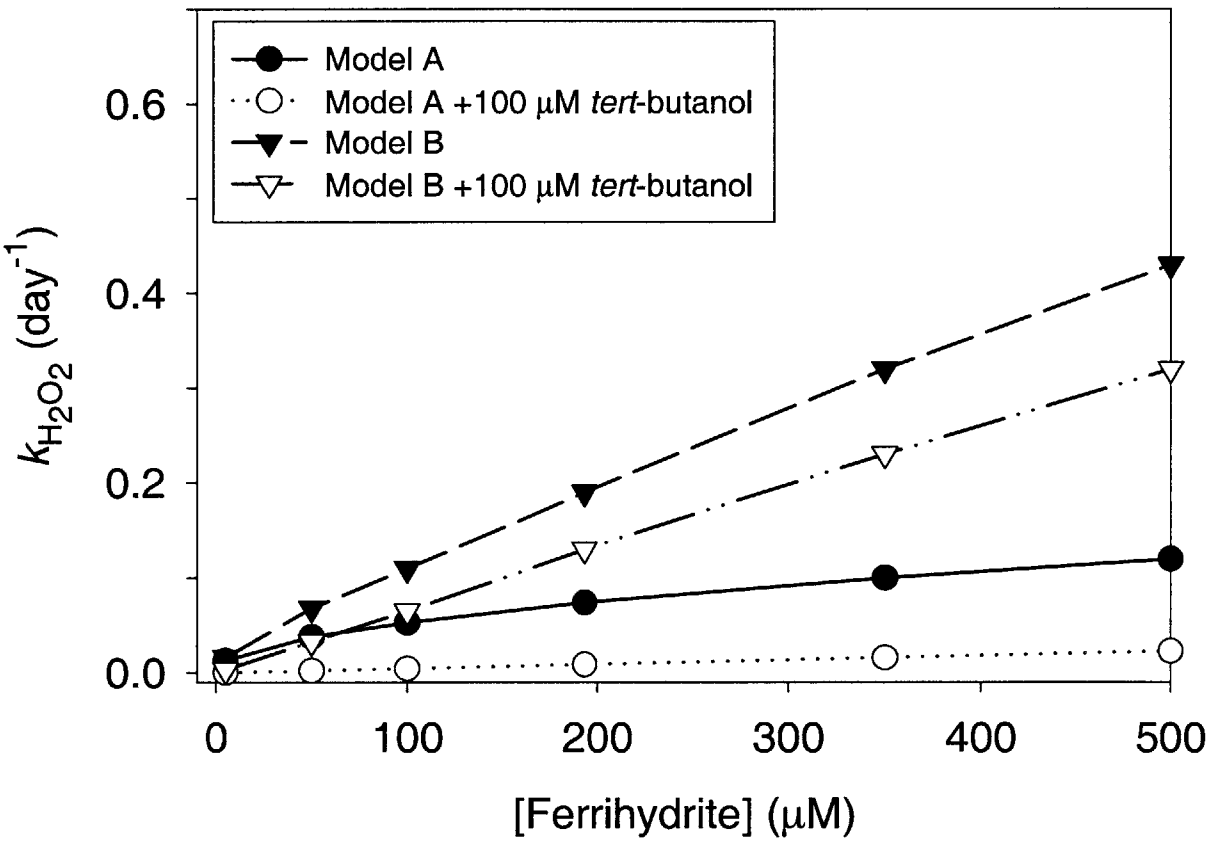

Figure 2-5b. Pseudo-first-order decomposition rates of $H^{14}COOH/H^{14}COO^-$ in an iron oxide/H_2O_2 system from Models A and B, with and without 100 μM *tert*-butyl alcohol.

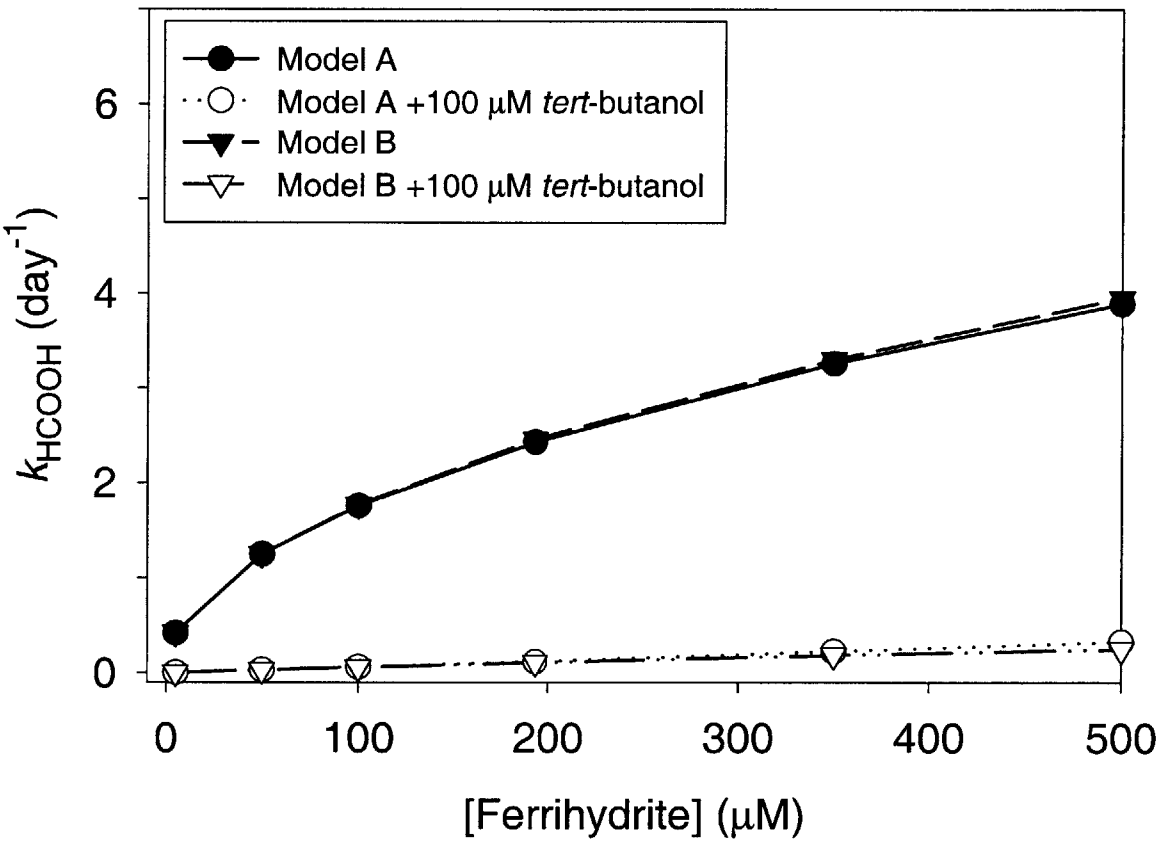

Figure 2-5c. Pseudo-first-order decomposition rates of H_2O_2 in an iron oxide/H_2O_2 system from Models C and D, with and without 100 μM *tert*-butyl alcohol.

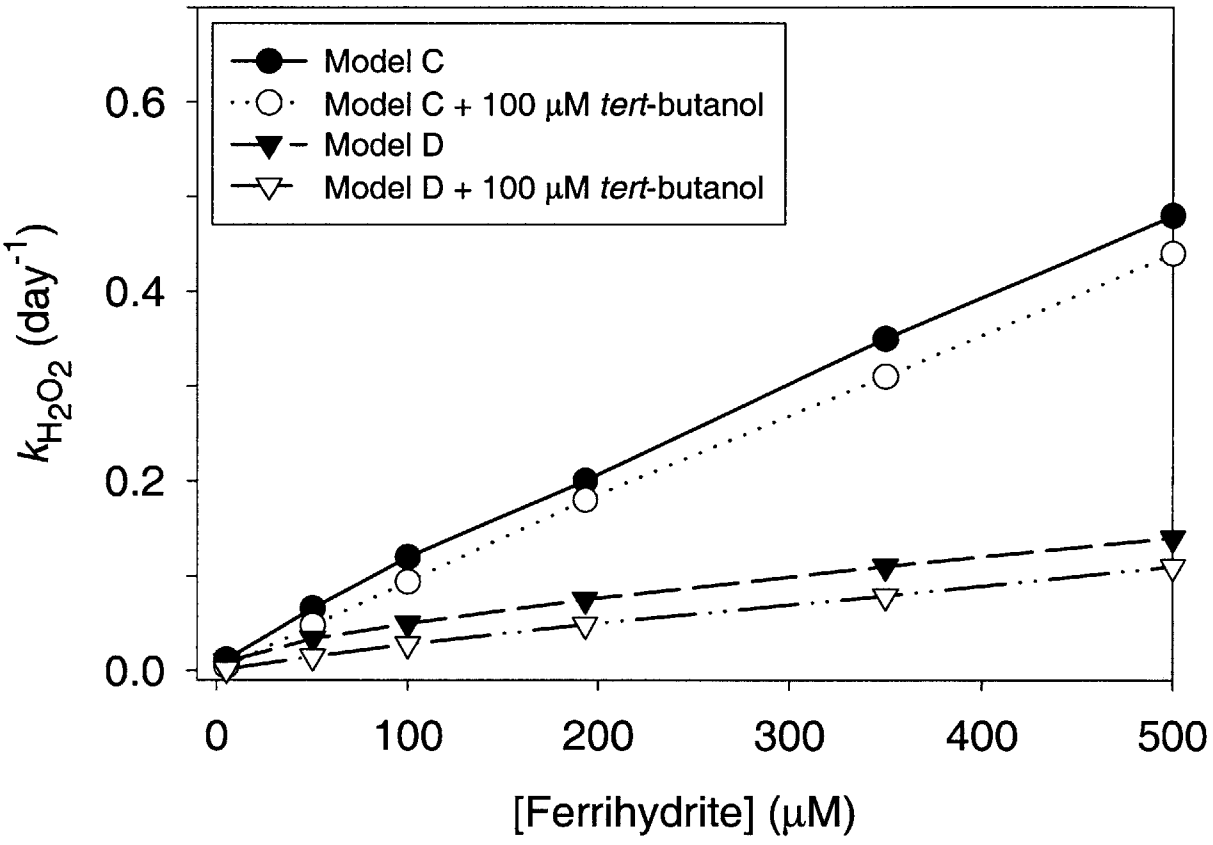

Figure 2-5d. Pseudo-first-order decomposition rates of $H^{14}COOH/H^{14}COO^-$ in an iron oxide/H_2O_2 system from Models C and D, with and without 100 μM *tert*-butyl alcohol.

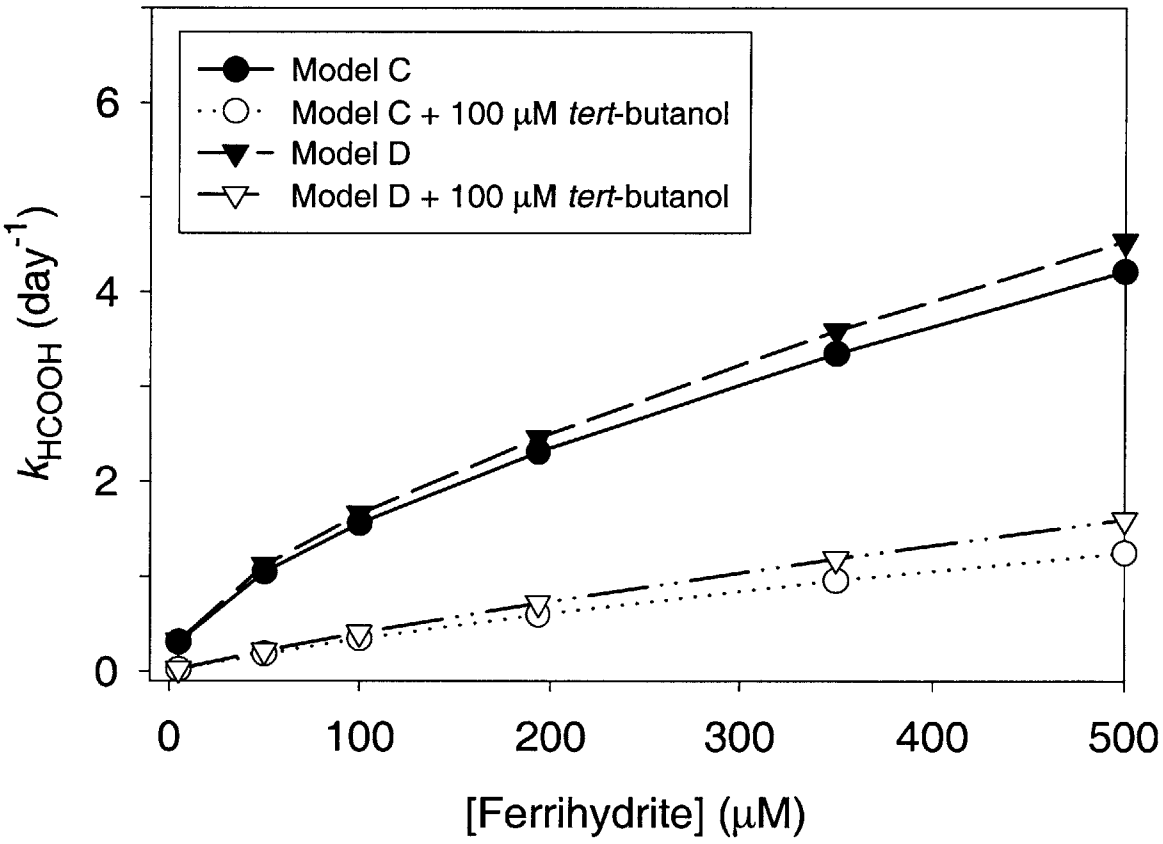

Chapter 3: Rates of Hydroxyl Radical Generation and Organic Compound Oxidation in Mineral-Catalyzed Fenton-like Systems

or

-Those iron oxides that I synthesized in my first year could be useful-

Reproduced with permission from Kwan, Wai P. and Voelker, Bettina M. "Rates of hydroxyl radical generation and organic compound oxidation in mineral-catalyzed Fenton-like systems." *Environmental Science and Technology*, **2003**, 37(6), 1150-1158.

© 2003 American Chemical Society

Abstract

The iron oxide-catalyzed production of hydroxyl radical (•OH) from hydrogen peroxide (H_2O_2) has been used to oxidize organic contaminants in soils and groundwater. The goals of this study are to determine which factors control the generation rate of •OH (V_{OH}) and to show that if V_{OH} and the rate constants of the reactions of •OH with the system's constituents are known, the oxidation rate of a dissolved organic compound can be predicted. Using ^{14}C-labeled formic acid as a probe, we measured V_{OH} in pH 4 slurries of H_2O_2 and either synthesized ferrihydrite, goethite, or hematite or a natural iron oxide-coated quartzitic aquifer sand. In all of our experiments, V_{OH} was proportional to the product of the concentrations of surface area of the iron oxide and H_2O_2, although different solids produced •OH at different rates. We used these results to develop a model of the decomposition rate of formic acid as a function of the initial formic acid and hydrogen peroxide concentrations and of the type and quantity of iron oxide. Our model successfully predicted the V_{OH} and organic compound oxidation rates observed in our aquifer sand experiment and in a number of other studies but overpredicted V_{OH} and oxidation rates in other cases, possibly indicating that unknown reactants are either interfering with •OH production or consuming •OH in these systems.

Introduction

A powerful method for the remediation of wastewater and contaminated groundwater is chemical oxidation, where a reactive chemical species such as the hydroxyl radical (•OH) is generated in aqueous solution. The hydroxyl radical is often chosen because it is a nonspecific oxidant that reacts with most organic compounds at near diffusion-limited rates (*1*). The common way to make hydroxyl radicals in situ in contaminated aquifers is to inject acidified solutions of ferrous iron into the groundwater, followed by concentrated hydrogen peroxide (H_2O_2). This is the well-known Fenton's reagent:

$$Fe(II) + H_2O_2 \rightarrow Fe(III) + \bullet OH + OH^- \quad (1)$$

If only Fe(III) is originally present, Fe(II) can be slowly generated by the following reactions:

$$Fe(III) + H_2O_2 = Fe(HO_2)^{2+} + H^+ \quad (2)$$

$$Fe(HO_2)^{2+} \rightarrow Fe(II) + HO_2 \quad (3)$$

In addition, the HO_2 formed in reaction 3 may deprotonate ($pK_a = 4.8$; *2*) and initiate a chain reaction sequence via the reaction

$$O_2^- + Fe(III) \rightarrow Fe(II) + O_2 \quad (4)$$

followed by reaction 1 and

$$\bullet OH + H_2O_2 \rightarrow HO_2 + H_2O \quad (5)$$

Thus •OH is formed from hydrogen peroxide when either Fe(II) or Fe(III) is present, although generation rates are much slower in the latter case, even when the chain reaction is significant (*3*, *4*).

Researchers have shown that common forms of iron oxide (goethite, hematite, magnetite, and ferrihydrite) can also catalyze the oxidation of organic compounds by H_2O_2 from pH 3 to pH 7 (*5-13*). Experiments that evaluated different iron oxides under the same conditions exhibited differences in the degradation rates of hydrogen peroxide and contaminants. Magnetite (Fe_3O_4) was the most effective catalyst as compared to the other iron oxides (*6*, *10*, *13*), possibly because it was the only one that had Fe^{2+} in its structure to enhance the production rate of •OH. Valentine and Wang (*11*) proposed that the surface area of the iron oxide accounts for the difference in reaction activity; they and Huang et al. (*14*) showed that the decomposition rates of H_2O_2 by goethite, ferrihydrite, and hematite were all relatively similar when normalized to surface area.

However, the consumption rate of H_2O_2 does not equal the generation rate of •OH (V_{OH}) because H_2O_2 can decompose to water and oxygen via nonradical-producing pathways. Examples of these include reactions involving biological enzymes (e.g., catalase) and inorganic chemical species such as manganese (*15*) and the iron oxide surface (*4*). As it is the concentration of •OH that determines the oxidation rate of the contaminant, it is therefore crucial to examine and understand the factors that control V_{OH} in addition to those that affect the lifetime of H_2O_2.

There have been only four publications (*9*, *16-18*) to our knowledge where the investigators explicitly measured V_{OH} from hydrogen peroxide decomposition and looked at the parameters that could affect it. Watts et al. (*9*, *16*) did two studies in systems containing either hematite or a goethite-silica sand and showed that V_{OH} remained constant when $[H_2O_2]$ was varied from 32 mM to 1.6 M and pH was varied from 4 to 7. Huling et al. (*17*) found that V_{OH} in peat-amended suspensions of silica sand mixed with goethite ore at pH ~6 was twice as much as that in unamended suspensions. Petigara et al. (*18*) measured the •OH formation rates of four different soil suspensions and concluded that •OH was a major product of H_2O_2 decomposition in soils with low organic matter but was a minor product in soils containing high amounts of organic matter or manganese. Variations in the yield of •OH from iron oxide/H_2O_2 systems have

also been noted previously (ref *4* and references therein). These studies illustrate that a more comprehensive study of the factors that control V_{OH} is needed. Although many other publications have documented the loss of an organic compound in the presence of H_2O_2 and iron oxide, those data cannot be used to study the behavior of V_{OH} because the compound was not completely dissolved in water, which complicates the data interpretation.

A deeper understanding of the factors that control the concentration of •OH in a pure iron oxide/H_2O_2 system would allow us to estimate the disappearance rate of any organic compound that can be oxidized by •OH in such systems. This would give us a way to interpret the differences between diverse systems and a basis for predicting the time needed for a contaminant to degrade in soils, where complications arise because of greater heterogeneity, sorption processes, and the presence of multiple sinks of H_2O_2 and •OH. Although many investigators have presented equations to predict pollutant destruction rates, most of them used empirical fits of experimental data. One exception is the work of Huling et al. (*19*), who showed that one can use the loss rate of one dissolved organic compound to calculate V_{OH} of a given H_2O_2/sand slurry and then use that V_{OH} to predict the loss rate of another dissolved organic compound under the same conditions. However, they did not attempt to develop a more generally applicable approach for predicting V_{OH}.

This study aims to provide greater comprehension of the parameters that control V_{OH} and to use that information to predict the degradation rate of any organic compound in an iron oxide/H_2O_2 system. Our experiments at pH 4 with three different iron oxides (ferrihydrite, goethite, and hematite) and ^{14}C-labeled formic acid as the •OH probe show that V_{OH} is proportional to the product of the concentrations of surface area of the iron oxide and H_2O_2. Using our results, we formulated a general model that predicts V_{OH} with four parameters: surface area, type and amount of iron oxide, and concentration of H_2O_2. Our model can also estimate the oxidation rate of any compound if we know its aqueous concentration and its reaction rate with •OH, along with the concentration and reaction rates of any other important •OH sinks in the system. We then compared our model predictions of V_{OH} and oxidation rates of organic compounds with a number of observations from published studies.

Materials and Methods

Materials

Detailed descriptions for materials and methods are in a previous publication (*4*). A brief

summary follows. All reagents were reagent grade and used as received. Solutions were prepared using 18 MΩ•cm Milli-Q water from a Millipore system. Glassware and containers were acid washed and rinsed before use. Colloidal ferrihydrite aggregates, mostly retained by 0.02-μm pore size filters, were prepared from $FeCl_3$•$6H_2O$ according to the method described by Wells et al. (*20*). $FeCl_3$•$6H_2O$ was dissolved to make a 4 x 10^{-4} M solution (5 x 10^{-4} M for experiments with high ferrihydrite concentrations). Within 1 h, the solution was heated in a 90 °C water bath for 5 min and then quickly cooled back to room temperature. It was used within 2 days as a colloidal suspension without further purification. Goethite was synthesized by aging ferrihydrite in a strong alkaline solution at 70 °C for 60 h (*21*). Hematite was made in the same manner as goethite except that the solution was aged for 8 days (*21*). The identities of both solids were verified by X-ray diffraction. The aquifer sand came from Georgetown, SC, and is an iron oxide-coated quartzitic sand that was previously characterized (*22*, *23*). It was sterilized before use by autoclaving, which has been shown to be very effective not only in killing microorganisms but also in deactivating enzymes (*24*).

Analytical Techniques

Hydrogen peroxide was measured spectrophotometrically using the DPD method (*25*) as modified by Voelker and Sulzberger (*26*) to minimize interference by Fe(II) and Fe(III). Samples were filtered when necessary to minimize light scattering from iron oxide particles and diluted when needed to ensure that the absorbance through a 1-cm path length cuvette was less than 1.2 au. The concentration of ferrihydrite was measured with ferrozine after reduction with hydroxylamine hydrochloride in strong HCl. $H^{14}COOH$ was measured using liquid scintillation (ScintiSafe Econo 1 Cocktail, Fisher) after an aliquot of experimental solution was air sparged to remove $^{14}CO_2$ (*4*). The surface areas of goethite and hematite were measured by single-point N_2 BET analysis (Porous Materials, Inc.) and were respectively 42.5 and 50.1 m^2/g, with a standard deviation of less than 0.5 m^2/g. BET analysis was not done on the ferrihydrite because we assumed that the drying step would alter its surface area. The bulk surface area of the sand was 15.2 m^2/g, calculated from mercury intrusion data (*22*). Its bulk fraction of organic carbon was 0.109 ± 0.025%, and the total iron content obtained after sediment digestion with HF-HCl-HNO_3 was 267 μmol/g (*22*). Ti(III)-citrate-EDTA-bicarbonate (TiCEB) and ammonium-oxalate-in-the-dark (AOD) extractions were also performed on the sand. TiCEB extraction measured 189 μmol/g of crystalline and amorphous surface iron, and AOD extraction determined that the

amorphous iron content was 16 μmol/g (*22*).

Kinetic Experiments

All experiments were performed in 250-mL Teflon bottles covered completely with black electrical tape to exclude light. The Milli-Q water was treated with a total organic carbon reduction unit (Aquafine) to oxidize traces of organic contamination. Unless noted otherwise, experimental solutions contained 10 mM $NaClO_4$ to control ionic strength and 1 μCi of ^{14}C. The bottles were loosely capped during the experiment, and the solutions were stirred magnetically while being kept in a recirculating water bath. The solutions were adjusted to pH 4 with $HClO_4$ and/or NaOH before the addition of H_2O_2 at time zero. Care was taken to avoid raising the pH of the solution above 6 during the adjustment. The pH of the solutions remained within ±0.5 unit of the initial pH throughout the experiment except for one instance discussed below. The temperature of the water was 22 ± 5 °C, but the variation was only ±1 °C for each individual set of experiments. A stock solution of sodium formate, kept in the dark at 4 °C and discarded after 2 weeks, was used to augment $[HCOOH]_T$ in some of the experiments ($[HCOOH]_T = [HCOOH] + [HCOO^-]$). In these experiments, the sum of the concentrations of $NaClO_4$ and sodium formate was 10 mM to maintain a constant ionic strength.

Loss of $H^{14}COOH$ appeared to follow pseudo-first-order kinetics in all experiments. Significant loss of H_2O_2 was detected only in experiments containing iron oxide and $[H_2O_2]_0$ of 1 mM or less and in some of the experiments with high $[HCOOH]_T$. $H^{14}COOH$ loss in H_2O_2-free control reactors containing iron oxide was insignificant. A control experiment consisting of autoclaved sand, Milli-Q water, and $H^{14}COOH$ showed no loss of $H^{14}COOH$ for at least 15 h.

For those experiments where $[HCOOH]_{T,0} = 10$ mM, the decomposition rate of $H^{14}COOH$ was obtained using the data points from 0 to 4 h because the pH rose above 5 afterward, which interfered with our sparging technique to separate $^{14}CO_2$ from $H^{14}COOH$. We believe the cause of this phenomenon was the high concentration of formic acid (see Appendix B) because in previous experiments at low formic acid concentrations, minimal pH changes were observed.

Calculating V_{OH}

A widely used method to measure V_{OH} is to introduce a hydroxyl radical sink and a dilute chemical probe that reacts with •OH in a well-defined manner (*27*). If the consumption of the •OH probe follows pseudo-first-order kinetics, then its loss rate is

$$-\frac{d[probe]}{dt} = k_{probe}[probe] \quad (6)$$

where k_{probe} is the observed pseudo-first-order rate constant (s^{-1}) and is also equal to $k_{OH,probe}[\bullet OH]_{ss}$, with $k_{OH,probe}$ as the second-order rate constant of the probe with •OH (M^{-1} s^{-1}). This gives us an equation for $[\bullet OH]_{ss}$:

$$[\bullet OH]_{ss} = \frac{k_{probe}}{k_{OH,probe}} \quad (7)$$

The generation rate of •OH must be equal to its scavenging rate at steady state:

$$V_{OH} = \text{scavenging rate} = \sum k_{OH,i}[S_i][\bullet OH]_{ss} \quad (8)$$

where S_i represents •OH sink i in solution. Substituting eq 7 into eq 8 yields

$$V_{OH} = \frac{k_{probe}\sum k_{OH,i}[S_i]}{k_{OH,probe}} \quad (9)$$

k_{probe} for our experiments was obtained by using SigmaPlot to do nonlinear least-squares regression fits of the concentration of our probe, $H^{14}COOH$, versus time (k_{HCOOH}). (Most of the rate coefficients obtained from linear regression fits to log transformed data differed from those obtained from nonlinear regressions by only a few percent. See Appendix B.) Since H_2O_2 and HCOOH were the only major sinks of •OH in our experiments, just their second-order rate constants with •OH were needed for our V_{OH} computation. We used 2.7 x 10^7 M^{-1} s^{-1} (*1*) for k_{OH,H_2O_2} and 2.2 x 10^9 M^{-1} s^{-1} (*4*) for $k_{OH,[HCOOH]_T}$. $k_{OH,[HCOOH]_T}$ is a composite rate constant and is the weighted sum of the two individual rate constants for formic acid and formate multiplied by the percentage of their respective chemical species at pH 4 (*4*). The pK_a of formic acid is 3.745 (*28*).

Our calculations do not need to distinguish between reactions in the bulk solution and reactions in the diffusion layer surrounding the particles if diffusion is fast as compared to the rate of decomposition of H_2O_2 and formic acid, so that the concentrations of these species are the same in the diffusion layer and bulk solution (*4*, *19*).

Results

We calculated V_{OH} values from the observed pseudo-first-order decay rates of our probe, k_{HCOOH}, in a variety of iron oxide/H_2O_2 systems and found that V_{OH} is proportional to the product of the concentrations of surface area (a surrogate for reactive sites, see Discussion) and hydrogen

peroxide (Figure 3-1a). However, the proportionality coefficient differed for the different iron oxides (solid lines in Figure 3-1a):

$$\text{Goethite: } V_{OH} = 1\ (\pm 0.1) \times 10^{-7}[\text{surface area}][H_2O_2] \quad (10)$$

$$\text{Hematite: } V_{OH} = 8\ (\pm 0.4) \times 10^{-9}[\text{surface area}][H_2O_2] \quad (11)$$

$$\text{Ferrihydrite: } V_{OH} = 1\ (\pm 0.02) \times 10^{-7}[\text{surface area}][H_2O_2] \quad (12)$$

Since we could not measure the surface area of our colloidal ferrihydrite, we plotted those data by assuming that it was 200 m^2/g. Ferrihydrite has a typical surface area of 100-400 m^2/g (*29*). In most of our experiments, V_{OH} and $[OH]_{ss}$ remained constant over time because $[H_2O_2]$ did not decrease considerably. In those experiments where H_2O_2 consumption was significant, it is more appropriate to consider our calculated V_{OH} values as initial •OH generation rates.

Although V_{OH} is directly proportional to $[H_2O_2]$ at a constant amount of iron oxide, changing $[H_2O_2]$ will have no effect on $[\bullet OH]_{ss}$ and, consequently, k_{HCOOH} if H_2O_2 is the dominant sink of •OH. This is apparent when eq 8 is rewritten:

$$[\bullet OH]_{ss} = \frac{V_{OH}}{k_{OH,H_2O_2}[H_2O_2] + k_{OH,[HCOOH]_T}[HCOOH]_T} \quad (13)$$

We replotted the data in Figure 3-1a to illustrate this point (Figure 3-1b). The model lines were generated by first using eqs 10-12 to determine V_{OH} and then using eq 14 to calculate the predicted values of the initial decomposition rate of formic acid:

$$-d[HCOOH]_T/dt|_{t=0} = k_{HCOOH}[HCOOH]_{T,0} \quad (14)$$

(We will use $d[HCOOH]_T/dt$ instead of $d[HCOOH]_T/dt|_{t=0}$ for simplicity.) k_{HCOOH} was modeled by multiplying $k_{OH,[HCOOH]_T}$ with $[\bullet OH]_{ss}$, which was computed using eq 13, with $[H_2O_2] = [H_2O_2]_0$ and $[HCOOH]_T = [HCOOH]_{T,0}$. The initial concentration of formic acid in these experiments was low (74-244 nM, with an average value of 131 nM), so hydrogen peroxide was the major sink of •OH. It is obvious from the figure that increasing $[H_2O_2]_0$ by 2-3 orders of magnitude had minimal impact on $d[HCOOH]_T/dt$ (normalized to $[Fe]_T$) for all three iron oxides.

Under conditions where $[HCOOH]_{T,0}$ is high enough that it is the main sink of •OH, increasing $[H_2O_2]_0$ should cause the oxidation rate of formic acid to increase. To demonstrate this and to ensure that high concentrations of formic acid would not compete with H_2O_2 for the active sites on the iron oxide surface and interfere with the production rate of •OH, we performed additional experiments at 0.6 g/L goethite with HCOOH as the dominant •OH sink. A comparison of the experiments in which HCOOH was the dominant •OH sink with those in

which H_2O_2 was the main sink shows that V_{OH} was unaffected by formic acid concentrations as high as 10 mM (Figure 3-2a) and that the expected increase in the rate of oxidation of formic acid with increasing $[H_2O_2]_0$ occurred (Figure 3-2b). The probe loss was well described by first-order kinetics (eq 6), implying that k_{HCOOH} was approximately constant over the course of the experiments (see Appendix B). As some H_2O_2 was consumed during the experiments, the V_{OH} values that we calculated using eq 9 with $[HCOOH]_{T,0}$ and $[H_2O_2]_0$ are more representative of the initial •OH generation rates. Figure 3-2b also illustrates that, at a given $[Fe]_T$ and $[HCOOH]_{T,0}$, there is a theoretical limit to the pseudo-first-order consumption rate of formic acid because there is a maximum value for $[•OH]_{ss}$. This is best shown by the data at $[HCOOH]_{T,0}$ = 50 μM (white squares and black hexagons): adding more H_2O_2 increased $d[HCOOH]_T/dt$ until $k_{OH,H_2O_2}[H_2O_2]_0$ became much greater than $k_{OH,[HCOOH]_T}[HCOOH]_{T,0}$, at which point $d[HCOOH]_T/dt$ approached its maximum value.

We used the Georgetown sand to examine if our findings from a pure iron oxide system would also apply to natural aquifer material. Goethite was the only type of crystalline iron oxide found in the sand (*23*). The results of experiments using either 25 or 60 g/L sand and either H_2O_2 or formic acid as the major •OH sink are shown in Figure 3-3a,b. Although we knew the surface area of the bulk sand, it was unlikely to be equal to the surface area of the goethite in the sand matrix. Instead, we plotted the data assuming that the goethite had a surface area of 40 m^2/g, which lies within the typical range of the surface area of goethite (8-200 m^2/g) (*29*), and that there was 173 μmol of goethite/g of sand (the difference between the TiCEB and AOD extractions). The behavior of V_{OH} with respect to the product of the concentrations of surface area and H_2O_2, with either H_2O_2 or formic acid as the dominant •OH sink, were analogous to that of the pure iron oxide system. Similar to the results of Figure 3-2b, $d[HCOOH]_T/dt$ of the aquifer sand/H_2O_2 system rose as $[H_2O_2]_0$ increased when HCOOH was the dominant •OH sink but remained steady when H_2O_2 was the major •OH sink. The two V_{OH} data points (they lie nearly on top of each other) that are outliers on the far left side of Figure 3-3a,b may have been caused by either of the following phenomena. One, there may have been contamination of the stock formate solution by bacteria whose activity was not suppressed significantly at $[H_2O_2]_0$ of 100 μM or less. The other explanation is that small amounts of Fe(II) could have been present in the sand, producing a small amount of •OH at a high rate. The effect of this reaction on V_{OH} would only be noticeable when the starting concentration of H_2O_2 was small, whereas at higher $[H_2O_2]_0$, its

contribution to V_{OH} would be negligible.

Our predictions for V_{OH} (eq 10) and $d[HCOOH]_T/dt$ were within a factor of 10 of the measured values (lines in Figure 3-3a,b). The range of predictions for $d[HCOOH]_T/dt$ was calculated based on the typical range of surface area of goethite. We neglected the contribution of amorphous Fe to V_{OH} and $d[HCOOH]_T/dt$ because it was only a small percentage (~10%) of the surface iron. Even if we assumed that the surface area of the amorphous iron was 10 times that of crystalline iron, it would only modify V_{OH} and $d[HCOOH]_T/dt$ by a factor of 2, which is of minor importance considering the uncertainty of other factors involved in the computation.

Discussion

In summary, we showed that V_{OH} is (i) proportional to the product of the concentrations of H_2O_2 and iron oxide surface area for goethite, hematite, ferrihydrite, and a natural aquifer sand and (ii) dependent on the type of iron oxide. The V_{OH} measurements from experiments that had similar $[H_2O_2]_0$ but different dominant •OH sinks (either formic acid or H_2O_2) agreed with each other. Besides being evidence that high concentrations of formic acid did not impact V_{OH}, this finding also supports our assumption that •OH was the primary oxidant of our system, which agrees with our previous work (*4*). A different oxidant would react with formic acid and H_2O_2 at second-order rates unlike those of •OH, causing the data sets to not coincide with each other.

Relationship between $[H_2O_2]$, Iron Oxide, and V_{OH}

Our observation that V_{OH} is proportional to the product of $[H_2O_2]$ and iron oxide surface area (indicated by the straight lines with a slope of 1 in Figure 3-1a) is consistent with a mechanism whose rate-limiting step involves H_2O_2 sorbed on the iron oxide surface. Although a consensus on the reaction mechanism does not exist, it is reasonable to assume that the surface reactions are analogous to those in solution:

$$\equiv Fe^{III} + H_2O_2 = \equiv Fe^{III}H_2O_2 \quad (15)$$

$$\equiv Fe^{III}H_2O_2 \rightarrow \equiv Fe^{II} + HO_2 + H^+ \quad (16)$$

$$\equiv Fe^{II} + H_2O_2 \rightarrow \equiv Fe^{III} + \bullet OH + OH^- \quad (17)$$

We assume that an identical Fe(III) site to that present in reaction 15 is regenerated by reaction 17. If reaction 16 is the rate-limiting step, then the rate of •OH production will be proportional to the concentration of $\equiv Fe^{III}H_2O_2$. If reaction 15 is fast enough to reach a pseudoequilibrium, then in accordance with the Langmuir isotherm expression:

$$\left[\equiv Fe^{III}H_2O_2\right] = \left[\equiv Fe^{III}\right]_T \frac{K_{ads}[H_2O_2]}{1 + K_{ads}[H_2O_2]} \quad (18)$$

where

$$K_{ads} = \frac{\left[\equiv Fe^{III}H_2O_2\right]}{\left[\equiv Fe^{III}\right][H_2O_2]} \quad (19)$$

and $[\equiv Fe^{III}]_T = [\equiv Fe^{III}H_2O_2] + [\equiv Fe^{III}]$. We do not expect $\equiv Fe^{II}$ to make up a significant portion of the surface sites because it is a transient species. If $K_{ads}[H_2O_2]$ is much less than 1, then eq 18 simplifies to

$$\left[\equiv Fe^{III}H_2O_2\right] = K_{ads}\left[\equiv Fe^{III}\right]_T[H_2O_2] \quad (20)$$

and V_{OH} will be proportional to the product of $[\equiv FeIII]_T$ and $[H_2O_2]$. This relationship should break down when $[H_2O_2]$ is sufficiently high for the surface to become saturated with sorbed H_2O_2 (when $K_{ads}[H_2O_2] >> 1$). We saw no evidence of this occurring at $[H_2O_2]$ as high as 3.7 M; so if this mechanism is correct, K_{ads} must be less than 0.27 M^{-1}.

Previous works have proposed that a chain reaction mechanism contributes to the decomposition of H_2O_2 and the generation of •OH in the presence of iron oxide surfaces. The chain reaction could be initiated by reactions 16 and 17 and then propagated by dissolved species (*4*, *30*). Nevertheless, we do not expect propagation of the solution chain reaction to be significant in most of the systems examined here. If the iron oxide/H_2O_2 system contains no iron complexing agents and is at pH 4 or greater, then there is very little dissolved iron because of the low solubility of Fe(III) above pH 4. Thus, the amount of hydroxyl radicals generated by reactions in the aqueous phase is likely to be negligible when compared to the amount produced at the oxide surface. We did observe evidence for a contribution of aqueous phase reactions at pH 4 at low concentrations of ferrihydrite (which is more soluble than goethite and hematite; *21*), which accounts for most of the deviation of these data points from the general trend (black circles in Figure 3-1a,b; see ref *4* for further discussion of these data points). Models including chain reaction kinetics would not be expected to yield a simple dependence of V_{OH} on the concentrations of H_2O_2 and iron oxide surface area (e.g., the models discussed in ref *4*), so our results suggest that the mechanism of •OH generation does not include a significant contribution by a chain reaction.

We graphed V_{OH} versus surface area instead of $[\equiv Fe^{III}]_T$ on the assumption that the number of sorption sites per unit surface area was a constant for each form of iron oxide.

However, goethite was better at producing •OH than hematite (Figure 3-1a) even when the same concentrations of surface area were used. (The surface areas of the two iron oxides that were measured with the N_2 BET method on dry surfaces might not be the same as the values in suspension because of, for example, changes due to drying, adsorption of water and/or solutes onto the oxide surface, and molecular size differences between N_2 and H_2O_2.) Petigara et al. (*18*) also commented on the higher reactivity of goethite, although their measurements were not normalized to surface area. This suggests that factors we did not consider, such as crystalline structure or impurities in the iron oxide, are also important in determining the •OH generation rate by affecting, for example, K_{ads} or the rate constant of reaction 16. Ferrihydrite has a greater solubility product (-log K_{sp} = 37.0-39.4) than either goethite (-log K_{sp} = 43.3-44.0) or hematite (-log K_{sp} = 42.2-43.3), and ferrihydrite (density = 3.96 g/cm^3) has a low crystallinity, whereas goethite (density = 4.26 g/cm^3) consists of edge-sharing octahedral crystals, and hematite (density = 5.26 g/cm^3) consists of edge- and face-sharing octahedral crystals (*21*). These variations between the three iron oxides could explain the differences in reactivity that we observed (Figure 3-1A). Interestingly, the decomposition of H_2O_2 by goethite and hematite has been observed to proceed at comparable rates when normalized to surface area (*11*, *14*), which implies that the yield of •OH from H_2O_2 is dependent on the type of iron oxide. We had examined this yield in our previous work, but the new data do not provide us with additional information because H_2O_2 loss was not measurable in most of our experiments.

Predicting V_{OH} and Organic Compound Degradation Rate

The success of our model prediction of the degradation rate of formic acid in the Georgetown sand at pH 4 shows that the iron oxide in a natural aquifer material with low organic matter content behaves fundamentally similar to pure iron oxide solids. However, the model prediction also illustrates the difficulty of determining the type and quantity of reactive iron oxides present in natural solids. Not all of the "crystalline" surface iron was necessarily goethite, as we assumed. Furthermore, the TiCEB extraction method may have dissolved some of the Fe present in clay minerals (*31*), so we could have (probably only slightly) overestimated the amount of crystalline surface iron in the aquifer sand. On a similar note, the effect of adsorbed silicate (*32*) and iron associated with aluminosilicates (approximately 35% of total, based on the difference between the HF-HCl-HNO_3 and TiCEB extractions, a mole fraction of 0.24 ± 0.08 Al/Fe for goethite aggregates, and a mole fraction of 0.44 ± 0.14 Al/Fe for amorphous iron; *33*)

on V_{OH} was unclear. While the surface reactivity of the iron oxides could be influenced by the presence of Al and/or adsorbed silicate, it is more certain that the close association between the two natural oxides and the adsorbed silicate reduced the amount of surface area, i.e., the number of reactive Fe sites, which was exposed to H_2O_2. This implies that the data points in Figure 3A should be closer to the predicted V_{OH} values. We chose the approach of using a range of possible goethite surface areas even though it is less satisfactory because it is difficult to obtain the actual value of this parameter.

To test the general applicability of our model, we also compared V_{OH} and organic compound oxidation rates observed in previous studies under a wide variety of conditions to our model's predictions. Since our model only predicts the oxidation rate of aqueous phase compounds by •OH, we considered only studies in which sorption of the organic compound was reported to be minor and in which the aqueous concentrations of the organic compound were measured. In other studies of iron oxide/H_2O_2 systems, the loss of hydrophobic compounds over time was measured using extraction techniques that detected the total (aqueous plus nonaqueous) quantity of the compounds remaining in the slurry.

To generate the predictions, we needed to assume that V_{OH} would not be affected by pH. This is not intuitive given that pH would be expected to control the extent of formation of a surface H_2O_2 complex, as observed for the solution complex of Fe(III) and H_2O_2 (*3*). Nevertheless, three studies found that V_{OH} was relatively invariant from pH 4 to pH 10, a range that encompasses almost all of the studies that were compared to our model: one in goethite/H_2O_2 systems from pH 5 to pH 9 (*8*), one in lepidocrite/H_2O_2 systems at initial pH values of 6.0 and 10.0 (*12*), and one in goethite-silica sand/H_2O_2 systems from pH 4 to pH 7 (*16*). At low pH values, proton-promoted dissolution of Fe from the oxide surface, as observed by Chou and Huang in their experiment at an initial pH value of 3.2 (*12*), could increase the importance of the solution phase chain reaction (*4*). It is unknown if there is a pH effect above pH 10.

When we compare V_{OH} values gathered from the literature (Table 3-1) to our predictions (Figure 3-4), our predictions were within a factor of 10 for slightly more than half of the measurements. All four publications measured V_{OH} with a nonsorbing probe and provided us with information about the type and amount of iron oxide plus the starting H_2O_2 concentration. Only in one study, however, was the iron oxide's surface area measured. For both studies by

Watts et al., the calculations that we did were based on the surface area reported in their other publications (*13*, *34*), which we assumed used the same iron oxides. For modeling the data from Petigara et al. (*18*), who examined natural soils, we took the approach used for the Georgetown sand, using typical ranges of surface area for goethite and hematite in the model.

Interestingly, our understanding of the relationship between $[H_2O_2]$ and V_{OH} contrasts with that of Watts et al. (*9*), who observed that the V_{OH} of hematite at pH 3 remained approximately constant as $[H_2O_2]_0$ increased from 0.1 to 5% (black circles in Figure 3-4). There is no obvious difference between the conditions of their experiments and ours, which were performed at similar concentration of H_2O_2 (0.03-1.6 vs 0.01-2 M) and surface area (9.6 vs 10 m^2/L). However, the V_{OH} values reported by Watts et al. (*9*), determined with nitrobenzene as the •OH probe and 2-propanol added as an additional •OH sink, were in some cases much greater than the decomposition rates of H_2O_2 measured in separate experiments at the same concentrations of H_2O_2 and hematite but without nitrobenzene and 2-propanol. The ratio of moles of •OH created to moles of hydrogen peroxide consumed can, at most, be 1:1. One possible explanation of this discrepancy is that Watts et al. (*9*) might have measured a fast initial production of •OH in their probe experiments, while their observations of H_2O_2 decomposition rates took place on a time scale of 1-3 days (more comparable to those of our experiments). Another possibility is that their probe or sink compounds affected V_{OH}. In contrast, our predictions agreed very well with the V_{OH} measurements in their other work using lower concentrations of the same probe but 1-octanol as the major •OH sink (*16*) (white triangles in Figure 3-4). The other two studies on V_{OH} included natural materials besides pure iron oxides. While our predictions generally agreed with the observations of Petigara et al. (*18*), we overestimated those reported by Huling et al. (*17*).

To further examine our model, we compared the pseudo-first-order loss rates of organic compounds (k_{org}) observed in a variety of systems (Table 3-2) with our predictions (Figure 3-5). (In every study except the one by Huling et al. (*19*), both the organic compound and H_2O_2 were initially important •OH sinks.) Our predictions successfully predicted the values of k_{org} measured by Lin and Gurol (*8*) but overpredicted the values of k_{org} observed in the other studies. We selected these six studies because they satisfied our criteria that the compound that was tracked is highly water-soluble and that the studies report most of the measurements of the parameters that our model needs to estimate V_{OH} and k_{org}: amount of H_2O_2, surface area, type and amount of iron

oxide, concentration of the major •OH sinks and organic compound in the system, and rate constants of their respective reactions with •OH. (We used a composite rate constant for the reaction between the organic compound and •OH if we needed to account for acid-base speciation of the organic compound at the specified pH.) Four of them, however, did not have values for the surface area of the iron oxide because they either used natural aquifer material or did not measure it, so we treated this deficiency in the same way as before.

When other solutes were present, their possible influence on k_{org} was considered. We included carbonate as a hydroxyl radical sink in calculating k_{org} when it was reported to be present (*11*, *36*, *37*), but its effect was insignificant. The fast reaction of Cl^- with •OH makes it a candidate as an important •OH scavenger in the studies done by Valentine and Wang (*11*) and Huling et al. (who included the reaction of Cl^- and •OH in their model of 2-Chlorophenol degradation; *19*). However, when •OH combines with chloride, the resulting intermediate can either dissociate back to the reactants or react with a proton to form a chlorine atom:

$$\bullet OH + Cl^- \rightarrow \bullet ClOH^- \quad (21)$$

$$\bullet ClOH^- \rightarrow \bullet OH + Cl^- \quad (22)$$

$$\bullet ClOH^- + H^+ \rightarrow Cl + H_2O \quad (23)$$

The respective rate constants of reactions 21-23 are 4.3×10^9 M^{-1} s^{-1}, 6.1×10^9 s^{-1}, and 2.1×10^{10} M^{-1} s^{-1} (*35*). A comparison of the rates of reactions 22 and 23 indicates that chloride should not be the major sink of •OH above pH 2 because reaction 22, the reverse of reaction 21, is then the dominant decomposition pathway of $\bullet ClOH^-$. We observed no difference in the decomposition rates of $H^{14}COOH$ and H_2O_2 in solutions with and without 1 mM NaCl (data not shown; other experimental conditions were pH 4, 1 mM H_2O_2, 100 nM $H^{14}COOH$, 10 mM $NaClO_4$, and 1 μM Fe(III) or 21 mg/L ferrihydrite), confirming chloride's ineffectiveness as an •OH sink at pH 4.

The possible effects of other system components are more difficult to predict, but they are likely to be unimportant. Sulfate is known to adsorb onto iron oxides, yet we did not find any connection between its presence and the deviations in our predictions. This is consistent with the results of Watts et al. (*16*), who observed similar V_{OH} values in experiments using unstabilized H_2O_2 or H_2O_2 containing 27.3 g/L $(NH_4)_2SO_4$ and 28.6 g/L $NaH_2PO_4 \bullet 7H_2O$. Finally, although natural organic matter could inhibit catalytic sites on the iron oxide or act as a radical sink, very little of it (<0.1%) was present in the natural materials that were used in the studies considered here.

There are three principal explanations for the disagreements between our predictions and the measurements. First, we do not have a complete understanding of all of the factors that determine the reactivity of an iron oxide. Hence, our model cannot always make accurate predictions, especially when the iron oxide is not in a pure form (e.g., associated with soil components or contains impurities) or when it is one that we did not examine, as illustrated by the large deviations between our estimates and those measured by Chou and Huang (*12*; black circles in Figure 3-5). They determined that their brick grain-supported iron oxide was lepidocrocite (γ-FeOOH), and we used goethite (α-FeOOH) in our model as an approximation. If the reactivity of lepidocrocite were instead similar to that of hematite, our predictions would be within 1 order of magnitude of the reported values. This reasoning also applies to the Valentine and Wang experiment (*11*) that used a semicrystalline iron oxide, which we assumed was equivalent to our ferrihydrite.

The second possible cause is that the compound being degraded or its oxidation products could interfere with the generation of •OH. The oxidation products of many of the aromatic compounds used in these studies are capable of complexing iron and, therefore, could also form complexes on the surfaces of iron oxides. Salicylic acid, for example, is a product of the oxidation of benzoic acid by •OH (*38-40*). We chose formic acid as our •OH probe to avoid the possibility of Fe reacting with the probe compound or its oxidation product.

Last, it is possible that unknown compounds associated with the solids in some of these systems were the main sinks of radicals. Miller and Valentine proposed that the oxide surface in their aquifer material competed with H_2O_2 and quinoline (or phenol, in a later study) for •OH and other radicals to explain the lack of increase in the decomposition rate of quinoline (or phenol) with an increase in the amount of solids at constant [H_2O_2] (*36*, *37*). Reactions representing this phenomenon were included in the mechanism that they used to successfully model the loss of quinoline and phenol in the presence of aquifer material and H_2O_2. However, we saw no evidence for similar reactions in our aquifer sand experiments.

In summary, we focused our study on determining the factors that affect V_{OH} in iron oxide/H_2O_2 systems and showed that if we know V_{OH} and the reaction rates of the important •OH sinks in the system, the oxidation rate of dissolved organic compounds can be predicted. The simple proportionality we observed between V_{OH} and the product of H_2O_2 and iron oxide surface area concentrations in our slurries suggests that it will be possible to predict organic compound

oxidation rates under a wide variety of conditions.

Nevertheless, application of our model to previous studies showed mixed results in its ability to make accurate predictions. The main reason for this may have been that, in most of these cases, the amount and reactivity of the iron oxide present was not precisely known (and in the case of natural solids, difficult to determine). Instead of trying to quantify the surface area and type of iron oxide present in a natural solid, an easier and probably more precise approach would be to measure V_{OH} at one $[H_2O_2]$ and solid concentration to find the proportionality factor M in the general relationship:

$$V_{OH} = M[H_2O_2][\text{solid concentration, e.g., g of solid/L}] \quad (24)$$

This approach should be effective for a wide range of concentrations of the organic compound, H_2O_2, and solid and would have accurately predicted the results of our experiments with the Georgetown sand, except at very low concentrations of H_2O_2.

More work is required to determine if other factors complicate our attempts to formulate a generally applicable model. Some compounds associated with natural solid material could act as the main radical sink. If this phenomenon is generally observed, then the importance of this mechanism will also need to be quantified experimentally for each material. It is conceivable that organic compounds and other solutes can affect V_{OH} via unknown mechanisms. Unlike most of the other studies we attempted to model, our data were obtained in systems containing no other solutes besides H_2O_2 and a probe compound, formic acid, that is highly water-soluble, does not complex iron, or sorb onto iron oxides and whose oxidation product, CO_2, also has these properties. If a wide range of solutes, especially the varied and poorly characterized oxidation products of organic contaminants, are found to significantly affect V_{OH}, then our ability to make general predictions will clearly be limited.

Further work is also needed to better understand several other important factors that control the oxidation rate of organic compounds. In cases where sorption is significant, we must consider the possibilities that the desorption rate could control the aqueous concentrations of the organic compound and that it could be oxidized at the surface or in the surface boundary layer at rates different from those in the bulk solution. In cases where H_2O_2 degradation is not slow as compared to the time needed for decomposition of the organic compound, for example, in soils that have rapid, nonradical-producing H_2O_2 sinks (*18*), accurate predictions of H_2O_2 decomposition rates will be necessary for successful application of our model.

Acknowledgments

This work was funded by a Gilbert Winslow Career Development Chair and by a grant from the American Chemical Society's Petroleum Research Fund.

Literature Cited

(1) Buxton, G. V.; Greenstock, C. L.; Helman, W. P.; Ross, A. B. *J. Phys. Chem. Ref. Data* **1988**, *17*, 513-886.

(2) Bielski, B. H. J.; Cabelli, D. E.; Arudi, R. L.; Ross, A. B. *J. Phys. Chem. Ref. Data* **1985**, *14*, 1041-1100.

(3) De Laat, J.; Gallard, H. *Environ. Sci. Technol.* **1999**, *33*, 2726-2732.

(4) Kwan, W. P.; Voelker, B. M. *Environ. Sci. Technol.* **2002**, *36*, 1467-1476.

(5) Watts, R. J.; Udell, M. D.; Rauch, P. A.; Leung, S. W. *Hazard. Waste Hazard. Mater.* **1990**, *7*, 335-345.

(6) Tyre, B. W.; Watts, R. J.; Miller, G. C. *J. Environ. Qual.* **1991**, *20*, 832-838.

(7) Khan, A. J.; Watts, R. J. *Water Air Soil Pollut.* **1996**, *88*, 247-260.

(8) Lin, S.-S.; Gurol, M. D. *Water Sci. Technol.* **1996**, *34*, 57-64.

(9) Watts, R. J.; Jones, A. P.; Chen, P.-H.; Kenny, A. *Water Environ. Res.* **1997**, *69*, 269-275.

(10) Kong, S. H.; Watts, R. J.; Choi, J. H. *Chemosphere* **1998**, *37*, 1473-1482.

(11) Valentine, R. L.; Wang, H. C. A. *J. Environ. Eng.* **1998**, *124*, 31-38.

(12) Chou, S.; Huang, C. *Chemosphere* **1999**, *38*, 2719-2731.

(13) Watts, R. J.; Udell, M. D.; Kong, S. H.; Leung, S. W. *Environ. Eng. Sci.* **1999**, *16*, 93-103.

(14) Huang, H.-H.; Lu, M.-C.; Chen, J.-N. *Water Res.* **2001**, *35*, 2291-2299.

(15) Pardieck, D. L.; Bouwer, E. J.; Stone, A. T. *J. Contam. Hydrol.* **1992**, *9*, 221-242.

(16) Watts, R. J.; Foget, M. K.; Kong, S.-H.; Teel, A. L. *J. Hazard. Mater.* **1999**, *69*, 229-243.

(17) Huling, S. G.; Arnold, R. G.; Sierka, R. A.; Miller, M. R. *Water Res.* **2001**, *35*, 1687-1694.

(18) Petigara, B. R.; Blough, N. V.; Mignerey, A. C. *Environ. Sci. Technol.* **2002**, *36*, 639-645.

(19) Huling, S. G.; Arnold, R. G.; Jones, P. K.; Sierka, R. A. *J. Environ. Eng.* **2000**, *126*, 348-353.

(20) Wells, M. L.; Mayer, L. M.; Guillard, R. R. L. *Mar. Chem.* **1991**, *33*, 23-40.

(21) Schwertmann, U.; Cornell, R. M. *Iron Oxides in the Laboratory*; VCH: New York, 1991.

(22) Holmén, B. A. Ph.D. Thesis, Massachusetts Institute of Technology, Cambridge, MA, 1995.

(23) Holmén, B. A.; Gschwend, P. M. *Environ. Sci. Technol.* **1997**, *31*, 1, 105-113.

(24) McLaren, A. D. *Soil Biol. Biochem.* **1969**, *1*, 63-73.

(25) Bader, H.; Sturzenegger, V.; Hoigné, J. *Water Res.* **1988**, *22*, 1109-1115.

(26) Voelker, B. M.; Sulzberger, B. *Environ. Sci. Technol.* **1996**, *30*, 1106-1114.

(27) Zepp, R. G.; Faust, B. C.; Hoigne´, J. *Environ. Sci. Technol.* **1992**, *26*, 313-319.

(28) Harris, D. C. *Quantitative Chemical Analysis*; W. H. Freeman and Company: New York, 1991.

(29) Cornell, R. M.; Schwertmann, U. *The Iron Oxides: Structure, Properties, Reactions, Occurrence and Uses*; VCH Publishers: New York, 1996.

(30) Lin, S.-S.; Gurol, M. D. *Environ. Sci. Technol.* **1998**, *32*, 1417-1423.

(31) Ryan, J. N.; Gschwend, P. M. *Clays Clay Miner.* **1991**, *39*, 509-518.

(32) Swartz, C. H.; Gschwend, P. M. *Environ. Sci. Technol.* **1998**, *32*, 1779-1785.

(33) Swartz, C. H.; Ulery, A. L.; Gschwend, P. M. *Geochim. Cosmochim. Ac.* **1997**, *61*, 707-718.

(34) Watts, R. J.; Udell, M. D.; Monsen, R. M. *Water Environ. Res.* **1993**, *65*, 839-844.

(35) Jayson, G. G.; Parsons, B. J.; Swallow, A. J. *J. Chem. Soc., Faraday Trans. 1* **1973**, 1597-1607.

(36) Miller, C. M.; Valentine, R. L. *Water Res.* **1995**, *29*, 2353-2359.

(37) Miller, C. M.; Valentine, R. L. *Water Res.* **1999**, *33*, 2805-2816.

(38) Armstrong, W. A.; Black, B. A.; Grant, D. W. *J. Phys. Chem.* **1960**, *64*, 1415-1419.

(39) Loeff, I.; Swallow, A. J. *J. Phys. Chem.* **1964**, *68*, 2470-2475.

(40) Zhou, X.; Mopper, K. *Mar. Chem.* **1990**, *30*, 71-88.

Table 3-1. Relevant information from the publications used in Figure 3-4.

Ref	$[Probe]_0$ (μM)	$k_{OH,\ compound}$ (10^{-9} M^{-1} s^{-1})	$[H_2O_2]_0$ (mM)	pH	Catalyst	Surface area conc. (m^2/l)	Solutes
9	Nitrobenzene: 3000	3.9	32, 320, 640, 1600	3	Hematite	9.6*	0.3 M 2-propanol, > 1 mM SO_4^{2-}
16	Nitrobenzene: 1.5	3.9	2.94	4-7	Goethite-silica sand	24.3**	30 μM 1-octanol, < 1 mM SO_4^{2-}
17	4POBN†: 665, 490	3.8	140, 130	5.7, 5.9	Goethite-silica sand	110	0.25 mM SO_4^{2-}
18	††	N/A	0.040	4-5‡	Goethite or hematite in natural soils	0.2-4.5, 8.2-204, 10.7-266.4, 1.8-79.6***	None

*Estimated using the surface area value from ref *13*.

**Estimated using the surface area value from ref *34*.

***Estimated using the typical range of surface area for goethite (8-200 m^2/g) and hematite (2-90 m^2/g) (*29*).

†α-(4-pyridyl-1-oxide)-*n*-tert-butylnitrone

††Petigara et al. used excess dimethyl sulfoxide to react with •OH to make a methyl radical that is trapped by 3-amino-2,2,5,5-tetramethyl-1-pyrrolidinyloxy to form a stable *O*-methylhydroxylamine.

‡Buffering to pH 7.4 with 0.1 M phosphate had no effect on V_{OH}.

Table 3-2. Relevant information from the publications used in Figure 3-5.*

Ref	Figure(s) examined	$[Compound]_0$ (μM)	$k_{OH,\ compound}$ ($10^{-9}\ M^{-1}\ s^{-1}$)	$[H_2O_2]_0$ (mM)	pH	Catalyst	Surface area conc. (m^2/l)	Solutes
36	7, all points	Quinoline: 81	9.28	54.0	7.8	Sandy Aquifer Material	3.8 – 96**	5 mM $NaHCO_3$ 3 mM Na_2SO_4 2 mM $CaCl_2$ 1 mM NaCl
8	1, all points†	Butyl chloride: 80	3.4	1.3, 2.2, 5.0, 10	7.5	Goethite	4 – 100**	Not reported
11	4b and 4c, 0-500 min	Quinoline: 78	9.28	14.7	7.0	Semi-Crystalline iron oxide, goethite	55.2, 146.8	5 mM $NaHCO_3$ 3 mM Na_2SO_4 2 mM $CaCl_2$ 1 mM NaCl
12	2a, all points; 3b, all points prior to the turning point	Benzoic acid: 950, 877	pH 3.2: 4.4 pH 6, 10: 5.9	5.88, 11.8, 23.5, 47.06	3.2, 6, 10	Lepidocrocite on a brick grain support	65.3	Not reported
37	6, all time points	Phenol: 110	6.60	58	7.6	Natural metal oxide-coated materials	2 – 52, 5 – 130, 10 – 260**	5 mM $NaHCO_3$ 3 mM Na_2SO_4 2 mM $CaCl_2$ 1 mM NaCl
19	Table 2	4POBN: 1060 2CP‡: 320, 350, 510, 530	4POBN: 3.8 2CP: 12	140	6.0	Goethite-silica sand	110***	0.25 mM SO_4^{2-}

*Some figures in some of the references were not evaluated due to complexities involving, for example, phosphate or humic acid.

**Estimated using the typical range of surface area for goethite (8-200 m^2/g) (*29*).

***Estimated using the surface area value from ref *17*.

[†]To account for the significant sorptive loss of butyl chloride (~35%), we calculated the decomposition rate of butyl chloride by subtracting the amount lost due to sorption from the concentration that remained at each time point.

[‡]2-Chlorophenol

Figure 3-1a. V_{OH} of three different iron oxides plotted as a function of the amount of surface area and hydrogen peroxide at pH 4. Ferrihydrite concentrations varied from 6-400 μM, with $[H_2O_2]_0$ ≤ 1 mM (●) and ≥ 5 mM (○); goethite concentrations of 0.02 (◈), 0.2 (◆), and 0.6 g/L (◇), and hematite concentrations of 0.2 (▲) and 1 g/L (△) are also shown. The initial concentration of formic acid for all experiments was 74-244 nM. The lines are regression fits of the data to eq 10-12.

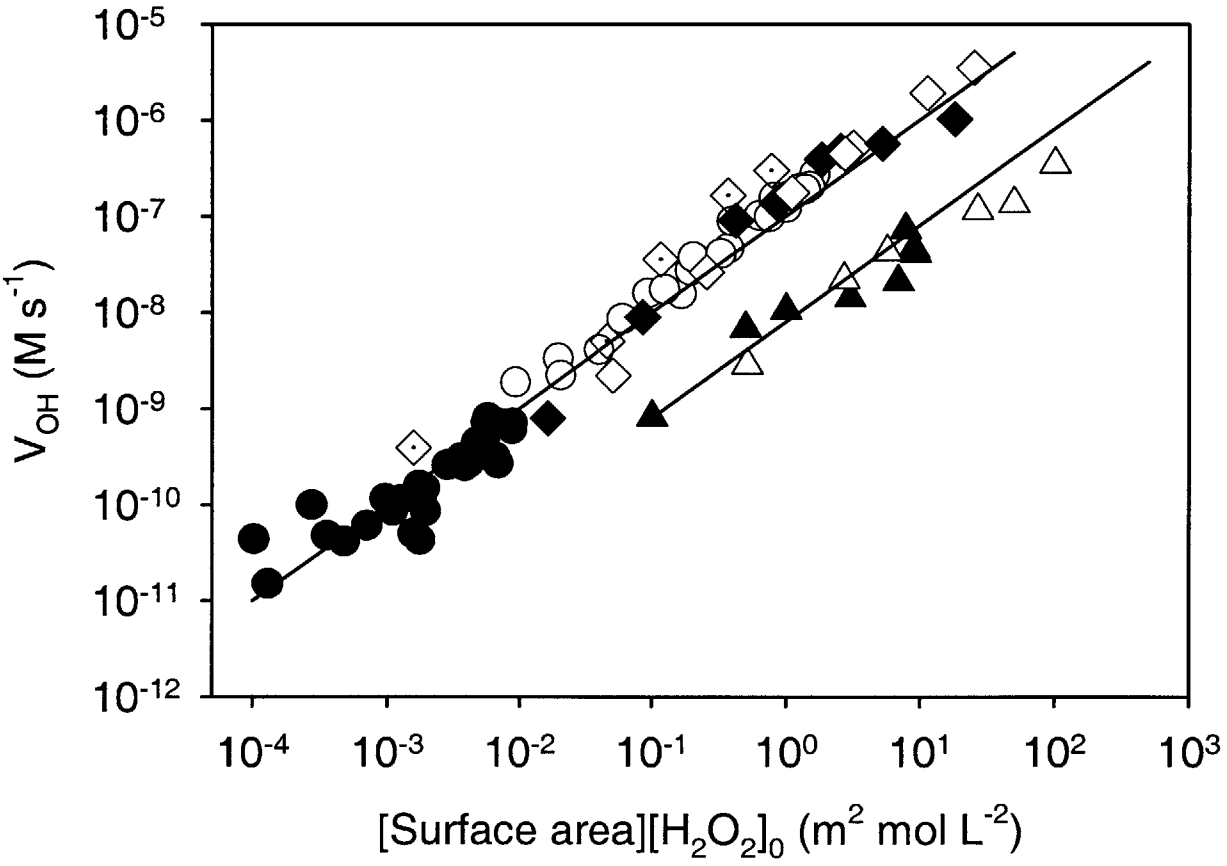

Figure 3-1b. Decomposition rate of formic acid in the experiments described in Figure 3-1a (same symbols), normalized to the concentration of total Fe and plotted as a function of the initial amount of hydrogen peroxide. The lines are the expected values based on the regressions.

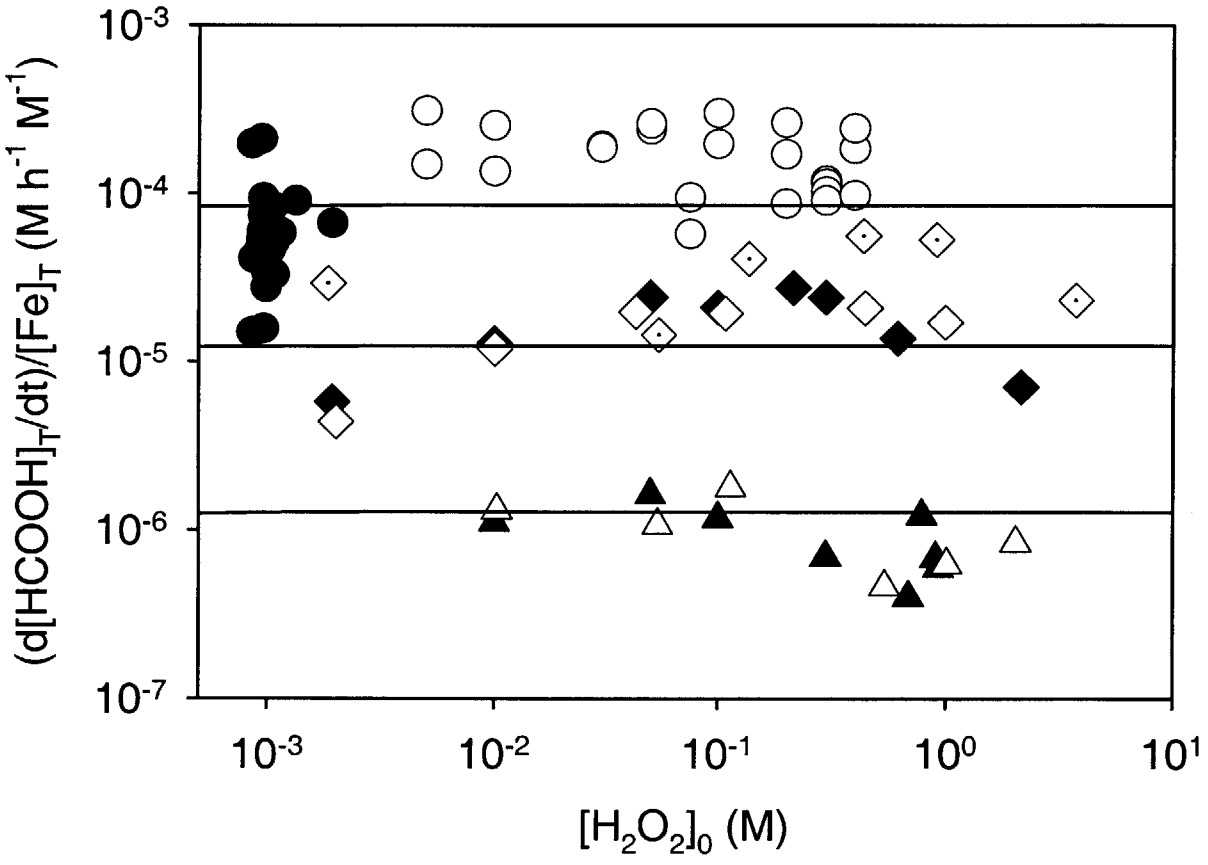

Figure 3-2a. V_{OH} from experiments containing 0.6 g/L of goethite with either H_2O_2 ($[HCOOH]_{T,0}$ = 100 nM (◇) or 50 μM (⬢)) or formic acid ($[HCOOH]_{T,0}$ = 50 μM (□), 0.3 mM (■) or 10 mM (▼)) as the dominant •OH sink at pH 4. The line is the predicted V_{OH} calculated from eq 10.

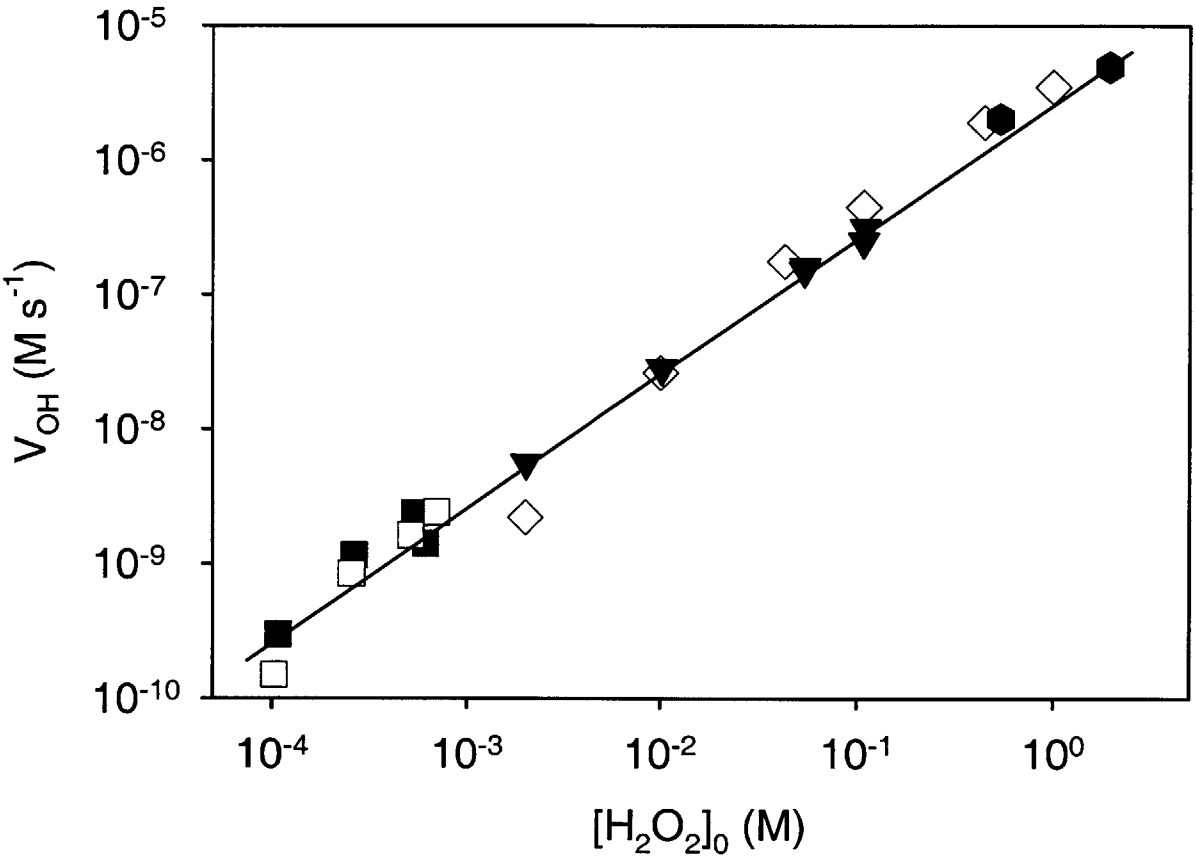

Figure 3-2b. Decomposition rate of formic acid in the experiments described in Figure 3-2a (same symbols), normalized to the concentration of total Fe and plotted as a function of the initial amount of hydrogen peroxide. The data for $[HCOOH]_{T,0}$ = 100 nM is the same as Figure 3-1b. The lines are the expected $(d[HCOOH]_T/dt)/[Fe]_T$ for each starting amount of formic acid, given the calculated V_{OH} shown in Figure 3-2a.

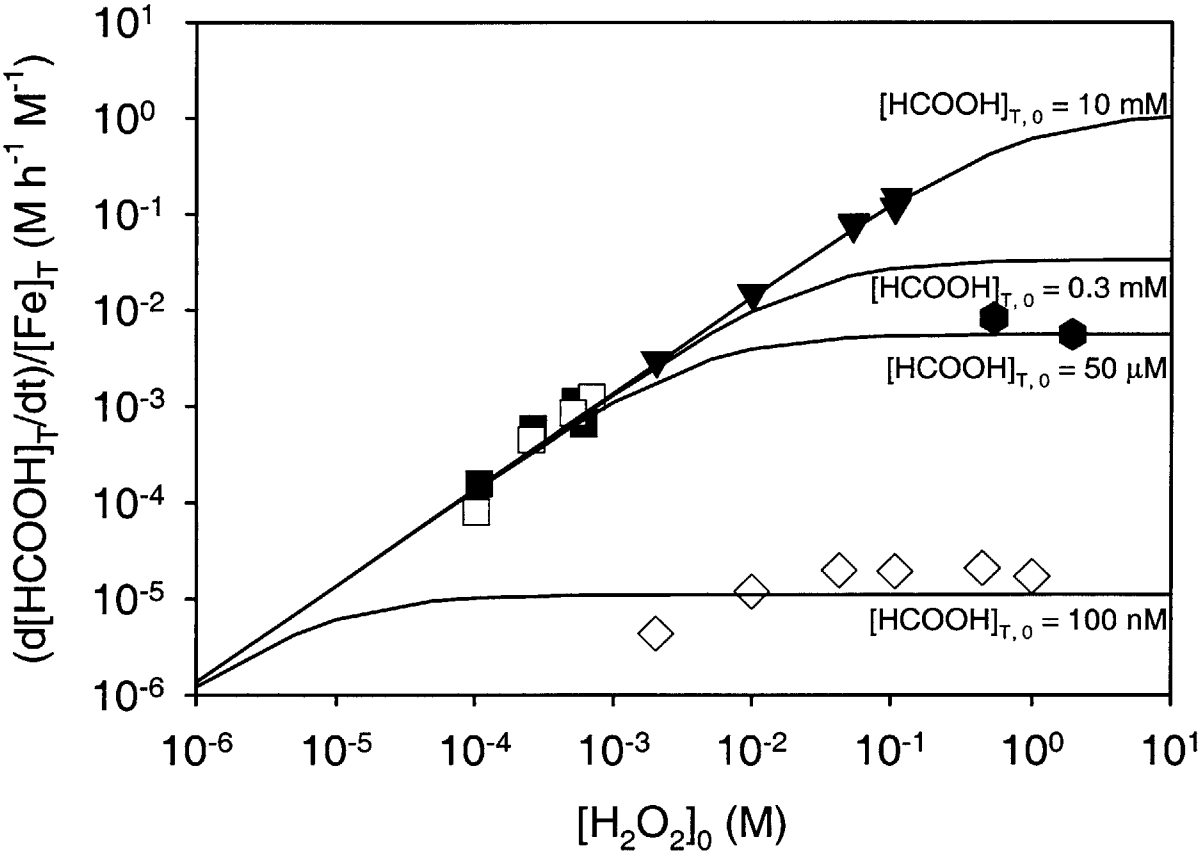

Figure 3-3a. V_{OH} from experiments at pH 4 with H_2O_2 as the dominant •OH sink and either 25 (●) or 60 g/L (▽) of sand and with formic acid as the dominant •OH sink and 60 g/L of sand (■). We assumed that all of the crystalline surface iron in the sand was goethite, and plotted all of the data points using a surface area of 40 m^2/g, with a range of 8-200 m^2/g depicted by the error bars. The line is the predicted V_{OH} calculated from eq 10.

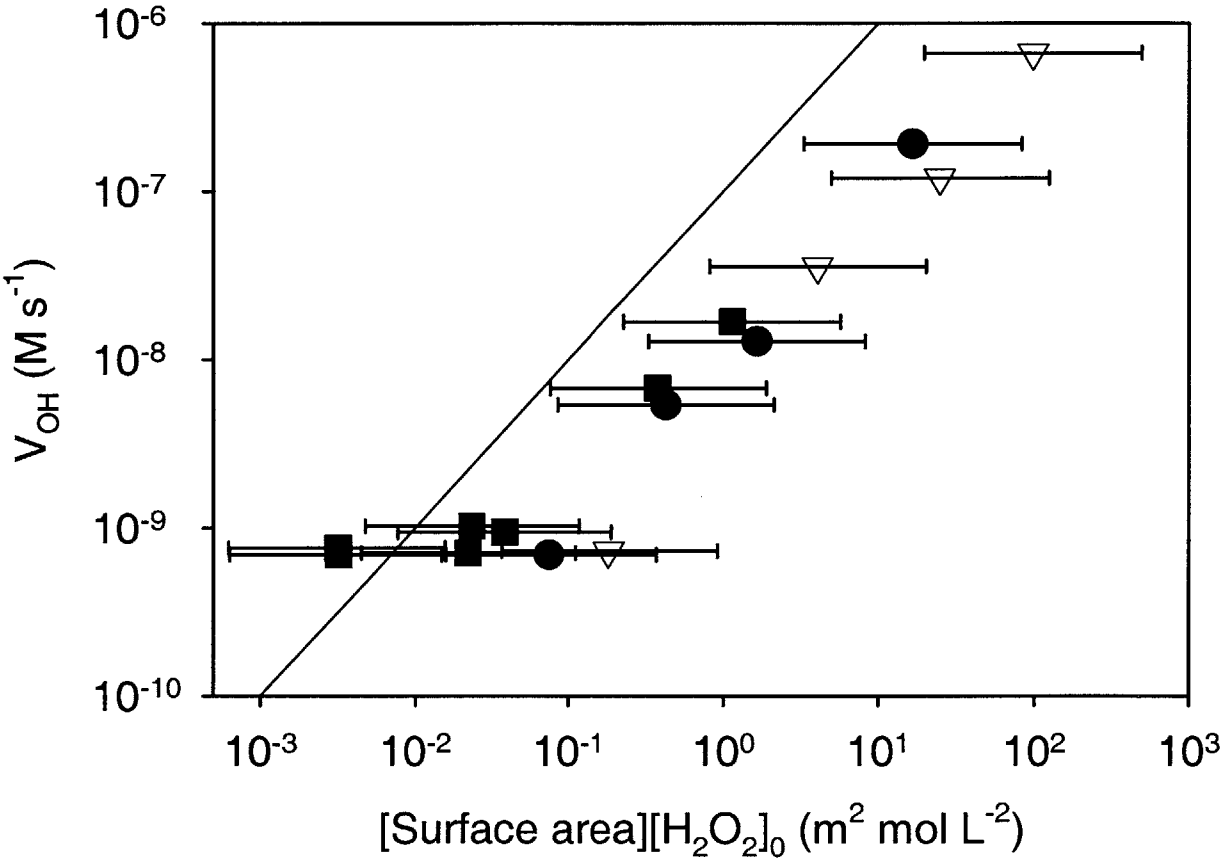

Figure 3-3b. Decomposition rate of formic acid in the experiments described in Figure 3-3a (same symbols), normalized to the concentration of total Fe and plotted as a function of the initial amount of hydrogen peroxide. The two sets of dashed lines represent the possible range of predicted values for the two systems, assuming that all of the crystalline iron in the sand was goethite, with a surface area ranging from 8 to 200 m^2/g.

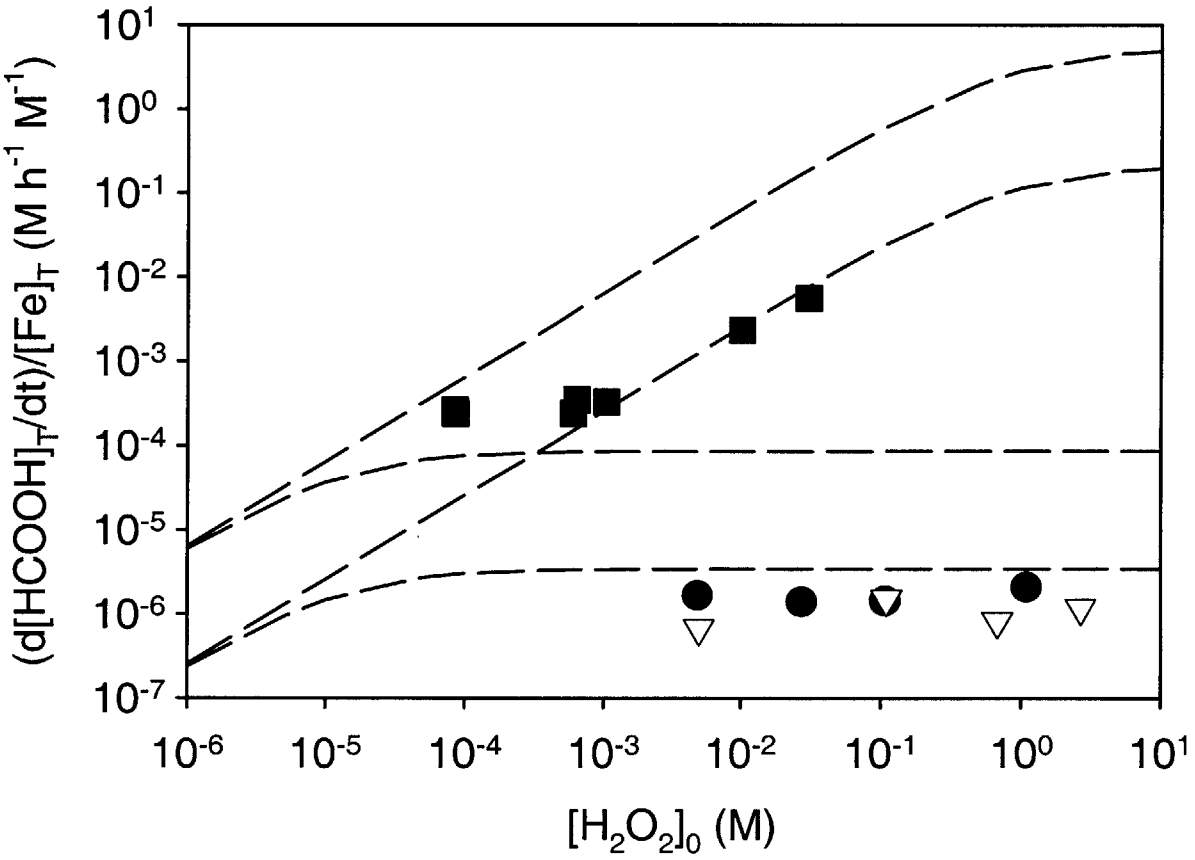

Figure 3-4. Comparison of measured V_{OH} from refs *9* (●), *16* (▽), *17* (■), and *18* (◇), versus our predictions. The line represents perfect agreement between predicted and measured V_{OH} values. Petigara et al. (*18*) did not have measurements of the surface area of their iron oxide because they used natural soils. Thus, we estimated the V_{OH} values using typical ranges of surface areas for goethite and hematite and presented the results with error bars.

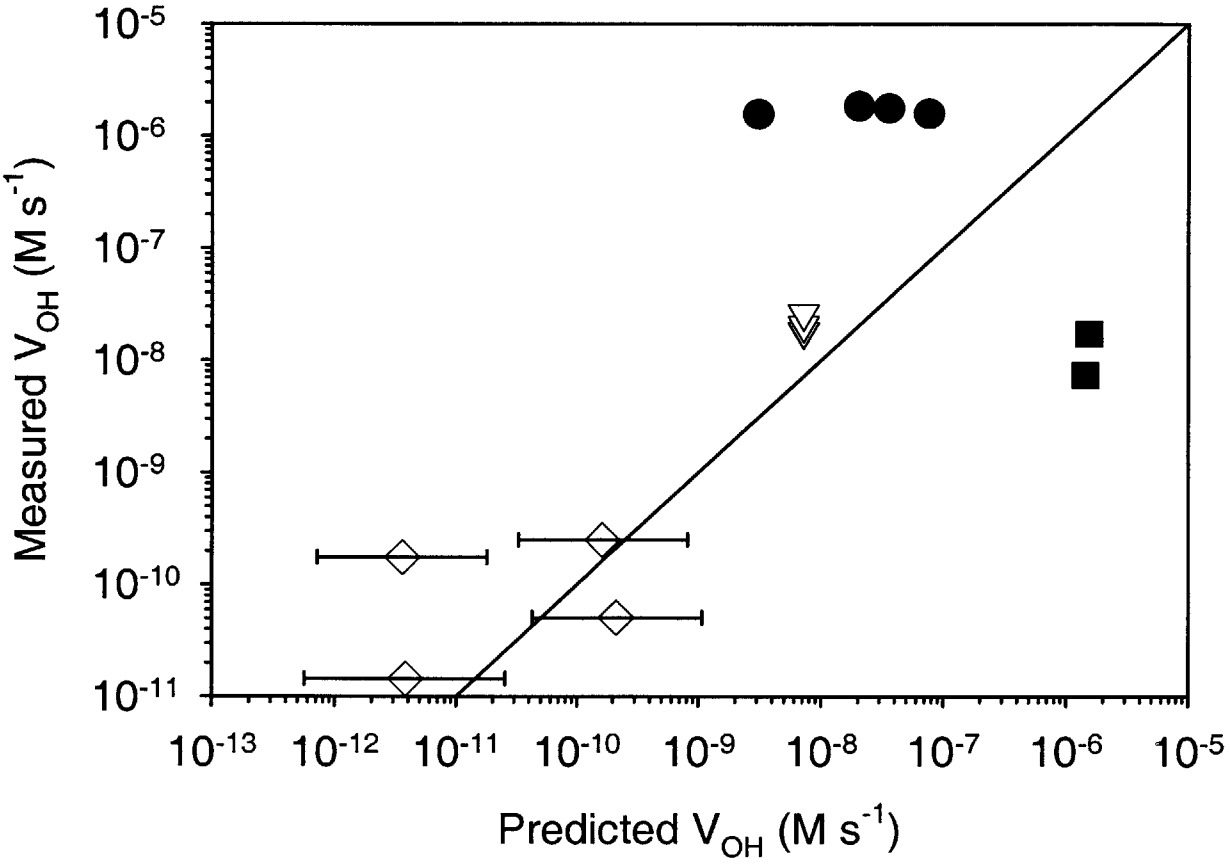

Figure 3-5. Comparison of the measured pseudo-first-order loss rate of various organic compounds, obtained from refs *36* (▼), *8* (○), *11* (▽), *12* (●), *37* (□), and *19* (■), versus our predictions. The line represents perfect agreement between predicted and measured k_{org} values. The error bars show the range of estimated k_{org} values using typical ranges of surface areas for goethite in studies where the surface area was not measured.

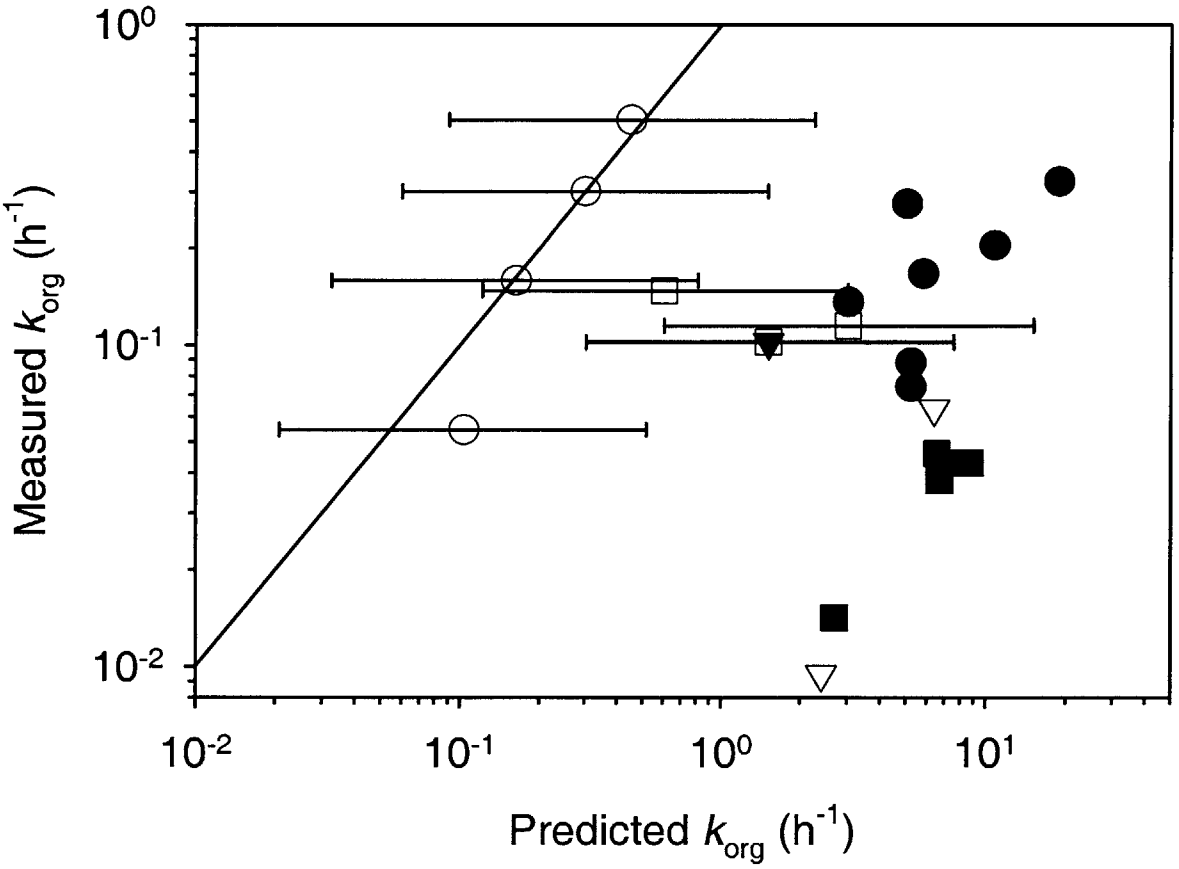

Chapter 4: Influence of Electrostatics on the Oxidation Rates of Organic Compounds in Heterogeneous Fenton Systems

or

-There is electricity in the air…and on the iron oxide-

Abstract

The objective of this work was to refine our model for predicting the pseudo-first-order oxidation rate coefficient of any dissolved organic compound (k_{org}) in systems where hydroxyl radicals (•OH) are produced by the iron oxide-catalyzed decomposition of hydrogen peroxide (H_2O_2). We investigated three hypotheses that could explain why our model overpredicted many of the k_{org} values that other investigators observed in systems containing iron oxide and H_2O_2: (1) there is a substantial difference in reactivity between our laboratory synthesized iron oxide and natural ores, (2) the electrostatic attraction between formate anions and the positively charged oxide surface caused ^{14}C-labeled formic acid, our •OH probe, to detect a greater concentration of •OH than the amount that reacts with neutral compounds, and (3) the organic compound being degraded or its oxidation products interfered with the •OH generation process at the oxide surface. Results from various experiments at pH 4 containing goethite, $H^{14}COOH$, and 2-Chlorophenol (2-CP) showed that our goethite had similar reactivity as natural goethite, and that electrostatic effects were important because $H^{14}COOH$ detected more •OH than 2-CP did in the same system. We also observed that the concentrations of •OH measured by $H^{14}COOH$ decreased with time, whereas the amount of •OH detected by 2-CP remained constant. This was attributed to the loss of positive charge on the oxide surface as the oxidation products of 2-CP complexed surface Fe species. There was no evidence that the oxidation products of 2-CP interfered with the •OH generation process at the concentrations of goethite that we used.

Introduction

The hydroxyl radical (•OH) reacts rapidly with numerous compounds (*1*) and is the key chemical species in many advanced oxidation processes to treat wastewater and polluted aquifers. There are various ways to create •OH in solution (*2-4*), including the use of iron oxide and hydrogen peroxide (H_2O_2). Although the iron oxide catalyzed mechanism is not yet fully understood, it most likely contains these reactions,

$$\equiv Fe^{III} + H_2O_2 = \equiv Fe^{III}H_2O_2 \quad (1)$$

$$\equiv Fe^{III}H_2O_2 \rightarrow \equiv Fe^{II} + HO_2 + H^+ \quad (2)$$

$$\equiv Fe^{II} + H_2O_2 \rightarrow \equiv Fe^{III} + \bullet OH + OH^- \quad (3)$$

where ≡Fe is a surface iron species. This system has been researched recently (*5-14*) because it can effectively catalyze the oxidation of different organic contaminants at circumneutral pH, whereas Fenton's reagent (Fe(II) + H_2O_2) is typically applied at low pH to ensure the Fe remains

dissolved throughout the entire remediation process. Therefore, using iron oxide instead of dissolved iron to treat contaminated aquifers would be advantageous when it would be difficult or destructive to lower the pH of the groundwater.

While there has been much research on the mechanism and factors that affect hydrogen peroxide and organic compound decomposition in the presence of iron oxide (*4, 5, 7-10, 12, 14-18*), none of them adequately answered the need for a general model that can predict the oxidation rate of any organic compound (k_{org}) in this system. We addressed this issue in a previous work (*14*) by creating a model that predicts the oxidation rate of any dissolved compound in an iron oxide/H_2O_2 system based on the generation rate of •OH (V_{OH}) and the reaction rate constants of the system's constituents with •OH. The model uses the following parameters to estimate the pseudo-first-order rate coefficient of oxidation of an organic compound: the surface area, type and amount of iron oxide, the concentrations of H_2O_2, organic compound and other important •OH sinks in the system, and their respective second-order rates with •OH. It successfully predicted the degradation rate of formic acid that we measured in sand from Georgetown at pH 4, but overpredicted many of the k_{org} values reported by other investigators who examined contaminant loss in iron oxide/H_2O_2 systems. We proposed potential explanations for the disagreements between our model predictions and the measured k_{org} values.

The first hypothesis was that there was a difference in reactivity between our laboratory synthesized iron oxide and those obtained from natural sources. These differences could be due to, for example, the presence of impurities or soil components that were associated with the natural iron oxide. If this were the case, then it could be difficult to create a generally applicable model to estimate the oxidation rate of any organic compound in an iron oxide/H_2O_2 system since every solid could have unique characteristics. A more practical approach would be to measure V_{OH} using one concentration of H_2O_2 and the solid of interest, and then apply our demonstrated linear proportionality between V_{OH}, [H_2O_2] and solid concentration (*14*) to extrapolate to conditions of interest.

The second possible explanation was electrostatics. Although we believed that this was not an important issue in our previous studies (*14*), we now think electrostatics could have affected the decomposition rate of formate. In this case, our predicted k_{org} values for neutral compounds would have to be adjusted. When oxides or oxyhydroxides are in an aqueous

solution, the surface hydroxyl groups can undergo proton exchange with the surrounding media and possibly acquire a surface charge:

$$\equiv FeOH_2^+ = \equiv FeOH + H^+ \quad (4)$$

$$\equiv FeOH = \equiv FeO^- + H^+ \quad (5)$$

The magnitude and sign of the charge can be determined qualitatively based on the pH of the solution and the equilibrium constants of reactions 4 and 5. The goethite surface has a net positive charge at our experimental pH of 4, so formate anions would be attracted toward the oxide surface where •OH is being produced. This would cause the actual loss rate of $H^{14}COOH$ to be greater than the value computed from bulk solution properties. On the other hand, neutral compounds are unaffected by the presence of surface charge, so a model based on formate decomposition rates could overpredict k_{org} for neutral compounds.

The third hypothesis was that the compound being degraded or its oxidation products interfered with the •OH generation process. Surface iron interacts with many functional groups, e.g., deprotonated hydroxy groups (*19, 20*), and it could become less reactive toward H_2O_2 when it is complexed. We avoided this possibility in our experiments to quantify V_{OH} by using $H^{14}COOH$ as our •OH probe, but many of the aromatic compounds in the studies that we modeled have oxidation products that could complex surface iron. If this caused V_{OH} to decrease with time, then the measured k_{org} would be less than the model prediction.

The goal of this work was to improve our model for predicting k_{org} by determining the factors that contributed to its overestimation, and we achieved this by testing the above conjectures. We used our goethite to reproduce the experiment done by Huling et al. (*21*) and measured a similar loss rate for 2-Chlorophenol (2-CP), thus showing that the reactivity of our goethite was not significantly different from that of the natural goethite used by Huling and coworkers. The results from parallel experiments at pH 4 containing 2-CP and/or nitrobenzene (NB) in goethite slurries, with and without $H^{14}COOH$, revealed that electrostatics caused $H^{14}COOH$ to detect a greater concentration of •OH than 2-CP and NB. They also indicated that the oxidation products of 2-CP complexed surface iron, but this did not significantly affect the decomposition rate of 2-CP at the amount of iron oxide and H_2O_2 that we used.

Materials and Methods

Materials

Detailed descriptions for materials and methods are in previous publications (*4, 14*). All reagents were reagent grade and used as received. 2-Chlorophenol (2-CP, 99+%) and nitrobenzene (NB, 99+%) were from Sigma-Aldrich. High load scintillation cocktail (ScintiSafe Plus 50% Cocktail) was from Fisher. The solutions were prepared using 18 MΩ•cm Milli-Q water from a Millipore system. All glassware was soaked in concentrated HCl for 8 hours or more and rinsed before use. Goethite was the same as that described in chapter 3.

Analytical Techniques

2-CP and NB were analyzed by gas chromatography. At each time point a 2-mL aliquot of the experimental solution was removed and centrifuged in a glass container at 5500 rpm for 10 mins. 1-μL of the supernatant was injected into a Perkin Elmer Auto System XL gas chromatograph fitted with a quartz liner at the injector port, 0.32 mm i.d. x 60 m DB-5 1-μm film capillary column, and flame ionization detector. Chromatographic conditions were: helium carrier gas at 25 psi, injector temperature at 125 °C, detector temperature at 300 °C, oven temperature at 120 °C from 0-1 min, rate of 17 °C/min until 190 °C, 5 °C/min until final oven temperature of 205 °C, hold for 0.4 min. ^{14}C activity was measured in a scintillation counter (*14*). The high load scintillation cocktail was used in those experiments involving goethite. Hydrogen peroxide was measured spectrophotometrically using the DPD method (*22*) as modified by Voelker and Sulzberger (*23*) to minimize interference by Fe(II) and Fe(III). Samples were diluted with Milli-Q water to ensure that the absorbance through a 1-cm path length cuvette was less than 1.2 au.

Experimental Setup

Experiments were done in 50-mL glass test tubes with glass stoppers. The Milli-Q water was treated with a total organic carbon reduction unit (Aquafine) to oxidize traces of organic contamination. Parallel experiments were set up so that both test tubes contained the same amounts (within weighing and measuring errors) of goethite, H_2O_2 and organic compound (2-CP and/or NB) in 40 mL of solution, with the difference being that one was spiked with ^{14}C-labeled formic acid. This allowed us to track the loss rate of $H^{14}COOH$ (k_{HCOOH}) in one tube and the organic compound in the other without contaminating the GC with radioactivity. The ionic strength was set at 10 mM with $NaClO_4$, and the pH was adjusted to 4 (unless noted otherwise)

with $HClO_4$ and/or NaOH after the goethite and all compounds but H_2O_2 were mixed together. H_2O_2 was introduced at time zero and the contents mixed by a wrist-action shaker. The temperature of the solutions was 23.5 ± 2.5 °C. The pH of the solutions remained within ±0.5 unit of the initial pH throughout the experiment. Control experiments (without H_2O_2) lasting for 43 hours showed no significant loss of 2-CP or NB to air, iron oxide, or glass.

In one set of experiments we examined electrostatic effects by comparing k_{HCOOH} at pH 4 and pH 5. Instead of adding goethite solids directly to the solution, we added equal volumes from the supernatant of a mixture that consisted of 90 mg of goethite in 150 mL of 0.010 M $NaClO_4$ that stood undisturbed for 2 h. This was done to let the larger goethite particles settle out and decrease the likelihood of coagulation at the higher pH. We can apply Stoke's law to estimate the size of the particles that remained in the supernatant:

$$\upsilon_s = \alpha \cdot \frac{2g(\rho_s - \rho_w)}{9\mu} \cdot r^2 \qquad (6)$$

where υ_s is the settling velocity, α is a nondimensional form factor and is equal to 1 for a sphere (we shall assume the goethite solids are spheres) (*24*), g is the acceleration due to gravity (9.81 m/s^2), ρ_s is the density of the solid (4260 kg/m^3 for goethite; *25*), ρ_w is the density of water (1000 kg/m^3), μ is the dynamic viscosity of the fluid (10^{-3} kg/m·s), and r is the sphere radius. The height of the goethite slurry in the flask was 5 cm, so theoretically only particles with a radius smaller than 1 μm would have stayed in the supernatant.

Results

The aim of our first set of experiments was to determine if our laboratory synthesized goethite crystals were drastically different from the natural goethite that Huling et al. (*21*) used in their work. The experimental conditions that we used were similar to Huling's (surface area concentration = 110 m^2/L, $[H_2O_2]_0$ = 150 mM, and $[2\text{-CP}]_0$ = 350 μM) except that we worked at pH 4 instead of pH 6 to facilitate our sparging technique to remove $^{14}CO_2$ from $H^{14}COOH$. The change in pH did not significantly affect 2-CP speciation, (pK_a = 8.49; *26*). We also assumed that it did not change how fast •OH was generated since three independent investigations have shown that V_{OH} is relatively invariant from pH 4 to pH 10 (*16-18*). Huling et al. (*21*) performed four experiments with $[2\text{-CP}]_0$ ranging from 320-530 μM and reported a 2-CP loss rate of 0.043 ± 0.003 h^{-1}, whereas we measured 0.16 ± 0.02 h^{-1} (n = 2) in our experiments. The similar 2-CP loss rates, in stark contrast to a difference of over two orders of magnitude between Huling's results

and those predicted by our model (*14*), led us to conclude that the two types of goethite were not significantly different from each other.

If electrostatics were important in our system, then k_{HCOOH} should decrease when we increase the ionic strength or pH. Raising the ionic strength compresses the thickness of the electric double layer, and increasing the pH reduces the net amount of positive charge on the iron oxide surface. In both cases, the net result is that fewer formate anions are attracted to the oxide surface where the concentration of hydroxyl radicals is the greatest. We tested this hypothesis by comparing the change in k_{HCOOH} in two different sets of experiments. In the first experiment, k_{HCOOH} decreased from ~1.0 h^{-1} to 0.16 h^{-1} when the ionic strength of a pH 4 goethite slurry was increased from 0.01 to 0.9 M. In the other experiment, k_{HCOOH} decreased from 0.081 h^{-1} to 0.032 h^{-1} when the pH of the goethite slurry was increased from 4 to 5 at I = 10 mM. (The k_{HCOOH} values at pH 4 and I = 10 mM were different because, as mentioned previously, goethite solids were not added directly to the solution used in the second experiment.) The percentage decrease of k_{HCOOH} in both cases was consistent with theoretical calculations (see Discussion).

To further assess the influence of electrostatics in the heterogeneous system, we compared the steady state concentration of •OH ($[•OH]_{ss}$) that $H^{14}COOH$ and 2-CP measured when both were mixed with 0.6 g/L of goethite and 2 M H_2O_2. If the rate of probe degradation via its reaction with •OH follows pseudo-first-order kinetics, then $[•OH]_{ss}$ is:

$$[\bullet OH]_{ss} = \frac{k_{probe}}{k_{OH,\,probe}} \tag{7}$$

where k_{probe} is the measured pseudo-first-order rate coefficient of $H^{14}COOH$ or 2-CP degradation, and $k_{OH,probe}$ is the second-order rate constant of the probe with •OH. In solutions where electrostatic effects are important, the concentration of a charged probe is a function of its distance from the iron oxide. Since there are high concentrations of both formate anions and •OH near the oxide surface, k_{HCOOH} would be higher than expected based on the bulk solution concentrations, and $[•OH]_{ss}$ calculated by eq 7 becomes a weighted average of the amount of •OH that the probe detected in the double layer and in the bulk solution. $[•OH]_{ss}$ will be greater for $H^{14}COOH$ than for 2-CP if electrostatic effects are indeed important. Figure 4-1 shows the probe loss data from one such experiment, and whereas 2-CP loss was pseudo-first-order, $H^{14}COOH$ loss clearly was not. This was surprising as $H^{14}COOH$ degradation was always pseudo-first-order in all of our previous experiments where 2-CP was not present (*14*).

Since adding 2-CP to the goethite/H_2O_2 system should not have introduced a new $H^{14}COOH$ degradation pathway (supported by experimental results discussed at the end of this section), the logical explanation for the behavior of the $H^{14}COOH$ data in Figure 4-1 is that as the experiment progressed $H^{14}COOH$ measured decreasing $[\bullet OH]_{ss}$. In order to obtain time-resolved information on [•OH] from the $H^{14}COOH$ data, we calculated the k_{probe} values of two consecutive time points assuming k_{probe} remained constant over the time interval:

$$k_{probe,\,interval} = -\ln\frac{[probe]_{t'}}{[probe]_t}(t'-t)^{-1} \qquad (8)$$

where t' was the next time after t at which the amount of probe compound remaining in solution was determined. $k_{probe,\,interval}$ should approximate k_{HCOOH} for the time interval as long as the difference between t' and t is small. We then substituted $k_{probe,\,interval}$ for k_{probe} in eq 7 to get $[\bullet OH]_{ss,\,interval}$ values for each interval (Figures 4-2a-c, negative $[\bullet OH]_{ss,\,interval}$ numbers were excluded). The results showed that (a) early on, $[\bullet OH]_{ss,\,interval}$ values for $H^{14}COOH$ were higher than those of 2-CP and NB, (NB is a well-known •OH probe that was used to confirm the $[\bullet OH]_{ss,\,interval}$ measurements made using 2-CP) and (b) $[\bullet OH]_{ss,\,interval}$ values for $H^{14}COOH$ decreased steadily until at approximately 5 hours, they were nearly equivalent to those of 2-CP and NB. As expected from the data in Figure 4-1, 2-CP detected the same amount of •OH in every time interval (within experimental uncertainty).

The non first-order behavior of k_{HCOOH} suggested that we should examine how 2-CP (or NB) or its oxidation products caused the $[\bullet OH]_{ss,\,interval}$ measurements for $H^{14}COOH$ to decrease with time. We did parallel experiments where 0.3, 3, 30 or 300 μM of 2-CP was added to 0.6 g/L of goethite and 2 M of H_2O_2, then computed $[\bullet OH]_{ss,\,interval}$ from the $H^{14}COOH$ data (Figures 4-3a,b). The results strengthened the idea that 2-CP or its oxidation products affected the degradation kinetics of $H^{14}COOH$ because the rate at which the $[\bullet OH]_{ss,\,interval}$ values measured using $H^{14}COOH$ decreased was a function of $[2\text{-}CP]_0$. There was also noticeable coagulation of the goethite particles in those experiments where $[2\text{-}CP]_0 \geq 30$ μM (Figures 4-4a,b). We believe these two observations are due to the loss of positive charge on the oxide surface as the intermediates and oxidation products of 2-CP (e.g., chlorocatechol, reaction 9) complexed surface Fe species.

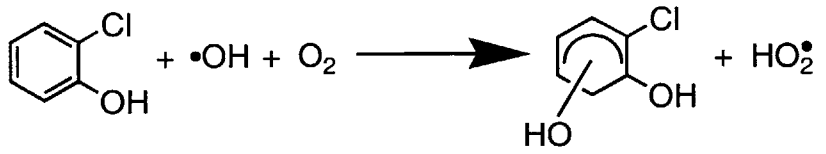

(9)

We did not determine the reaction products from our 2-CP experiments. Although there is no direct evidence that 2-Chlorocatechol is formed, 4-Chlorocatechol is a known intermediate of the reaction between •OH and 4-Chlorophenol (*27-32*), and a study of 2-CP degradation in an irradiated aqueous suspension of TiO_2 detected eight intermediates, of which only chlorohydroquinone, hydroxyhydroquinone, and catechol were identified (*33*). We did not observe any oxidative coupling products, i.e., polyphenols (*32, 34*), in our suspensions.

Coagulation alone cannot explain the results of Figures 4-2a-c because it leads to the loss of surface area, which should decrease the oxidation rates of both $H^{14}COOH$ and 2-CP by the same amount. It may be that not enough surface area was lost to significantly affect the oxidation rates of $H^{14}COOH$ and 2-CP.

By the same token, any decrease of Fe reactivity toward H_2O_2 caused by the oxidation products of 2-CP also cannot explain the results of Figures 4-2a-c because in that case, $[\bullet OH]_{ss,\ interval}$ measured by both $H^{14}COOH$ and 2-CP would be expected to decrease with time. We confirmed this by doing two experiments at pH 3 where 25 and 75 μM of Fe was introduced as dissolved Fe(III) (in the form of $Fe(ClO_4)_3 \bullet 9H_2O$) instead of goethite into solutions containing 2 M H_2O_2 and 200 μM 2-CP (Figures 4-5a,b). Figures 4-6a,b show that both probes measured the same concentration of •OH (within experimental uncertainty), confirming that adding 2-CP to our experiments did not introduce a new $H^{14}COOH$ degradation pathway. Moreover, Fe(III) interacted with the oxidation products of 2-CP and became less reactive toward H_2O_2, as evidenced by the decrease in $[\bullet OH]_{ss,\ interval}$ for both $H^{14}COOH$ and 2-CP with time, in contrast to the data in Figures 4-2a-c. These results suggest that the reactivity of surface Fe toward H_2O_2 could also decrease when the Fe is complexed by the oxidation products of 2-CP, but as discussed above, we did not observe this in our experiments. Most likely, the number of surface Fe sites that were complexed was too low to adversely affect the production rate of •OH. Nevertheless, the loss of some of the charged surface Fe sites, which make up only a small fraction of the total surface Fe sites, to complexation could still have a substantial effect on the surface charge, causing the observed effects: a decrease in k_{HCOOH} and coagulation.

Discussion

The goal of this work was to improve our model for predicting the oxidation rate of organic compounds in mineral-catalyzed, Fenton-like systems. The model successfully predicted the decomposition rate of $H^{14}COOH$ in slurries containing iron oxide and a natural iron oxide-coated quartzitic aquifer sand, but overpredicted many of the k_{org} values that other researchers reported (*14*). We tested three hypotheses that could explain the disagreements between the model predictions and the measurements, and concluded that electrostatics, which was not considered in our model, played a crucial role by enriching the concentration of formate near the positively charged iron oxide surface where •OH is generated.

Lifetime of •OH

One method of judging the possible influence of electrostatics on k_{HCOOH} is to compute the lifetime of •OH. If •OH is relatively long-lived, then it can diffuse far away from the oxide surface. This would imply that k_{HCOOH} is determined by the solute concentrations in the bulk solution, which are unaffected by electrostatics. The lifetime of a chemical species (τ) that is consumed according to first-order kinetics is equal to the inverse of the sum of the product of the concentration of all chemical species that react with it and their respective second-order reaction rate constants:

$$\tau = \frac{1}{\sum k_i [S_i]} \tag{10}$$

τ_{OH} is estimated to be ~20 ns in a solution containing 2 M H_2O_2, 200 μM 2-CP, with k_{OH,H_2O_2} = 2.7 x 10^7 M^{-1} s^{-1} (*1*) and $k_{OH,2\text{-}CP}$ = 1.2 x 10^{10} M^{-1} s^{-1} (*1*). The double layer thickness is the reciprocal of the Debye parameter, which at 25 °C is equal to 3.29 x 10^9 $I^{1/2}$ (*35*), and is ~3 nm at I = 10 mM. The typical time for a molecule to diffuse across this boundary is 9 ns, calculated by squaring the length of the double layer and dividing by 10^{-5} cm^2/s, the diffusivity of a solute (*24*). As τ_{OH} is only twice the time needed to travel across the double layer, it agrees with our theory that k_{HCOOH} was significantly affected by electrostatics.

Quantifying Electrostatic Effects

To further determine how electrostatic effects affected our system, we needed a method of predicting how k_{HCOOH} changes as a result of the migration of formate anions toward the positively charged iron oxide surface. It has been shown that the Coulombic correction factor, $\exp(-\Delta Z F \Psi_0 / RT)$, can quantify the electrostatic interactions between solutes and solid surfaces in

solution, i.e., the change in the concentration of charged solutes at the oxide surface caused by the surface charge (*35*). ΔZ is the change in the charge of the surface species for the reaction under consideration, F is the Faraday constant (96485 C/mol), Ψ_0 is the surface potential, R is the gas constant (8.314 J/K·mol), and T is the temperature. Ψ_0 determines the strength of the attraction or repulsion between the ions and the oxide surface and is given by (*24*):

$$\Psi_0 = \frac{2RT}{zF}\sinh^{-1}\left(\sigma\sqrt{\frac{\pi F^2 10^{-3}}{2\varepsilon RTI}}\right) \tag{11}$$

where z is the valence of the background electrolyte and is equal to 1 in our experiments, ε is the dielectric constant of water (7.2×10^{-10} C/V·m), and I is the ionic strength. σ in eq 11 is the surface charge density, which is the difference between $[\equiv FeOH_2^+]$ and $[\equiv FeO^-]$:

$$\sigma = \frac{[\equiv FeOH][H^+]e^{-F\Psi_0/RT}}{K_{a1}^{int}} - \frac{[\equiv FeOH]K_{a2}^{int}}{[H^+]e^{-F\Psi_0/RT}} \tag{12}$$

where [≡FeOH] is the density of the reactive surface Fe sites, and K_{a1}^{int} and K_{a2}^{int} are the intrinsic surface acid-base equilibrium constants of reactions 4 and 5, respectively. The Coulombic correction factor is required for H^+ since we are dealing with surface Fe species and thus need the concentration of protons at the surface. We assumed our goethite had a pK_{a1}^{int} of 6, a pK_{a2}^{int} of 9, and a site density of 2×10^{-6} mol/m^2 (*24*) because we did not measure these parameters. Table 4-1 lists Ψ_0 of the oxide surface in the experiments that were done to assess the importance of electrostatic effects in the goethite/H_2O_2 system.

With Ψ_0 known, we can predict how k_{HCOOH} changes with ionic strength or pH. Generally speaking, the pseudo-first-order rate constant that we measure, k_{HCOOH}, is a weighted sum of the rates at which $H^{14}COOH$ is oxidized in the bulk solution and near the surface:

$$k_{HCOOH} = k_{HCOOH,\,bulk}\left(\frac{vol_{bulk}}{total\ vol}\right) + k_{HCOOH,\,surf}\left(\frac{vol_{surf}}{total\ vol}\right) \tag{13}$$

where "bulk" designates the bulk solution concentration of the solutes, "surf" denotes the surface concentration of the solutes, and the volume fractions weigh the contribution from each region. For electrostatic effects to be important, the contribution from the bulk region must be much less than the surface region, so as a first approximation:

$$k_{HCOOH} \approx k_{HCOOH,\,surf}\left(\frac{vol_{surf}}{total\ vol}\right) \tag{14}$$

Using eq 7 to substitute for $k_{HCOOH,\ surf}$,

$$k_{HCOOH} \approx k_{OH,\ HCOOH,\ surf}\,[\bullet OH]_{ss,\ surf}\left(\frac{vol_{surf}}{total\ vol}\right) \tag{15}$$

which shows that the ratio of k_{HCOOH} measured from two experiments is the same as the ratio of $k_{OH,\ HCOOH,\ surf}$ for those two experiments as long as the perturbations to $[\bullet OH]_{ss,\ surf}$ and the volume fraction are minor. $k_{OH,\ HCOOH,\ surf}$ is equal to:

$$k_{OH,\ HCOOH,\ surf} = k_{OH,\ HCOOH}\frac{[HCOOH]_{bulk}}{[HCOOH]_T} + k_{OH,\ HCOO^-}\frac{[HCOO^-]_{bulk}}{[HCOOH]_T}e^{F\Psi_0/RT} \tag{16}$$

where the Coulombic factor corrects for the amount of formate present at the oxide surface and can be computed once Ψ_0 is known. Although pK_{a1}^{int} for goethite ranges from 6.0-7.47 (neglecting one study reporting it as 4.2) (*25*), pK_{a2}^{int} ranges from 9.0-11.11 (*25*), and the site density ranges from 2-4.7 x 10^{-6} mol/m^2 (*35*), our calculations indicated that the change in Ψ_0 at pH 4 due to these variations was less than 0.05 V and more importantly, the ratio of $k_{OH,\ HCOOH,\ surf}$ was unaffected. We predicted $k_{OH,\ HCOOH,\ surf}$ would decrease by a factor of 6.9 when the ionic strength was raised from 10 to 900 mM, and the measured decrease of k_{HCOOH} was by a factor of 6.3. k_{HCOOH} decreased by a factor of 2.5 in the experiment where the pH was raised from 4 to 5, which was close to the predicted decrease of a factor of 3.2. The good agreement between the measurements and predictions for both experiments support the hypothesis that electrostatics affected k_{HCOOH}.

Ionic strength dictates the extent of interactions between charged components in solution. The theoretical calculations that we did accounted for the change in the width of the double layer and the influence of surface charge on the distribution of ions in solution. However, they do not consider the change in the activity coefficient within the localized environment of the double layer, or that excess counterions restrict the number of ions that can approach the surface. More experiments would help elucidate the relationship between ionic strength and k_{HCOOH}.

Implications For Our Model

In order to improve the ability of our model to predict the k_{org} of dissolved neutral compounds, we need a method to rectify the higher oxidation rate of $H^{14}COOH$ so that it is the same as that of any dissolved neutral compound. While the previous evaluations were useful for confirming the importance of electrostatics in our system, neither of them met the requirement.

The full analysis involves examining how the consumption rate of $H^{14}COOH$ is affected by Ψ and $[\bullet OH]_{ss}$, both of which decrease with distance away from the iron oxide:

$$\left(-\frac{d[HCOOH]}{dt}\right)_{el} = \frac{A}{V}\int_0^x \left(k_{OH,HCOOH}[\bullet OH]_{ss}(x)[HCOOH]_{bulk} + k_{OH,HCOO^-}[\bullet OH]_{ss}(x)[HCOO^-]_{bulk} e^{-\Delta Z F \Psi(x)/RT}\right)dx \quad (17)$$

where "el" denotes electrostatic effects, A is the total amount of iron oxide surface area in solution, and V is the volume of the solution. $\Psi(x)$ can be approximated by $\Psi_0 e^{-\kappa x}$ (*35*), where κ is the Debye parameter. We can determine how •OH changes with distance by applying the law of mole conservation, which says that at steady state the mole inflow rate plus any gains into a control volume must equal the mole outflow rate and any losses within the control volume. The resulting equation for our system is:

$$D\frac{\partial^2[\bullet OH]_{ss}(x)}{\partial x^2} = \sum k_{OH,i}[\bullet OH]_{ss}(x)[S_i](x) \quad (18)$$

where D is the diffusion coefficient, and S_i represents •OH sink *i* in solution. The boundary conditions are:

$$-D\frac{\partial[\bullet OH]_{ss}}{\partial x}\Big|_{x=0} = \tilde{V}_{OH} \quad (19)$$

and $[\bullet OH]_{ss} = 0$ at an infinite distance away from the oxide surface. Eq 19 is Fick's law and describes the influx of •OH, assuming it is generated only at the oxide surface (x = 0). $\tilde{V}_{OH}$ is the mole flux per unit area per unit time (equivalent to V_{OH} multiplied by a unit length). If $[S_i]$ is not a function of x, then the solution to eq 18 is:

$$[\bullet OH]_{ss}(x) = \frac{\tilde{V}_{OH}}{\sqrt{D\sum k_{OH,i}[S_i]}}\exp\left(-x\sqrt{\frac{\sum k_{OH,i}[S_i]}{D}}\right) \quad (20)$$

We can now refine our model for predicting k_{org} by correcting for the percent increase in the loss rate of formate in the double layer due to electrostatic effects. This was achieved by dividing the increased oxidation rate of $H^{14}COOH$ in the double layer due to formate enrichment (integrating eq 17 from 0 to infinity) by the oxidation rate of $H^{14}COOH$ in which electrostatic effects are ignored (integrating eq 21 from 0 to infinity).

$$-\frac{d[HCOOH]}{dt} = \frac{A}{V}\int_0^x \left(k_{OH,HCOOH}[\bullet OH]_{ss}(x)[HCOOH]_{bulk} +\right.$$

$$k_{OH,HCOO^-}[\bullet OH]_{ss}(x)[HCOO^-]_{bulk}\Big)dx \qquad (21)$$

We assumed the major sink of •OH was H_2O_2, which was true in the experiments that we did to quantify V_{OH} using $H^{14}COOH$ (Figure 3-1a), and used numerical integration (adaptive Simpson quadrature, adaptive Lobatto quadrature, and Clenshaw-Curtis quadrature) to integrate eq 17 because it does not appear to have an analytical solution. The quotient is approximately proportional to $[H_2O_2]^{1/2}$, as expected given the behavior of $[\bullet OH]_{ss}(x)$. It is ~58 at pH 4, I = 10 mM, $\Psi_0 = 0.16$ V, $[H_2O_2]_0 = 2$ M, and a total $H^{14}COOH$ concentration of 100 nM, which agrees with the difference in $[\bullet OH]_{ss,\,interval}$ observed in Figures 4-2a-c at the beginning of the experiment. Using this information, we divided the predicted k_{org} values shown in Figure 3-5 by 58 (Figure 4-7). All of the model predictions now are within a factor of 10 of the measurements, even the butyl chloride experiments done by Lin and Gurol (*16*).

We re-examined the benzoic acid data ($pK_a = 4.19$; *26*) for electrostatic effects because those experiments were done at pH 3.2, 6, and 10 (black circles in Figure 4-7). Using the above approach and assuming that lepidocrocite has the same surface charge properties as goethite, we would expect the oxidation rate of benzoic acid, compared to a neutral probe compound under the same conditions, to increase by a factor of 3 at pH 3.2, be approximately the same at pH 6, and decrease by a factor of 2 at pH 10. These correction factors do not have a significant impact on the agreement between the predicted and measured k_{org}.

Most researchers do not consider the effects of electrostatic on the oxidation rates of organic compounds in heterogeneous systems because they deal with pollutants that have pK_a values of 7 or greater. Nevertheless, we showed that electrostatics was the most probable explanation for the discrepancy between our model predictions and the k_{org} values reported by other researchers because $H^{14}COOH$ measured a concentration of •OH that was much greater than the amount that reacted with neutral organic compounds. The difference between the two $[\bullet OH]_{ss}$ was similar to the difference between the predicted and measured k_{org}. Since some organic compounds, for example benzoic acid, have charged species at pH values of 7 or less, it is important to know that electrostatics affects the interactions between organic compounds and iron oxide. Electrostatics could also influence the concentration of any charged •OH sinks in the boundary layer, which would impact the oxidation rate of the compound of interest if the charged sink were an important sink of •OH.

Acknowledgments

We thank Phil Gschwend, John MacFarlane, and Yang-hsin Shih for their help with GC instrumentation and insightful discussions. This work was funded by a grant from the American Chemical Society's Petroleum Research Fund.

Literature Cited

(1) Buxton, G. V.; Greenstock, C. L.; Helman, W. P.; Ross, A. B. *J. Phys. Chem. Ref. Data* **1988**, *17*, 513-886.

(2) Bauer, R.; Fallmann, H. *Res. Chem. Intermediat.* **1997**, *23*, 341-354.

(3) Bhattacharjee, S. *Rev. Chem. Eng.* **1998**, *14*, 1-45.

(4) Kwan, W. P.; Voelker, B. M. *Environ. Sci. Technol.* **2002**, *36*, 1467-1476.

(5) Watts, R. J.; Udell, M. D.; Rauch, P. A.; Leung, S. W. *Hazard. Waste Hazard. Mater.* **1990**, *7*, 335-345.

(6) Khan, A. J.; Watts, R. J. *Water Air Soil Pollut.* **1996**, *88*, 247-260.

(7) Watts, R. J.; Jones, A. P.; Chen, P.-H.; Kenny, A. *Water Environ. Res.* **1997**, *69*, 269-275.

(8) Kong, S. H.; Watts, R. J.; Choi, J. H. *Chemosphere* **1998**, *37*, 1473-1482.

(9) Lin, S.-S.; Gurol, M. D. *Environ. Sci. Technol.* **1998**, *32*, 1417-1423.

(10) Valentine, R. L.; Wang, H. C. A. *J. Environ. Eng.* **1998**, *124*, 31-38.

(11) Miller, C. M.; Valentine, R. L. *Water Res.* **1999**, *33*, 2805-2816.

(12) Watts, R. J.; Udell, M. D.; Kong, S. H.; Leung, S. W. *Environ. Eng. Sci.* **1999**, *16*, 93-103.

(13) Lu, M.-C.; Chen, J.-N.; Huang, H.-H. *Chemosphere* **2002**, *46*, 131-136.

(14) Kwan, W. P.; Voelker, B. M. *Environ. Sci. Technol.* **2003**, *37*, 1150-1158.

(15) Tyre, B. W.; Watts, R. J.; Miller, G. C. *J. Environ. Qual.* **1991**, *20*, 832-838.

(16) Lin, S.-S.; Gurol, M. D. *Water Sci. Technol.* **1996**, *34*, 57-64.

(17) Chou, S.; Huang, C. *Chemosphere* **1999**, *38*, 2719-2731.

(18) Watts, R. J.; Foget, M. K.; Kong, S.-H.; Teel, A. L. *J. Hazard. Mater.* **1999**, *69*, 229-243.

(19) McBride, M. B. *Soil Sci. Soc. Am. J.* **1987**, *51*, 1466-1472.

(20) Kung, K.-H. S.; McBride, M. B. *Environ. Sci. Technol.* **1991**, *25*, 702-709.

(21) Huling, S. G.; Arnold, R. G.; Jones, P. K.; Sierka, R. A. *J. Environ. Eng.* **2000**, *126*, 348-353.

(22) Bader, H.; Sturzenegger, V.; Hoigné, J. *Water Res.* **1988**, *22*, 1109-1115.

(23) Voelker, B. M.; Sulzberger, B. *Environ. Sci. Technol.* **1996**, *30*, 1106-1114.

(24) Schwarzenbach, R. P.; Gschwend, P. M.; Imboden, D. M. *Environmental Organic Chemistry*; John Wiley & Sons, Inc.: New York, 1993.

(25) Cornell, R. M.; Schwertmann, U. *The Iron Oxides: Structure, Properties, Reactions, Occurrence and Uses*; VCH Publishers: New York, NY, 1996.

(26) Lide, D. R., Ed. *Handbook of Chemistry and Physics*; CRC Press: New York, 1995.

(27) Mills, A.; Morris, S. *J. Photochem. Photobiol. A-Chem.* **1993**, *71*, 285-289.

(28) Mills, A.; Davies, R. H.; Worsley, D. *Chem. Soc. Rev.* **1993**, *22*, 417-425.

(29) Martin, S. T.; Morrison, C. L.; Hoffmann, M. R. *J. Phys. Chem.* **1994**, *98*, 13695-13704.

(30) Stafford, U.; Gray, K. A.; Kamat, P. V. *J. Phys. Chem.* **1994**, *98*, 6343-6351.

(31) Martin, S. T.; Lee, A. T.; Hoffmann, M. R. *Environ. Sci. Technol.* **1995**, *29*, 2567-2573.

(32) Martin, S. T.; Kesselman, J. M.; Park, D. S.; Lewis, N. S.; Hoffmann, M. R. *Environ. Sci. Technol.* **1996**, *30*, 2535-2542.

(33) D'Oliveira, J.-C.; Alsayyed, G.; Pichat, P. *Environ. Sci. Technol.* **1990**, *24*, 990-996.

(34) O'Shea, K. E.; Cardona, C. *J. Photochem. Photobiol. A-Chem.* **1995**, *91*, 67-72.

(35) Stumm, W.; Morgan, J. J. *Aquatic Chemistry*; John Wiley & Sons, Inc.: New York, 1996.

(36) Miller, C. M.; Valentine, R. L. *Water Res.* **1995**, *29*, 2353-2359.

Table 4-1. Effect of ionic strength and pH on Ψ_0.

I (mM)	pH	Ψ_0 (V)
10	4	0.16
900	4	0.11
10	5	0.12

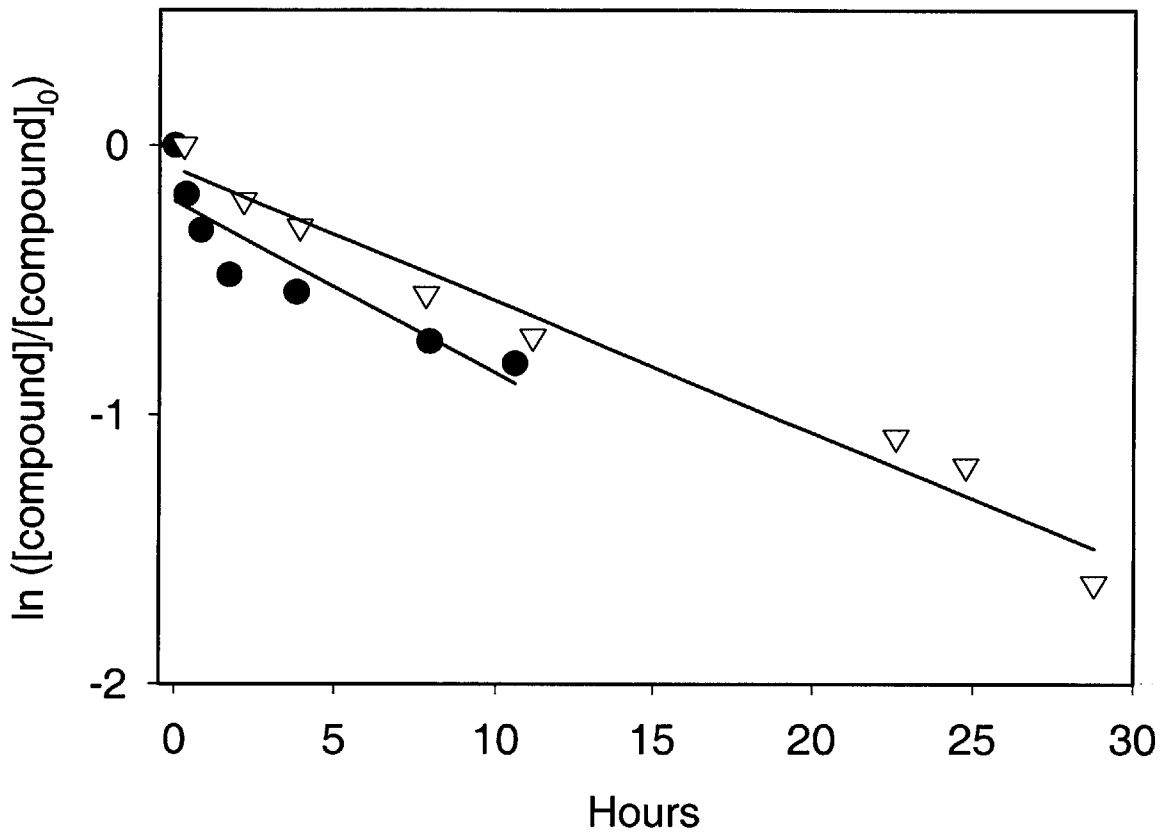

Figure 4-1. Typical data set of the concentration of ^{14}C-labeled formic acid (●) and 2-CP (▽) in an experiment containing 0.6 g/L goethite, $[H_2O_2]_0$ = 2 M, $[2\text{-CP}]_0$ = 300 μM, and initial ^{14}C of 10000 DPM at pH 4. The lines are linear regression fits to log transformed data.

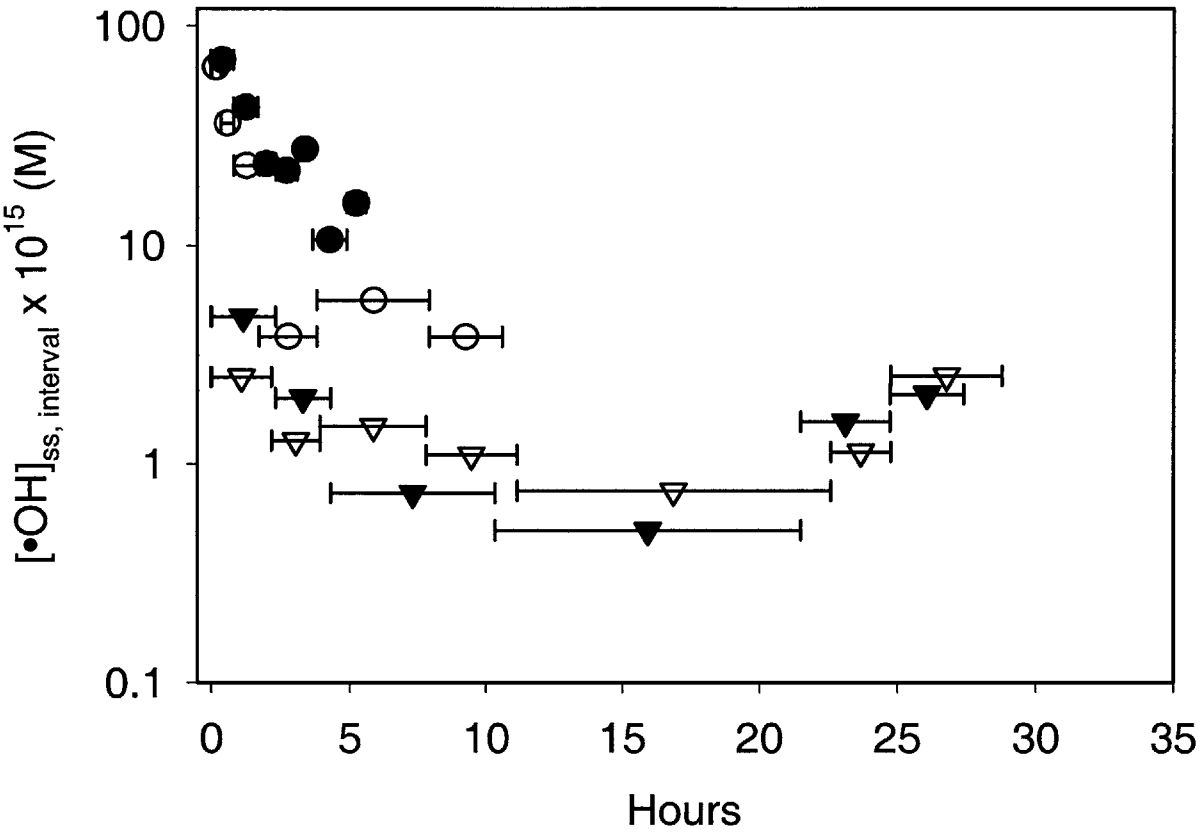

Figure 4-2a. $[\bullet OH]_{ss,\ interval}$ for ^{14}C-labeled formic acid (●, ○) and 2-CP (▼, ▽) in experiments containing 0.6 g/L goethite, $[H_2O_2]_0 = 2$ M, initial ^{14}C of 20000 (●) or 10000 (○)DPM, and $[2\text{-CP}]_0 = 130$ (▼) or 300 (▽) μM at pH 4. The horizontal bars denote the time interval between the two consecutive data points that were used to calculate $[\bullet OH]_{ss,\ interval}$.

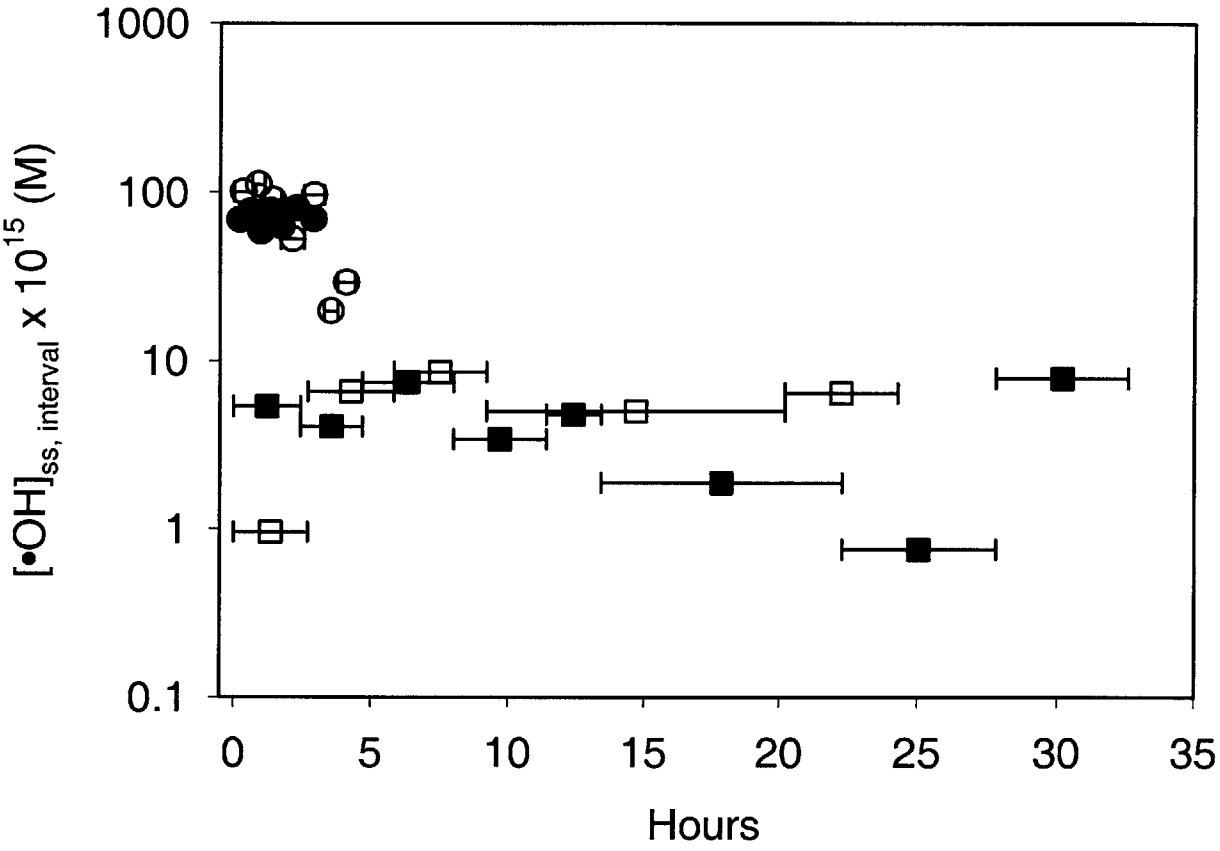

Figure 4-2b. $[\bullet OH]_{ss,\ interval}$ for ^{14}C-labeled formic acid (●, ○) and NB(■, □) in experiments containing 0.6 g/L goethite, $[H_2O_2]_0$ = 2 M, $[NB]_0$ = 100 μM, and initial ^{14}C of 40000 (●) or 10000 (○) DPM at pH 4. The horizontal bars denote the time interval between the two consecutive data points that were used to calculate $[\bullet OH]_{ss,\ interval}$.

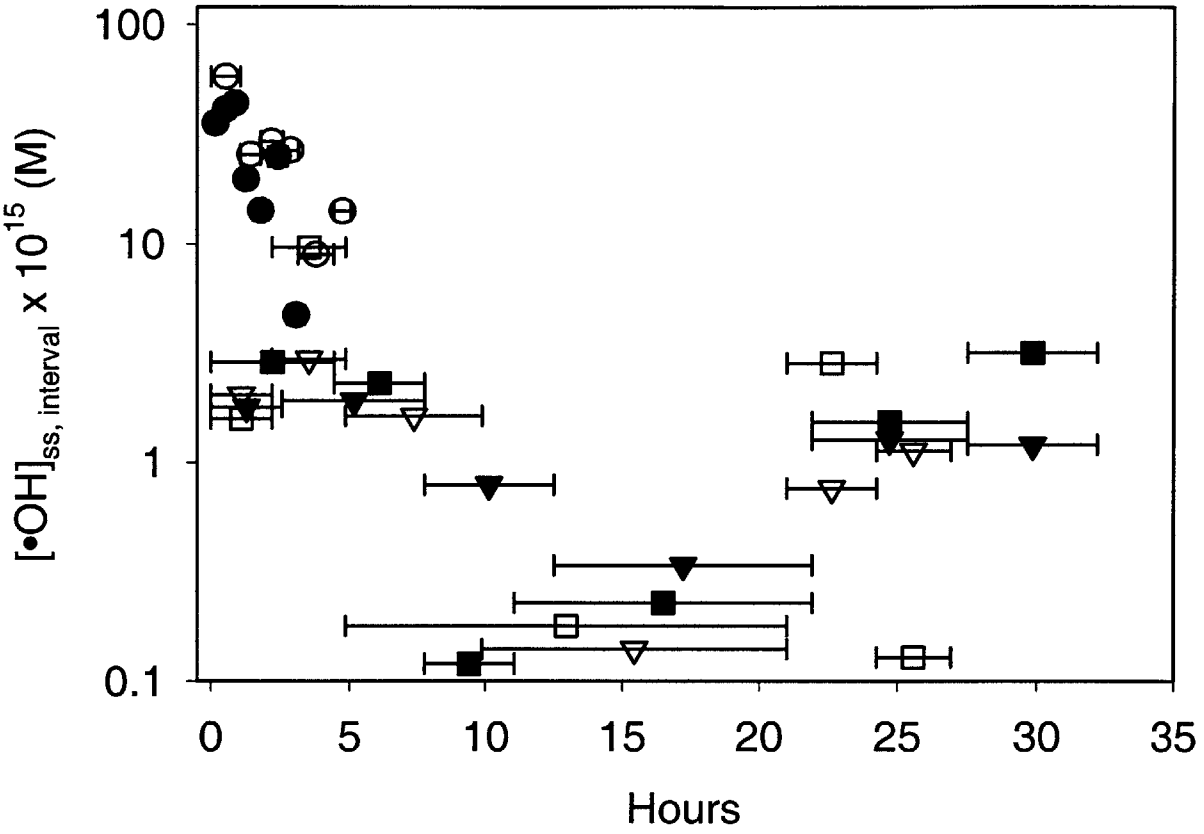

Figure 4-2c. $[\bullet OH]_{ss,\ interval}$ for ^{14}C-labeled formic acid (●, ○), 2-CP (▼, ▽), and NB (■, □) in experiments containing 0.6 g/L goethite, $[H_2O_2]_0$ = 2 M, $[2\text{-CP}]_0 = [NB]_0$ = 100 μM, and initial ^{14}C of 40000 (●) or 20000 (○) DPM at pH 4. The horizontal bars denote the time interval between the two consecutive data points that were used to calculate $[\bullet OH]_{ss,\ interval}$.

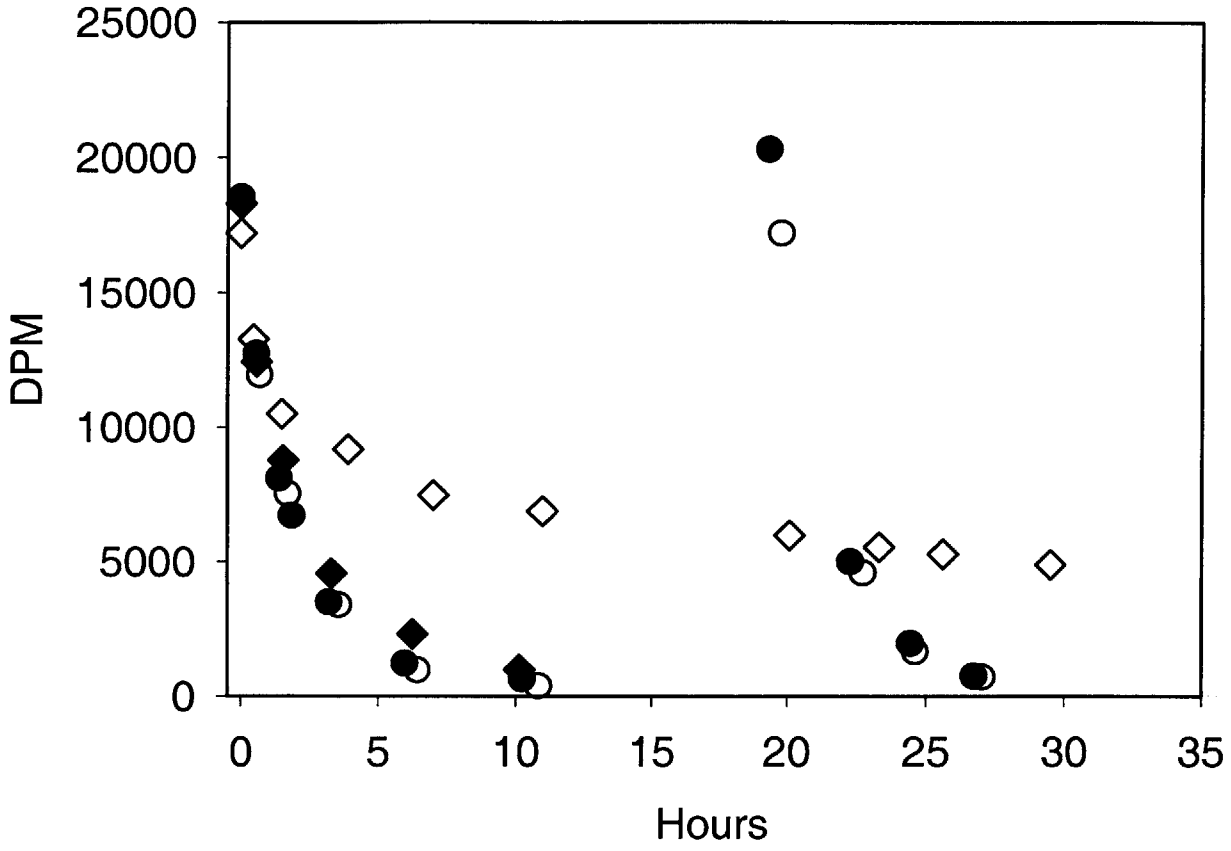

Figure 4-3a. ^{14}C activity of $H^{14}COOH$ in four experiments containing 0.6 g/L goethite, $[H_2O_2]_0$ = 2 M, and $[2\text{-CP}]_0$ = 0.3 (●), 3 (○), 30 (◆), or 300 (◇) μM at pH 4. The experiments with $[2\text{-CP}]_0$ = 0.3 and 3 μM were re-spiked with $H^{14}COOH$ after ~20 hours.

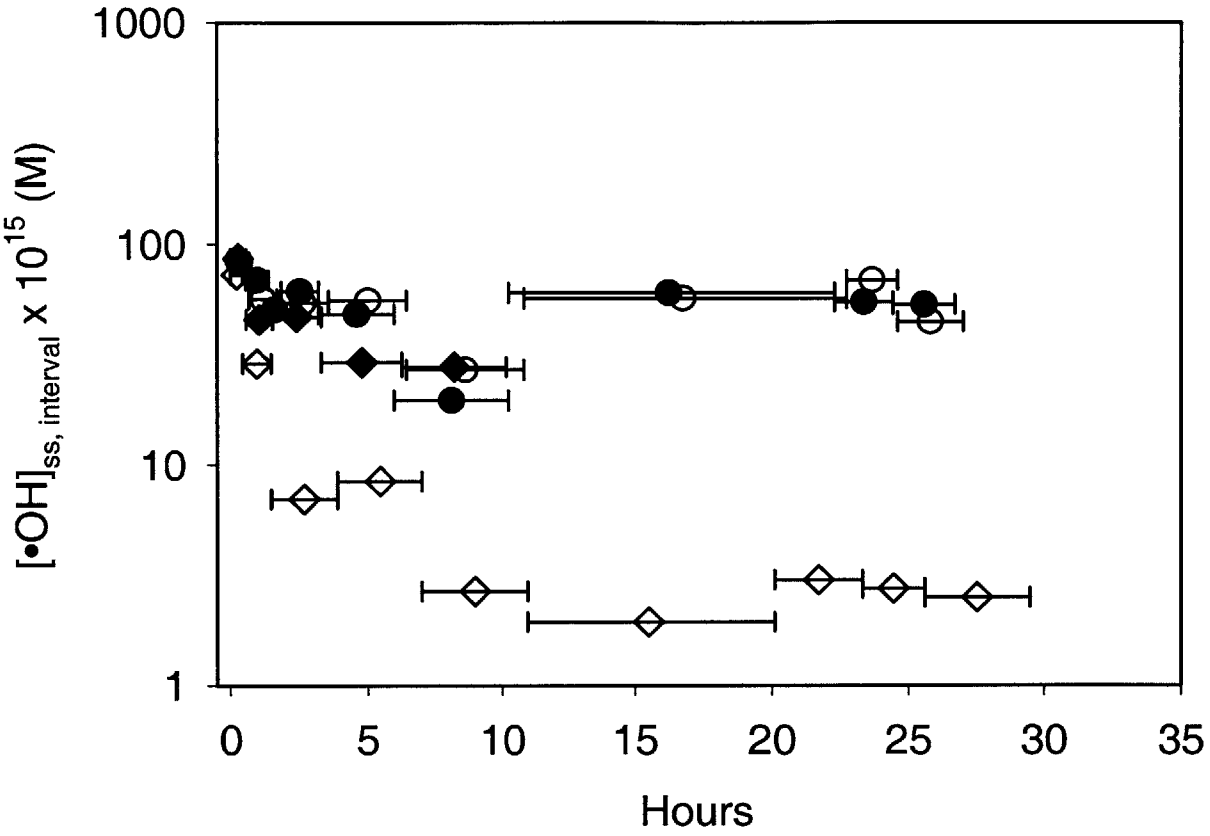

Figure 4-3b. $[\bullet OH]_{ss,\ interval}$ for the data shown in Figure 4-3a. The horizontal bars denote the time interval between the two consecutive data points that were used to calculate $[\bullet OH]_{ss,\ interval}$.

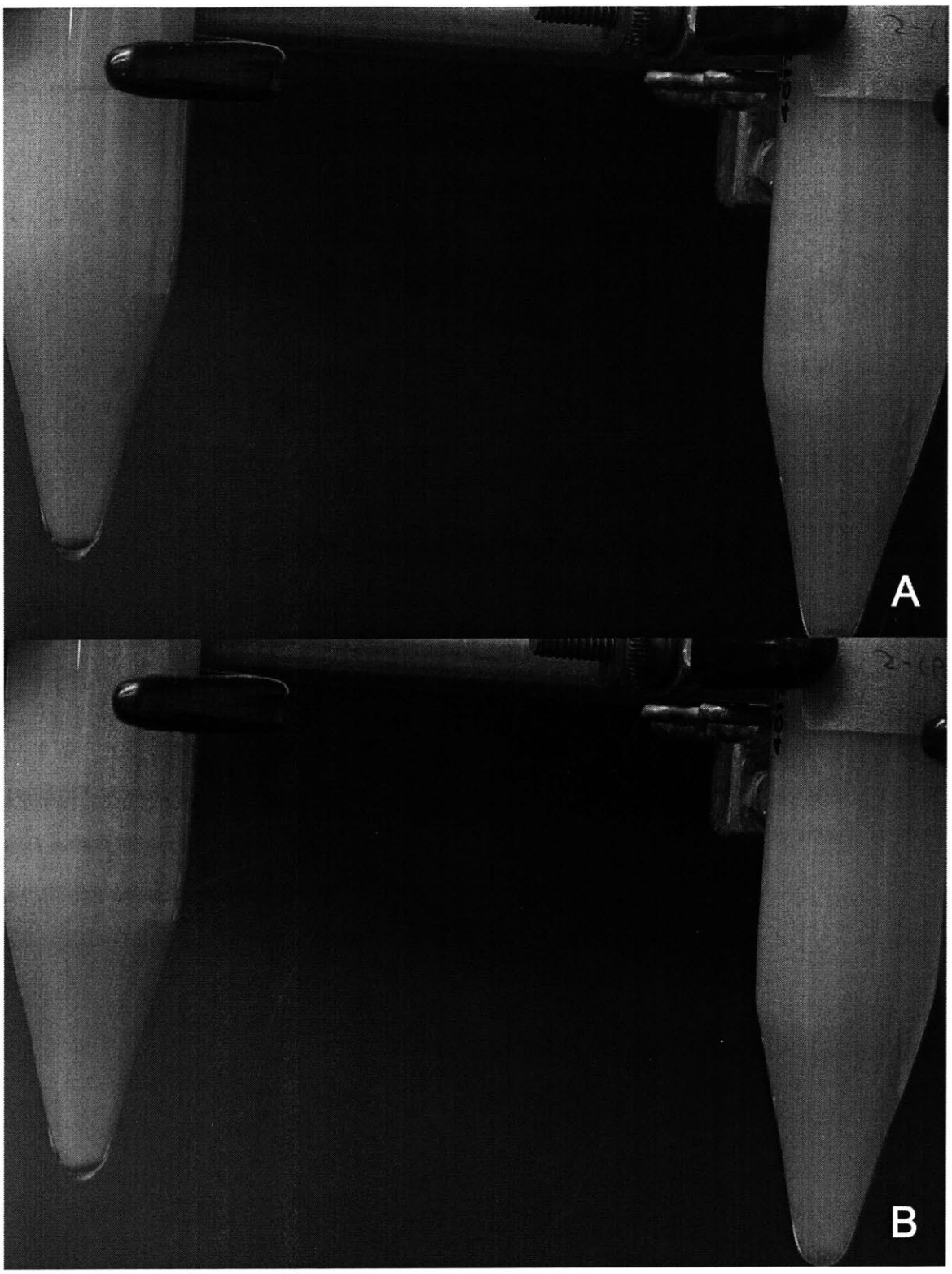

Figure 4-4a. Photos of two test tubes containing 0.6 g/L of goethite, $[H_2O_2]_0$ = 2 M and $[2\text{-CP}]_0$ = 3 (left) or 300 (right) μM at pH 4. (A) was taken immediately after the test tubes had been shaking for 1.5 hours. They were then left undisturbed for 15 minutes before (B) was taken.

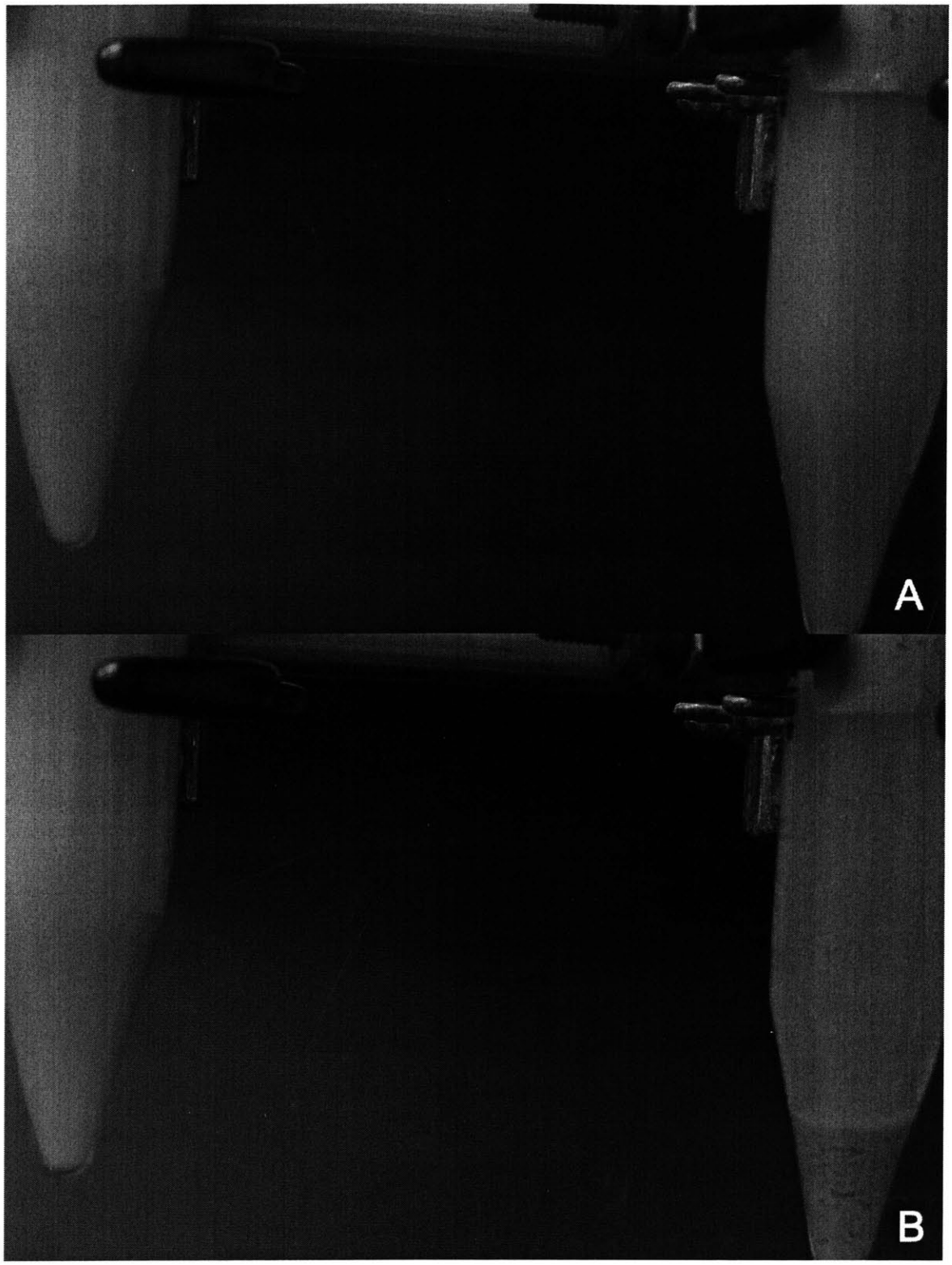

Figure 4-4b. Continuation of the experiment described in Figure 4-4a. (A) was taken immediately after the test tubes had been shaking for 10 hours. They were then left undisturbed for 15 minutes before (B) was taken.

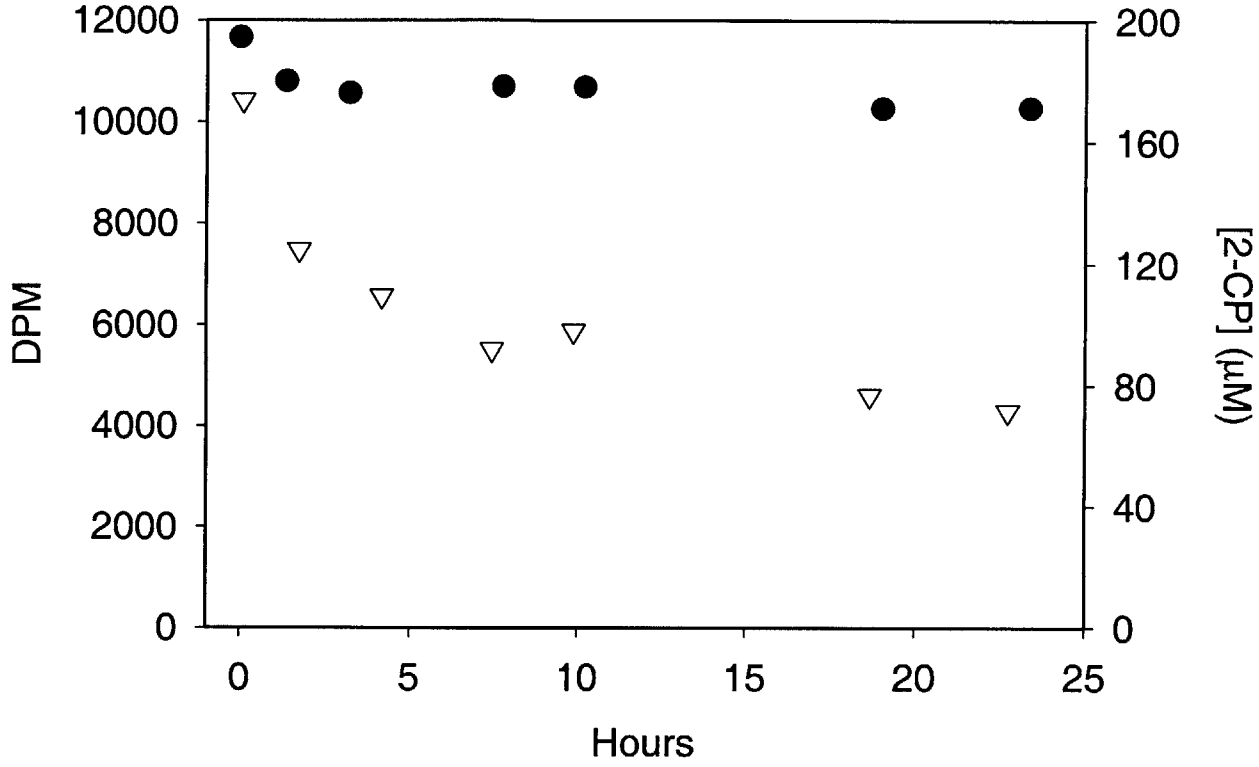

Figure 4-5a. ^{14}C activity of $H^{14}COOH$ (●) and [2-CP] (▽) in an experiment with [Fe(III)] = 25 μM, $[H_2O_2]_0$ = 2 M, and $[2\text{-CP}]_0$ = 170 μM at pH 3.

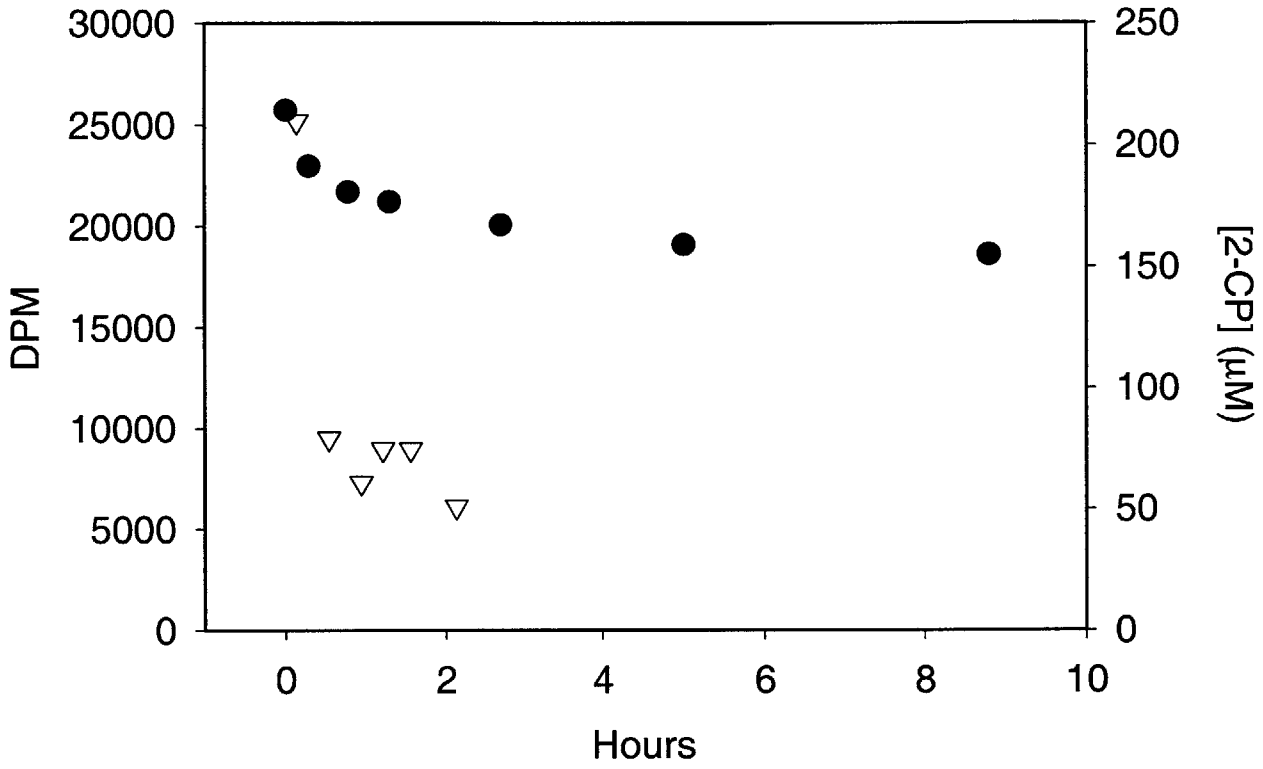

Figure 4-5b. ^{14}C activity of $H^{14}COOH$ (●) and [2-CP] (▽) in an experiment with [Fe(III)] = 75 μM, $[H_2O_2]_0$ = 2 M, and $[2\text{-CP}]_0$ = 200 μM at pH 3.

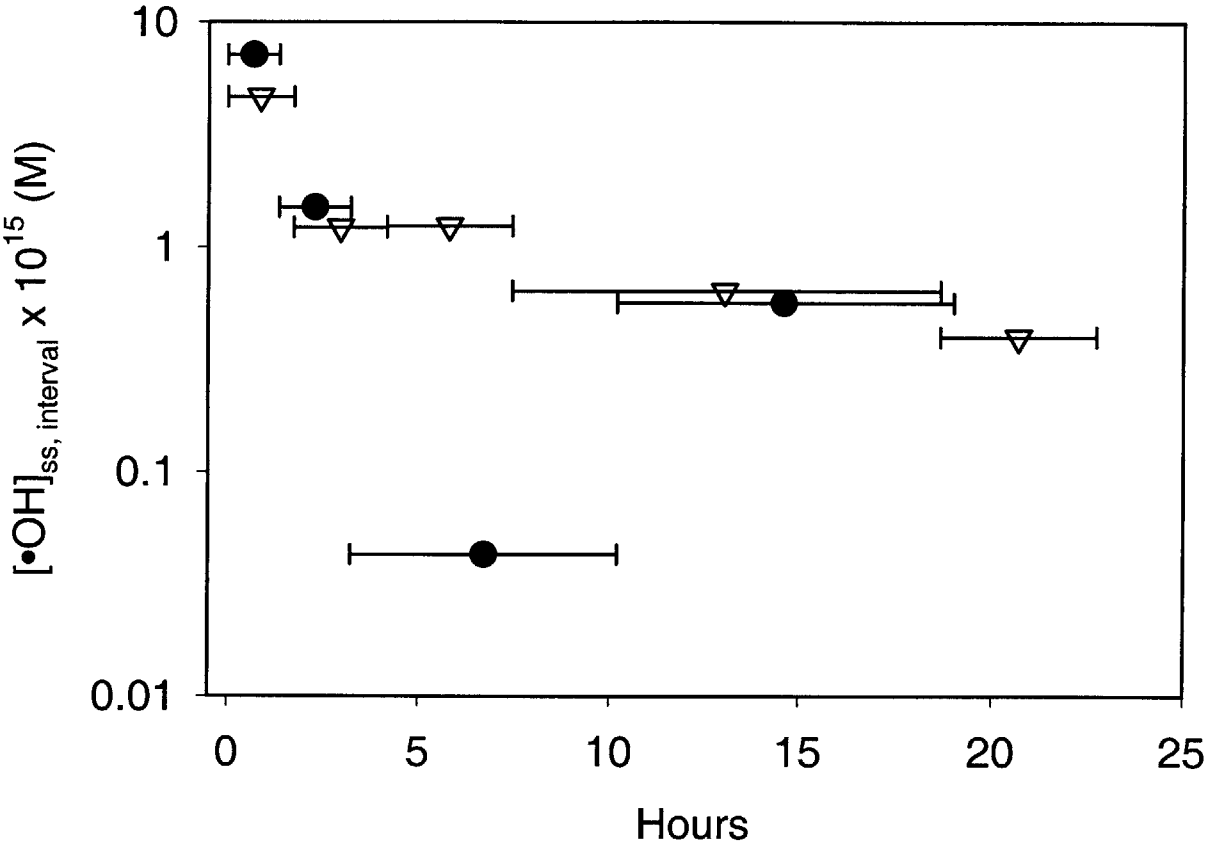

Figure 4-6a. $[\bullet OH]_{ss,\ interval}$ for the data shown in Figure 4-5a. The horizontal bars denote the time interval between the two consecutive data points that were used to calculate $[\bullet OH]_{ss,\ interval}$.

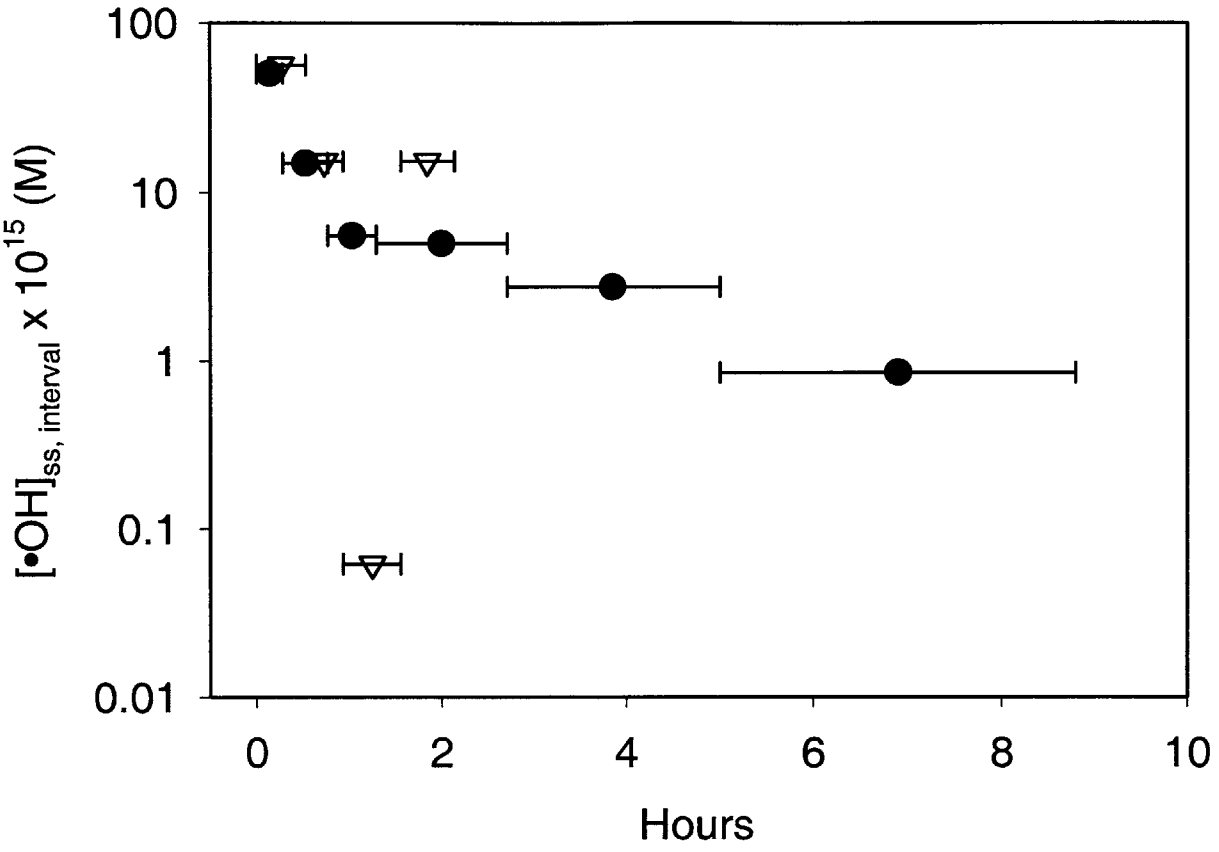

Figure 4-6b. $[\bullet OH]_{ss,\ interval}$ for the data shown in Figure 4-5b. The horizontal bars denote the time interval between the two consecutive data points that were used to calculate $[\bullet OH]_{ss,\ interval}$.

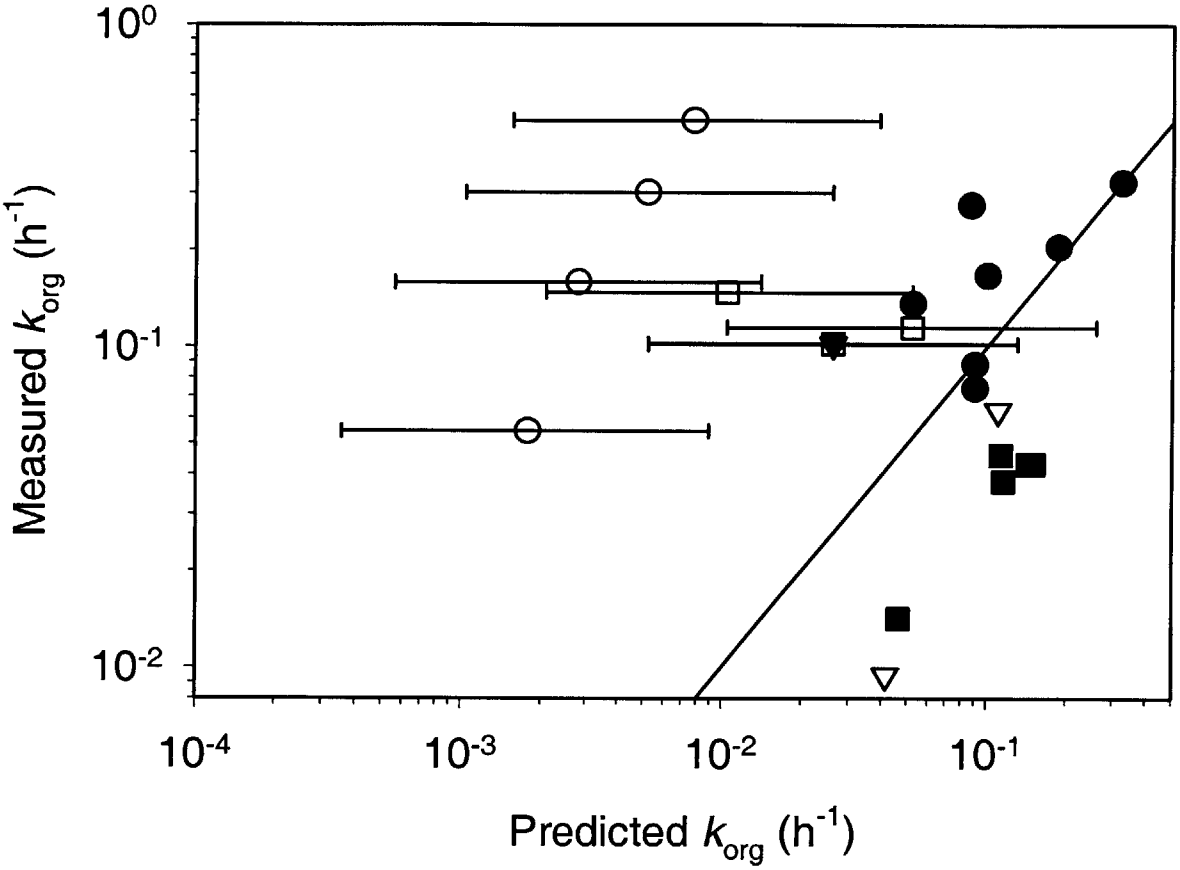

Figure 4-7. Comparison of the measured pseudo-first-order loss rate of various organic compounds, obtained from refs *36* (▼), *16* (○), *10* (▽), *17* (●), *11* (□), and *21* (■), versus our model predictions that account for electrostatic effects. The line represents perfect agreement between predicted and measured k_{org} values. The horizontal bars show the range of estimated k_{org} values using typical ranges of surface areas for goethite in studies where the surface area was not measured.

Chapter 5: Conclusions and Future Research Topics

or

-Just one more experiment...-

Contributions of This Thesis

This dissertation focused on understanding the factors that control the oxidation rates of organic compounds in Fenton and Fenton-like systems. The solution chain reaction was shown to be the dominant decomposition pathway of H_2O_2 and $H^{14}COOH$ at pH 4 in the presence of dissolved Fe, but this was not the case when the Fe source was ferrihydrite. The probable explanation, based on comparing modeling results from hypothetical mechanisms to experimental data, is that there were insufficient amounts of dissolved Fe to effectively propagate the solution phase chain reaction. Further work in the iron oxide/H_2O_2 system showed that the generation rate of •OH (V_{OH}) was proportional to the product of the concentrations of surface area of the iron oxide and H_2O_2. A model to estimate the pseudo-first-order rate loss rate coefficients of organic compounds (k_{org}) based on this relationship and the chemical reactions of the Fenton-like system was created. It successfully predicted V_{OH} and the loss rate of $H^{14}COOH$ in aquifer sand experiments, but yielded mixed results when it was used to estimate V_{OH} and k_{org} observed in iron oxide/H_2O_2 systems that other investigators had examined. Subsequent experimental results showed that the most likely explanation was that the attraction between formate anions and the positively charged goethite surface caused $H^{14}COOH$ to measure a greater $[•OH]_{ss}$ than the concentration that a neutral •OH probe would detect. Given this analysis, a better model was made that accounted for electrostatic effects, which involves knowing the speciation of the compound of interest, the pH of the solution, and the intrinsic surface acid-base equilibrium constants of the iron oxide.

This work showed that electrostatics affected the oxidation rate of formic acid in the iron oxide/H_2O_2 system. Researchers who study the oxidation rates of organic compounds in heterogeneous systems usually do not need to think about electrostatic effects because many organic pollutants have pK_a values greater than 7 and therefore are uncharged in neutral and acidic media. Nevertheless, some organic compounds such as benzoic acid have charged species at pH values of 7 or less. It then becomes important to know that electrostatics does affect the interactions between organic compounds and iron oxide. Electrostatics could also influence the concentration of any charged •OH sinks in the boundary layer, which would impact the oxidation rate of the compound of interest if the charged sink were an important sink of •OH.

This work also demonstrated that models could be used to understand key characteristics of the decomposition of hydrogen peroxide and organic compounds in the presence of iron

oxide. Researchers can use models to easily test and constrain mechanistic possibilities, and thus modeling is an efficient approach to investigate the behavior of complicated systems where only some parameters are known. Modeling results should always be compared against experimental data since that is the true test of a model's accuracy and robustness. When differences occur, as it did in this work, new areas of research become available for those who desire to improve on the current model.

Once some requirements and assumptions are satisfied, our model for predicting k_{org} from V_{OH} can be used to determine the proper H_2O_2 dosage to oxidize a pollutant in a given period of time. The oxidation process should take place in a well-mixed reactor that is not a continuous flow-through system. The organic pollutant must be primarily in the aqueous phase, and the type and concentration of the contaminant and the iron oxide has to be identified. The pH must be controlled as it dictates chemical speciation and the extent of electrostatic interactions between the various components in the system. The k_{org} that we are aiming for is then calculated by choosing the time and the factor that the organic compound must be reduced by:

$$k_{org} = \frac{-\ln([org]_t/[org]_0)}{t} \quad (1)$$

The corresponding steady state concentration of •OH is:

$$[\bullet OH]_{ss} = \frac{k_{org}}{k_{OH,org}} \quad (2)$$

where k_{org} has been corrected for electrostatic effects (if necessary), and the second-order rate constant of the contaminant with •OH ($k_{OH,org}$) is known. This is substituted into the expression for V_{OH} (refer to eq 8 of chapter 3),

$$V_{OH} = \left(k_{OH,org}[org]_0 + k_{OH,H_2O_2}[H_2O_2]_0\right)[\bullet OH]_{ss} \quad (3)$$

where we assume that all other •OH sinks in the groundwater, e.g., dissolved organic carbon and microorganisms, are at negligible concentrations. Lastly, we solve for the initial concentration of H_2O_2 by setting eq 3 equal to eq 10, 11, or 12 of chapter 3, depending on the form of the iron oxide in the soil. This assumes that all of the H_2O_2 reacts with the iron oxide, i.e., other H_2O_2 degradation pathways such as microbial enzymes are unimportant. Once considerable quantities of the pollutant and H_2O_2 have been consumed, V_{OH} will be significantly less than the value that we desire. We would therefore also have to determine when to put in more H_2O_2 to the system in order to maintain a steady V_{OH}. For instance, we could decide that the H_2O_2 in the reactor should

be replenished when V_{OH} has fallen to 90% of our expected V_{OH}, which tells us when more H_2O_2 must be added. Then, the contaminant concentration at that time is used in eq 3 to determine how much H_2O_2 we need to add to restore V_{OH} back to its original value. This is done iteratively until the pollutant level is reduced to our goal.

For a contaminant that is highly hydrophobic and thus sorbed on soil particles, we would need to know whether or not it is oxidized only in the aqueous phase. This would help us decide if the time that it would require to clean up the polluted soil is dictated by the desorption rate of the compound. If the compound can be oxidized in its sorbed state, then the contribution of the surface oxidation rate to the total oxidation rate has to be evaluated.

If an in situ remediation scheme is used to treat groundwater, then a model for predicting the proper dosage of H_2O_2 must also consider issues such as soil porosity, dispersion, and transport of pollutants downstream due to the gradient caused by the well injections. The successful model would likely incorporate our model into a groundwater flow model that is appropriate for the site.

Future Work

Many topics related to the Fenton and Fenton-like systems remain to be explored. For instance, the mechanism to describe the iron oxide catalyzed decomposition of H_2O_2 is still incomplete. The correct mechanism should show that V_{OH} is proportional to the concentrations of H_2O_2 and iron oxide, and explain why V_{OH} is relatively constant from pH 4 to pH 10. Understanding whether H_2O_2 is chemisorbed or physisorbed onto the iron oxide could help in formulating this mechanism.

Reactive species such as superoxide (O_2^-), perhydroxyl radical ($HO_2^{\bullet}$), and hydroperoxide anion (HO_2^-) are also produced in the Fenton-like system, and they could be involved in reactions that transform organic compounds via reduction instead of oxidation (*1-3*). A greater understanding of this non-hydroxyl radical degradation pathway could increase the applicability of the Fenton-like system for waste treatment and remediation.

The experiments in this thesis were done in solutions containing only a few solutes, but groundwater typically contains metals, carbon (dissolved and particulate), anions such as phosphate, sulfate, and carbonate, and microorganisms. The impact of these constituents on the kinetics of the reactions of the Fenton system and the oxidation rates of contaminants has not been completely explored (*4-9*). For example, microbes could be an important nonradical

producing sink of H_2O_2 because they use catalase and peroxidase to decompose H_2O_2 to water and oxygen:

$$2H_2O_2 \xrightarrow{\text{catalase}} 2H_2O + O_2 \quad (4)$$

$$H_2O_2 + NADH + H^+ \xrightarrow{\text{peroxidase}} 2H_2O + NAD^+ \quad (5)$$

[Although this is a disadvantage from the viewpoint of chemical oxidation, H_2O_2 has been used as a way of delivering oxygen to aerobic microorganisms that are responsible for bioremediation in aquifers (*10-12*).] Other metal oxides also react with H_2O_2 (*13*), but not all make •OH and so they would represent another set of nonradical producing sinks. Experiments will be needed to determine the effect of each component and their interactions as a whole.

Contaminants in the subsurface are often sorbed onto soil particles and may be harder to oxidize in this state (*14*). Therefore, the rates at which they adsorb and desorb would control their aqueous and sorbed concentrations and determine how quickly they are oxidized by •OH. This subject has not been explored in-depth in the literature (*15-17*), but understanding it could potentially increase the accuracy of the model predictions of k_{org} for organic compounds that sorb strongly onto solids.

Literature Cited

(1) Watts, R. J.; Bottenberg, B. C.; Hess, T. F.; Jensen, M. D.; Teel, A. L. *Environ. Sci. Technol.* **1999**, *33*, 3432-3437.

(2) Teel, A. L.; Watts, R. J. *J. Hazard. Mater.* **2002**, *94*, 179-189.

(3) Hess, T. F.; Renn, T. S.; Watts, R. J.; Paszczynski, A. J. *Analyst* **2003**, *128*, 156-160.

(4) Tyre, B. W.; Watts, R. J.; Miller, G. C. *J. Environ. Qual.* **1991**, *20*, 832-838.

(5) Lipczynska-Kochany, E.; Sprah, G.; Harms, S. *Chemosphere* **1995**, *30*, 9-20.

(6) Voelker, B. M.; Sulzberger, B. *Environ. Sci. Technol.* **1996**, *30*, 1106-1114.

(7) Valentine, R. L.; Wang, H. C. A. *J. Environ. Eng.* **1998**, *124*, 31-38.

(8) Lindsey, M. E.; Tarr, M. A. *Water Res.* **2000**, *34*, 2385-2389.

(9) Huling, S. G.; Arnold, R. G.; Sierka, R. A.; Miller, M. R. *Water Res.* **2001**, *35*, 1687-1694.

(10) Aggarwal, P. K.; Means, J. L.; Downey, D. C.; Hinchee, R. E. *J. Hazard. Mater.* **1991**, *27*, 301-314.

(11) Hinchee, R. E.; Downey, D. C.; Aggarwal, P. K. *J. Hazard. Mater.* **1991**, *27*, 287-299.

(12) Morgan, P.; Watkinson, R. J. *Water Res.* **1992**, *26*, 73-78.

(13) Pardieck, D. L.; Bouwer, E. J.; Stone, A. T. *J. Contam. Hydrol.* **1992**, *9*, 221-242.

(14) Sedlak, D. L.; Andren, A. W. *Water Res.* **1994**, *28*, 1207-1215.

(15) Watts, R. J.; Kong, S.; Dippre, M.; Barnes, W. T. *J. Hazard. Mater.* **1994**, *39*, 33-47.

(16) Watts, R. J.; Jones, A. P.; Chen, P.-H.; Kenny, A. *Water Environ. Res.* **1997**, *69*, 269-275.

(17) Watts, R. J.; Stanton, P. C.; Howsawkeng, J.; Teel, A. L. *Water Res.* **2002**, *36*, 4283-4292.

Appendix A

or

-The nitty-gritty, revealed!-

Table A-1. Concentration of dissolved iron (defined as iron that passed through a 0.02-μm filter) in the ferrihydrite experiments. Ferrihydrite was diluted from a freshly prepared 4 x 10^{-4} M stock solution, except where noted, into 200 mL. The detection limit for Fe is 0.03 μM.

[Ferrihydrite] (μM)	Number of hours in experiment	$[Fe]_{diss}$ at start (μM)	$[Fe]_{diss}$ at end (μM)	$[Fe]_{diss}$ (μM)[a]
10	56.7		0.83	
50	56.7		0.90	
100	56.8		0.56	
300	72.1		0.49	
10	55.4		0.46	
40	55.3		0.30	
100	55.3		0.31	
150	55.2		0.043	
60	73.0	0.036	0.14	
100	73.0	0.15	0.071	
415[b]	27.8	2.17	1.80	
350	9.6	5.37	7.23	
436[b]	9.6	2.72	1.04	
200	24.7	<0.03	<0.03	

360	13.0	<0.03	<0.03	
200	23.8	<0.03	<0.03	
200	23.9	<0.03	<0.03	
200	25.6			<0.03
100	34.9			19.83
100	47.4	<0.03	<0.03	
200[c]	25.9	<0.03	0.62	
200[c]	26.0	<0.03	0.36	
100	55.9			0.62
100[d]	55.9			0.91
100[d]	56.0			2.89
200	26.6			0.57
200[d]	26.5			0.84
60	50.0			1.34
60[d]	50.1			1.10

[a] In this column, the time when the sample was taken was not written down.

[b] Diluted from a 5×10^{-4} M solution of ferrihydrite.

[c] Experiment contained 100 μM *tert*-butyl alcohol.

[d] Experiment contained 10 μM *tert*-butyl alcohol.

Kelvin effect

The Kelvin effect (*1*) states that colloids and small crystals have a greater solubility than their larger counterparts because they are thermodynamically less stable. It is quantified as follows (*2*):

$$\log K_{sp}(r) = \log K_{sp}(r = \infty) + \frac{2\gamma(MW)}{2.303RT\rho r} \qquad (1)$$

where log K_{sp}(r) is the solubility product of the colloid with radius r, r is the colloidal radius, log K_{sp}(r = ∞) is the solubility product of the large crystals, γ is the interfacial tension of the solid-water interface, MW is the molecular weight, R is the gas constant, T is the absolute temperature, and ρ is the mineral density. γ for ferrihydrite is not known, but can be estimated from the values for goethite and hematite because mineral hardness correlates positively with γ (*2*). Therefore, γ for ferrihydrite is expected to be less than 1600 and 1200 mJ/m^2 (*1*), the respective values for goethite and hematite. Assuming a value of 250 mJ/m^2 and a colloidal radius of 0.02 μm (this filter size retained most of the ferrihydrite colloids),

$$\frac{2(2.5 \times 10^{-5}\ J\ cm^{-2})(107\ g\ mol^{-1})}{2.303(8.31\ J\ mol^{-1}\ deg^{-1})(298.15\ deg)(3.96\ g\ cm^{-2})(2 \times 10^{-6}\ cm)} = 0.1 \qquad (2)$$

then the change to the solubility product is small compared to the known range for K_{sp} ($10^{-39.4}$-$10^{-37.0}$; *3*).

Literature Cited

(1) Stumm, W.; Morgan, J. J. *Aquatic Chemistry*; John Wiley & Sons, Inc.: New York, 1996.

(2) Gschwend, P. M.; Reynolds, M. D. *J. Contam. Hydrol.* **1987**, *1*, 309-327.

(3) Schwertmann, U.; Cornell, R. M. *Iron Oxides in the Laboratory*; VCH Publishers: New York, 1991.

Appendix B

or

-0 = 1?-

pH increase due to oxidation of formic acid

The oxidation of formic acid by •OH is expected to increase the pH of the system in this manner:

$$\bullet OH + HCOO^- + O_2 \rightarrow CO_2 + O_2^- + H_2O \quad (1)$$

$$H^+ + O_2^- \rightarrow HO_2 \quad (2)$$

$$2HO_2 \rightarrow H_2O_2 + O_2 \quad (3)$$

The first two reactions are a significant sink of H^+ in our experiments because the dominant species of formic acid and superoxide at pH 4 are formate and perhydroxyl radical, respectively. The oxygen that reaction 1 consumes is plentiful since the solutions are open to air ($[O_2]_{sat}$ = 258 μM at 25 °C; *1*) and constantly stirred, which facilitates air-liquid transfer.

Experiments with H_2O_2 as the dominant •OH sink

Figures B1a-e show typical data sets of loss of ^{14}C-labeled formic acid and H_2O_2 over time from experiments containing ferrihydrite, goethite, hematite, or Georgetown sand. We compared two methods of determining k_{HCOOH}, non-linear regression fits of the ^{14}C data and linear regression of the log-transformed data, for all experiments except those that used ferrihydrite. The average percent difference in the k_{HCOOH} obtained was insignificant (4.1, with a standard deviation of 5.2).

Experiments with formic acid as the dominant •OH sink

Figures B2a-f show pseudo-first order and zeroth-order fits to formic acid loss data in experiments containing 0.6 g/L of goethite. Both types of regression produce similarly good fits for most of the data sets.

Given that formic acid is initially the main sink of •OH, if one assumes that $[H_2O_2]$, and therefore also V_{OH}, remain constant over time, then the loss of $H^{14}COOH$ should follow zeroth-order kinetics. However, some H_2O_2 was consumed during the experiments, thus decreasing V_{OH}, and in the later parts of some experiments H_2O_2 became a competing •OH sink because $[HCOOH]_T$ decreased more rapidly than $[H_2O_2]$ (see Figures B2a-f and B3). Strictly speaking, then, neither first-order nor zeroth-order kinetics should precisely describe formic acid loss in these experiments. However, since we observed that the loss of formic acid is well described by first-order kinetics, using k_{HCOOH} from eq 6 to calculate V_{OH} in eq 9 still provides an excellent estimate of the initial rate of •OH formation.

Literature Cited

(1) Wetzel, R. G. *Limnology*; Harcourt Brace College Publishers: Fort Worth, 1983.

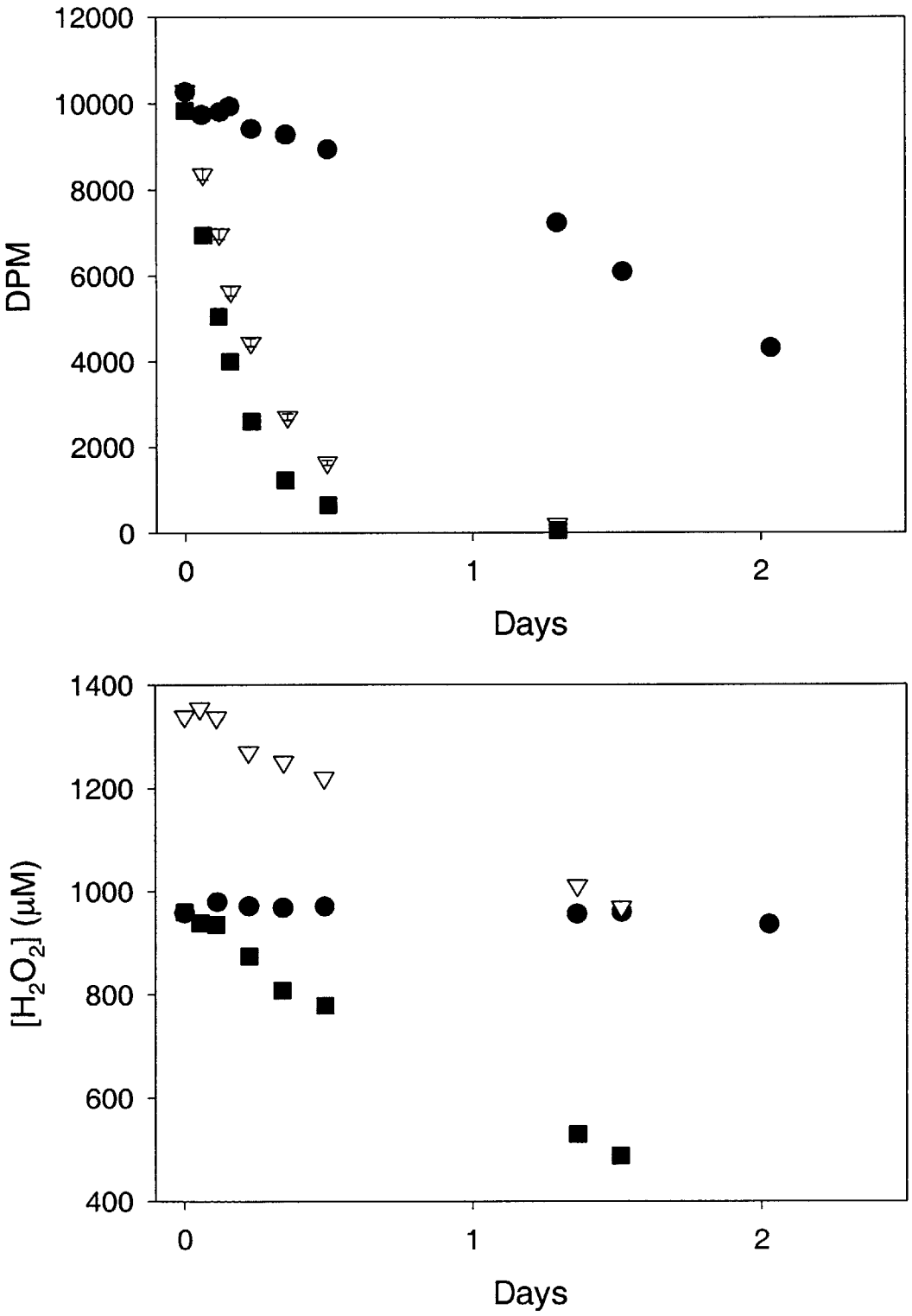

Figure B1a. Representative data set of the concentration of ^{14}C-labeled formic acid (given as disintegrations per minute) and hydrogen peroxide over time in experiments at pH 4, containing 20 μM (●), 200 μM (▽), or 280 μM (■) ferrihydrite. $[HCOOH]_{T,0}$ was 110 nM.

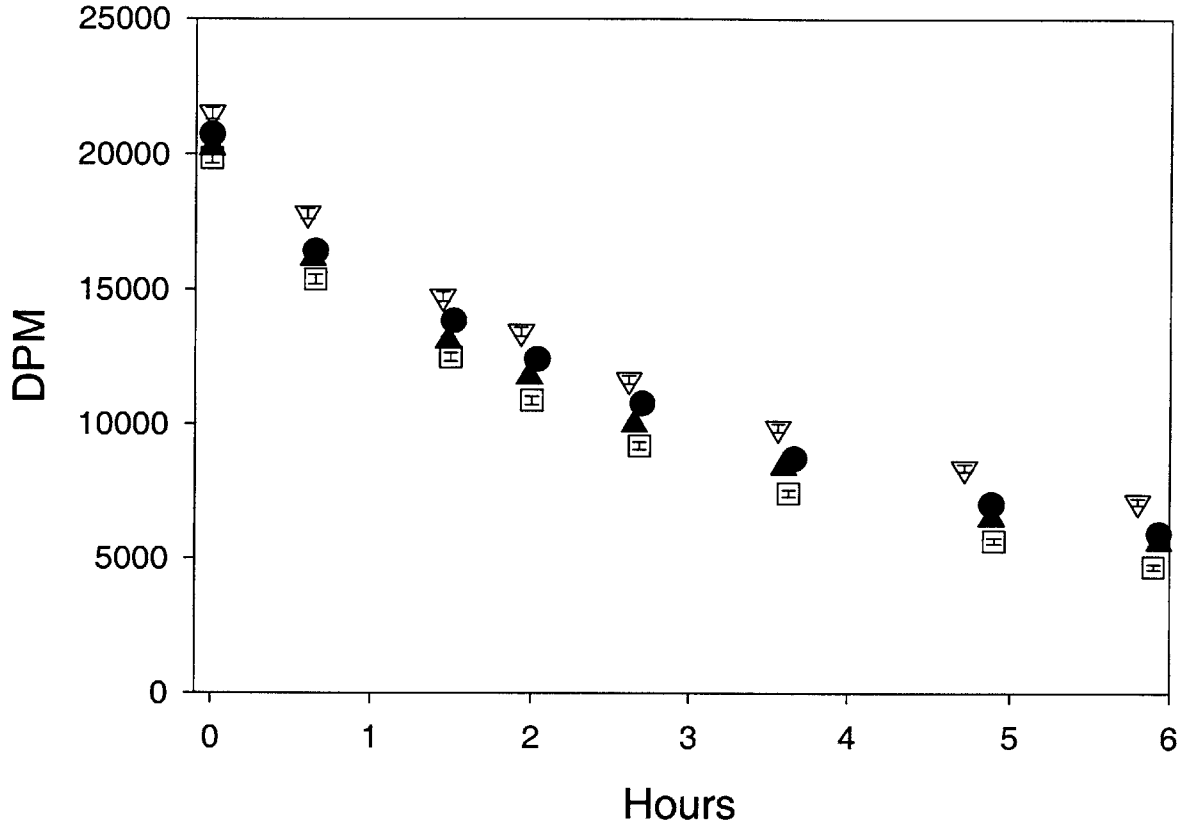

Figure B1b. Representative data set of the concentration of ^{14}C-labeled formic acid (given as disintegrations per minute) over time in experiments at pH 4, 190 μM ferrihydrite, $[HCOOH]_{T,0}$ = 212-219 nM, and $[H_2O_2]_0$ = 50 mM(●), 100 mM (□), 200 mM (▲), or 400 mM(▽).

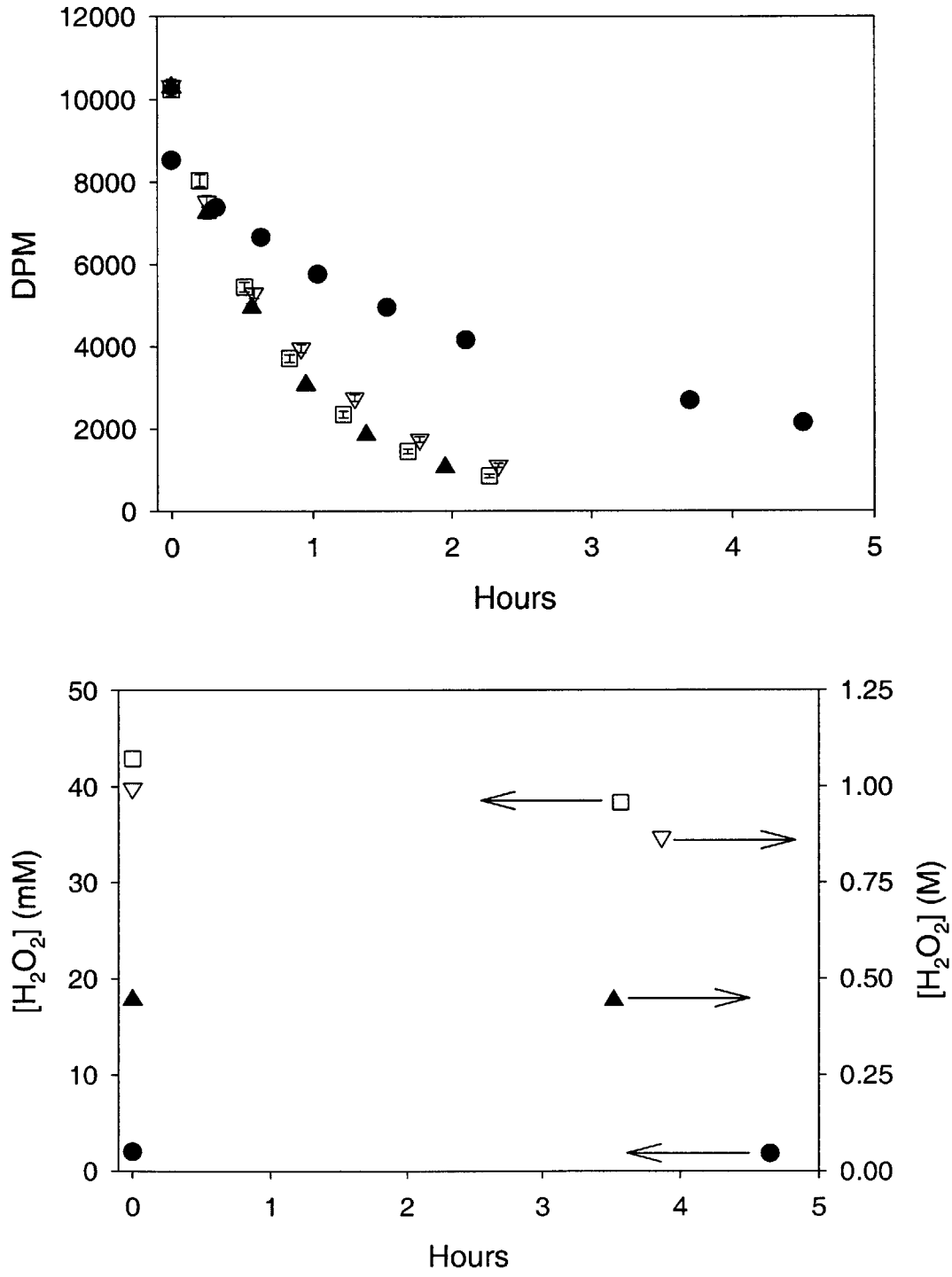

Figure B1c. Representative data set of the concentration of ^{14}C-labeled formic acid (given as disintegrations per minute) and hydrogen peroxide over time in experiments at pH 4, containing 0.6 g/L of goethite, $[HCOOH]_{T,0}$ = 92-112 nM, and $[H_2O_2]_0$ = 2 mM (●), 40 mM (□), 0.4 M (▲), or 1 M (▽).

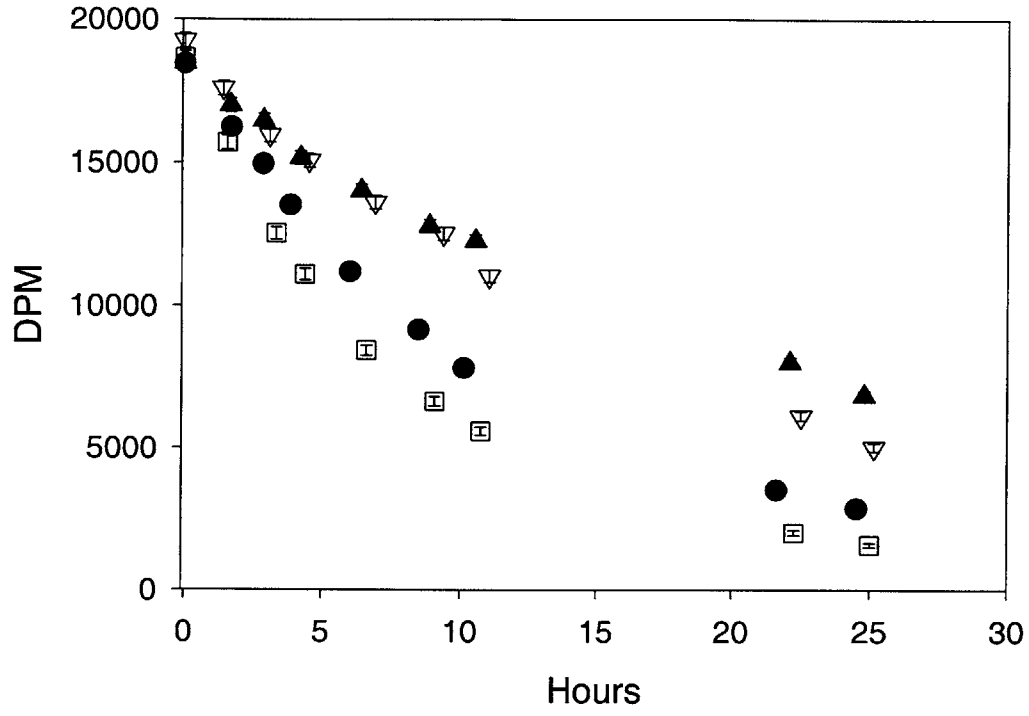

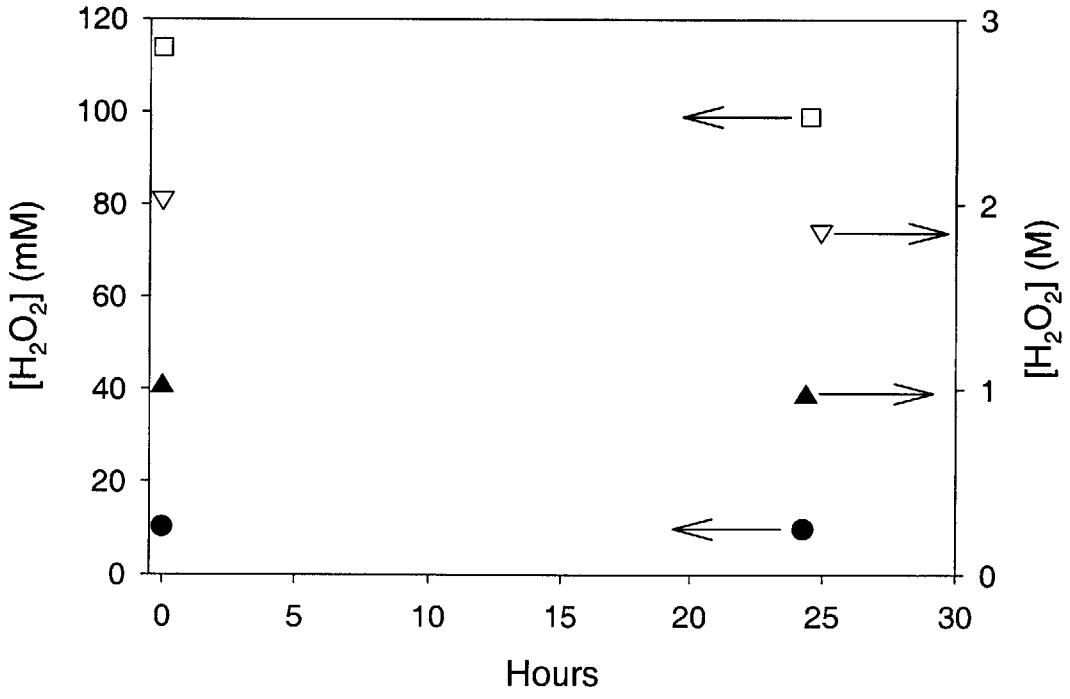

Figure B1d. Representative data set of the concentration of ^{14}C-labeled formic acid (given as disintegrations per minute) and hydrogen peroxide over time in experiments at pH 4, containing 1 g/L of hematite, $[HCOOH]_{T,0}$ = 201-210 nM, and $[H_2O_2]_0$ = 10 mM (●), 100 mM (□), 1 M (▲), or 2 M (▽).

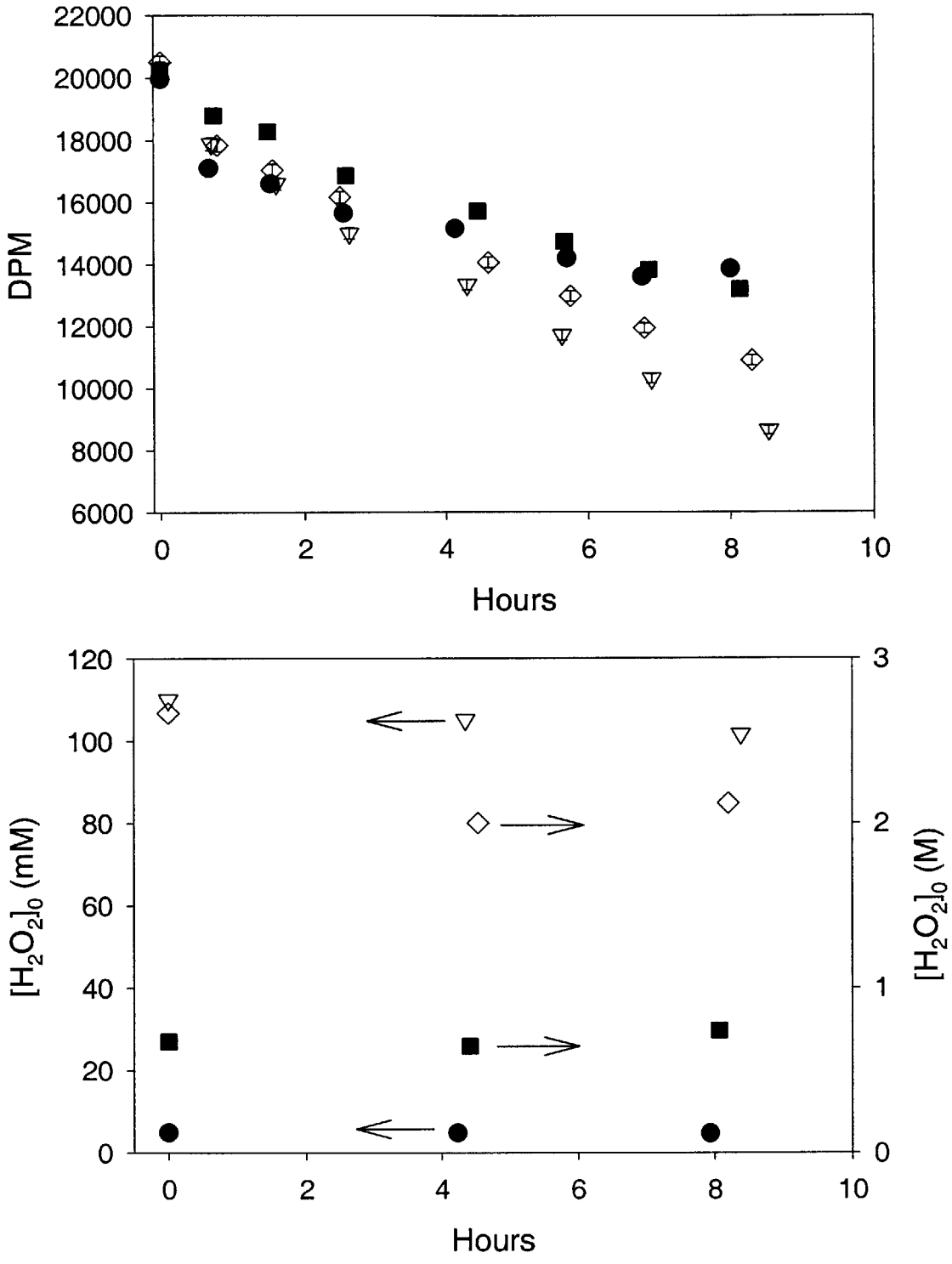

Figure B1e. Representative data set of the concentration of ^{14}C-labeled formic acid (given as disintegrations per minute) and hydrogen peroxide over time in experiments at pH 4, containing 60 g/L of Georgetown sand, $[HCOOH]_{T,0}$ = 162-166 nM, and $[H_2O_2]_0$ = 5 mM (●), 110 mM (▽), 675 mM (■), or 2.7 M (◇).

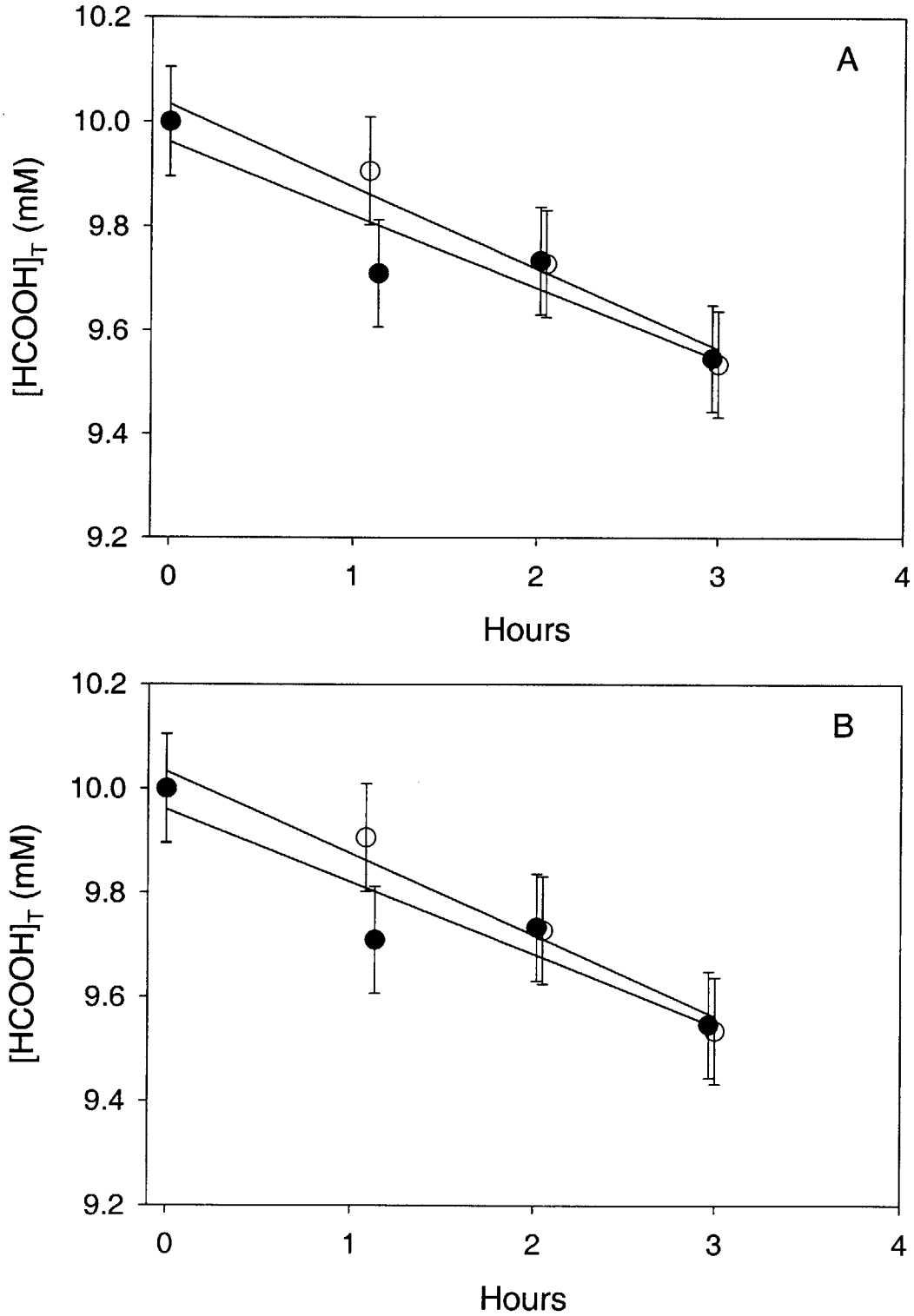

Figure B2a. Concentration of HCOOH versus time from experiments containing 0.6 g/L of goethite, $[HCOOH]_{T,0}$ = 10 mM, and $[H_2O_2]_0$ = 2 mM (●) or 10 mM (○). (A) shows the nonlinear regression fits to the data, while (B) shows the linear regression fits.

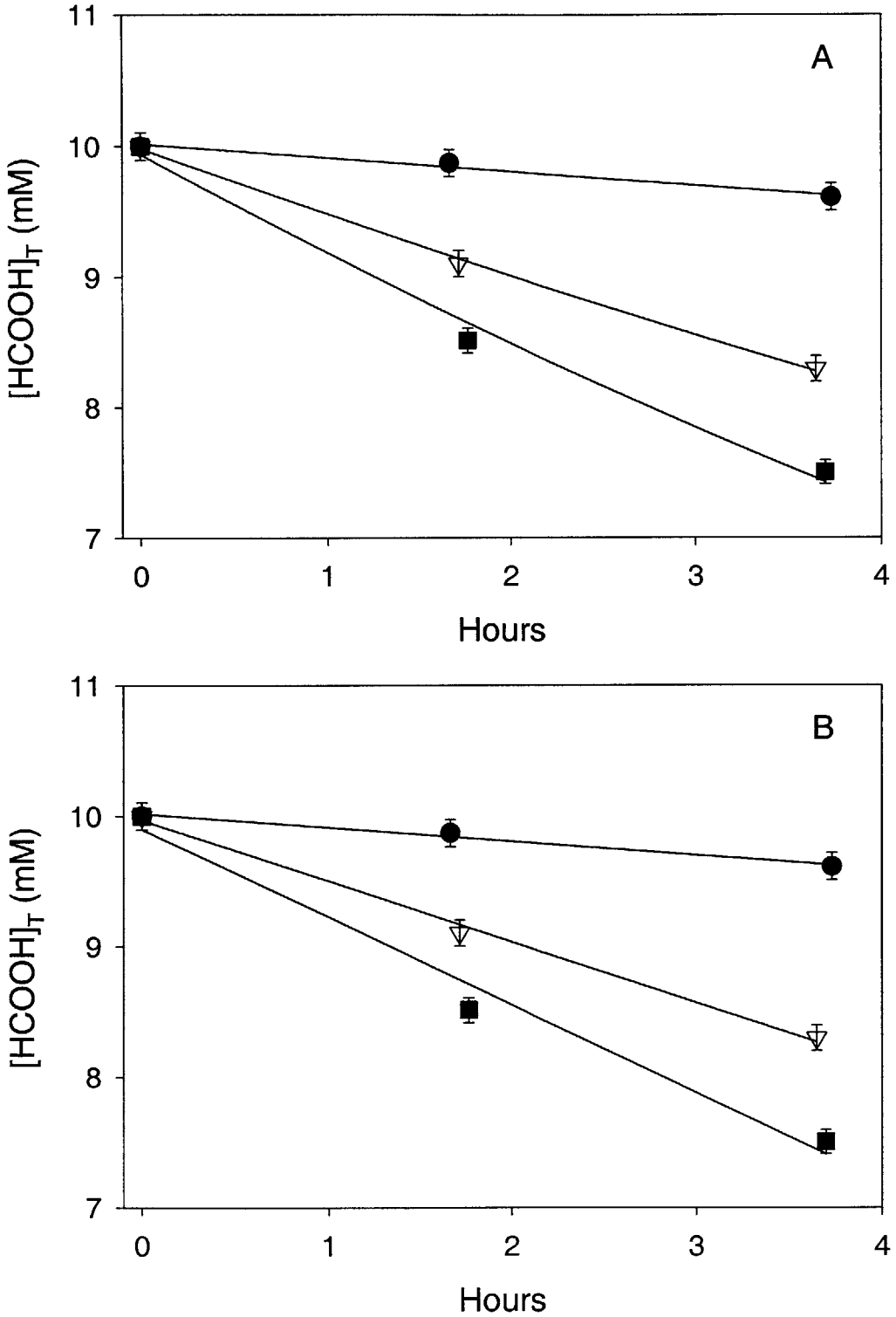

Figure B2b. Concentration of HCOOH versus time from experiments containing 0.6 g/L of goethite, $[HCOOH]_{T,0}$ = 10 mM, and $[H_2O_2]_0$ = 10 mM (●), 50 mM (▽), or 100 mM (■). (A) shows the nonlinear regression fits to the data, while (B) shows the linear regression fits.

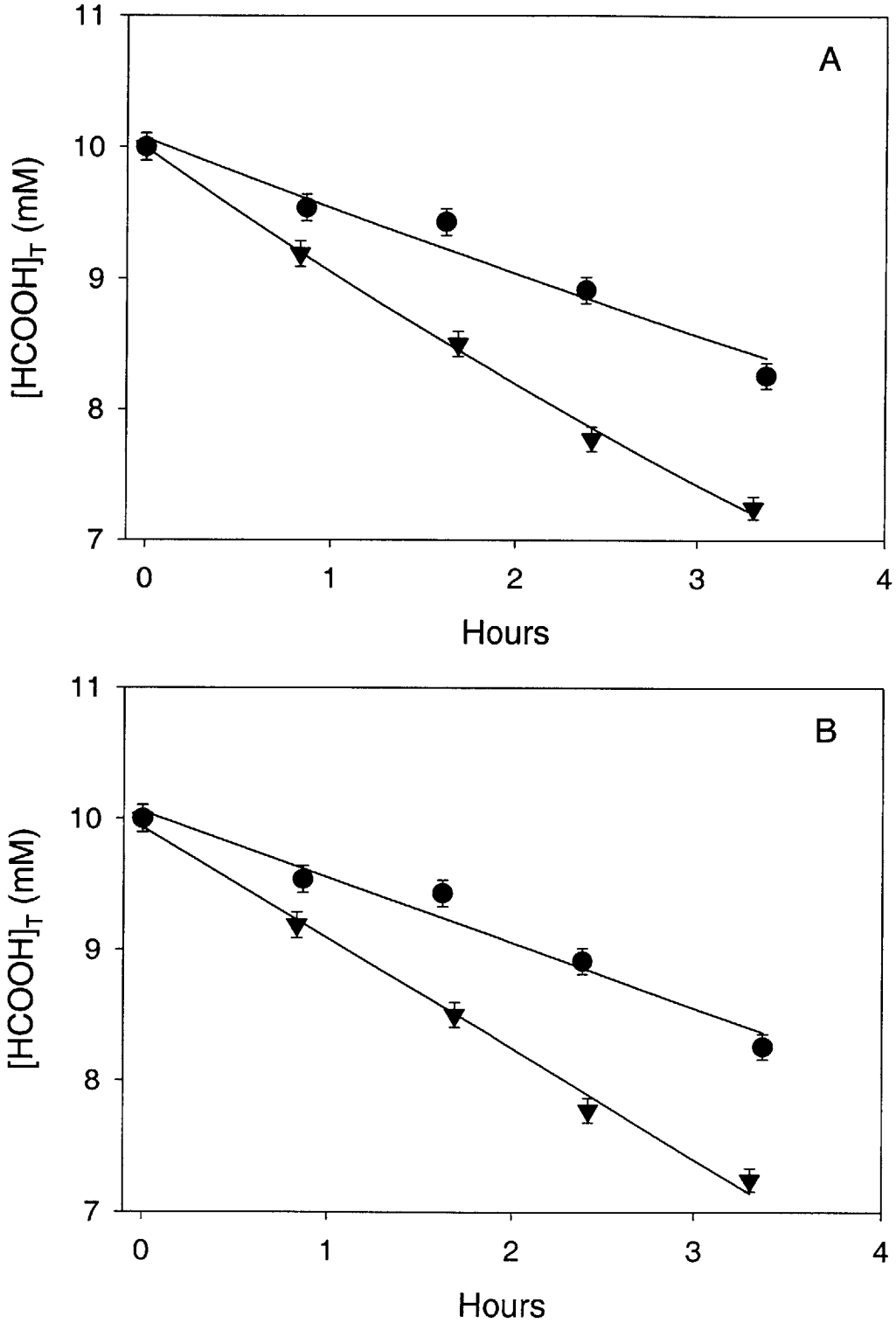

Figure B2c. Concentration of HCOOH versus time from experiments containing 0.6 g/L of goethite, $[HCOOH]_{T,0}$ = 10 mM, and $[H_2O_2]_0$ = 50 mM (●) or 100 mM (▼). (A) shows the nonlinear regression fits to the data, while (B) shows the linear regression fits.

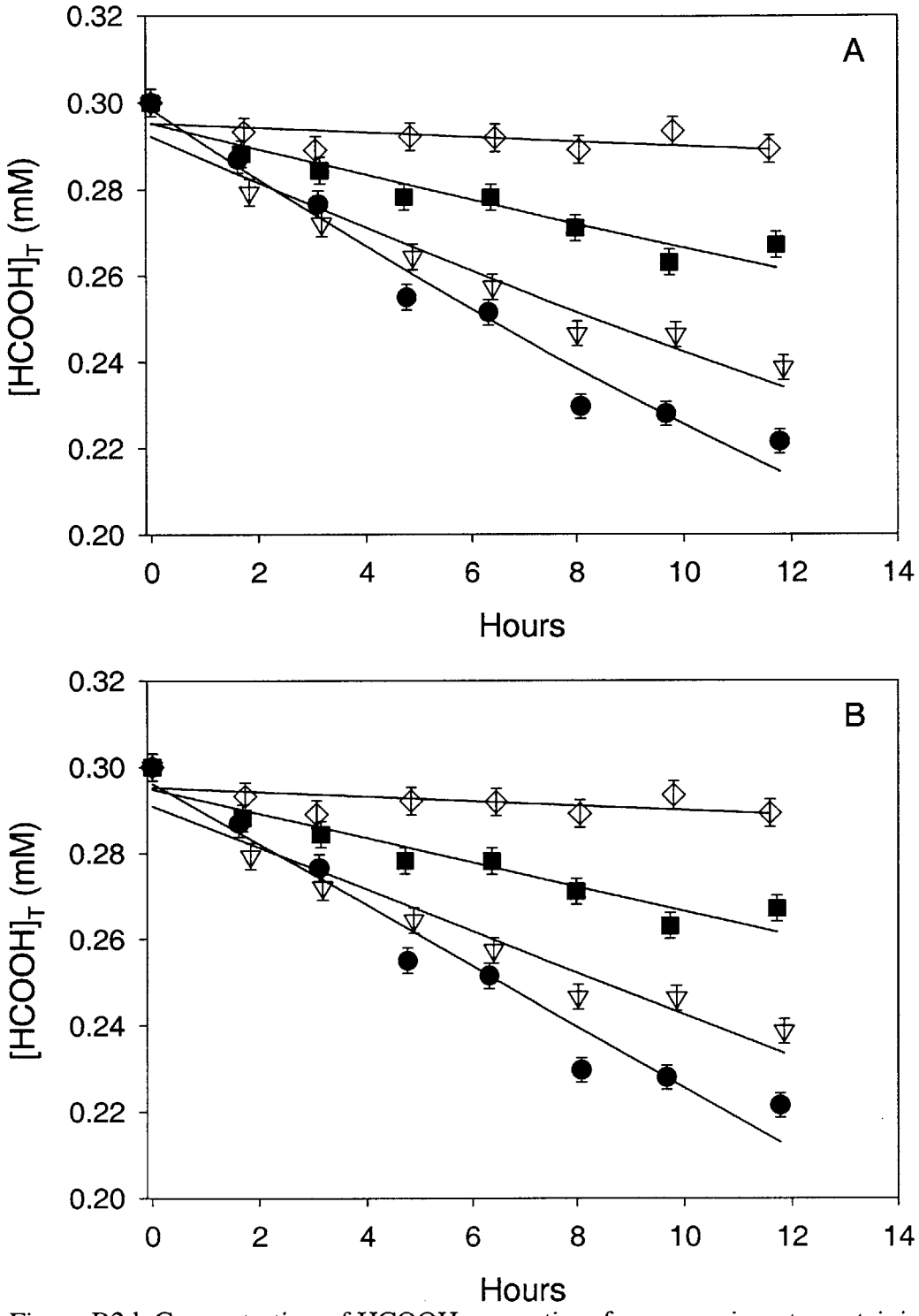

Figure B2d. Concentration of HCOOH versus time from experiments containing 0.6 g/L of goethite, $[HCOOH]_{T,0}$ = 0.3 mM, and $[H_2O_2]_0$ = 700 μM (●), 500 μM (▽), 250 μM (■), or 100 μM (◇). (A) shows the nonlinear regression fits to the data, while (B) shows the linear regression fits.

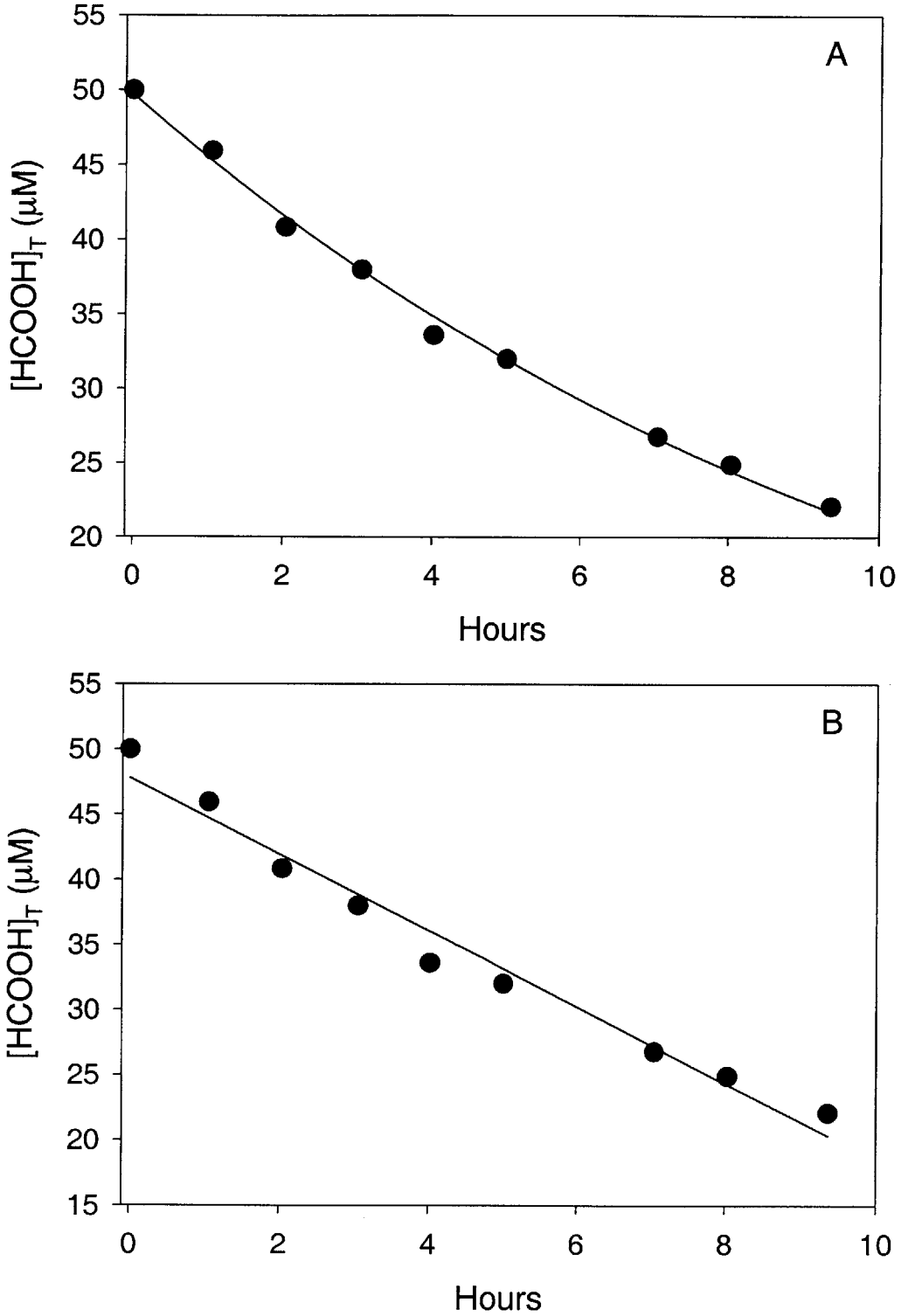

Figure B2e. Concentration of HCOOH versus time from experiments containing 0.6 g/L of goethite, $[HCOOH]_{T,0}$ = 50 μM, and $[H_2O_2]_0$ = 600 μM. (A) shows the nonlinear regression fit to the data, while (B) shows the linear regression fit.

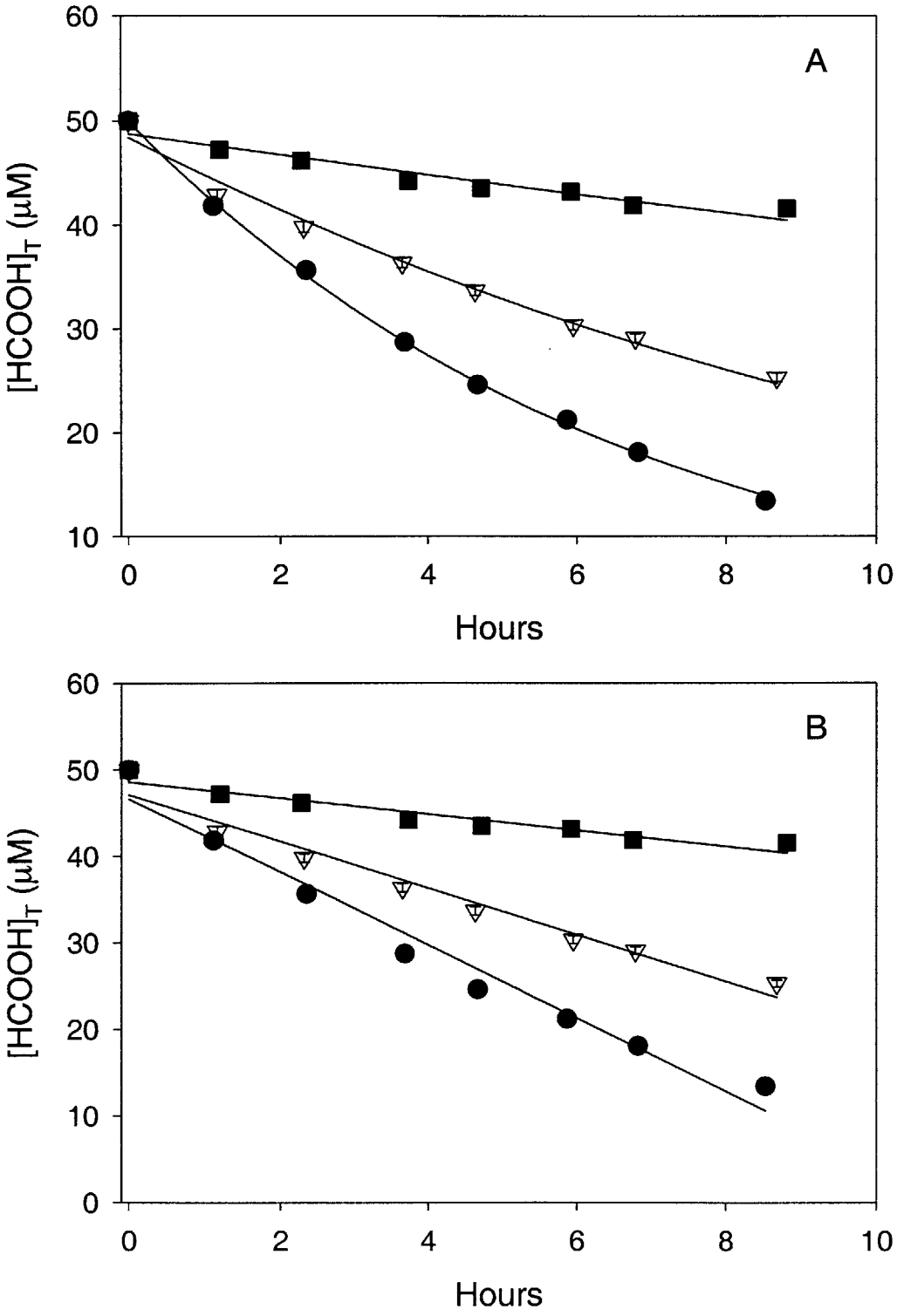

Figure B2f. Concentration of HCOOH versus time from experiments containing 0.6 g/L of goethite, $[HCOOH]_{T,0}$ = 50 μM, and $[H_2O_2]_0$ = 500 μM (●), 250 μM (▽), or 100 μM (■). (A) shows the nonlinear regression fits to the data, while (B) shows the linear regression fits.

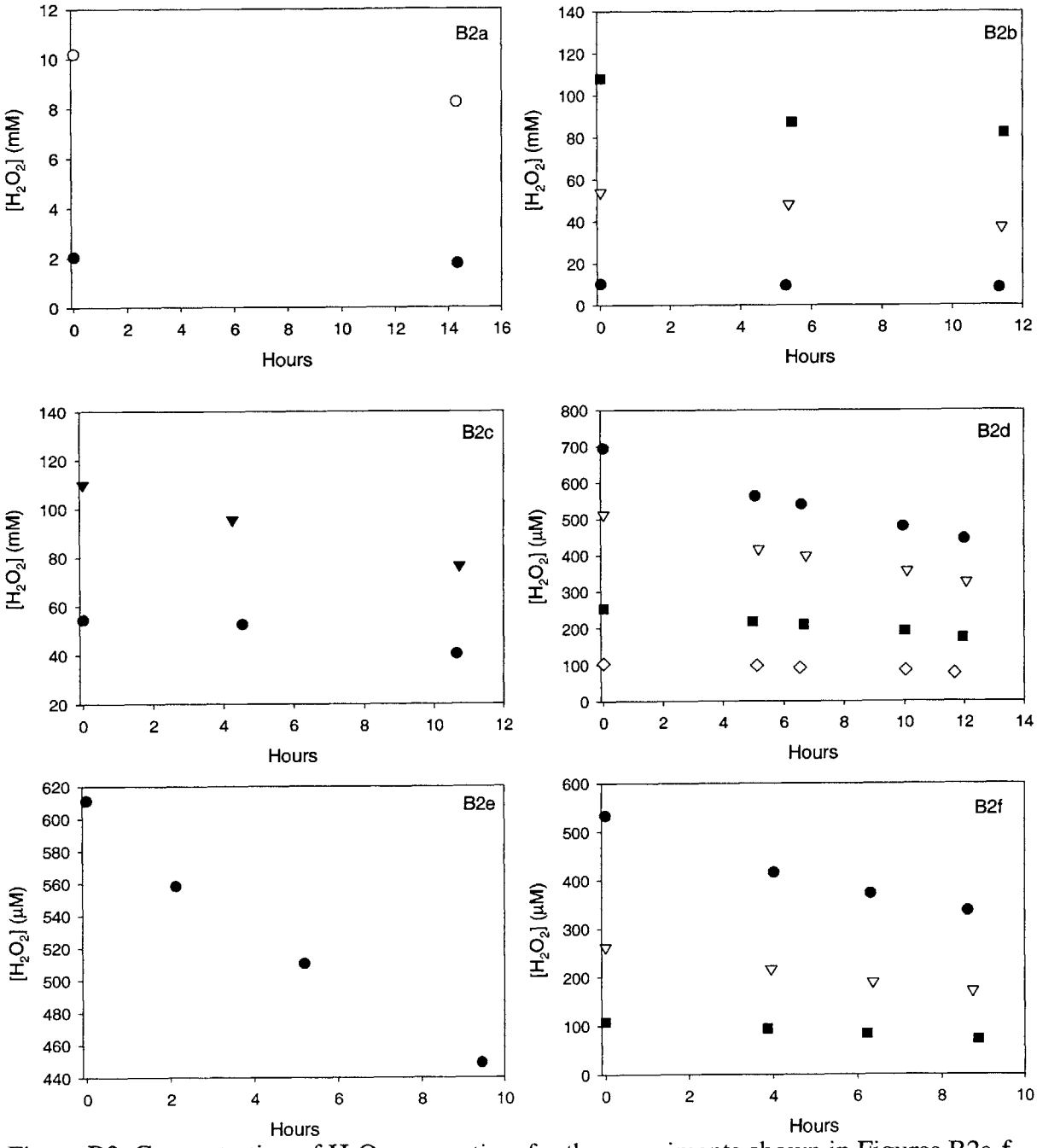

Figure B3. Concentration of H_2O_2 versus time for the experiments shown in Figures B2a-f.

Appendix C

or

-Details, details-

Table C-1. Final pH of experiments using goethite and H_2O_2 to oxidize 2-CP. The initial pH was 4.0.

[goethite] (g/L)	$[H_2O_2]_0$ (mM)	$[2\text{-CP}]_0$ (μM)	Number of hours in experiment	Final pH
2.5	160	350	9.3	3.3
2.5	160	330	7.7	3.5
2.5	142	310	6.4	3.5

We used eq 17 from chapter 4 (shown below) to determine the impact on electrostatics as a result of a decrease of 0.5-0.7 pH units over the course of an experiment.

$$\left(-\frac{d[HCOOH]}{dt}\right)_{el} = \frac{A}{V}\int_0^x \left(k_{OH,HCOOH}[\bullet OH]_{ss}(x)[HCOOH]_{bulk} + k_{OH,HCOO^-}[\bullet OH]_{ss}(x)[HCOO^-]_{bulk}\, e^{-\Delta ZF\Psi(x)/RT}\right)dx \qquad (1)$$

The results (Table C-2) indicate that Ψ_0 increases as pH decreases, as expected, but ζ remains relatively constant because the percentage of total formic acid that is formate decreases as pH decreases. Therefore, the changes in pH that we observed have no significant impact on the electrostatics modeling.

Table C-2. $\int_0^\infty k_{OH,HCOO^-}[\bullet OH]_{ss}(x)[HCOO^-]_{bulk}e^{-\Delta ZF\Psi(x)/RT}dx$ (ζ) as a function of pH. Ψ_0 was calculated in the same manner as described in chapter 4, and ζ was evaluated at I = 10 mM and $[H_2O_2]_0$ = 160 mM.

pH	Ψ_0 (V)	Percent of total formic acid as formate	ζ
4	0.16	64	4.8×10^{-7}
3.5	0.17	36	5.1×10^{-7}
3.3	0.18	26	5.0×10^{-7}

Appendix D

or

-If a picture is worth a thousand words, then I wrote much more than I thought!-

The graphs in the following pages depict the raw data for the experiments discussed in chapters 2-4. All experiments were done at I = 10 mM $NaClO_4$ and pH 4 unless stated otherwise. The rate constants were obtained by fitting the data to the function $[C] = [C]_0 \exp(-kt)$.

Figures D1-14 show data discussed in chapter 2.

Figures D1-7, D11C-D12, and D15-26 show data discussed in chapter 3.

Figures D27-35 show data discussed in chapter 4.

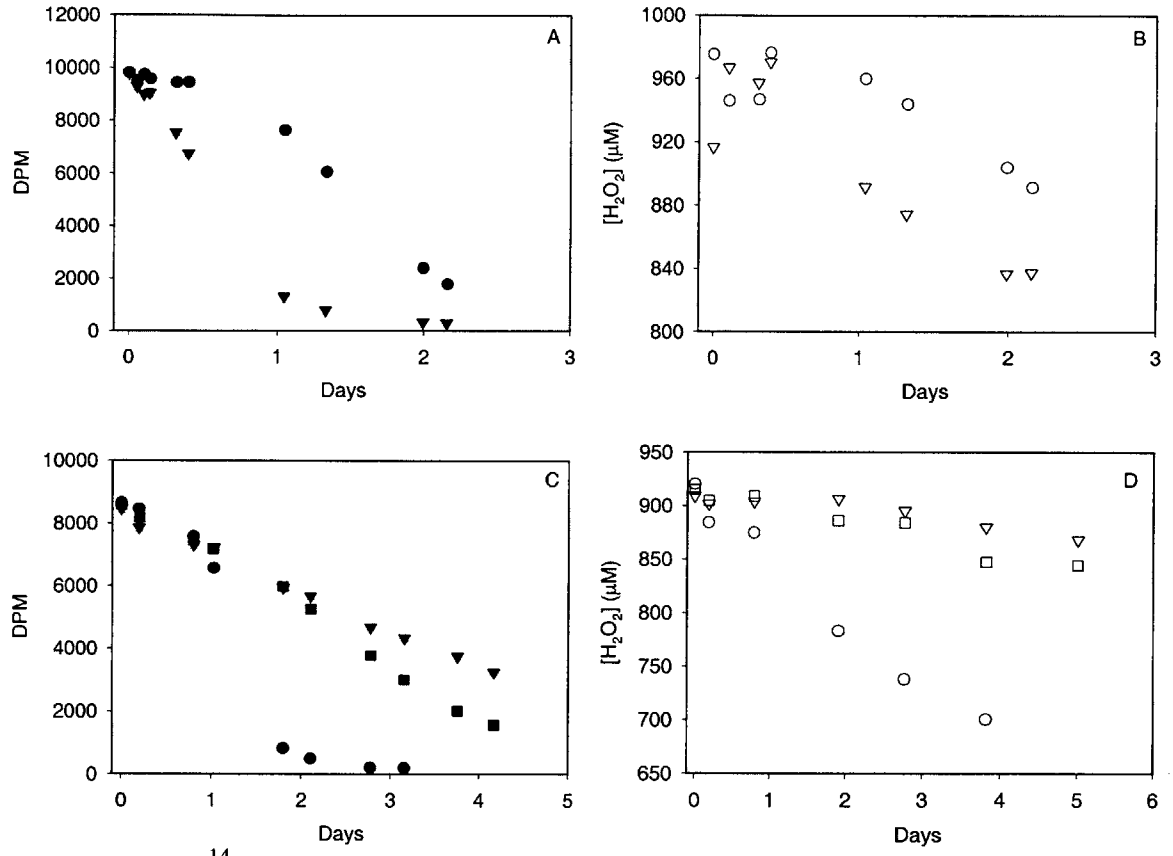

Figure D1. (A) ^{14}C activity in experiments with [Fe(III)] = 0.79 (●) or 2.11 (▼) μM, and k = 0.53 and 1.45 d^{-1}, respectively. (B) $[H_2O_2]$ in experiments described in (A), with k = 0.033 (○) and 0.066 (▽) d^{-1}. (C) ^{14}C activity in experiments with [Fe(III)] = 1.30 (●), 0.58 (▼), or 0.73 (■) μM, and k = 0.76, 0.21, and 0.32 d^{-1}, respectively. (D) $[H_2O_2]$ in experiments described in (C), with k = 0.072 (○), 0.0082 (▽), and 0.017 (□) d^{-1}.

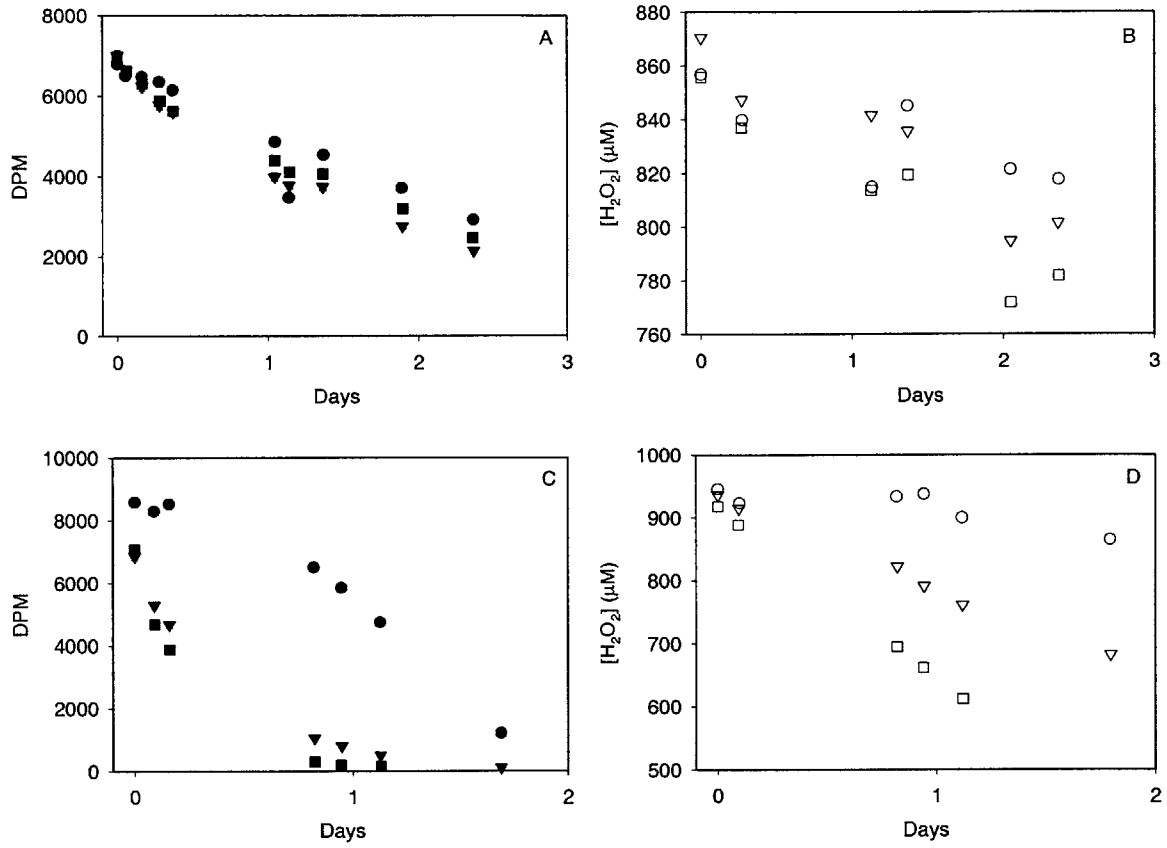

Figure D2. (A) ^{14}C activity in experiments with [ferrihydrite] = 5.59 (●), 37.66 (▼) or 85.69 (■) μM, and k = 0.36, 0.49, and 0.41 d^{-1}, respectively. (B) $[H_2O_2]$ in experiments described in (A), with k = 0.016 (○), 0.035 (▽), and 0.040 (□) d^{-1}. (C) ^{14}C activity in experiments with [ferrihydrite] = 16.85 (●), 178.56 (▼) or 276.19 (■) μM, and k = 0.63, 2.30, and 3.89 d^{-1}, respectively. (D) $[H_2O_2]$ in experiments described in (C), with k = 0.039 (○), 0.18 (▽), and 0.35 (□) d^{-1}.

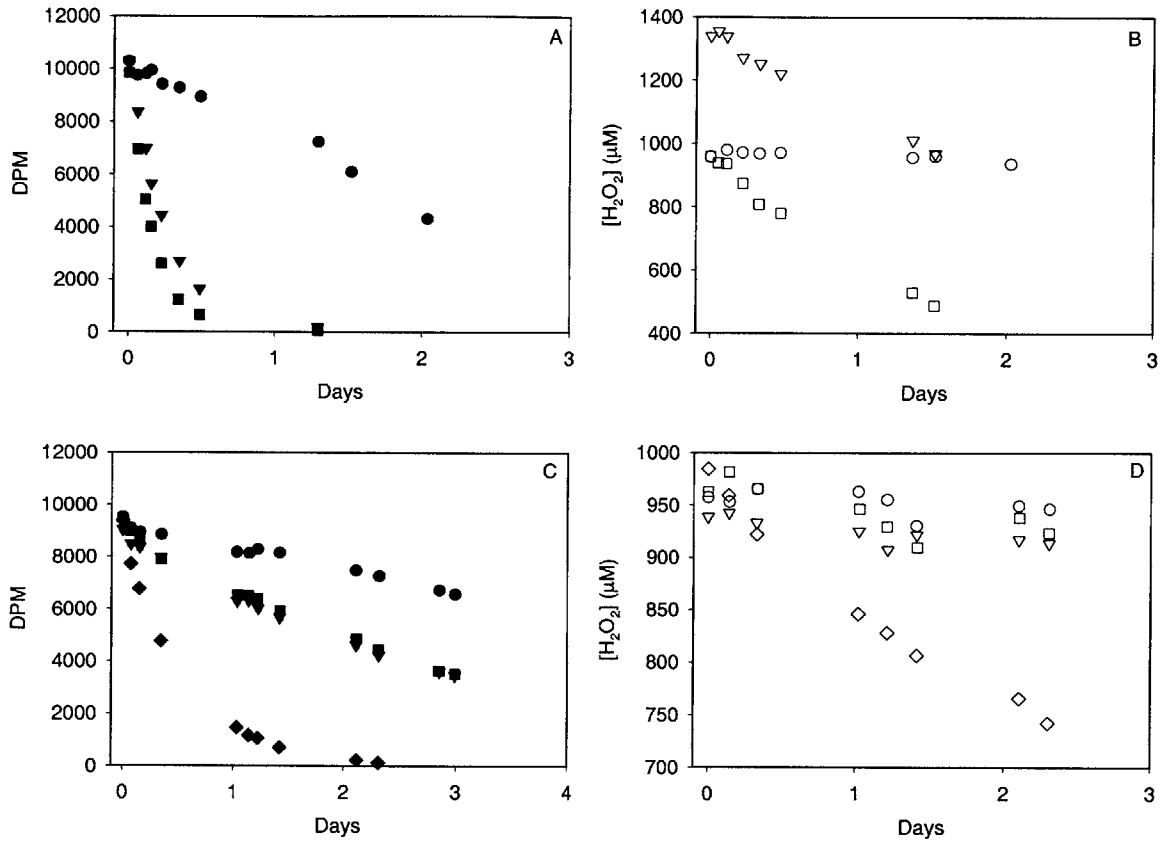

Figure D3. (A) ^{14}C activity in experiments with [ferrihydrite] = 20.31 (●), 192.93 (▼), or 276.76 (■) μM, and k = 0.36, 0.49, and 0.41 d^{-1}, respectively. (B) $[H_2O_2]$ in experiments described in (A), with k = 0.11 (○), 0.035 (▽), and 0.040 (□) d^{-1}. (C) ^{14}C activity in experiments with [ferrihydrite] = 6.35 (●), 23.74 (▼), 85.34 (■), or 133.91 (◆) μM, and k = 0.11, 0.31, 0.31, and 1.84 d^{-1}, respectively. (D) $[H_2O_2]$ in experiments described in (C), with k = 0.0067 (○), 0.013 (▽), 0.024 d^{-1} (□), and 0.12 (◇) d^{-1}.

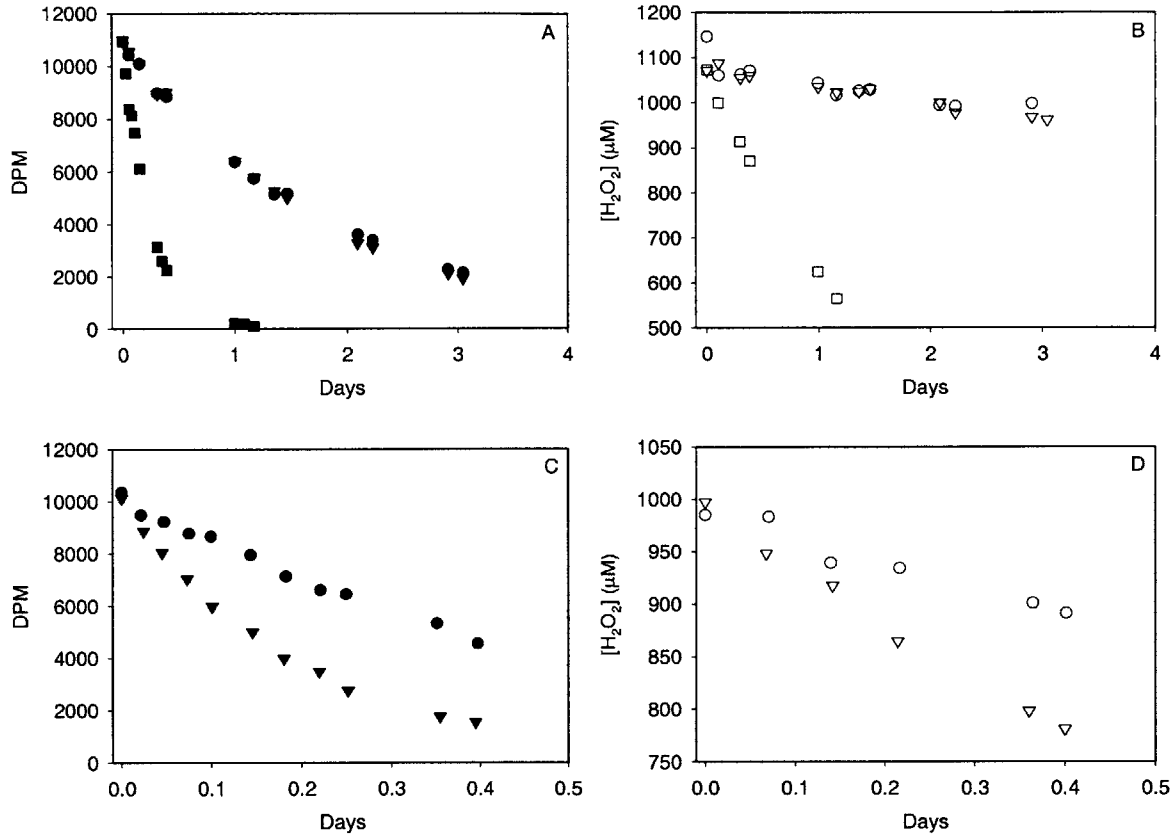

Figure D4. (A) ^{14}C activity in experiments with [ferrihydrite] = 44.86 (●), 84.41 (▼), or 378.99 (■) μM, and k = 0.53, 0.56, and 4.00 d^{-1}, respectively. (B) $[H_2O_2]$ in experiments described in (A), with k = 0.040 (○), 0.038 (▽), and 0.54 (□) d^{-1}. (C) ^{14}C activity in experiments with [ferrihydrite] = 323.31 (●) or 411.83 (▼) μM, and k = 1.91 and 4.97 d^{-1}, respectively. (D) $[H_2O_2]$ in experiments described in (C), with k = 0.26 (○) and 0.61 (▽) d^{-1}.

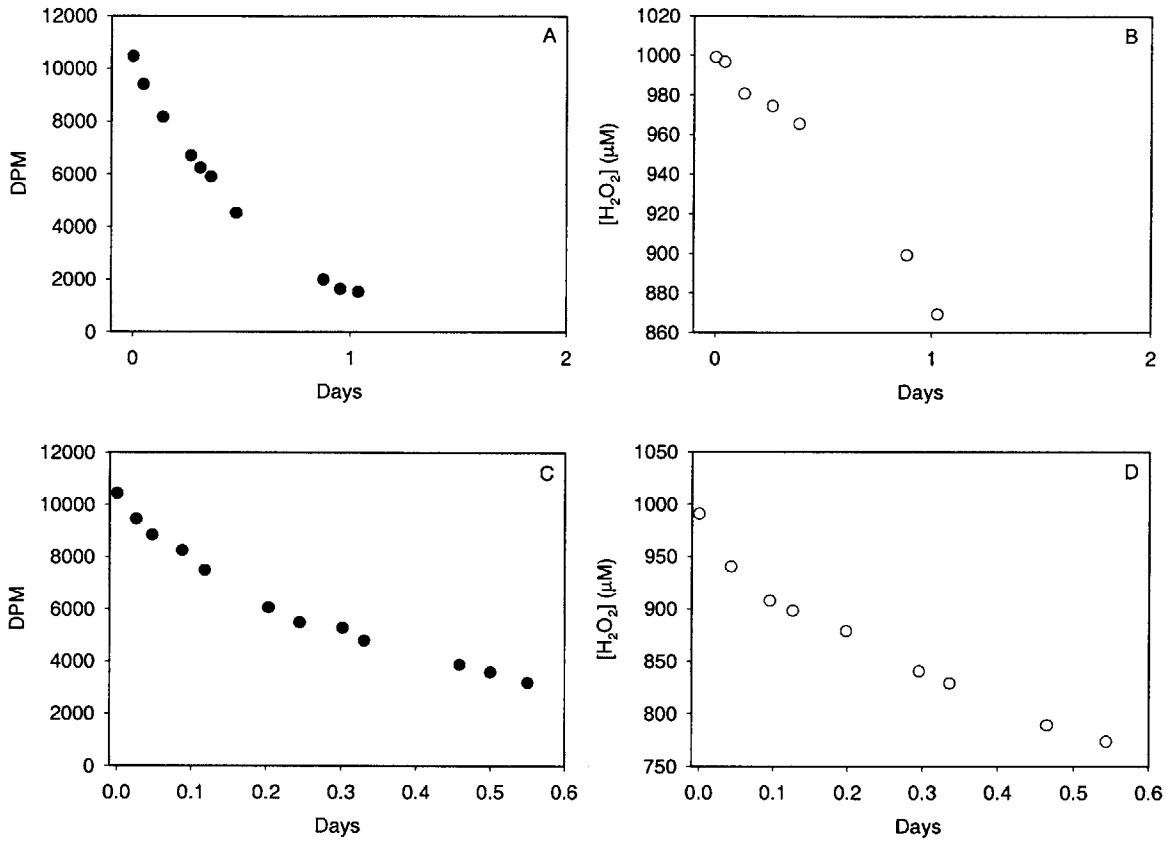

Figure D5. (A) ^{14}C activity in experiments with [ferrihydrite] = 178.22 μM and k = 1.77 d^{-1}. (B) $[H_2O_2]$ in experiments described in (A), with k = 0.13 d^{-1}. (C) ^{14}C activity in experiments with [ferrihydrite] = 306.45 μM and k = 2.20 d^{-1}. (D) $[H_2O_2]$ in experiments described in (C), with k = 0.43 d^{-1}.

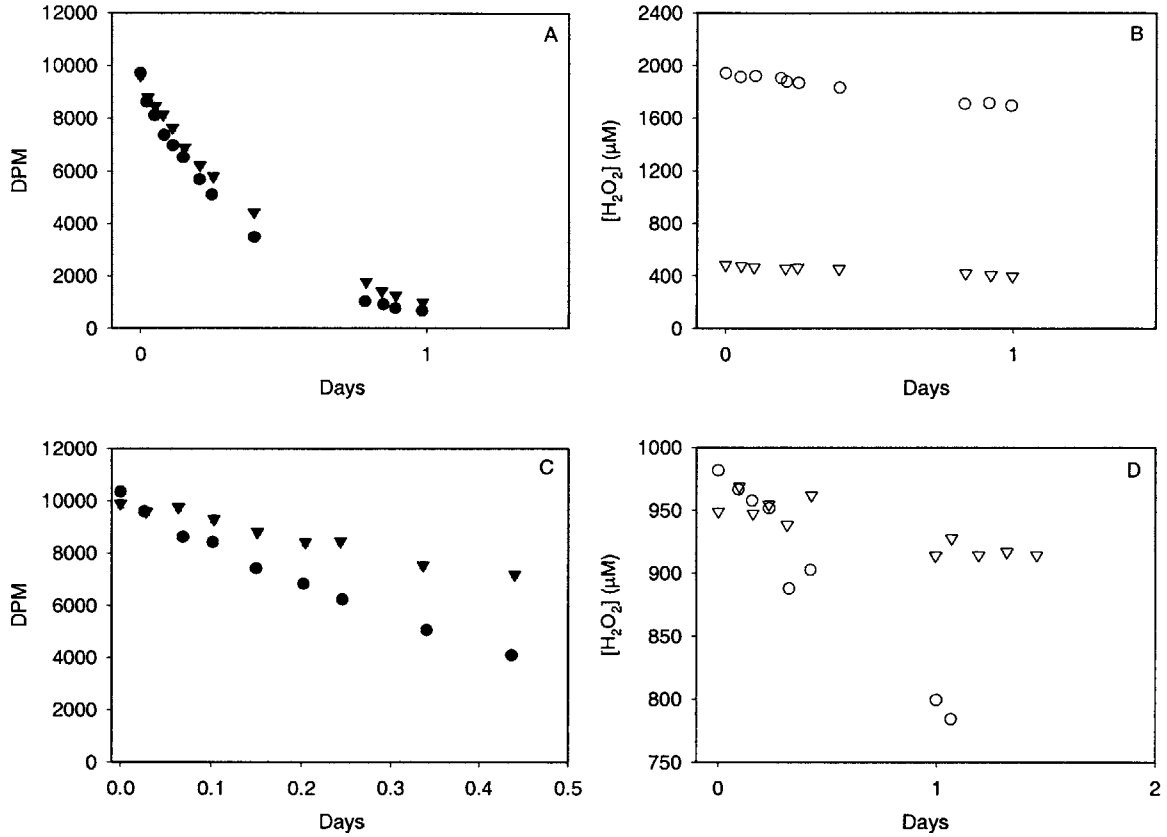

Figure D6. (A) ^{14}C activity in experiments with [ferrihydrite] = 166.77 (●) or 183.94 (▼) μM, and k = 2.63 and 2.13 d^{-1}, respectively. (B) $[H_2O_2]$ in experiments described in (A), with k = 0.14 (○) and 0.18 (▽) d^{-1}. (C) ^{14}C activity in experiments with [ferrihydrite] = 212.85 (●) or 61.80 (▼) μM, and k = 2.22 and 0.83 d^{-1}, respectively. (D) $[H_2O_2]$ in experiments described in (C), with k = 0.21 (○) and 0.036 (▽) d^{-1}.

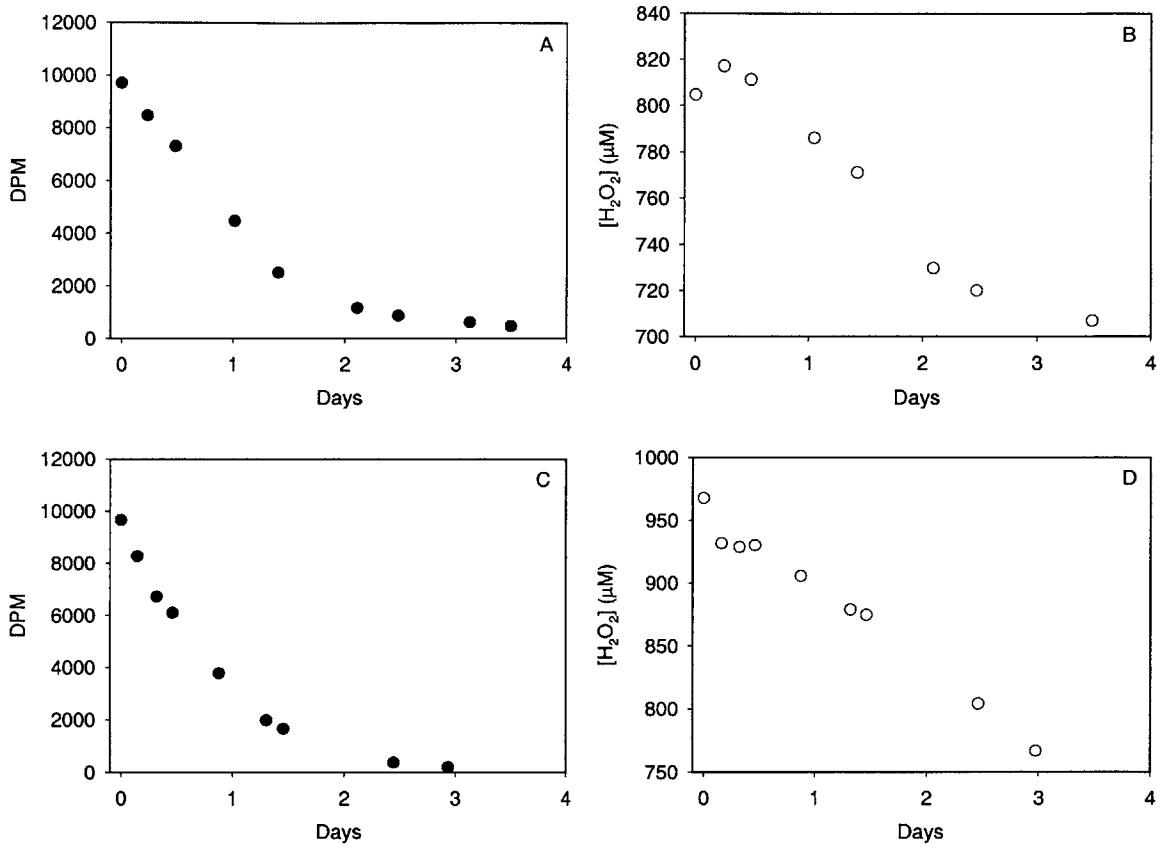

Figure D7. (A) ^{14}C activity in experiments with [Fe(III)] = 1.30 μM and k = 0.89 d^{-1}. (B) $[H_2O_2]$ in experiments described in (A), with k = 0.046 d^{-1}. (C) ^{14}C activity in experiments with [ferrihydrite] = 83.68 μM and k = 1.15 d^{-1}. (D) $[H_2O_2]$ in experiments described in (C), with k = 0.071 d^{-1}.

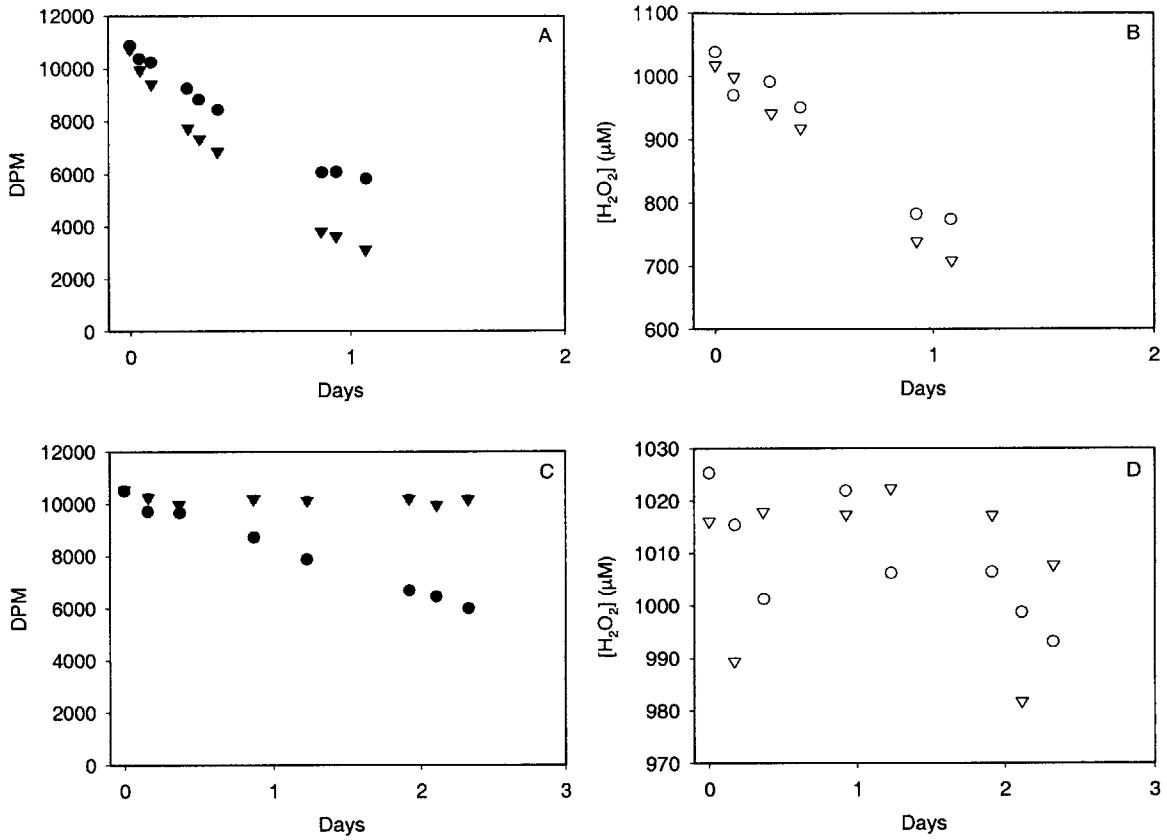

Figure D8. (A) ^{14}C activity in experiments with 0.1 mM *tert*-butyl alcohol and [ferrihydrite] = 192.63 (●) or 196.87 (▼) μM, and k = 0.62 and 1.16 d^{-1}, respectively. (B) $[H_2O_2]$ in experiments described in (A), with k = 0.27 (○) and 0.34 (▽) d^{-1}. (C) ^{14}C activity in experiments with [Fe(III)] = 2.70 (●) or 2.73 and 0.1 mM *tert*-butyl alcohol (▼) μM, and k = 0.23 and 0.0095 d^{-1}, respectively. (D) $[H_2O_2]$ in experiments described in (C), with k = 0.0090 (○) and 0.0031 (▽) d^{-1}.

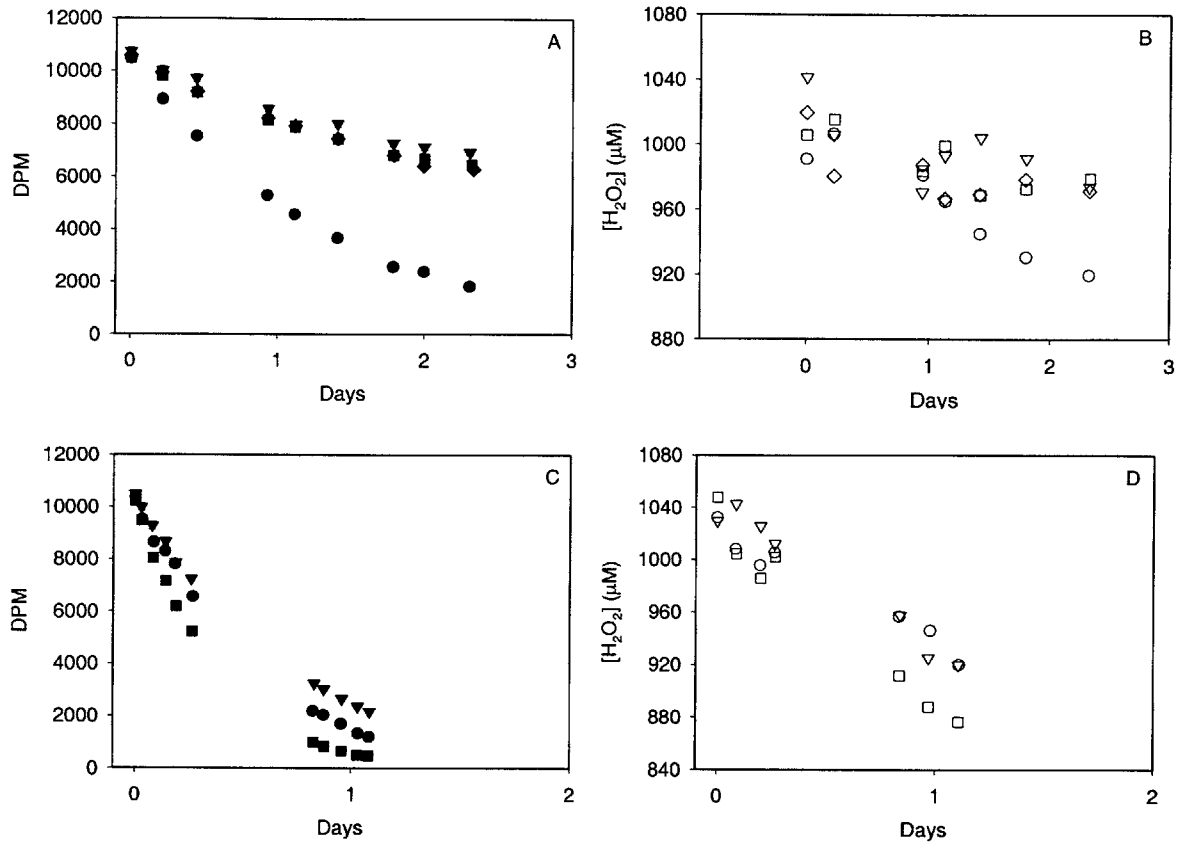

Figure D9. (A) ^{14}C activity in experiments with 10 μM *tert*-butyl alcohol (except ●) and [ferrihydrite] = 85.70 (●), 78.34 (▼), 85.08 (■), or 84.93 and 1 μM Fe(III) (◆) μM, and k = 0.75, 0.20, 0.22, and 0.23 d^{-1}, respectively. (B) $[H_2O_2]$ in experiments described in (A), with k = 0.039 (○), 0.020 (▽), 0.018 (□), and 0.015 (◇) d^{-1}. (C) ^{14}C activity in experiments with [ferrihydrite] = 185.46 (●), 192.95 and 10 μM *tert*-butyl alcohol (▼), or 181.93 and 1.5 μM Fe(III) (■) μM, and k = 1.86, 1.43, and 2.74 d^{-1}, respectively. (D) $[H_2O_2]$ in experiments described in (C), with k = 0.088 (○), 0.11 (▽), and 0.15 (□) d^{-1}.

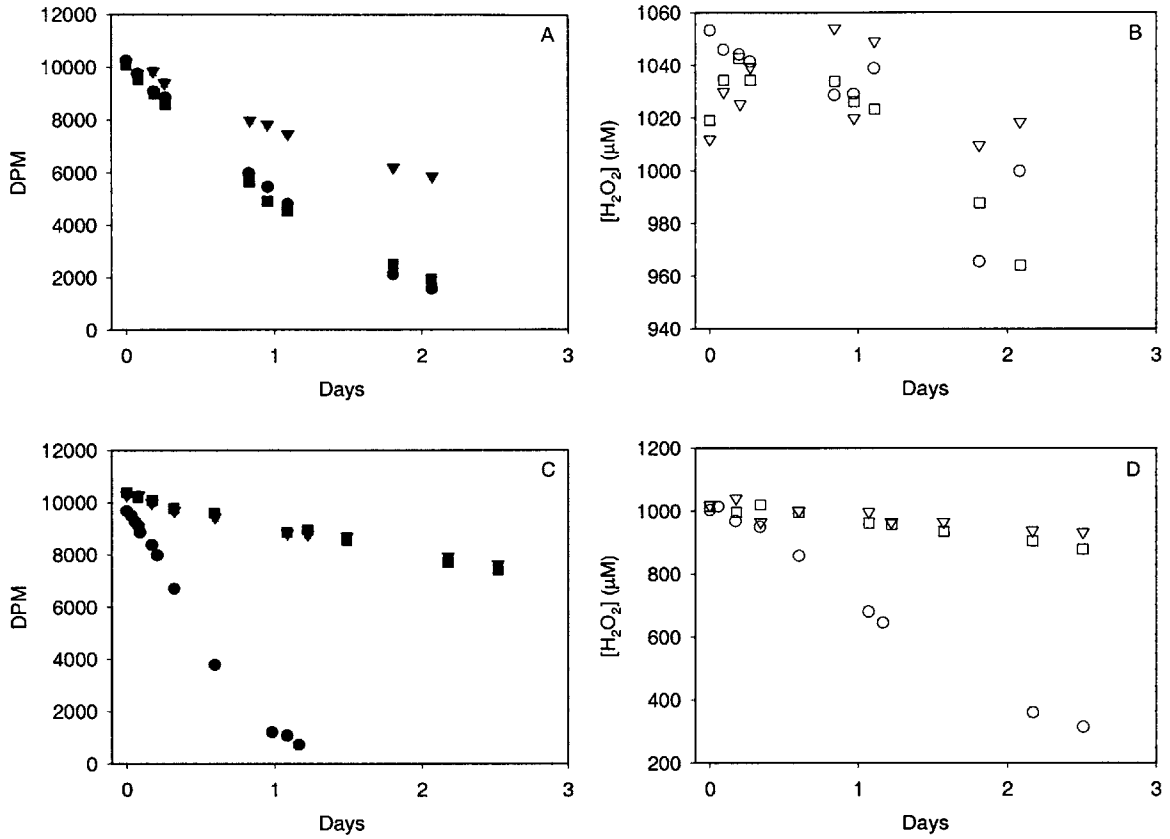

Figure D10. (A) ^{14}C activity in experiments with [ferrihydrite] = 42.68 (●), 48.93 and 10 μM *tert*-butyl alcohol (▼), or 42.15 and 1.5 μM Fe(III) (■) μM, and k = 0.77, 0.27, and 0.76 d^{-1}, respectively. (B) $[H_2O_2]$ in experiments described in (A), with k = 0.031 (○), 0.0037 (▽), and 0.028 (□) d^{-1}. (C) ^{14}C activity in experiments with [ferrihydrite] = 190.11 (●), 187.86 and 10 μM *tert*-butyl alcohol (▼), or 187.77 and 10 μM *tert*-butyl alcohol (■) μM, and k = 1.73, 0.12, and 0.13 d^{-1}, respectively. (D) $[H_2O_2]$ in experiments described in (C), with k = 0.44 (○), 0.036 (▽), and 0.057 (□) d^{-1}.

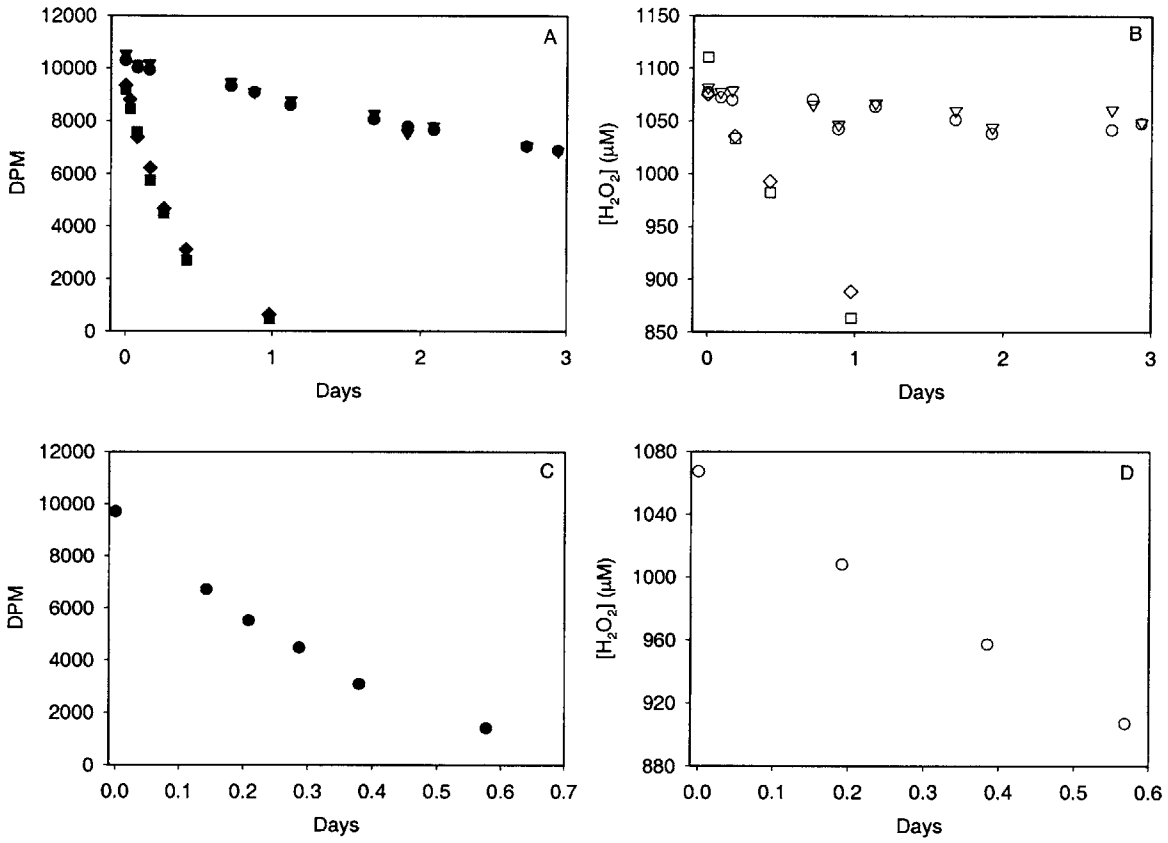

Figure D11. (A) ^{14}C activity in experiments with [Fe(III)] = 0.90 (●) or 1.18 and 1 mM NaCl (▼) μM, [ferrihydrite] = 197.95 (■) or 197.35 and 1 mM NaCl (◆) μM, and k = 0.14, 0.14, 2.85, and 2.63 d^{-1}, respectively. (B) $[H_2O_2]$ in experiments described in (A), with k = 0.011 (○), 0.0087 (▽), 0.25 (□), and 0.19 (◇) d^{-1}. (C) ^{14}C activity in experiments with [ferrihydrite] ~200 μM and k = 2.93 d^{-1}. (D) $[H_2O_2]$ in experiments described in (C), with k = 0.28 d^{-1}.

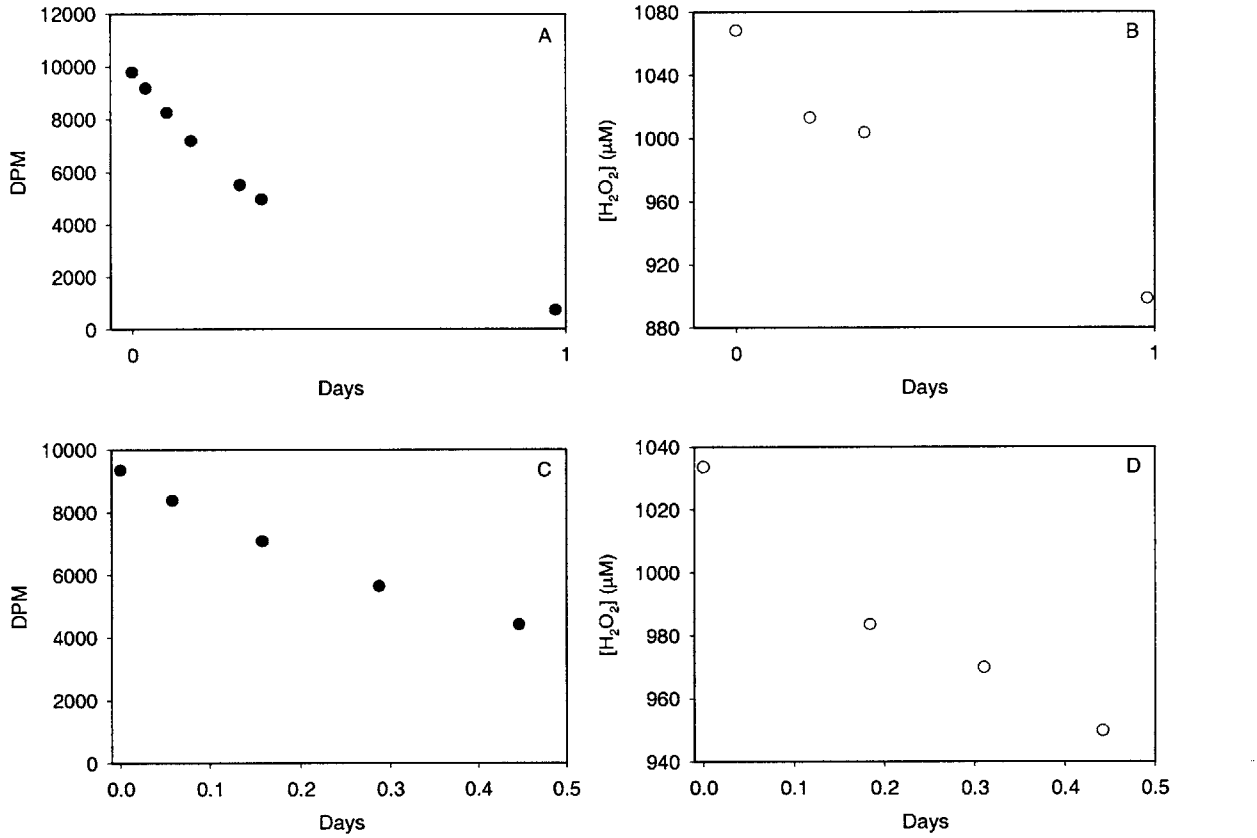

Figure D12. (A) ^{14}C activity in experiments with [ferrihydrite] = 198.75 μM and k = 2.40 d^{-1}. (B) $[H_2O_2]$ in experiments described in (A), with k = 0.17 d^{-1}. (C) ^{14}C activity in experiments with [ferrihydrite] ~200 μM and k = 1.71 d^{-1}. (D) $[H_2O_2]$ in experiments described in (C), with k = 0.19 d^{-1}.

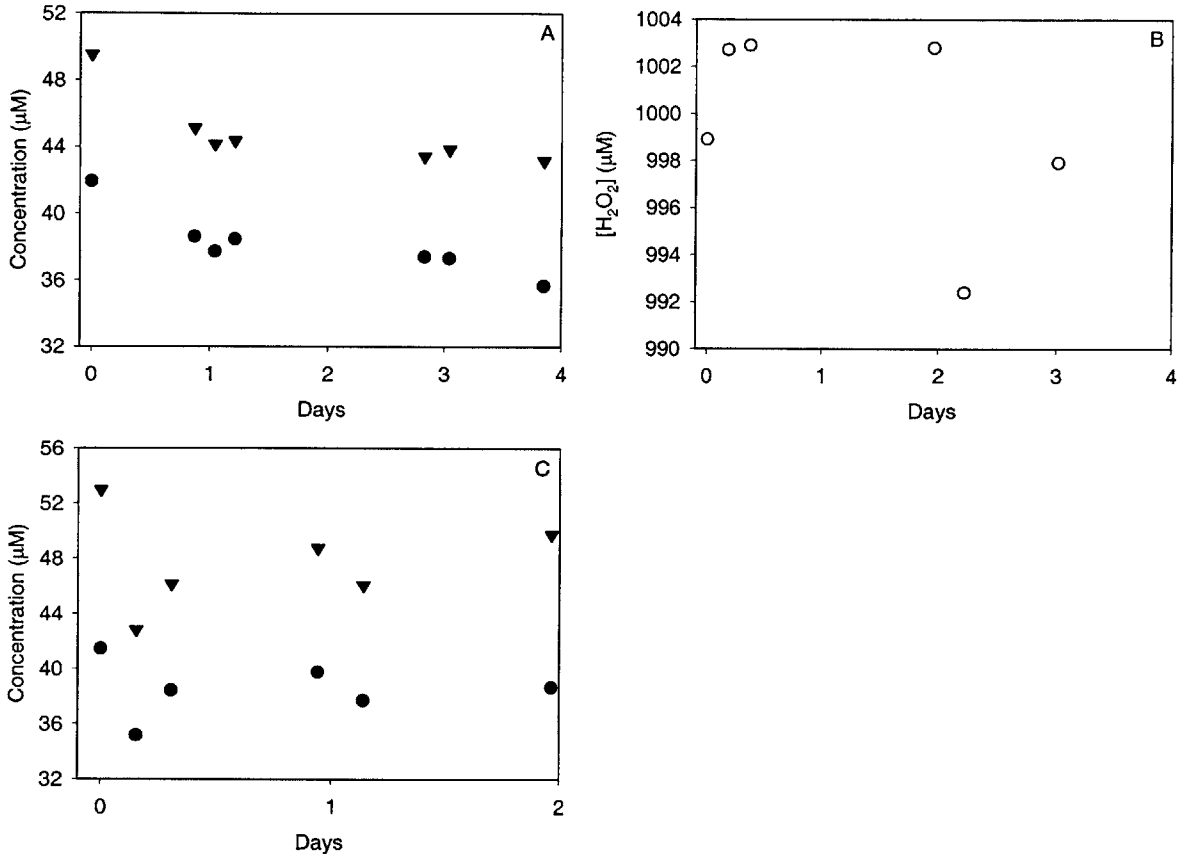

Figure D13. (A) Concentration of benzoic acid (●) and formic acid (▼) in a control experiment containing H_2O_2 and no iron. (B) [H_2O_2] in the experiment described in (A). (C) Concentration of benzoic acid (●) and formic acid (▼) in a control experiment with [ferrihydrite] = 300 μM and no H_2O_2.

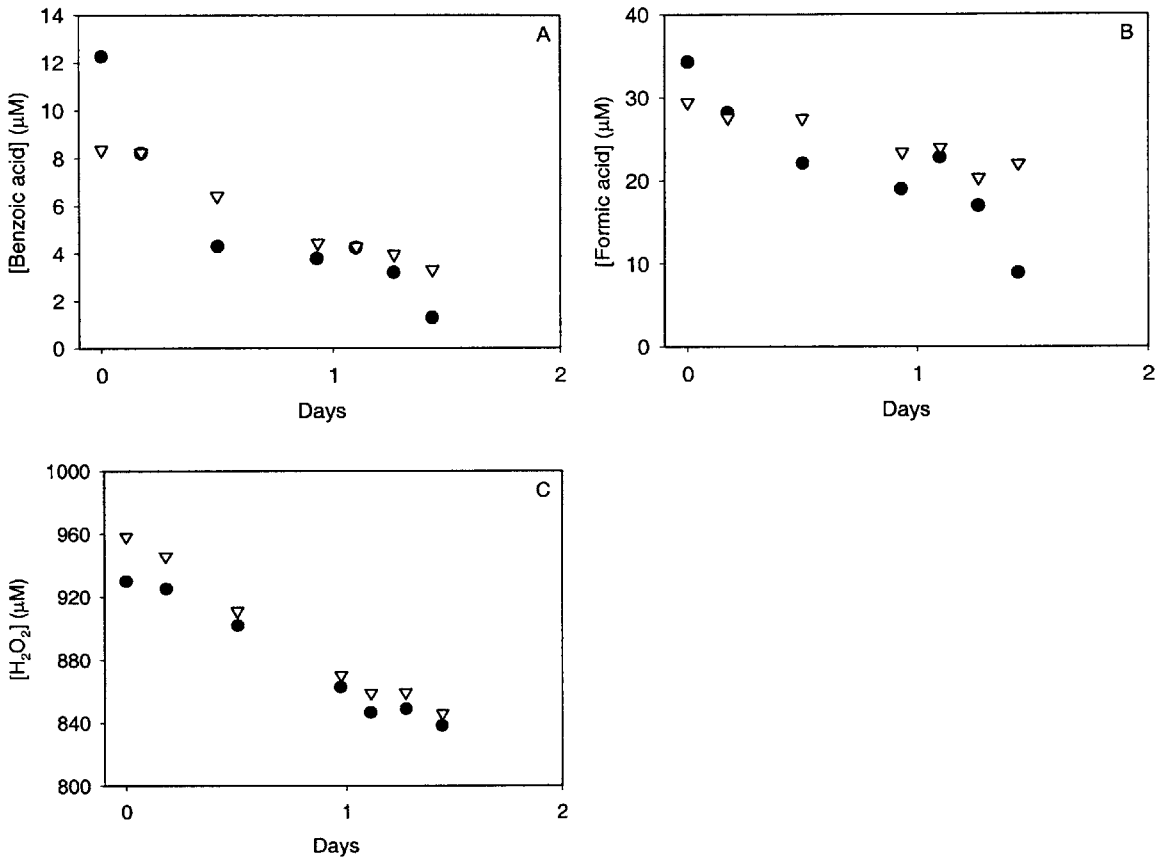

Figure D14. (A) Concentration of benzoic acid in duplicate experiments with [ferrihydrite] = 190 μM, and k = 1.26 (●) and 0.66 (▽) d^{-1}. (B) Concentration of benzoic acid in duplicate experiments with [ferrihydrite] = 190 μM, and k = 0.59 (●) and 0.23 (▽) d^{-1}. (C) $[H_2O_2]$ in experiments described in (A) and (B), with k = 0.078 (●) and 0.090 (▽) d^{-1}.

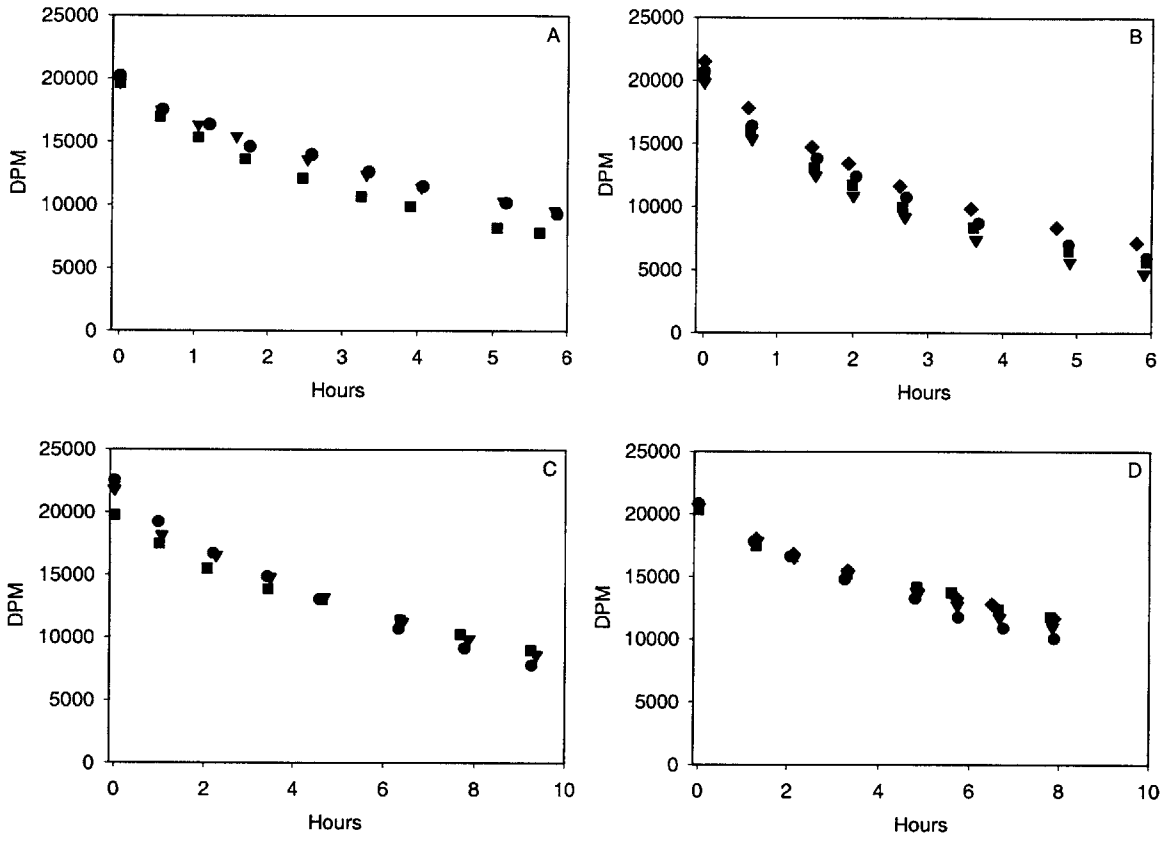

Figure D15. (A) ^{14}C activity in experiments with [ferrihydrite] = 190 μM and $[H_2O_2]_0$ = 5 (●), 10 (▼) or 30 (■) mM, and k = 0.13, 0.12, and 0.17 h^{-1}, respectively. (B) ^{14}C activity in experiments with [ferrihydrite] = 190 μM and $[H_2O_2]_0$ = 50 (●), 100 (▼), 200 (■) or 400 (◆) mM, and k = 0.22, 0.26, 0.23, and 0.20 h^{-1}, respectively. (C) ^{14}C activity in experiments with [ferrihydrite] = 90 μM and $[H_2O_2]_0$ = 5 (●), 10 (▼) or 30 (■) mM, and k = 0.11, 0.098, and 0.084 h^{-1}, respectively. (D) ^{14}C activity in experiments with [ferrihydrite] = 90 μM and $[H_2O_2]_0$ = 50 (●), 100 (▼), 200 (■) or 400 (◆) mM, and k = 0.093, 0.080, 0.068, and 0.072 h^{-1}, respectively.

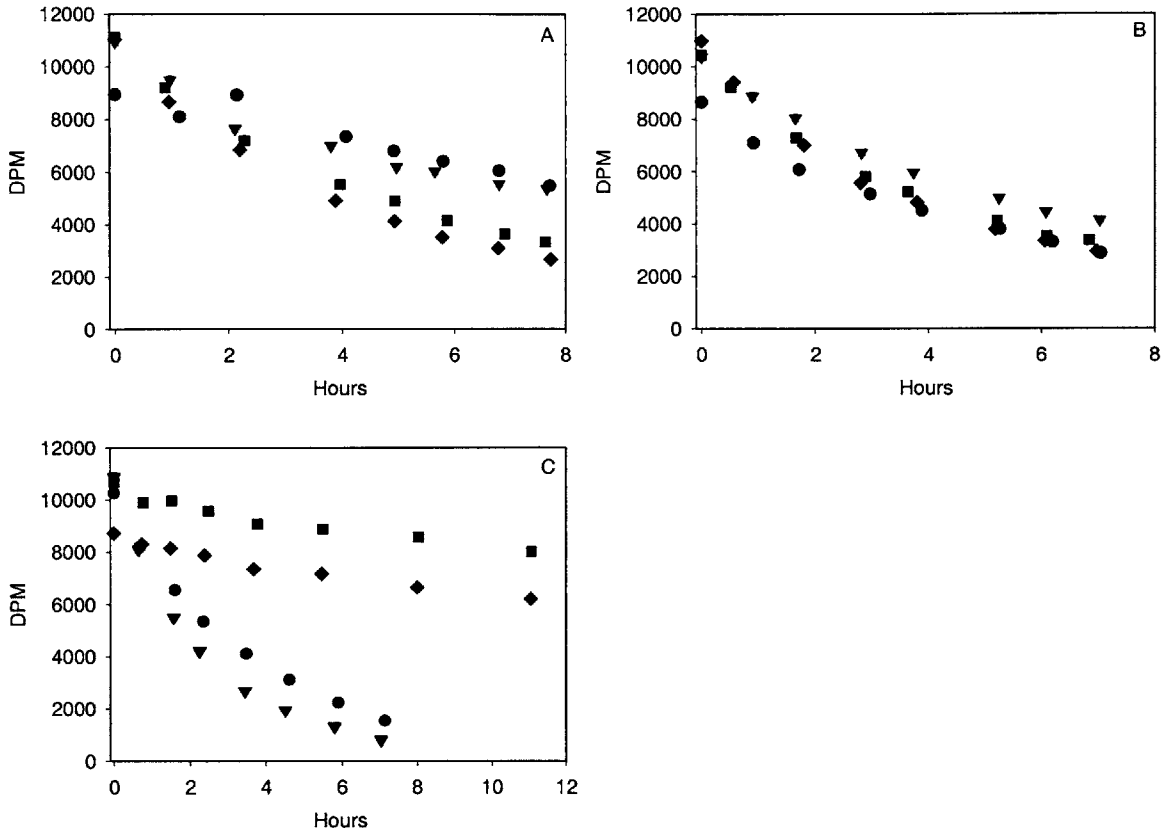

Figure D16. (A) ^{14}C activity in experiments with [ferrihydrite] = 100 μM and $[H_2O_2]_0$ = 75 (●) or 300 (▼) mM, or [ferrihydrite] = 200 μM and $[H_2O_2]_0$ = 75 (■) or 300 (◆) mM, and k = 0.061, 0.099, 0.16 and 0.19 h^{-1}, respectively. (B) ^{14}C activity in experiments with [ferrihydrite] = 160 μM and $[H_2O_2]_0$ = 0.3 (●) or 0.4 (▼) M, or [ferrihydrite] = 230 μM and $[H_2O_2]_0$ = 0.2 (■) or 0.3 (◆) M, and k = 0.16, 0.14, 0.18 and 0.20 h^{-1}, respectively. (C) ^{14}C activity in experiments with 0.2 g/L goethite and $[H_2O_2]_0$ = 10 (●) or 100 (▼) mM, or [hematite] = 0.2 g/L and $[H_2O_2]_0$ = 10 (■) or 100 (◆) mM, and k = 0.26, 0.40, 0.024 and 0.031 h^{-1}, respectively.

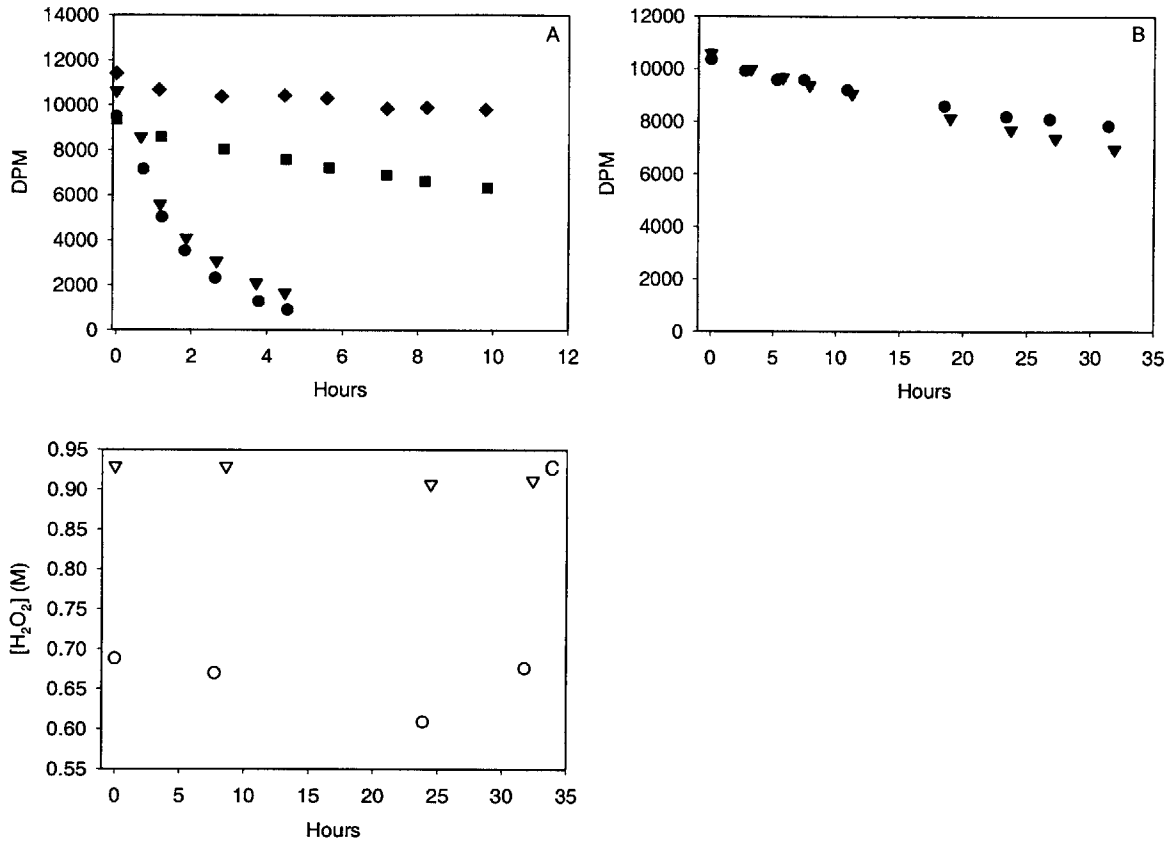

Figure D17. (A) ^{14}C activity in experiments with 0.2 g/L goethite and $[H_2O_2]_0$ = 50 (●) or 300 (▼) mM, or 0.2 g/L hematite and $[H_2O_2]_0$ = 50 (■) or 300 (◆) mM, and k = 0.53, 0.47, 0.040 and 0.014 h^{-1}, respectively. (B) ^{14}C activity in experiments with 0.2 g/L hematite with k = 0.0089 (●) and 0.013 (▼) h^{-1}. (C) $[H_2O_2]$ in experiments described in (B), with $[H_2O_2]_0$ = 0.7 (○) or 0.9 (▽) M.

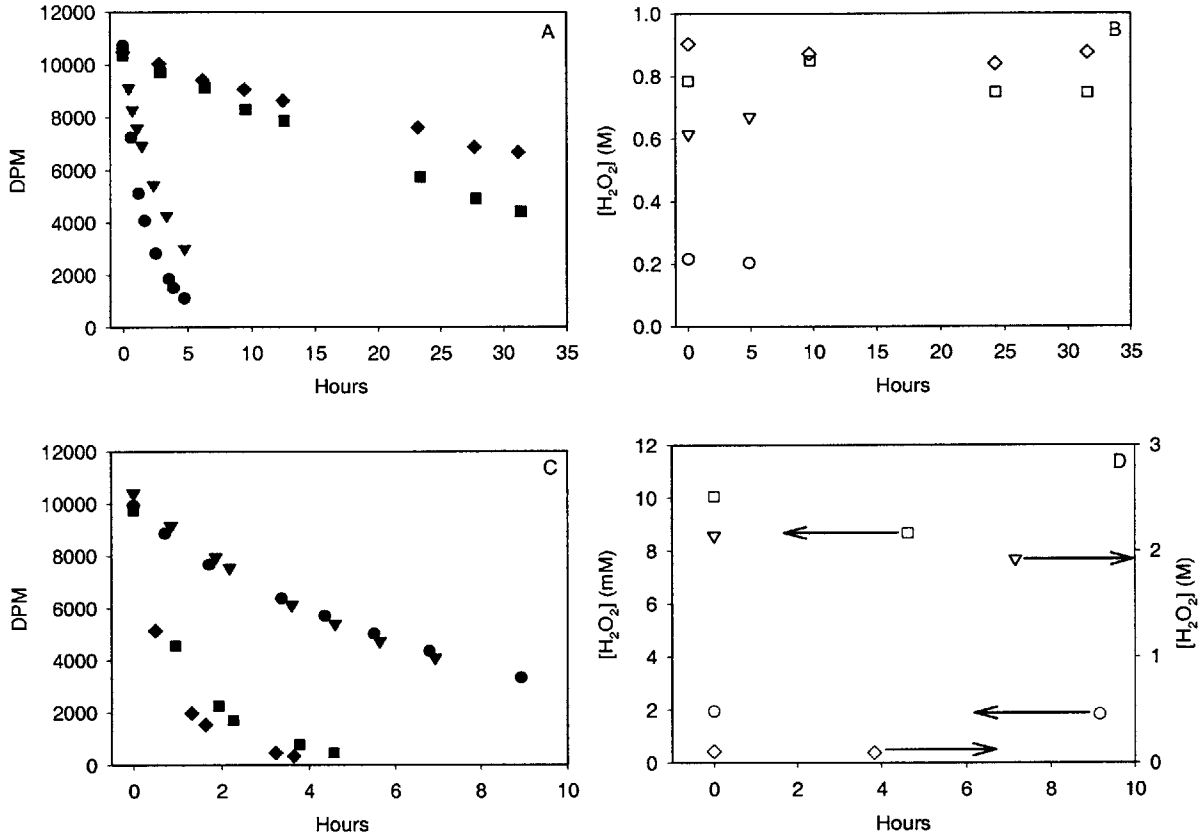

Figure D18. (A) ^{14}C activity in experiments with 0.2 g/L goethite and k = 0.53 (●) and 0.27 (▼) h^{-1}, or 0.2 g/L hematite and k = 0.027 (■) and 0.015 (◆) h^{-1}. (B) $[H_2O_2]$ in experiments described in (A), with $[H_2O_2]_0$ = 0.2 (○), 0.6 (▽), 0.8 (□), or 0.9 (◇) M. (C) ^{14}C activity in experiments with 0.2 g/L goethite and k = 0.12 (●) and 0.14 (▼) h^{-1}, or 0.6 g/L goethite and k = 0.76 (■) and 1.21 (◆) h^{-1}. (D) $[H_2O_2]$ in experiments described in (C), with $[H_2O_2]_0$ = 0.002 (○), 2 (▽), 0.010 (□), or 0.1 (◇) M.

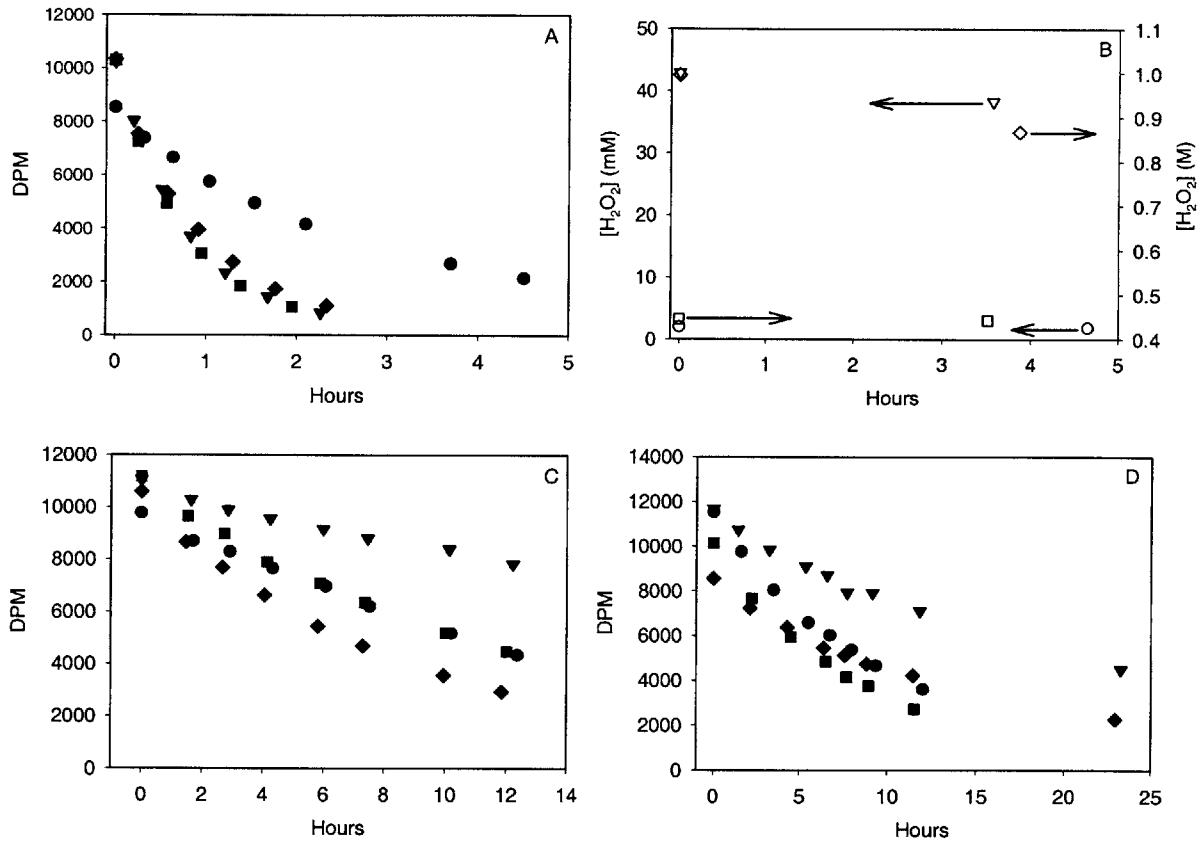

Figure D19. (A) ^{14}C activity in experiments with 0.6 g/L goethite and k = 0.32 (●), 1.20 (▼), 1.26 (■) and 1.03 (◆) h^{-1}. (B) $[H_2O_2]$ in experiments described in (A), with $[H_2O_2]_0$ = 2 (○) or 40 (▽) mM, or 0.4 (□) or 1.0 (◇) M. (C) ^{14}C activity in experiments with 0.02 g/L goethite and $[H_2O_2]_0$ = 2 (●), 50 (▼), 140 (■) or 440 (◆) mM, with k = 0.062, 0.027, 0.076, and 0.11 h^{-1}, respectively. (D) ^{14}C activity in experiments with 0.2 g/L goethite and $[H_2O_2]_0$ = 0.9 (●) or 3.7 (▼) M, or 1.0 g/L hematite and $[H_2O_2]_0$ = 50 (●) or 540 (▼) mM, with k = 0.12, 0.062, 0.096, and 0.041 h^{-1}, respectively.

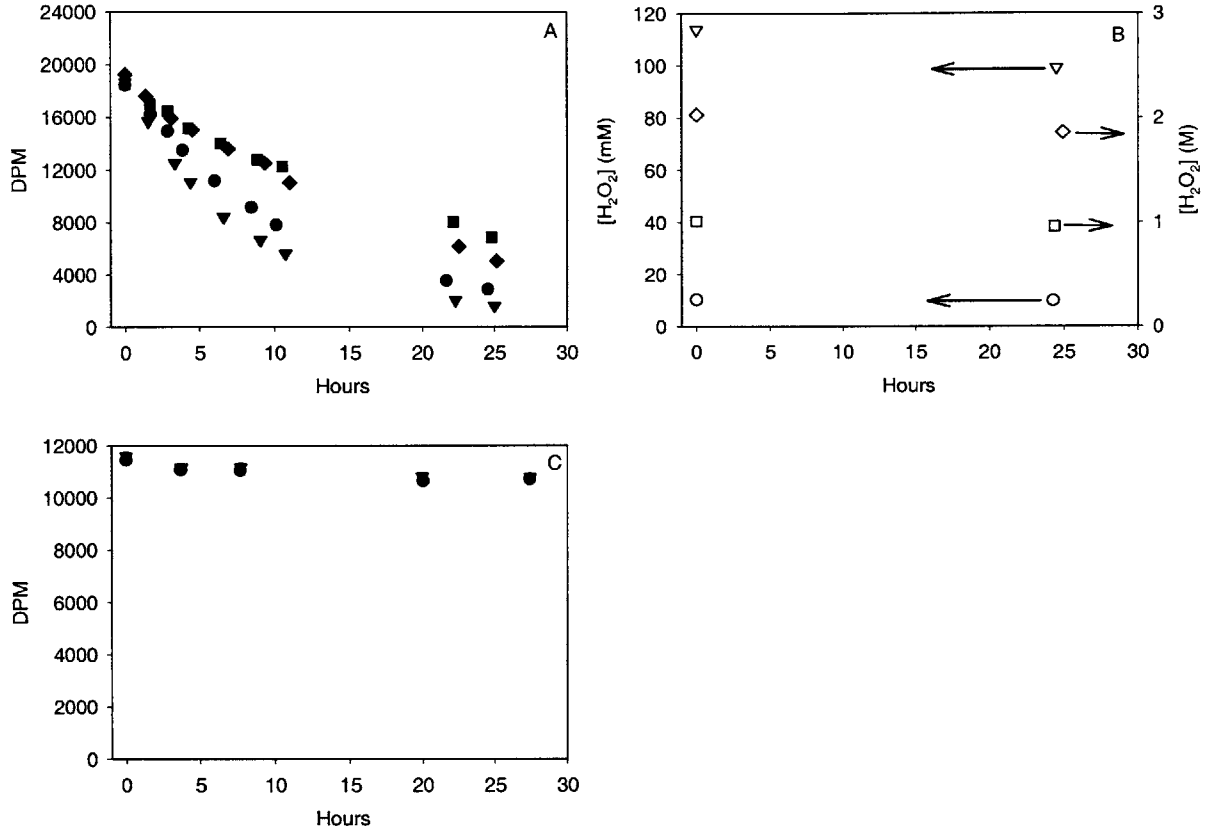

Figure D20. (A) ^{14}C activity in experiments with 1.0 g/L hematite and k = 0.081 (●), 0.11 (▼), 0.039 (■) and 0.050 (◆) h^{-1}. (B) $[H_2O_2]$ in experiments described in (A), with $[H_2O_2]_0$ = 10 (○) or 110 (▽) mM, or 1.0 (□) or 2.0 (◇) M. (C) ^{14}C activity in control experiments with 0.02 g/L goethite (●) or hematite (▼) and no H_2O_2.

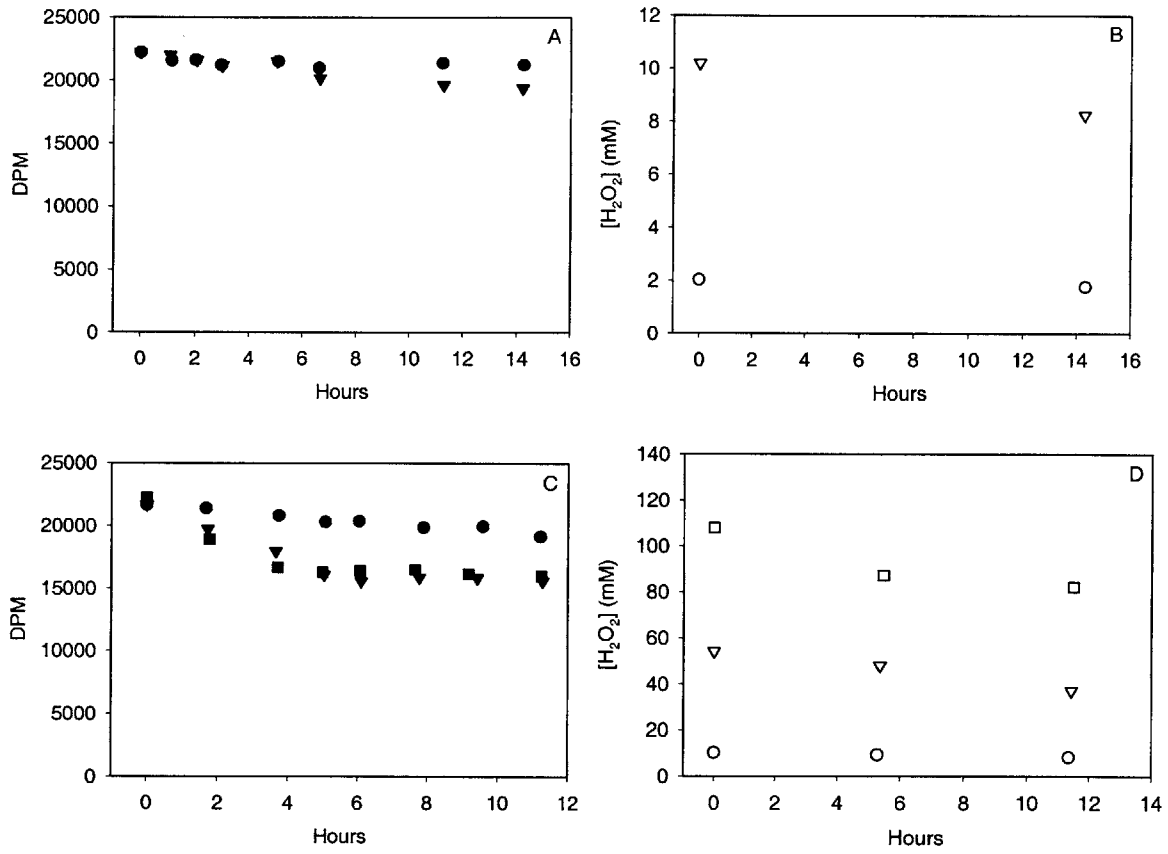

Figure D21. (A) ^{14}C activity in experiments with 0.6 g/L goethite, I = [NaHCOO] = 10 mM, and k = 0.0020 (●) and 0.010 (▼) h^{-1}. (B) $[H_2O_2]$ in experiments described in (A), with $[H_2O_2]_0$ = 2 (○) or 10 (▽) mM. (C) ^{14}C activity in experiments with 0.6 g/L goethite, I = [NaHCOO] = 10 mM, and k = 0.010 (●), 0.051 (▼) and 0.079 (■) h^{-1}. The second and third k values were obtained using the data points from the first four hours as the pH of the solutions rose above 5 afterwards. (D) $[H_2O_2]$ in experiments described in (C), with $[H_2O_2]_0$ = 10 (○), 50 (▽), or 100 (□) mM.

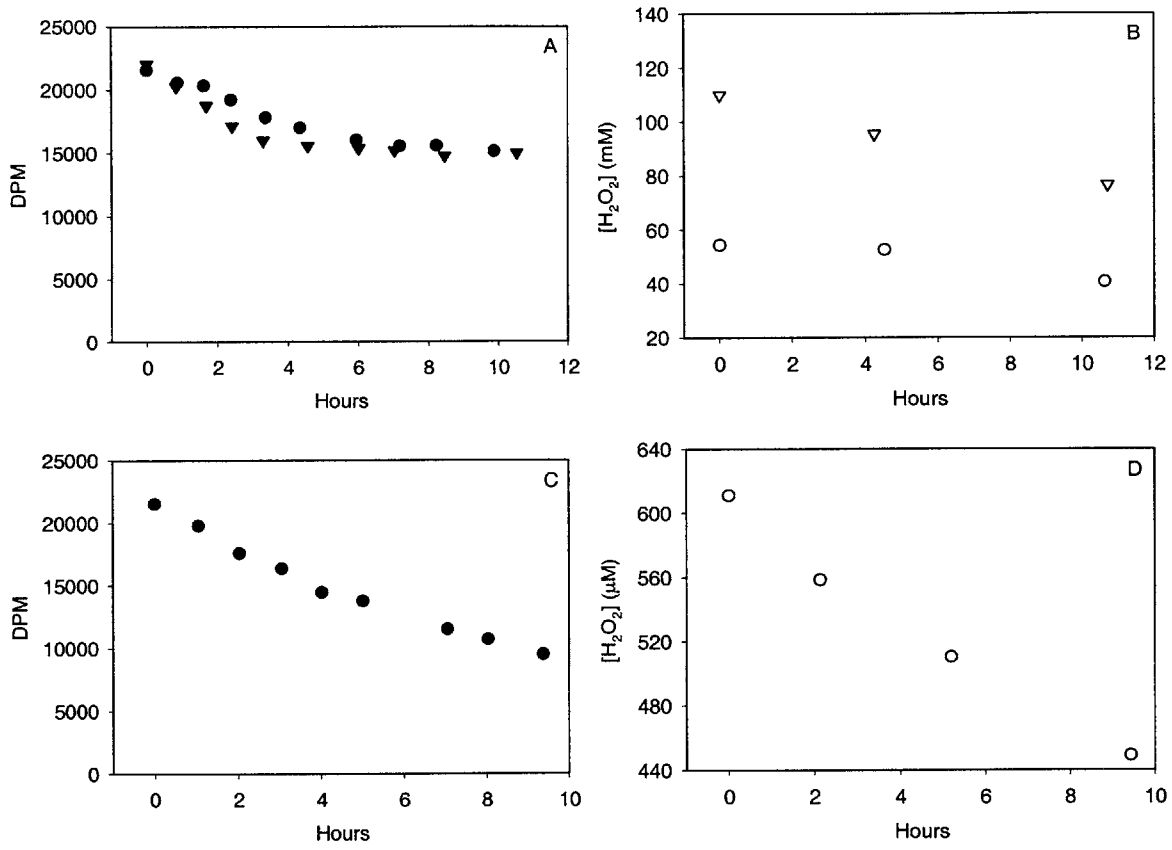

Figure D22. (A) ^{14}C activity in experiments with 0.6 g/L goethite, I = [NaHCOO] = 10 mM, and k = 0.054 (●) and 0.099 (▼) h^{-1}. The k values were obtained using the data points from the first four hours as the pH of the solutions rose above 5 afterwards. (B) $[H_2O_2]$ in experiments described in (A), with $[H_2O_2]_0$ = 50 (○) or 110 (▽) mM. (C) ^{14}C activity in experiments with 0.6 g/L goethite, [NaHCOO] = 50 μM (I = 10 mM), and k = 0.088 h^{-1}. (D) $[H_2O_2]$ in experiments described in (C), with $[H_2O_2]_0$ = 610 μM and k = 0.032 h^{-1}.

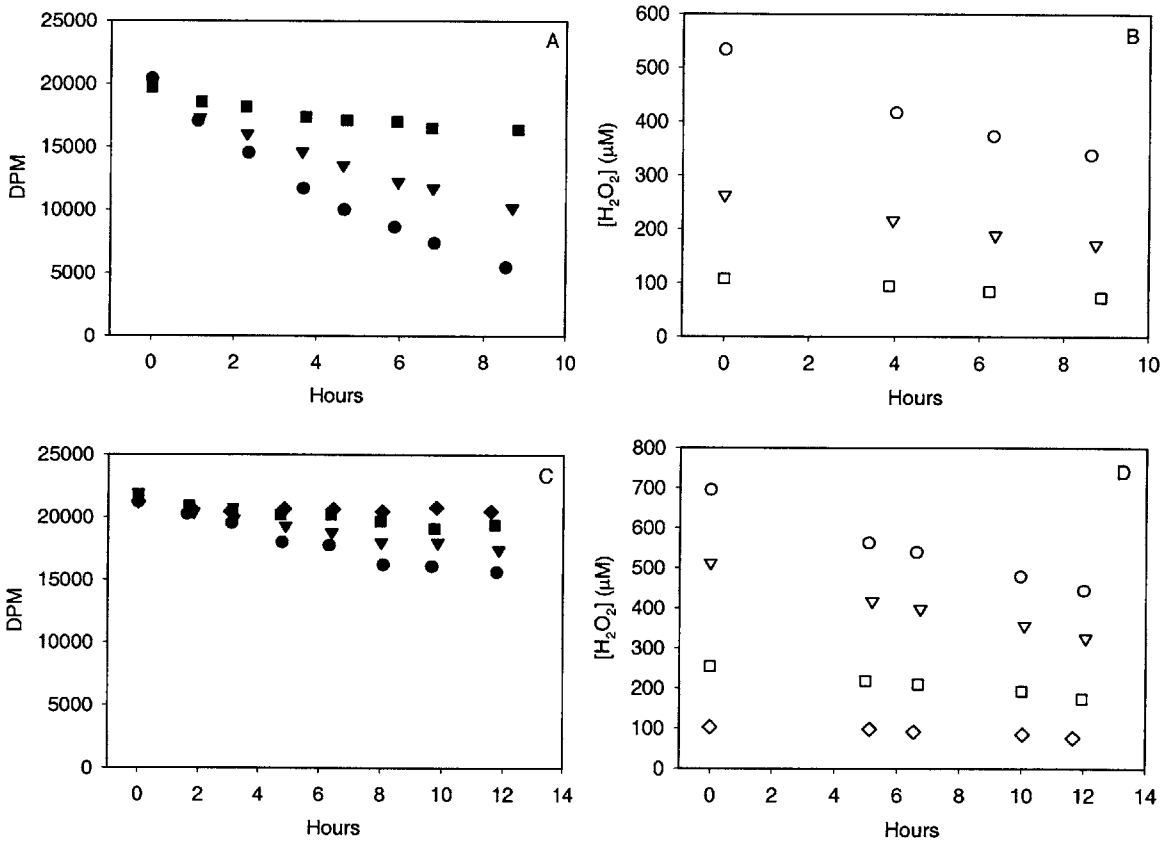

Figure D23. (A) ^{14}C activity in experiments with 0.6 g/L goethite, [NaHCOO] = 50 μM (I = 10 mM), and k = 0.15 (●), 0.078 (▼), and 0.021 (■) h^{-1}. (B) $[H_2O_2]$ in experiments described in (A), with $[H_2O_2]_0$ = 530 (○), 260 (▽), or 110 (□) μM, and k = 0.055, 0.050, and 0.043 h^{-1}, respectively. (C) ^{14}C activity in experiments with 0.6 g/L goethite, [NaHCOO] = 300 μM (I = 10 mM), and k = 0.028 (●), 0.019 (▼), 0.010 (■), and 0.0018 (◆) h^{-1}. (D) $[H_2O_2]$ in experiments described in (C), with $[H_2O_2]_0$ = 700 (○), 500 (▽), 250 (□), or 100 (◇) μM and k = 0.037, 0.037, 0.030, and 0.023 h^{-1}, respectively.

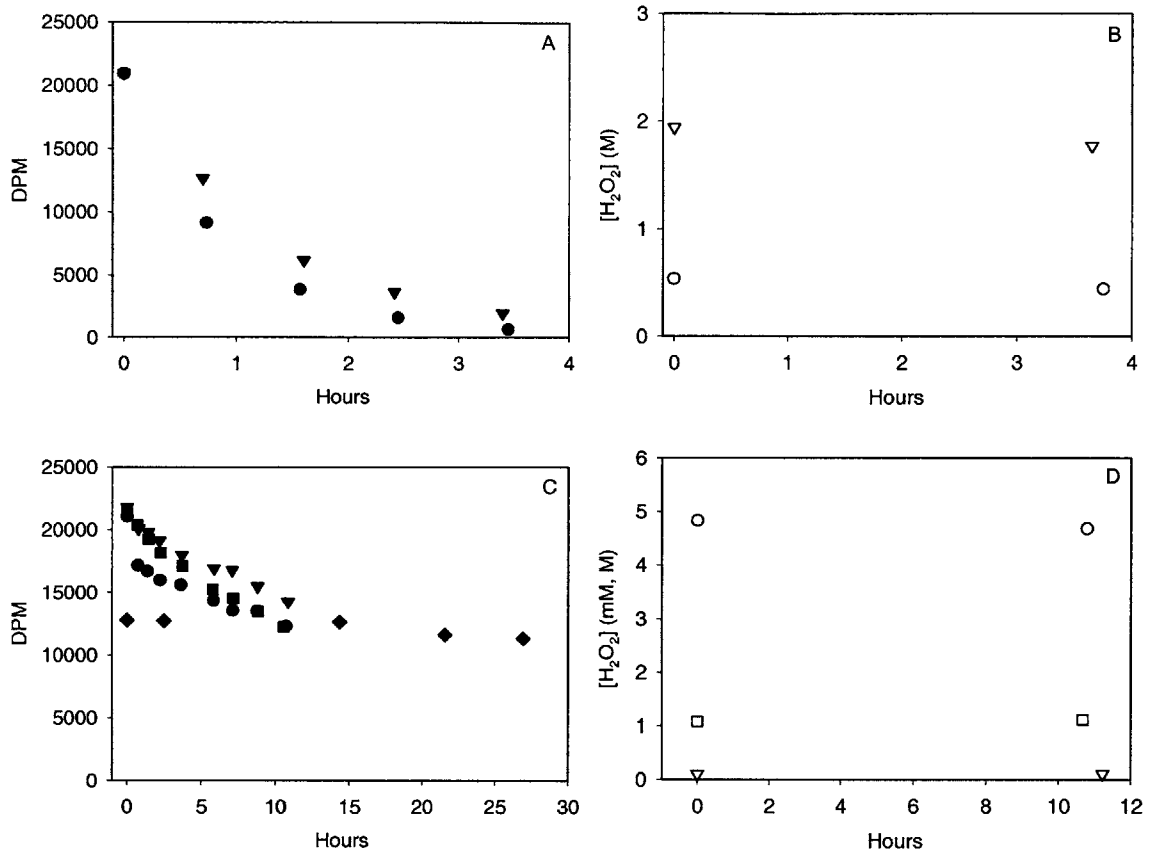

Figure D24. (A) ^{14}C activity in experiments with 0.6 g/L goethite, [NaHCOO] = 50 μM (I = 10 mM), and k = 1.10 (●) and 0.74 (▼) h^{-1}. (B) $[H_2O_2]$ in experiments described in (A), with $[H_2O_2]_0$ = 0.5 (○) or 1.9 (▽) M. (C) ^{14}C activity in experiments with 25 g/L Georgetown sand, and k = 0.042 (●), 0.035 (▼), and 0.052 (■) h^{-1}. (◆) is the control experiment with k = 0.0044 h^{-1}. (D) $[H_2O_2]$ in experiments described in (C), with $[H_2O_2]_0$ = 4.8 (○) or 100 (▽) mM, or 1.1 (□) M.

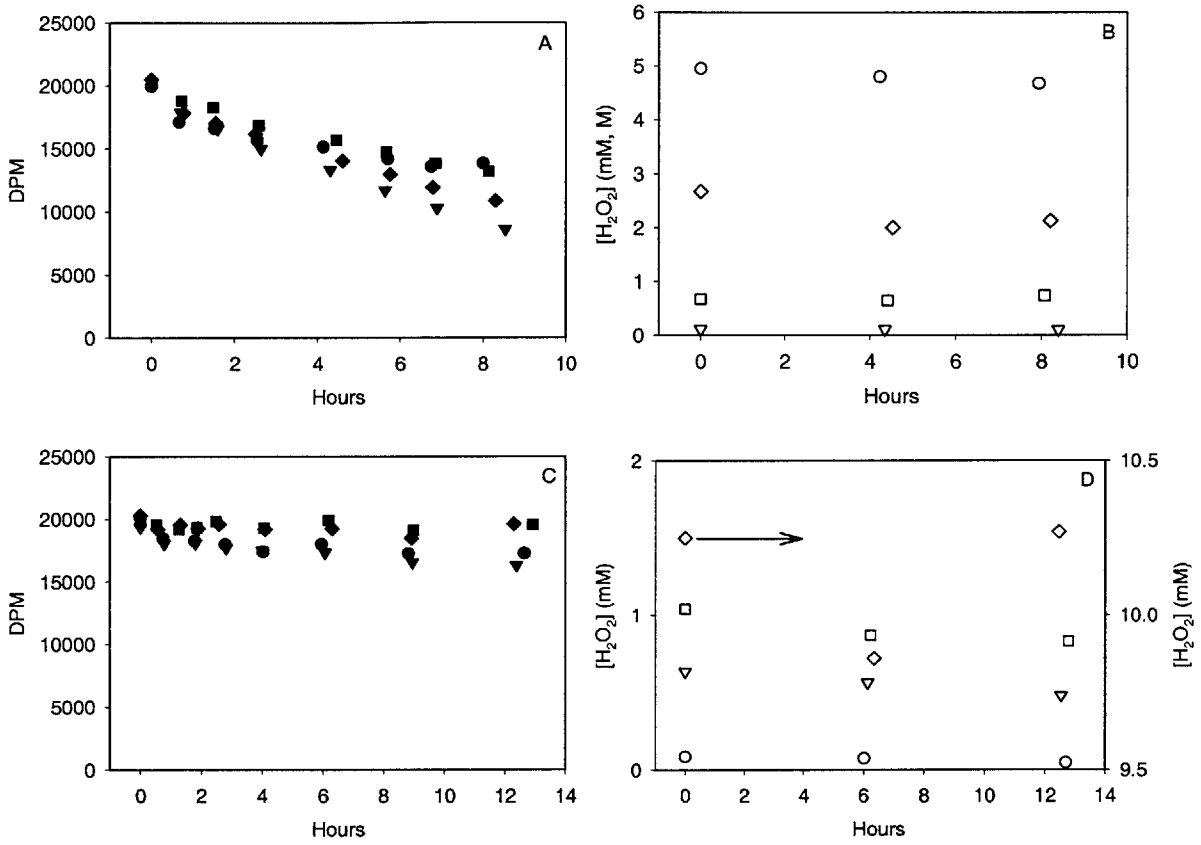

Figure D25. (A) ^{14}C activity in experiments with 60 g/L Georgetown sand and k = 0.043 (●), 0.095 (▼), 0.052 (■), and 0.073 (◆) h^{-1}. (B) $[H_2O_2]$ in experiments described in (A), with $[H_2O_2]_0$ = 5.0 (○), 110 (▽), 675 (□), or 2700 (◇) mM. (C) ^{14}C activity in experiments with 60 g/L Georgetown sand, and k = 0.0091 (●), 0.012 (▼), 0.00034 (■), and 0.0024 (◆) h^{-1}. (■) and (◆) contained 10 mM NaHCOO instead of $NaClO_4$. (D) $[H_2O_2]$ in experiments described in (C), with $[H_2O_2]_0$ = 85 (○) or 630 (▽) μM, or 1.0 (□) or 10 (◇) mM.

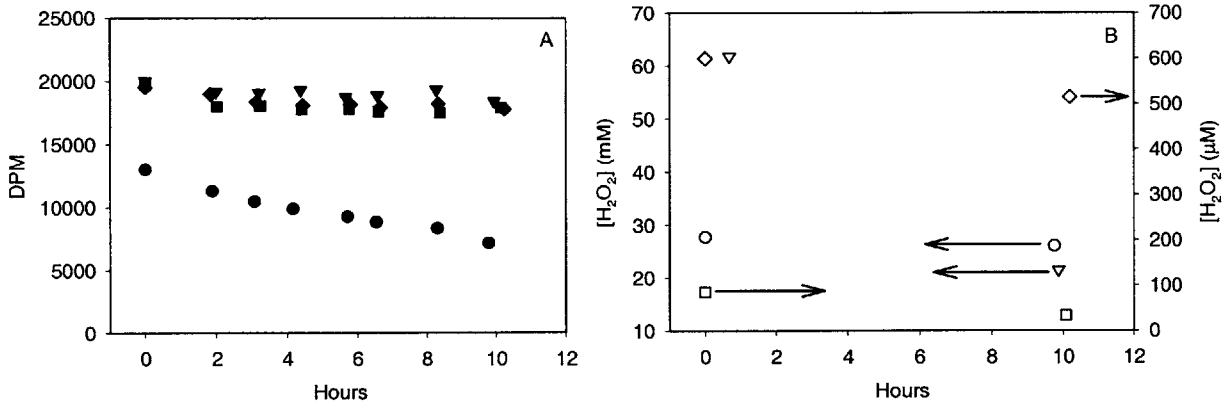

Figure D26. (A) ^{14}C activity in experiments with 25 g/L Georgetown sand (●), or 60 g/L Georgetown sand and [NaHCOO] = 10 mM (▼) or [NaHCOO] = 300 μM (I = 10 mM) (■), (◆). k = 0.057, 0.0058, 0.0083, and 0.0083 h^{-1}, respectively. (B) $[H_2O_2]$ in experiments described in (A), with $[H_2O_2]_0$ = 30 (○), 60 (▽), 0.086 (□), or 0.6 (◇) mM.

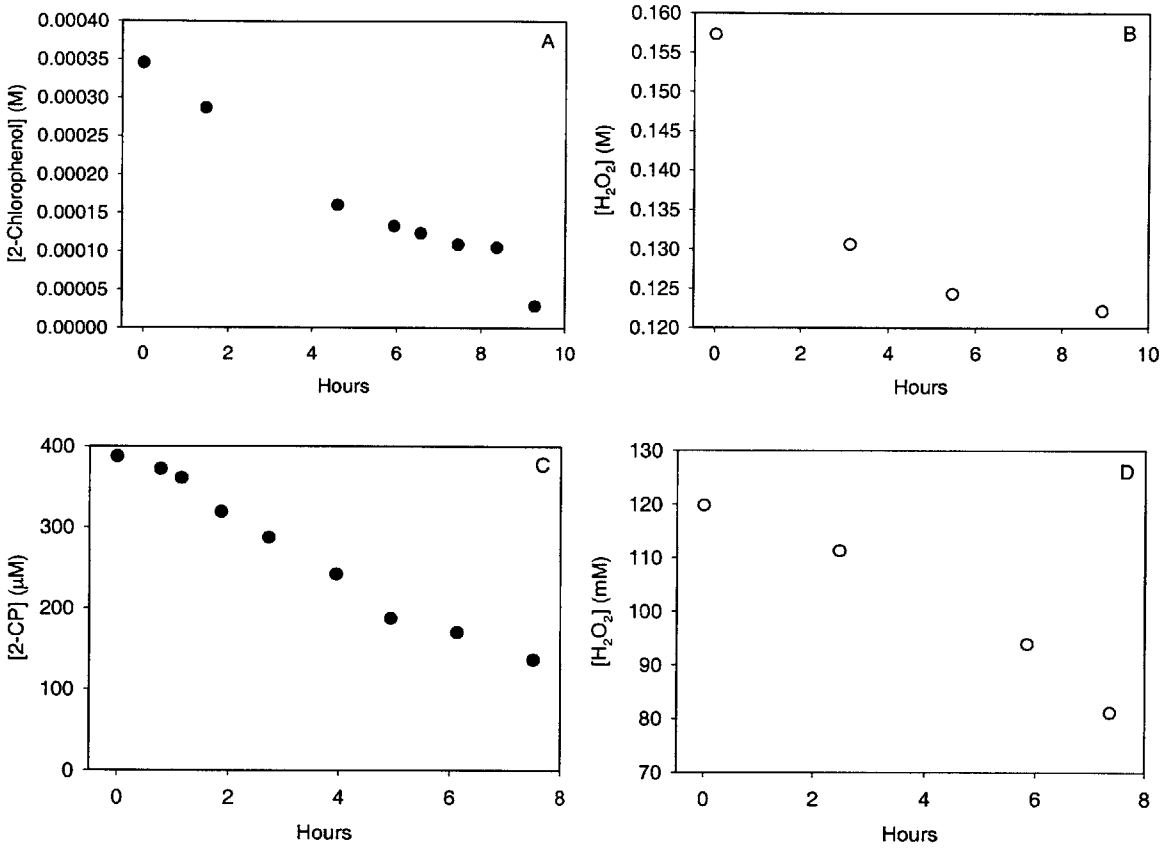

Figure D27. (A) [2-CP] in an experiment with 2.5 g/L goethite and $k = 0.17\ h^{-1}$. (B) $[H_2O_2]$ in the experiment described in (A), with $k = 0.030\ h^{-1}$. (C) [2-CP] in an experiment with 2.5 g/L goethite and $k = 0.14\ h^{-1}$. (D) $[H_2O_2]$ in the experiment described in (C), with $k = 0.050\ h^{-1}$.

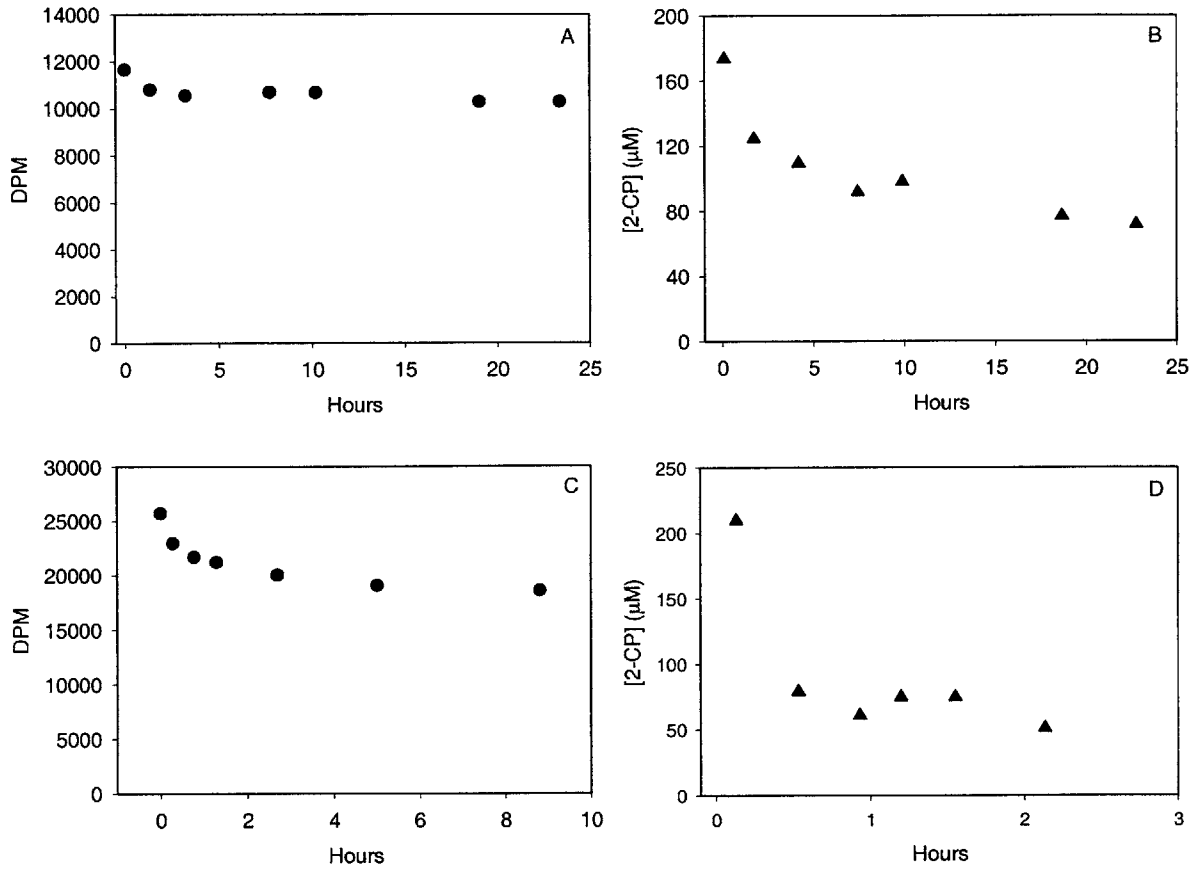

Figure D28. (A) ^{14}C activity in an experiment with [Fe(III)] = 25 μM, $[H_2O_2]_0$ = 1.9 M, and [2-CP]$_0$ = 200 μM, with k = 0.0038 h^{-1}. (B) [2-CP] in an experiment with [Fe(III)] = 25 μM and $[H_2O_2]_0$ = 2.0 M, with k = 0.039 h^{-1}. (C) ^{14}C activity in an experiment with [Fe(III)] = 75 μM, $[H_2O_2]_0$ = 1.7 M, and [2-CP]$_0$ = 200 μM, with k = 0.032 h^{-1}. (D) [2-CP] in an experiment with [Fe(III)] = 75 μM and $[H_2O_2]_0$ = 1.8 M, with k = 0.97 h^{-1}.

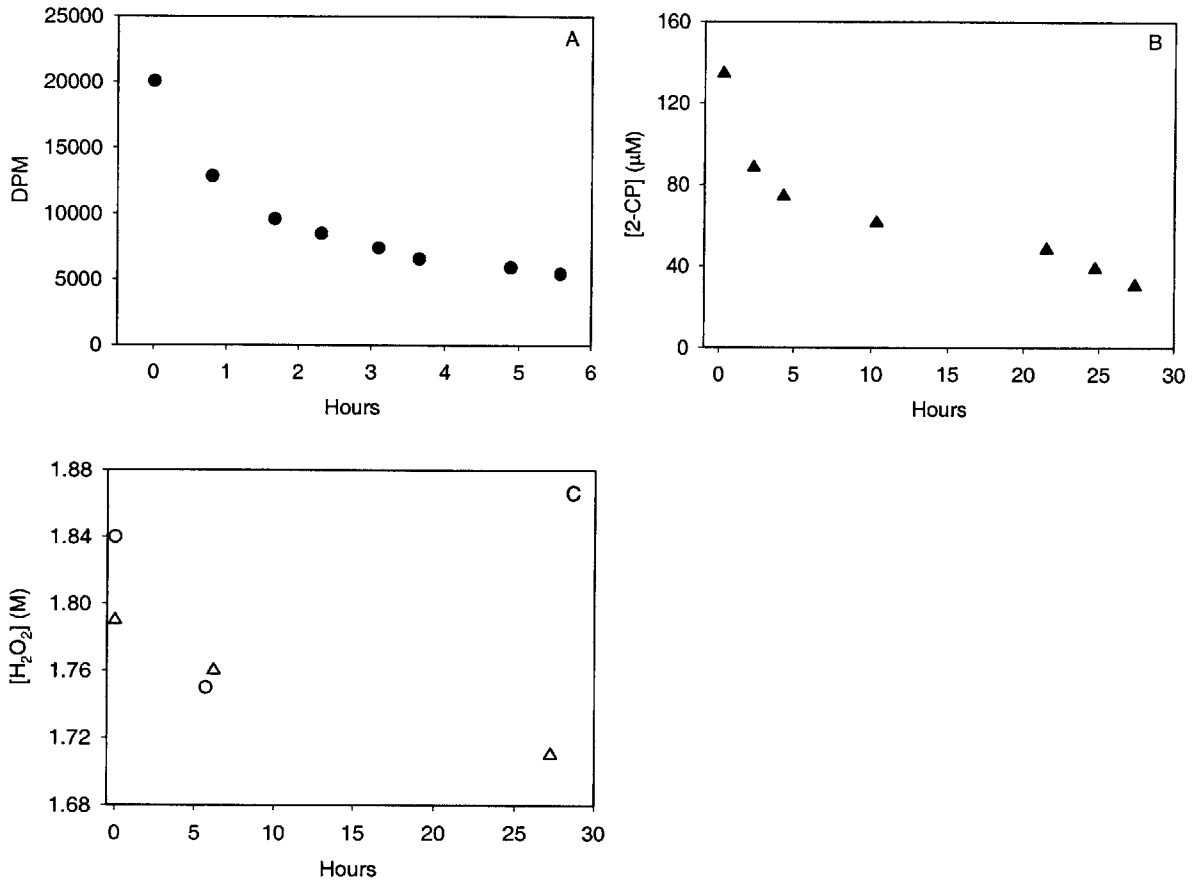

Figure D29. (A) ^{14}C activity in an experiment with 0.6 g/L goethite, $[H_2O_2]_0 = 2$ M, and $[2\text{-CP}]_0 = 130$ μM, with $k = 0.28$ h^{-1}. (B) [2-CP] in an experiment with 0.6 g/L goethite, $[H_2O_2]_0 = 2$ M, and $k = 0.049$ h^{-1}. (C) $[H_2O_2]$ in the experiments described in (A, ○) and (B, △), with $k = 0.0016$ (△) h^{-1}.

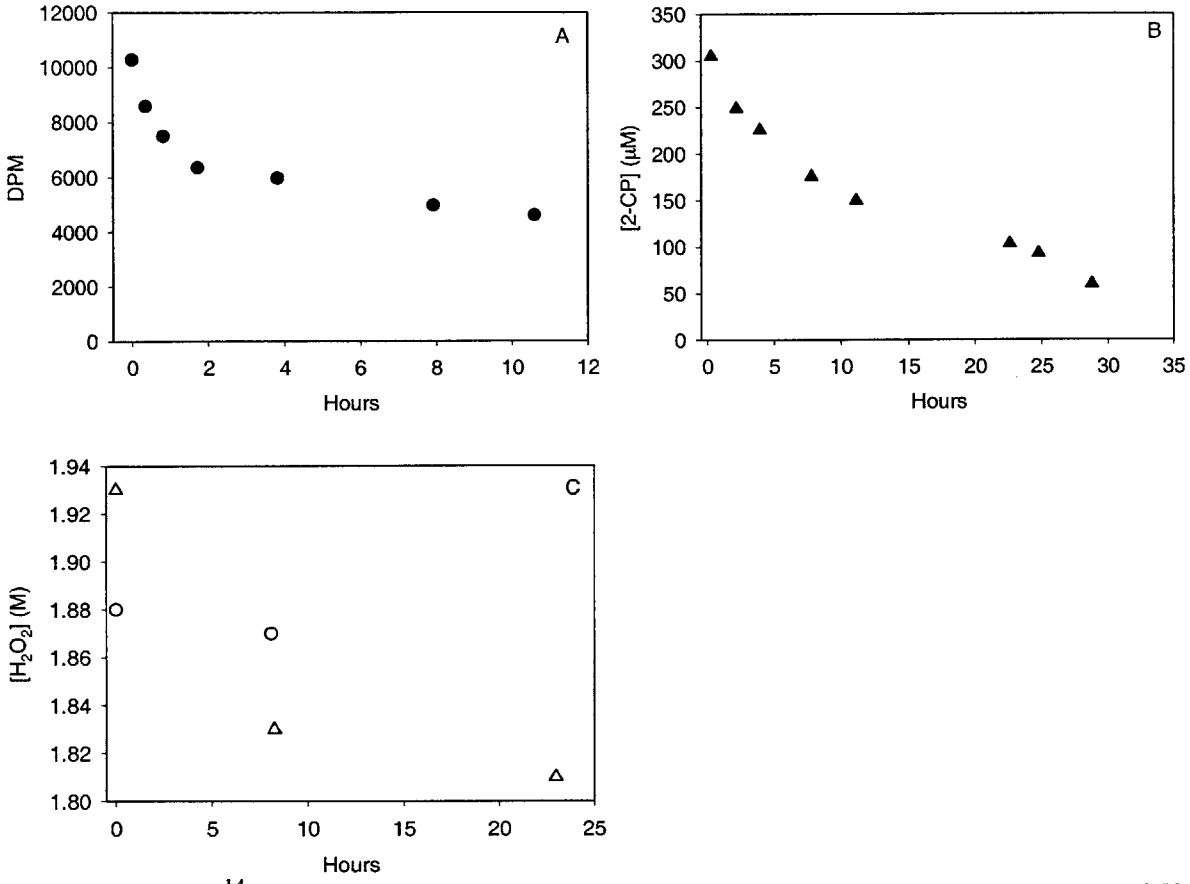

Figure D30. (A) ^{14}C activity in an experiment with 0.6 g/L goethite, $[H_2O_2]_0 = 2$ M, and $[2\text{-CP}]_0 = 300$ μM, with $k = 0.075$ h^{-1}. (B) [2-CP] in an experiment with 0.6 g/L goethite, $[H_2O_2]_0 = 2$ M, and $k = 0.052$ h^{-1}. (C) $[H_2O_2]$ in the experiments described in (A, ○) and (B, △), with $k = 0.0026$ (△) h^{-1}.

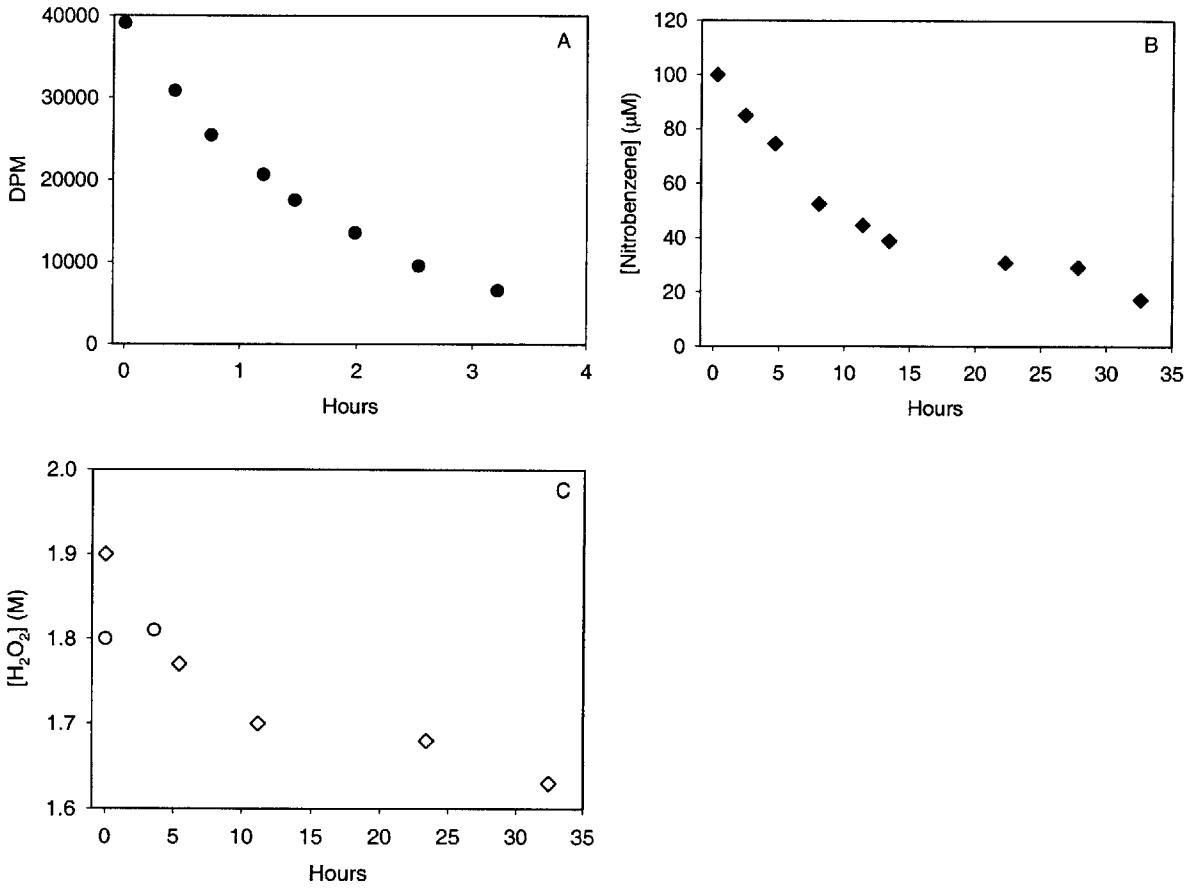

Figure D31. (A) ^{14}C activity in an experiment with 0.6 g/L goethite, $[H_2O_2]_0 = 2$ M, and $[NB]_0 = 100$ μM, with $k = 0.55$ h^{-1}. (B) [NB] in an experiment with 0.6 g/L goethite, $[H_2O_2]_0 = 2$ M, and $k = 0.058$ h^{-1}. (C) $[H_2O_2]$ in the experiments described in (A, ○) and (B, ◇), with $k = 0.0042$ (◇) h^{-1}.

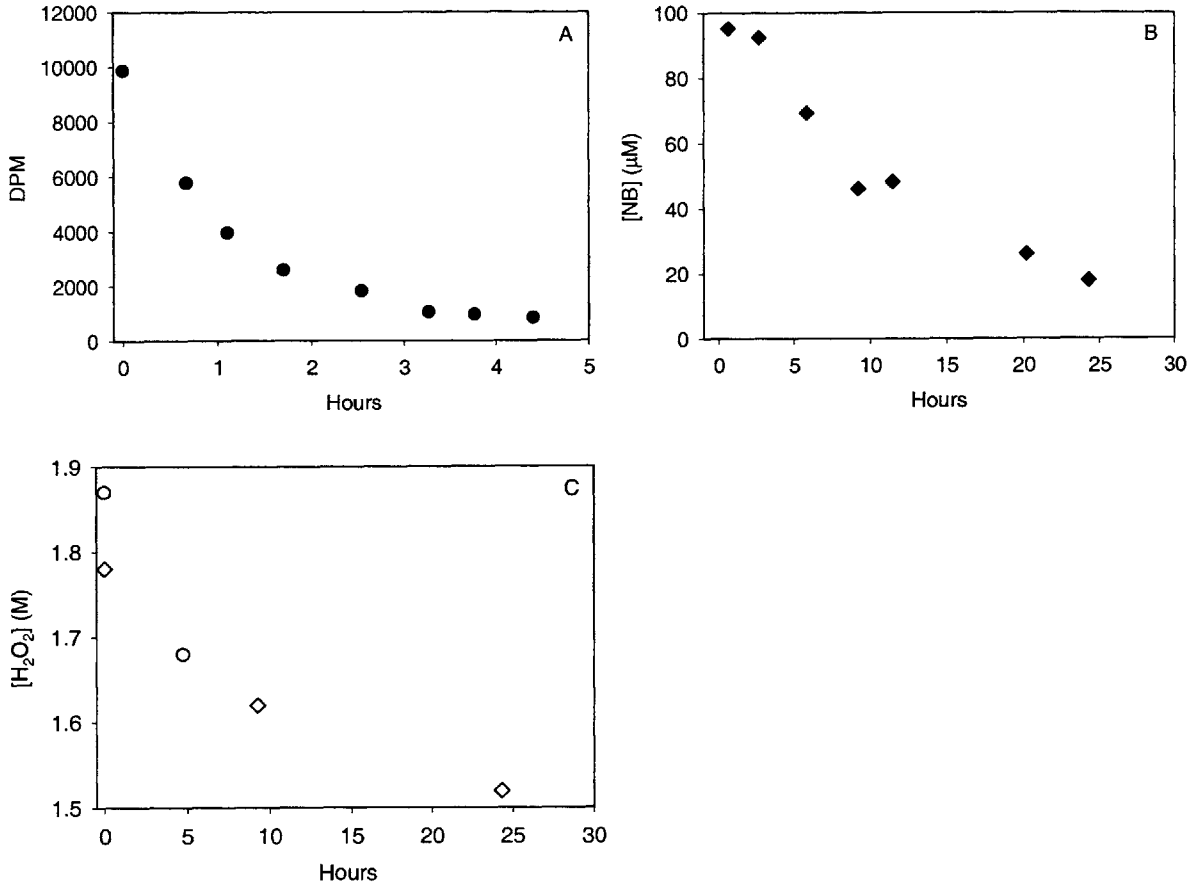

Figure D32. (A) ^{14}C activity in an experiment with 0.6 g/L goethite, $[H_2O_2]_0 = 2$ M, and $[NB]_0 = 100$ μM, with $k = 0.73$ h^{-1}. (B) [NB] in an experiment with 0.6 g/L goethite, $[H_2O_2]_0 = 2$ M, and $k = 0.072$ h^{-1}. (C) $[H_2O_2]$ in the experiments described in (A, ○) and (B, ◇), with $k = 0.0064$ (◇) h^{-1}.

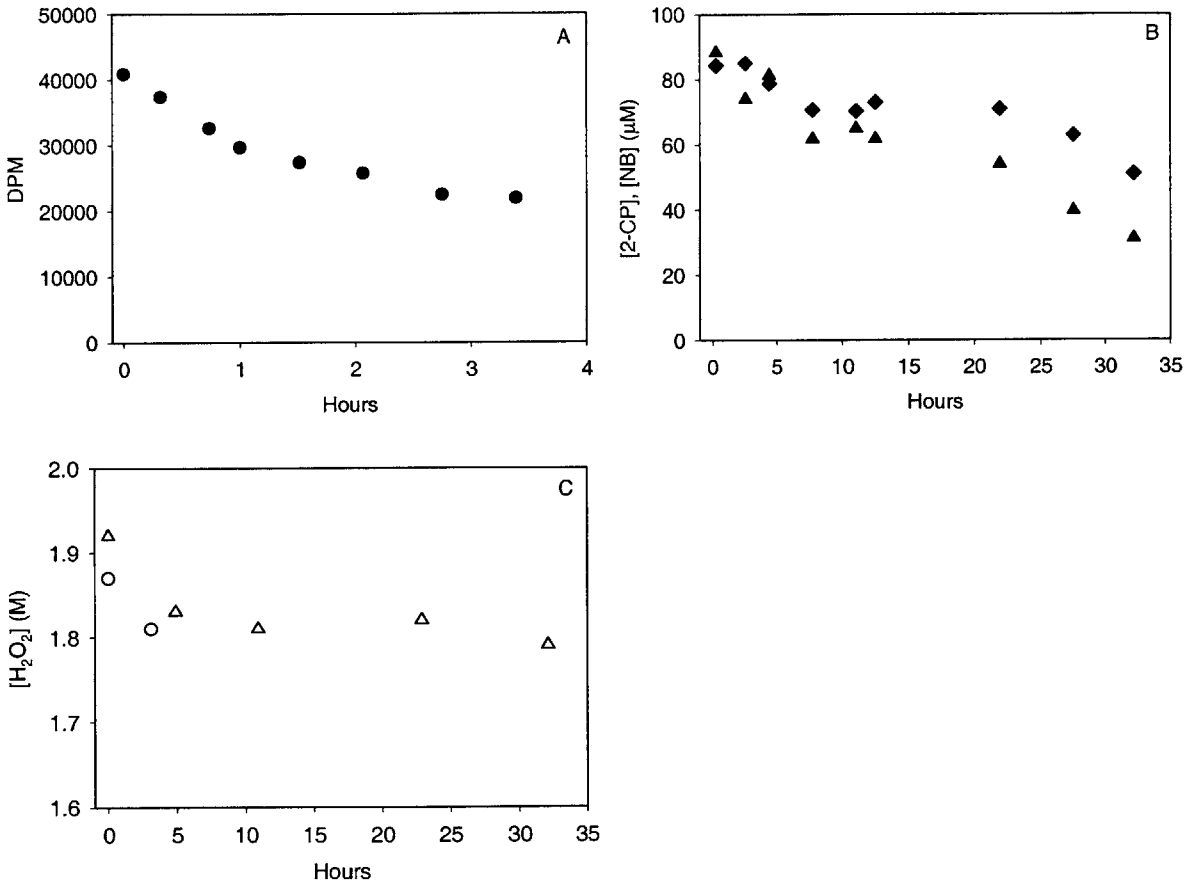

Figure D33. (A) ^{14}C activity in an experiment with 0.6 g/L goethite, $[H_2O_2]_0 = 2$ M, and $[2\text{-CP}]_0 = [NB]_0 = 90$ μM, with $k = 0.20$ h^{-1}. (B) [2-CP] (▲) and [NB] (◆) in an experiment with 0.6 g/L goethite, $[H_2O_2]_0 = 2$ M, with $k = 0.028$ (▲) and 0.012 (◆) h^{-1}. (C) $[H_2O_2]$ in the experiments described in (A, ○) and (B, △), with $k = 0.0016$ (△) h^{-1}.

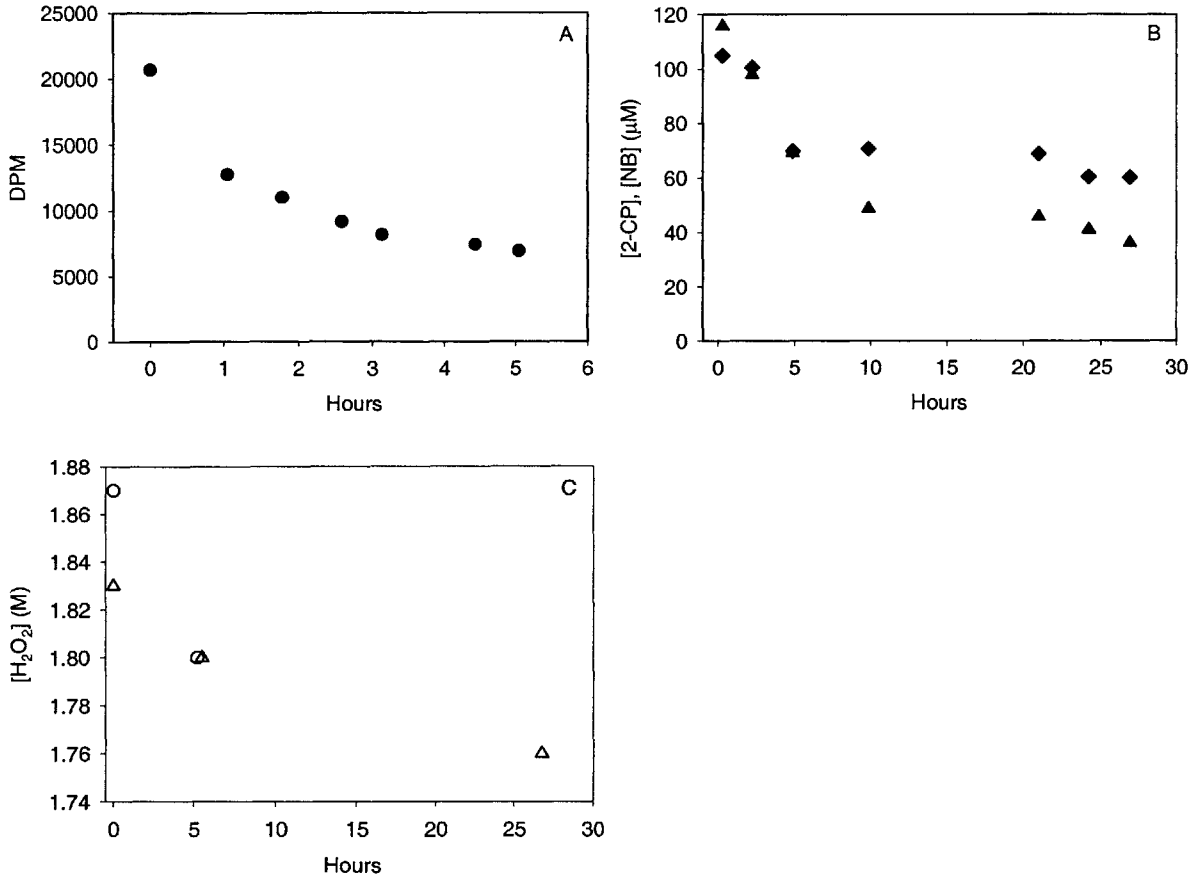

Figure D34. (A) ^{14}C activity in an experiment with 0.6 g/L goethite, $[H_2O_2]_0 = 2$ M, and $[2\text{-CP}]_0 = [NB]_0 = 100$ μM, with $k = 0.25$ h^{-1}. (B) [2-CP] (▲) and [NB] (◆) in an experiment with 0.6 g/L goethite, $[H_2O_2]_0 = 2$ M, with $k = 0.046$ (▲) and 0.019 (◆) h^{-1}. (C) $[H_2O_2]$ in the experiments described in (A, ○) and (B, △), with $k = 0.0014$ (△) h^{-1}.

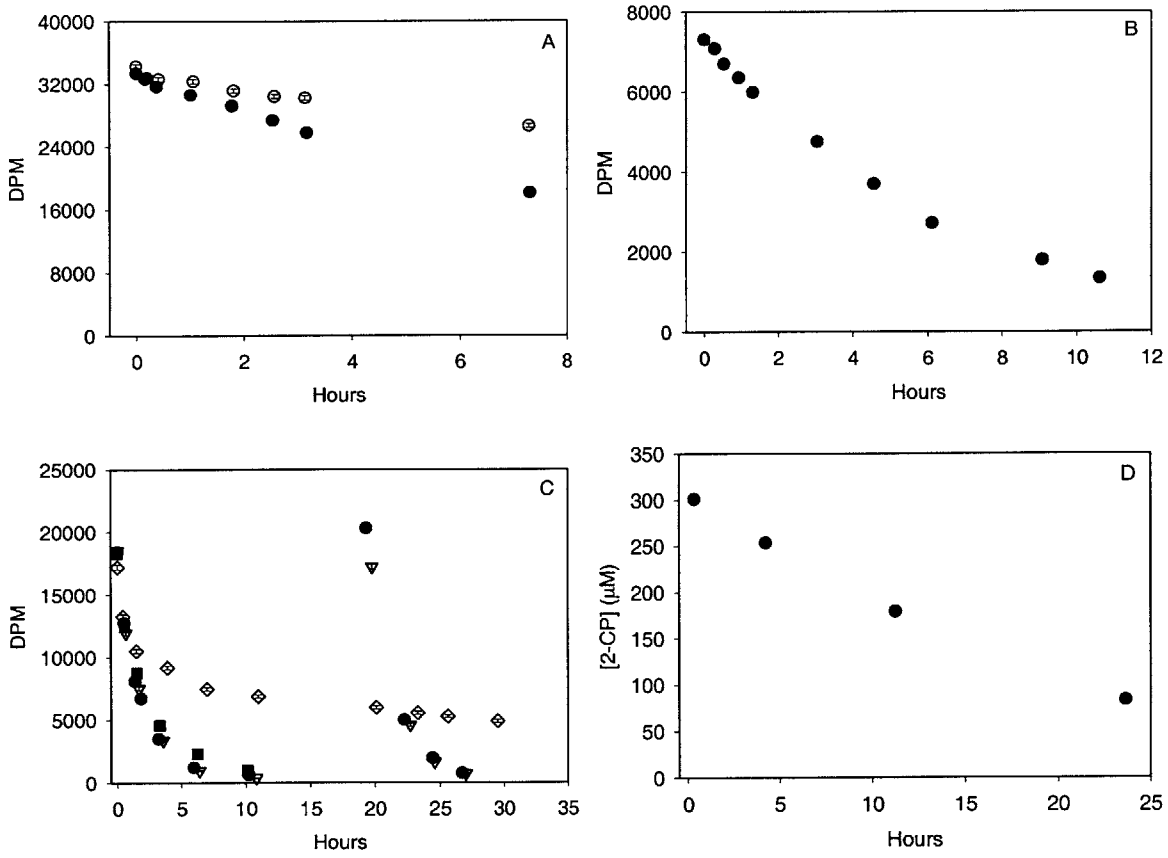

Figure D35. (A) ^{14}C activity in an experiment where the iron was from the supernatant of a 0.6 g/L goethite suspension (see chapter 4 for details) and $[H_2O_2]_0 = 1$ M at pH 4 (●) or 5 (○), with $k = 0.081$ and 0.032 h^{-1}, respectively. (B) ^{14}C activity in an experiment with 0.6 g/L goethite, $[H_2O_2]_0 = 1$ M, and I = 0.9 M $NaClO_4$, with $k = 0.016$ h^{-1}. (C) ^{14}C activity in four experiment with 0.6 g/L goethite, $[H_2O_2]_0 = 2$ M, and $[2\text{-CP}]_0 = 0.3$ (●), 3 (▽), 30 (■), or 300 (◇) μM, with $k = 0.55$, 0.52, 0.42 and 0.043 h^{-1}, respectively. The experiments with $[2\text{-CP}]_0 = 0.3$ and 3 μM were re-spiked with $H^{14}COOH$ after ~20 hours. (D) [2-CP] in the experiment described in (C) with $[2\text{-CP}]_0 = 300$ μM, with $k = 0.052$ h^{-1}.

2607
11